Leveraging Open Microfluidic Patterning and Home Blood Sampling and Stabilization to Advance Tissue Engineering and Translational Research

Amanda J. Haack

A dissertation
submitted in partial fulfillment of the
requirements for the degree of

Doctor of Philosophy

University of Washington
2023

Reading Committee:
Ashleigh B. Theberge, Chair
Matthew F. Bush
Robert E. Synovec

Program Authorized to Offer Degree:
Chemistry

University of Washington

Abstract

Leveraging Open Microfluidic Patterning and Home Blood Sampling and Stabilization to Advance Tissue Engineering and Translational Research

Amanda J. Haack

Chair of the Supervisory Committee:
Ashleigh B. Theberge, Ph.D.
Department of Chemistry

Engineered systems and microfluidic devices have long been used to gain insight into a range of disciplines in the medical sciences, from three-dimensional (3D) bioprinting to home biofluid sampling devices. This dissertation explores engineering tools and the use of open microfluidics to further develop tissue engineering and translational medicine. Chapter 1 introduces the field of open microfluidics and provides background into existing technologies for 3D tissue patterning and home sampling of biological fluids. Chapter 2 outlines a novel, additive technique for the fabrication of complex 3D hydrogel structures using removable open microfluidic patterning devices. This technique takes advantage of surface tension and capillary forces to drive flow and define the shape of the hydrogel structure, allowing for the use of native hydrogels (e.g., collagen, fibrin, and Matrigel) as well as engineered dynamic hydrogels. Chapter 3 expands upon open microfluidic tissue patterning in which a suspended removable open microfluidic channel is used to generate spatially patterned multi-component suspended engineered tissues. Chapter 4 introduces *home*RNA: a kit comprising a commercially available lancet-based blood sampling device from Tasso and a custom engineered fluidic tube for delivery of a stabilizer solution to a self-collected blood sample. *home*RNA enables fully remote user-directed blood sampling and RNA stabilization. Chapter 5 further explores the use of *home*RNA in high temperature settings via two pilot studies conducted in the summer months in western US and in Doha, Qatar. Chapter 6 describes a study

investigating the use of *home*RNA to evaluate the systemic inflammatory response to wildfire smoke in the Western US by utilizing a remote and flexible study design; the results show that *home*RNA is feasible for collecting biological samples in challenging environments, including unpredictable natural disasters such as wildfires. Finally, Chapter 7 provides an overarching summary of the technologies presented in this dissertation for home-sampling and tissue engineering applications. Chapter 7 also outlines future outlooks and current directions for these technologies. This dissertation leverages open microfluidics principles to advance tissue engineering, allowing for additional 3D control over a range of materials to study dynamic and structurally relevant engineered tissues. Looking beyond *in vitro* engineered tissue modelling, this work also presents technology to expand the study of human health outside of the laboratory and into the home – exploring the use of home-sampling and stabilization technologies to enable fully remote translational research.

Table of Contents

List of Figures

Dedication

I would like to dedicate this dissertation to my parents, Alan and Valerie, to my sisters, Stacey and Allison, and to my husband, Christopher.

Acknowledgments

I can only touch the surface of describing everyone who has helped and supported me during the process of creating this work. From my family to my peers and research mentors, thank you.

To everyone I crossed paths with in the Theberge lab, each have shaped my development as a bourgeoning scientist, and I am incredibly grateful for the camaraderie and companionship I have felt. I would like to thank Ulri, Tammi, Sam, John, Tianzi, and Jing for their support and welcoming during the early years of my PhD. I am also deeply grateful to Lauren, Jodie, Filip, Jamison, Maddie, Wan-Chen, Dakota and Yuting for their support, laughter, and wonderful creative endeavors, experiments and coffee breaks.

Thank you especially to my coauthors who worked on tissue patterning projects including Lauren, Ulri, Ross and John. It was fantastic to work with all of you. And thank you to Yun, Dakota, Lauren, Filip, and Yuting and Jing — coauthors on *home*RNA projects – the collaboration and camaraderie to bring this technology to fruition has been incredible.

To the many undergraduate students that I have had the absolute pleasure of working with throughout the years, thank you for all the hard work you have all put into the lab and the projects. Thank you to Serena, Jenny, Kathleen, Shayla, Lauren, Alex, Aaliyah, Ingrid and many more. I am excited to see where your careers take you and hope we can continue to work together in the future.

Thank you to my mentor, Prof. Ashleigh Theberge, for your mentorship and guidance throughout my PhD. Your expertise, insight, and dedication to research have been invaluable, and I could not have achieved this milestone without your support.

Thank you to Bingjie and Tessa for your friendship and support throughout medical school and graduate school. I am deeply grateful for your companionship.

Thank you to my family, my sisters Stacey and Allison, and my parents, Alan and Valerie. Thank you for always being there to support me throughout this long journey and to celebrate the milestones with me.

And finally thank you to my husband, Chris. You left your much-loved California sunshine to be in rainy Seattle for this MD/PhD journey and have been an invaluable source of motivation and support. You have encouraged me to strive for excellence, pushing me to go beyond what I thought was possible. Your enthusiasm and support have been a source of strength. Thank you.

Chapter 1: Introduction[1]

1.1 Open microfluidics overview

Microfluidics is an interdisciplinary field that involves the manipulation and control of small volumes of fluids in systems with at least one dimension on the micron scale. [1] It combines principles from physics, chemistry, engineering, and biology to develop technologies such as lab-on-a-chip platforms and biosensors. [1, 2] Emerging in the broader microfluidics community is an interest in developing open microfluidic systems. [3, 4] In comparison to closed or conventional microfluidics, open microfluidic systems are characterized by the lack of physical walls on at least one side of the microfluidic channel. [3] In conventional microfluidics, fluid within the microfluidic chip is typically only accessible via an inlet and an outlet, and flow is often driven by positive pressure via a flow pump such as a syringe pump. [3, 5] In contrast, the open geometry of open microfluidics enables access to the channels via standard laboratory tools such as pipettes, thus allowing the fluid within channels can be manipulated or added throughout the channel. Furthermore, open channel geometry utilizes capillary forces and surface tension to manipulate fluid flow. [3, 5] As equipment (such as fluid pumps) is not needed to drive the system, open microfluidics offer the potential to reduce cost and complexity of the overall system. This makes open microfluidics an attractive platform for researchers in a variety of fields looking for greater accessibility to microfluidic technologies.

Open microfluidic systems are attractive to use due to their accessibility with pipettes and lack of reliance on external equipment. However, open systems must be carefully designed; the geometry of the open channels as well as the surface chemistry with respect to the fluid both must be considered as flow is dictated by surface tension and capillary forces. [3, 6] In an open microfluidic system, flow can occur via spontaneous capillary flow or SCF. A simplified equation has been described [5] that indicates the conditions for whether SCF will occur and can be summarized in Equation 1.1:

[1] Portions of this chapter have been excerpted or paraphrased from Chapters 2-6 of this dissertation.

$$\frac{p_f}{p_w} < \cos(\theta) \qquad (Eq. 1.1)$$

where p_f refers to the free perimeter of a cross-section of a channel, or the portion of the perimeter that contains an air-liquid interface, p_w refers to the wetted perimeter, or the portion of the cross-section perimeter where liquid is in contact with a surface, and θ refers to the contact angle of the fluid on that surface. By manipulating these parameters such that the inequality is satisfied, researchers can design open microfluidic systems where fluid flow is driven by SCF.

1.2 Open microfluidic hydrogel patterning applications in engineered tissues

Generation of physiologically relevant tissue constructs *in vitro* is a significant driving force in the tissue engineering field. [7] Particularly important in achieving the goal of physiological relevance is achieving spatially controlled heterogeneous constructs; tissues are not homogenous *in vivo,* but rather contain regions of various cell type and extracellular matrix (ECM) composition, and can vary greatly in shape which can further affect tissue function. [7] ECM materials are typically made up of a biologically relevant hydrogel, such as collagen or fibrin. [7] The ability to develop 3D tissue constructs with precise hydrogel patterning and cellular compositional control would improve the physiological relevance of *in vitro* tissue models used for drug testing and disease progression applications. [8, 9]

There are many established methods for hydrogel patterning. Amongst these methods, photopolymerization techniques are robust and offer resolution on the order of microns, [10-19] however photo-initiators have been shown to cause cellular damage [20, 21] and the necessity for chemical functionalization of the gel precludes the use of native (unmodified) gels. Other broadly used hydrogel patterning methods include inkjet [22-24] and microextrusion [25-29] printing. In these methods, the hydrogel is jetted through a nozzle that exposes cells encapsulated within the hydrogel to shear stress, which can mechanically damage the cells and limit the types of cells that can be patterned. [30, 31] Casting

hydrogels using a fabricated negative mold provides an alternative approach, but the complexity of the gel structures obtainable is limited due to demolding considerations. [32-34]

In this dissertation, I introduce an alternative method for controlling hydrogel deposition to generate 3D patterned extracellular matrix for tissue engineering applications utilizing open microfluidics. Taking advantage of surface tension, open channels are designed to drive the flow of a hydrogel precursor and control the shape of the gel deposition via capillary pinning. In this work, channels for patterning either comprise a ceiling and a floor with no walls in the case of layer-by-layer patterning (Chapter 2) or contain walls with no ceiling or floor in the case of suspended open microfluidic patterning (Chapter 3); the two modes of open microfluidic hydrogel patterning are depicted in Figure 1.1. Open channels are accessible via pipette across the channel geometry, and cells can be added to native hydrogel precursors, thereby patterning distinct regions of tissues. A blocker such as bovine serum albumin (BSA) can be used to coat patterning devices to prevent cellular adhesion, patterning devices can be removed after the ECM-cell mixture has gelled, leaving behind a 3D engineered tissue construct. With open microfluidic tissue patterning, pen microfluidics is employed as a tool for controlling the deposition of tissues, but not in the final engineered tissue model itself which can be entirely made up of living tissue.

1.2.1 Layer by layer open microfluidic patterning: towards 3D spatial control over tissue models

Layer by layer open microfluidic hydrogel patterning is a method that uses open microfluidic principles and surface tension driven flow to deposit and sequentially form hydrogel layers in user-defined patterns, each delivered directly using a pipette. [35] To form each hydrogel layer in a controlled shape, we use a ‘patterning device,’ which is either a plastic physical ‘rail’ or a hydrophilic track delineated on a hydrophobic flat surface; both enable the pre-gel solution to flow via capillary action without external pressure and constrain the pre-gel solution under the rail footprint via capillary pinning. [5, 36] The patterning device is placed above an existing hydrogel layer, or bottom of a plastic tissue culture well plate if it is the first layer, at a designed height (Figure 1.1A). The gap between the patterning device and the existing hydrogel layer forms an open microfluidic ‘channel’ in which liquid pre-gel solution can flow,

where the channel 'ceiling' is the patterning device, the 'floor' is the previous gel layer, and the 'sides' are free air-liquid interfaces (Figure 1.1A). The patterning device can be removed once the gel layer has formed, and another patterning device can be applied to pattern the next layer, providing the ability to build three-dimensional structures layer-by-layer.

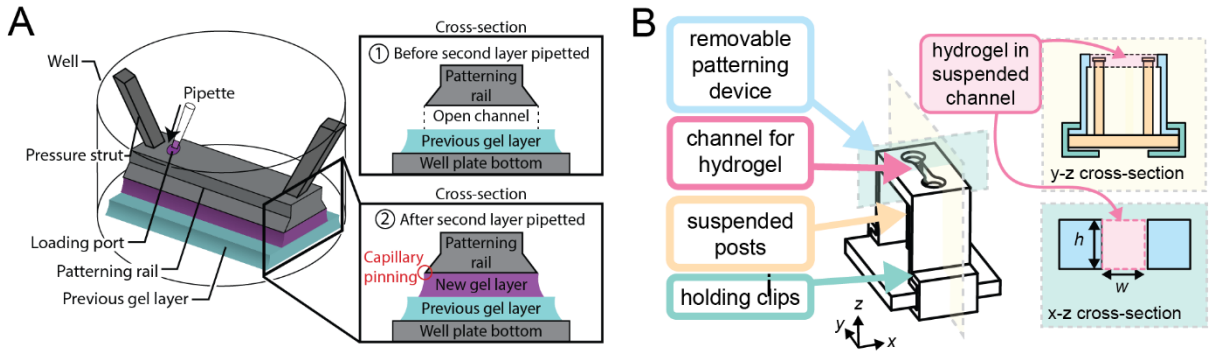

Figure 1.1. Open microfluidic hydrogel patterning. A) Schematic demonstrating layer-by-layer open microfluidic hydrogel patterning. B) Schematic demonstrating suspended open microfluidic hydrogel patterning.

1.2.2 Suspended tissue patterning with open microfluidics

Many engineered 3D tissue models lack the ability to apply mechanical forces, such as stress- and strain-induced mechanotransduction, that play a crucial role in cell morphology, alignment, proliferation, and differentiation. [37-39] To address this limitation, flexible cantilevers and pillars have been used to fabricate suspended 3D tissue structures that can experience tensile forces in real time; [40-43] these platforms have been used to develop engineered heart, [44, 45] muscle, [46, 47] and lung tissues, [48, 49] as well as wound healing skin models. [50] While being able to apply mechanical force to these engineered tissues is critical for understanding and studying these tissue types, what can further enhance the biological relevance and allow for more complex studies to recapitulate these tissues is adding spatial control across a suspended tissue.

In Chapter 3, I describe an additional implementation of open microfluidic patterning, distinct from the layer-by-layer patterning described in Chapter 2, to generate a 3D, multi-region suspended hydrogel culture. This suspended model is developed using a removable open microfluidic patterning device that

interfaces two posts, generating a suspended hydrogel over an open space without the use of a sacrificial material (Figure 1.1B). This technology expands on an existing model that uses casting to generate suspended engineered heart tissues, but our method offers the unique advantage of spatial control over material and cell composition. [51, 52] Utilizing surface tension to drive flow and capillary pinning to stop flow, we can selectively place tissue components in different areas to pattern multiple regions within a single suspended tissue. Next, taking advantage of the cellular behavior to contract and remodel ECM, cells pull away from the walls of the patterning device while remaining compacted on the suspended posts, thereby allowing gentle removal of the patterning device. This system can be used to unlock frontiers in modeling complex biological functions such as border regions between tissues (e.g., disease and healthy tissue borders), myotendinous junctions (e.g., bone-ligament or muscle-tendon interfaces), or recapitulating *in vivo* zonal patterning (e.g., modeling liver zonation or gradients).

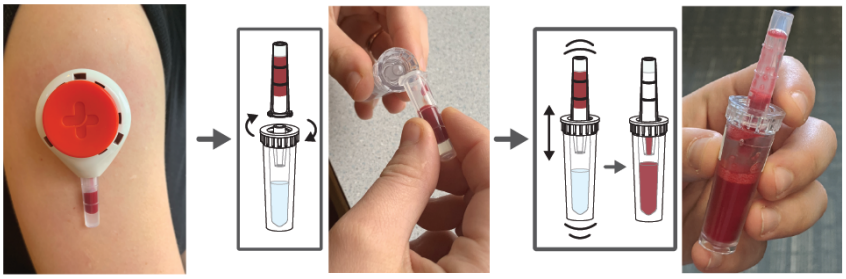

Figure 1.2. Workflow for self-blood collection and stabilization with *home*RNA.

1.3 Remote blood sampling: emerging tools for remote research studies

Remote and contact-free laboratory testing is rapidly emerging as the new standard in patient care and clinical research, especially considering the COVID-19 pandemic. However, blood sample collection remains a challenging procedure to perform remotely as venipuncture is resource-intensive, physically uncomfortable, and inflexible regarding collection time and location. [53, 54] Remote self-administered blood collection, on the other hand, offers many practical advantages, including (1) expanded lab testing for rural and remote medicine applications (i.e., telemedicine), (2) convenience for clinical research studies

as well as the ability to recruit participants that are not able to come to the clinic (due to work schedules, caregiver responsibilities, mobility challenges, etc.), (3) the ability to capture acute and transient biomarker fluctuations (e.g., immediately following an acute exposure, an asthma attack, or a flare in an autoimmune disease), and (4) opportunities to conduct longitudinal research studies that require frequent sample collections from the same individual over a short time course (e.g., daily blood collections). To date, these applications have been limited due to the logistical challenges associated with in-person venipuncture.

1.3.1 Challenges with remote blood RNA stabilization

There is an obvious advantage to decentralizing blood collection beyond a phlebotomy clinic; consequently, there have been many technological advances in self-blood collection. [55-59] However, blood collection is often only the first step in blood-based laboratory tests. Blood is not a static tissue sample; it contains living cells that can continue reacting to changes in their ex vivo environment. Post collection sample handling is critical, and there have been numerous studies determining the best way to store, stabilize, and handle blood samples for various target analytes. [60-63] For transcriptomics profiling, RNA stabilization in liquid whole blood is particularly critical. Changes in mRNA transcripts that can happen in the *ex vivo* environment after blood collection can be highly unfavorable for research intended to understand *in vivo* cellular expression landscapes. RNA can either be highly degraded from ribonucleases and other processes such that it cannot be analyzed, and other *ex vivo* changes (e.g., inducement of mRNA expression in blood cells post-collection) can lead to an inaccurate representation of the *in vivo* transcriptome in question. [64, 65]

In a traditional outpatient venipuncture setting, stabilization of whole blood RNA is accomplished by collecting venous blood directly into vacutainers containing RNA stabilizers (e.g., Tempus or Paxgene) or immediately pipetting anticoagulated blood into vials containing RNA*later*. This procedure is incompatible with a self-sampling protocol as users cannot be expected to pipette their own blood or do venipuncture into a vacutainer tube on themselves. To fully enable remote sampling and transcriptomic profiling of liquid blood samples, one must eliminate the need for a phlebotomist-assisted blood draw and

enable the patient or research participants to act as their own laboratory technician, allowing them to perform necessary steps to stabilize their blood sample without the use of pipettes, gloves, or syringes.

1.3.2 home*RNA as a kit for the self-collection and stabilization of whole blood RNA*

In Chapter 4, I describe the development of *home*RNA: a kit aimed at accomplishing the goal of both collection and RNA stabilization in at-home settings. [66] With *home*RNA we combine a commercially available lancet-based blood sampling device (Tasso-SST), a liquid RNA stabilizer (RNA*later*), and a custom-engineered fluid transfer and stabilizer tube into a single sampling unit that can be mailed to remote study participants. Figure 1.2 illustrates the process for collecting and stabilizing blood with *home*RNA. Participants collect a liquid sample (~0.1−0.5 mL) of whole blood, stabilize it, and ship it back to the laboratory for analysis. To demonstrate our liquid stabilization technology, we chose to target total whole blood cellular RNA with RNA*later*. However, our technology is broadly generalizable in that a researcher interested in using a different stabilizer or targeting a different class of biomarkers can replace the stabilizer in the stabilizer tube with another liquid stabilizer.

To assess the usability and feasibility of this sampling methodology, we conducted a pilot study (n = 47 participants) to answer two fundamental research questions: (1) are the design and instructions for the kit comprehensive and user- friendly enough to allow users to collect and stabilize a sample of their own blood without in-person training? and (2) is the stabilization process sufficient to enable isolation of high-quality RNA suitable for standard gene expression analyses? In the pilot study, the *home*RNA kit was sent to 47 participants, aged between 21 and 69 and living across 10 different US states (WA, CA, CO, NE, WI, IN, PA, NY, MA, and ME). We measured successful blood collection and RNA stabilization by total RNA yield and RNA integrity number (RIN). Our kit and methodology open the potential for a new class of transcriptomics studies, enabling increased sampling frequency for longitudinal studies and access to populations that have been historically hard to reach.

1.3.3. home*RNA and challenges with remote sampling in high temperature climates*

In contrast to Chapter 4, where most of the samples in the pilot feasibility study were collected in regions with relatively moderate summer temperatures or during the fall/winter, in Chapter 5 I describe additional investigations into *home*RNA in higher temperature climates. Establishing ways to remotely probe the human whole blood transcriptome in elevated temperature settings has important implications, including enabling clinical research or personalized medicine applications in areas with high temperature and studying diseases/events that are specific to warm climates or warm times of year. [58, 67, 68] For example, regions more highly burdened by tropical diseases would benefit from a better understanding of the stability of RNA because many of these areas often have persistently elevated temperatures. Further, even in regions with more moderate climates for part of the year, researchers may wish to conduct remote sampling studies in the summer months, particularly when tied to a specific seasonal event. For example, a study aiming to understand wildfire smoke exposure in the Western and South Central USA would necessitate sampling in the summer months where temperatures are elevated, as these months are when wildfires occur. Overall, the ability to reliably stabilize RNA with *home*RNA in high temperature settings will open remote transcriptome studies to regions with a warmer climate, seasonally or permanently.

In Chapter 5 I describe two small pilot studies exploring the application of *home*RNA in high temperature settings. In the first pilot study, *home*RNA was used by a small group in the city of Doha, Qatar before the sample was exposed to simulated shipping conditions of fluctuating temperatures. [68] In the second study, *home*RNA was used at a regional scale, where participants used *home*RNA in their own homes during the summer months in several Western and South Central USA states, which included regions that are typically very hot (e.g., Reno, Nevada and Southern California) as well as the Pacific Northwest during the June 2021 heat wave. For samples collected from both studies, we examine quality control metrics typical to determining suitability of isolated RNA for downstream RNA transcript analysis, including the RNA integrity number (RIN) and total cellular RNA yield. Overall, our data demonstrate

successful RNA stabilization as a function of yield and RIN values using *home*RNA in high temperature settings.

1.3.4. Sampling unpredictable exposures: home*RNA as a tool for understanding inflammatory transcriptome response to wildfire smoke exposure*

The frequency, size, and intensity of wildfire events have increased dramatically in the past decades across the western United States and are projected to continue increasing by 56% through 2100. [69] Given the increasing impact of wildfire smoke on general population health, there has also been a push to understand the impacts of wildfire smoke, from a mechanistic perspective, particularly on respiratory tract and systemic inflammation. [70-74] Investigating a transcriptome-wide systemic response to wildfire smoke on the general population is difficult due to the logistical challenges inherent to conducting such a study. Because wildfire smoke exposure can be unpredictable, running a clinic-based blood draw study would require either (1) relying on historical data to choose a location that has infrastructure to support clinic based blood draws (i.e., a urban or suburban environment), which has a historically high prevalence of wildfire smoke, (2) setting up a multi-site study or (3) relying on retrospective studies or capturing smoke exposure incidentally on a study investigating a different question where longitudinal blood samples are collected. [72, 75] Having one study location runs the risk of no smoke exposure occurring during the study period in that location. In contrast, setting up a multi-site study with multiple clinic-based phlebotomy sites or remote phlebotomy sites would increase logistical burden of the study design. Finally, many cases of wildfire smoke exposure occur in remote locations, which may be inaccessible via traditional phlebotomy or require study participants to travel large distances for each blood draw timepoint.

In Chapter 6 I describe a large-scale longitudinal study utilizing *home*RNA to collect samples in response to wildfire smoke throughout the Western U.S. In this study, we collected samples from participants who were exposed to varying levels of wildfire smoke throughout the wildfire season to study the short-term changes in gene expression in response to wildfire smoke exposure, as well as 3 and 6 months after the wildfire season to assess long-term effects of wildfire smoke exposure. The study design is fully remote, enabling a wide range of geographic locations and timepoints to be collected. *home*RNA thus

provides a tool for fully remote, responsive, and flexible study design in response to unpredictable events such as wildfire smoke exposures.

1.4 Dissertation Summary

In this dissertation I present technologies and methods that harness principles of open microfluidics to expand the range of questions that can be asked in biological research. Applications of the technologies presented here range from methods to advance *in vitro* engineered tissues in the laboratory to technology to collect and stabilize blood in the home. Open microfluidic tissue patterning introduces new possibilities to the existing repertoire of engineered in vitro tissue models, allowing for the patterning of more complex geometries and the manipulation of spatial, temporal, and mechanical cues. And lastly, *home*RNA allows for probing of the immune response a to events that occur beyond the clinic and laboratory and provides a new paradigm for fully remote longitudinal blood transcriptome studies.

1.5 References

1. G. M. Whitesides, *Nature 2006 442:7101*, 2006, **442**, 368–373.
2. D. J. Beebe, G. A. Mensing and G. M. Walker, *https://doi.org/10.1146/annurev.bioeng.4.112601.125916*, 2003, **4**, 261–286.
3. E. Berthier, A. M. Dostie, U. N. Lee, J. Berthier and A. B. Theberge, *Anal Chem*, 2019, **91**, 8739–8750.
4. Open Microfluidics - Jean Berthier, Kenneth A. Brakke, Erwin Berthier (accessed 30 January 2023).
5. B. P. Casavant, E. Berthier, A. B. Theberge, J. Berthier, S. I. Montanez-Sauri, L. L. Bischel, K. Brakke, C. J. Hedman, W. Bushman, N. P. Keller and D. J. Beebe, *Proc Natl Acad Sci U S A*, 2013, **110**, 10111–10116.
6. B. P. Casavant, E. Berthier, A. B. Theberge, J. Berthier, S. I. Montanez-Sauri, L. L. Bischel, K. Brakke, C. J. Hedman, W. Bushman, N. P. Keller and D. J. Beebe, *Proc Natl Acad Sci U S A*, 2013, **110**, 10111–10116.
7. Y. Park, K. M. Huh and S. W. Kang, *International Journal of Molecular Sciences 2021, Vol. 22, Page 2491*, 2021, **22**, 2491.
8. R. Daniel Pedde, B. Mirani, A. Navaei, T. Styan, S. Wong, M. Mehrali, A. Thakur, N. Khadem Mohtaram, A. Bayati, A. Dolatshahi-Pirouz, M. Nikkhah, S. M. Willerth, M. Akbari, R. D. Pedde, B. Mirani, N. Khadem Mohtaram, M. Akbari, A. Navaei, M. Nikkhah, T. Styan, S. Wong, A. Bayati, S. M. Willerth, M. Mehrali, A. Thakur and A. Dolatshahi-Pirouz, *Advanced Materials*, 2017, **29**, 1606061.

9. E. L. Elson and G. M. Genin, *Interface Focus*, , DOI:10.1098/RSFS.2015.0095.
10. D. J. Beebe, J. S. Moore, J. M. Bauer, Q. Yu, R. H. Liu, C. Devadoss and B. H. Jo, *Nature*, 2000, **404**, 588–590.
11. V. Chan, P. Zorlutuna, J. H. Jeong, H. Kong and R. Bashir, *Lab Chip*, 2010, **10**, 2062–2070.
12. W. G. Koh and M. v. Pishko, *Anal Bioanal Chem*, 2006, **385**, 1389–1397.
13. M. S. Hahn, J. S. Miller and J. L. West, *Advanced Materials*, 2006, **18**, 2679–2684.
14. V. A. Liu and S. N. Bhatia, *Biomed Microdevices*, 2002, **4**, 257–266.
15. C. K. Arakawa, B. A. Badeau, Y. Zheng and C. A. DeForest, *Advanced Materials*, , DOI:10.1002/ADMA.201703156.
16. J. Liu, D. Gao, H. F. Li and J. M. Lin, *Lab Chip*, 2009, **9**, 1301–1305.
17. J. Decock, M. Schlenk and J. B. Salmon, *Lab Chip*, 2018, **18**, 1075–1083.
18. S. J. Bryant, J. L. Cuy, K. D. Hauch and B. D. Ratner, *Biomaterials*, 2007, **28**, 2978–2986.
19. G. Papavasiliou, P. Songprawat, V. Pérez-Luna, E. Hammes, M. Morris, Y. C. Chiu and E. Brey, *Tissue Eng Part C Methods*, 2008, **14**, 129–140.
20. C. G. Williams, A. N. Malik, T. K. Kim, P. N. Manson and J. H. Elisseeff, *Biomaterials*, 2005, **26**, 1211–1218.
21. L. Xu, N. Sheybani, W. A. Yeudall and H. Yang, *Biomater Sci*, 2015, **3**, 250–255.
22. T. Boland, X. Tao, B. J. Damon, B. Manley, P. Kesari, S. Jalota and S. Bhaduri, *Materials Science and Engineering C*, 2007, **27**, 372–376.
23. C. Xu, W. Chai, Y. Huang and R. R. Markwald, *Biotechnol Bioeng*, 2012, **109**, 3152–3160.
24. T. Xu, W. Zhao, J. M. Zhu, M. Z. Albanna, J. J. Yoo and A. Atala, *Biomaterials*, 2013, **34**, 130–139.
25. A. Bandyopadhyay, V. K. Dewangan, K. Y. Vajanthri, S. Poddar and S. K. Mahto, *Biocybern Biomed Eng*, 2018, **38**, 158–169.
26. S. Sakai, K. Mochizuki, Y. Qu, M. Mail, M. Nakahata and M. Taya, *Biofabrication*, , DOI:10.1088/1758-5090/AADC9E.
27. J. H. Shim, J. S. Lee, J. Y. Kim and D. W. Cho, *Journal of Micromechanics and Microengineering*, , DOI:10.1088/0960-1317/22/8/085014.
28. F. Pati, J. Jang, D. H. Ha, S. Won Kim, J. W. Rhie, J. H. Shim, D. H. Kim and D. W. Cho, *Nat Commun*, , DOI:10.1038/NCOMMS4935.
29. T. J. Hinton, Q. Jallerat, R. N. Palchesko, J. H. Park, M. S. Grodzicki, H. J. Shue, M. H. Ramadan, A. R. Hudson and A. W. Feinberg, *Sci Adv*, , DOI:10.1126/SCIADV.1500758.
30. K. Nair, M. Gandhi, S. Khalil, K. C. Yan, M. Marcolongo, K. Barbee and W. Sun, *Biotechnol J*, 2009, **4**, 1168–1177.
31. A. Blaeser, D. F. Duarte Campos, U. Puster, W. Richtering, M. M. Stevens and H. Fischer, *Adv Healthc Mater*, 2016, **5**, 326–333.
32. Y. Zheng, J. Chen, M. Craven, N. W. Choi, S. Totorica, A. Diaz-Santana, P. Kermani, B. Hempstead, C. Fischbach-Teschl, J. A. López and A. D. Stroock, *Proc Natl Acad Sci U S A*, 2012, **109**, 9342–9347.

33. Y. Ling, J. Rubin, Y. Deng, C. Huang, U. Demirci, J. M. Karp and A. Khademhosseini, *Lab Chip*, 2007, **7**, 756–762.

34. S. Cosson and M. P. Lutolf, *Sci Rep*, , DOI:10.1038/SREP04462.

35. U. N. Lee, J. H. Day, A. J. Haack, R. C. Bretherton, W. Lu, C. A. Deforest, A. B. Theberge and E. Berthier, *Lab Chip*, 2020, **20**, 525–536.

36. S. B. Berry, T. Zhang, J. H. Day, X. Su, I. Z. Wilson, E. Berthier and A. B. Theberge, *Lab Chip*, 2017, **17**, 4253–4264.

37. B. D. Riehl, J. H. Park, I. K. Kwon and J. Y. Lim, *Tissue Eng Part B Rev*, 2012, **18**, 288–300.

38. W. Zhang, G. Huang and F. Xu, *Front Bioeng Biotechnol*, 2020, **8**, 1151.

39. J. J. Tomasek, G. Gabbiani, B. Hinz, C. Chaponnier and R. A. Brown, *Nature Reviews Molecular Cell Biology 2002 3:5*, 2002, **3**, 349–363.

40. W. R. Legant, A. Pathak, M. T. Yang, V. S. Deshpande, R. M. McMeeking and C. S. Chen, *Proc Natl Acad Sci U S A*, 2009, **106**, 10097–10102.

41. R. K. Christensen, C. von Halling Laier, A. Kiziltay, S. Wilson and N. B. Larsen, *Biomacromolecules*, 2020, **21**, 356–365.

42. N. Gaio, B. van Meer, W. Q. Solano, L. Bergers, A. van de Stolpe, C. Mummery, P. M. Sarro and R. Dekker, *Micromachines 2016, Vol. 7, Page 120*, 2016, **7**, 120.

43. J. Eyckmans and C. S. Chen, *J Cell Sci*, 2017, **130**, 63–70.

44. B. M. Ulmer, A. Stoehr, M. L. Schulze, S. Patel, M. Gucek, I. Mannhardt, S. Funcke, E. Murphy, T. Eschenhagen and A. Hansen, *Stem Cell Reports*, 2018, **10**, 834–847.

45. M. Lux, B. Andrée, T. Horvath, A. Nosko, D. Manikowski, D. Hilfiker-Kleiner, A. Haverich and A. Hilfiker, *Acta Biomater*, 2016, **30**, 177–187.

46. H. Vandenburgh, J. Shansky, F. Benesch-Lee, V. Barbata, J. Reid, L. Thorrez, R. Valentini and G. Crawford, *Muscle Nerve*, 2008, **37**, 438–447.

47. I.-C. Liao, J. B. Liu, N. Bursac and K. W. Leong, *Cellular and Molecular Bioengineering 2008 1:2*, 2008, **1**, 133–145.

48. Z. Chen, Q. Wang, M. Asmani, Y. Li, C. Liu, C. Li, J. M. Lippmann, Y. Wu and R. Zhao, *Scientific Reports 2016 6:1*, 2016, **6**, 1–11.

49. A. R. West, N. Zaman, D. J. Cole, M. J. Walker, W. R. Legant, T. Boudou, C. S. Chen, J. T. Favreau, G. R. Gaudette, E. A. Cowley and G. N. Maksym, *Am J Physiol Lung Cell Mol Physiol*, 2013, **304**, 4–16.

50. M. S. Sakar, J. Eyckmans, R. Pieters, D. Eberli, B. J. Nelson and C. S. Chen, *Nature Communications 2016 7:1*, 2016, **7**, 1–8.

51. A. Leonard, A. Bertero, J. D. Powers, K. M. Beussman, S. Bhandari, M. Regnier, C. E. Murry and N. J. Sniadecki, *J Mol Cell Cardiol*, 2018, **118**, 147–158.

52. S. Bremner, A. J. Goldstein, T. Higashi and N. J. Sniadecki, *Methods in Molecular Biology*, 2022, **2485**, 87–97.

53. L. C. Martial, R. E. Aarnoutse, M. F. Schreuder, S. S. Henriet, R. J. M. Brüggemann and M. A. Joor, *PLoS One*, , DOI:10.1371/JOURNAL.PONE.0167433.

54. C. A. James, M. D. Barfield, K. F. Maass, S. R. Patel and M. D. Anderson, *Nat Med*, 2020, **26**, 1810.

55. S. M. Lofgren, A. B. Morrissey, C. C. Chevallier, A. I. Malabeja, S. Edmonds, B. Amos, D. J. Sifuna, L. von Seidlein, W. Schimana, W. S. Stevens, J. A. Bartlett and J. A. Crump, *AIDS*, 2009, **23**, 2459–2466.

56. K. Li, J. C. Naviaux, J. M. Monk, L. Wang and R. K. Naviaux, *Metabolites*, , DOI:10.3390/METABO10030082.

57. K. Malsagova, A. Kopylov, A. Stepanov, T. Butkova, A. Izotov and A. Kaysheva, *Diagnostics*, , DOI:10.3390/DIAGNOSTICS10040248.

58. M. D. Lim, *American Journal of Tropical Medicine and Hygiene*, 2018, **99**, 256–265.

59. T. M. Blicharz, P. Gong, B. M. Bunner, L. L. Chu, K. M. Leonard, J. A. Wakefield, R. E. Williams, M. Dadgar, C. A. Tagliabue, R. el Khaja, S. L. Marlin, R. Haghgooie, S. P. Davis, D. E. Chickering and H. Bernstein, *Nat Biomed Eng*, 2018, **2**, 151–157.

60. L. A. Matheson, T. T. Duong, A. M. Rosenberg and R. S. M. Yeung, *J Immunol Methods*, 2008, **339**, 82–89.

61. N. Duale, G. Brunborg, K. S. Ronningen, T. Briese, J. Aarem, K. K. Aas, P. Magnus, C. Stoltenberg, E. Susser and I. W. Lipkin, *BMC Res Notes*, , DOI:10.1186/1756-0500-5-510.

62. N. Duale, W. I. Lipkin, T. Briese, J. Aarem, K. S. Rønningen, K. K. Aas, P. Magnus, K. Harbak, E. Susser and G. Brunborg, *BMC Res. Notes*, 2014, **7**, 633.

63. A. Gautam, D. Donohue, A. Hoke, S. A. Miller, S. Srinivasan, B. Sowe, L. Detwiler, J. Lynch, M. Levangie, R. Hammamieh and M. Jett, *PLoS One*, , DOI:10.1371/JOURNAL.PONE.0225137.

64. L. Opitz, G. Salinas-Riester, M. Grade, K. Jung, P. Jo, G. Emons, B. M. Ghadimi, J. Gaedcke and T. Beißbarth, *BMC Med Genomics*, , DOI:10.1186/1755-8794-3-36.

65. A. T. Bender, B. P. Sullivan, L. Lillis and J. D. Posner, *Journal of Molecular Diagnostics*, 2020, **22**, 1030–1040.

66. A. J. Haack, F. Y. Lim, D. S. Kennedy, J. H. Day, K. N. Adams, J. J. Lee, E. Berthier and A. B. Theberge, *Anal Chem*, 2021, **93**, 13196–13203.

67. D. Chaussabel, *Semin Immunol*, 2015, **27**, 58–66.

68. L. G. Brown, A. J. Haack, D. S. Kennedy, K. N. Adams, J. E. Stolarczuk, M. G. Takezawa, E. Berthier, S. Thongpang, F. Y. Lim, D. Chaussabel, M. Garand and A. B. Theberge, *Front Digit Health*, 2022, **4**, 903153.

69. M. D. Hurteau, A. L. Westerling, C. Wiedinmyer and B. P. Bryant, *Environ Sci Technol*, 2014, **48**, 140203132416003.

70. J. R. Swiston, W. Davidson, S. Attridge, G. T. Li, M. Brauer and S. F. van Eeden, *European Respiratory Journal*, 2008, **32**, 129–138.

71. H. Jia, Y. Liu, D. Guo, W. He, L. Zhao and S. Xia, *Environ Toxicol*, 2021, **36**, 298–307.

72. K. Huttunen, T. Siponen, I. Salonen, T. Yli-Tuomi, M. Aurela, H. Dufva, R. Hillamo, E. Linkola, J. Pekkanen, A. Pennanen, A. Peters, R. O. Salonen, A. Schneider, P. Tiittanen, M. R. Hirvonen and T. Lanki, *Environ Res*, 2012, **116**, 44–51.

73. A. M. Hejl, O. Adetona, D. Diaz-Sanchez, J. D. Carter, A. A. Commodore, S. L. Rathbun and L. P. Naeher, *J Occup Environ Hyg*, 2013, **10**, 173–180.

74. G. Mu, M. Zhou, B. Wang, L. Cao, S. Yang, W. Qiu, X. Nie, Z. Ye, Y. Zhou and W. Chen, *Science of The Total Environment*, 2021, **755**, 142522.

75. A. M. Parenteau, N. v. Alen, J. La, A. T. Luck, D. J. Teichrow, E. M. Daang, A. T. Nissen, L. B. K. Deer and C. E. Hostinar, *New Dir Child Adolesc Dev*, 2022, **2022**, 125–154.

Chapter 2: Layer-by-Layer Fabrication of 3D Hydrogel Structures Using Open Microfluidics

Reproduced in part from U. N. Lee, J. H. Day,* A. J. Haack,* R. C. Bretherton, W. Lu, C. A. DeForest,‡ A. B. Theberge,‡ and E. Berthier,‡ "Layer-by-layer fabrication of 3D hydrogel structures using open microfluidics." Lab on a Chip, 2020,* ***20****, 525–536.*
**Equal contribution*
‡Co-corresponding authors

UNL, JHD, AJH, and RCB conducted the experiments, WL collected preliminary data, CAD, ABT, and EB supervised and UNL, JHD, AJH, ABT, and EB interpreted the results.

Abstract: Patterned deposition and 3D fabrication techniques have enabled the use of hydrogels for a number of applications including microfluidics, sensors, separations, and tissue engineering in which form fits function. Devices such as reconfigurable microvalves or implantable tissues have been created using lithography or casting techniques. Here, we present a novel open microfluidic patterning method that utilizes surface tension forces to form hydrogel layers on top of each other, in a patterned 3D structure. We use a patterning device to form a temporary open microfluidic channel on an existing gel layer, allowing the controlled flow of unpolymerized gel in device-regions. After layer gelation and device removal, the process can be repeated iteratively to create multi-layered 3D structures. The use of open-microfluidic and surface tension-based methods to define the shape of each individual layer enables patterning to be performed with a simple pipette and with minimal dead-volume. Our method is compatible with unmodified (native) biological hydrogels, and other non-biological materials with precursor fluid properties compatible with capillary flow. With our open-microfluidic layer-by-layer fabrication method, we demonstrate the capability to build agarose, type I collagen, and polymer-peptide 3D structures featuring asymmetric designs, multiple components, overhanging features, and cell laden regions.

2.1 Introduction

Hydrogels are configurable and functional materials whose 3D geometries can be patterned to obtain desired functions ranging from mechanical responses (e.g., microfluidic valves, pumps) to organotypic functions (e.g., biological models, implantable materials). Many of these applications have simple geometric requirements, such integration in microfluidic devices as valves, [1, 2] for encapsulating

colorimetric indicators, [3] or for chemical separation of desired analytes. [4, 5] For cell culture applications, patterned hydrogels are used for encapsulating cells in a controlled position relative to additional cell types, microchannels, or extracellular matrix components. [6-14] Reliable and low-entrance barrier solutions to these applications would have the potential of widespread adoption in biology, fluidics, and engineering labs that seek prototyping solutions. Here, we present a method for multilayer hydrogel patterning in three dimensions that uses a simple setup: patterning devices are positioned above a substrate to guide the flow of hydrogel precursors using surface tension forces. Hydrogel materials are delivered with standard pipettes, minimizing dead volume, a key consideration when patterning expensive hydrogels and/or including rare cell types.

There are many established methods for hydrogel patterning, each with their own set of benefits and limitations. Researchers may choose one method based on unique application considerations. Amongst these methods, photopolymerization techniques are robust and offer resolution on the order of microns, [1, 6, 10, 12, 13, 15-19] however photo-initiators have been shown to cause cellular damage, [20, 21] and the necessity for chemical functionalization of the gel precludes the use of native (unmodified) gels. Other broadly used hydrogel patterning methods include inkjet [22-24] and microextrusion [25-29] printing. In these methods, the hydrogel is jetted through a nozzle that exposes any cells encapsulated within the hydrogel to shear stress, which can mechanically damage the cells and limit the types of cells that can be patterned. [31, 32] Inkjet and extrusion-based printing methods can also require optimization depending on the viscosity and type of gel used. Many of these hydrogel patterning techniques can require large volumes of fluid to fill vats, fluidic channels, or tubing used in typical gel 3D printing setups, limiting the use of rare cell types or expensive gels. Casting hydrogels using a fabricated negative mold provides an alternative approach, but the complexity of the gel structures obtainable is limited due to demolding considerations. [7, 33-35] A hydrogel patterning method that does not rely on photoinitiators, external pressure, tubing, or reservoirs of gel could reduce material waste and alleviate some of the stresses that can affect cell health, rendering it well suited for applications that require fragile, primary, or rare cell types.

In this chapter, we present a novel layer-by-layer patterning method that uses open microfluidic principles and surface tension driven flow to deposit and sequentially form hydrogel layers in user-defined patterns, each delivered directly using a pipette. To form each hydrogel layer in a controlled shape, we use a 'patterning device,' which is either a plastic physical 'rail' or a hydrophilic track delineated on a hydrophobic flat surface; both enable the pre-gel solution to flow via capillary action without external pressure and constrain the pre-gel solution under the rail footprint via capillary pinning. [36, 37] The patterning device is placed above an existing hydrogel layer at a designed height. Most of the structures presented in this work were made with layer heights between 100-500 μm, although the method is not limited to heights within this range; demonstrations of the range of layer heights achieved are included in Figure A1-4. The gap between the patterning device and the existing hydrogel layer forms an open microfluidic 'channel' in which liquid pre-gel solution can flow, where the channel 'ceiling' is the patterning device, the 'floor' is the previous gel layer, and the 'sides' are free air-liquid interfaces (Figure 2.1). The patterning device can be removed once the gel layer has formed, and another patterning device can be applied to pattern the next layer, providing the ability to build three-dimensional structures layer-by-layer. This work builds on prior publications demonstrating the use of rails to pattern a single hydrogel layer to partition a well plate for coculture [37-40] where due to the design constraints of the previous rail devices, the patterning device could not be removed once the hydrogel was polymerized, and thus a three dimensional hydrogel structure could not be fabricated. Here, we built multilayer hydrogel structures from native and engineered hydrogels which included unsupported overhanging features, objects comprising multiple materials and components both within a layer and across layers, asymmetric designs, and a cell-laden gel architecture. We also demonstrate the capability to spatially control the initial structure of engineered enzymatically degradable dynamic poly(ethylene glycol) (PEG)-based hydrogels. The ability to establish a full layer in a single dispensing step is distinct from extrusion or inkjet patterning methods, which require multiple passes of material deposition for a single layer. Further, in contrast to methods that use photopolymerizable gels and light as a means of patterning hydrogels, which then require washing away

of unused, pre-gel solution, [1, 6, 16, 17] we limit waste; all of the pre-gel solution that is dispensed is polymerized and incorporated as part of the patterned material.

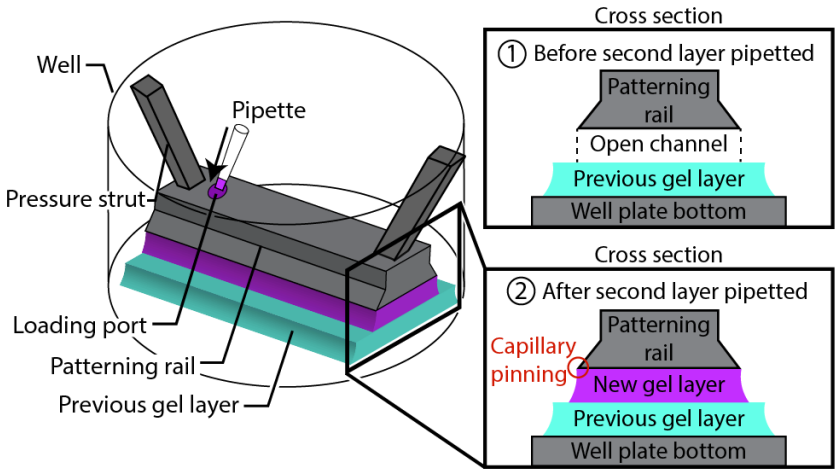

Figure 2.1. Schematic showing the mechanism of layer-by-layer gel patterning using open microfluidics. An open channel is created above an existing gel layer using a rail-based patterning device.

2.2 Open microfluidic flow principles that drive layer-by-layer patterning

Our layer-by-layer patterning method uses open microfluidic principles to create temporary open channels on a plastic or existing hydrogel surface allowing pre-gel solution to flow in a spatially controlled area defined by a patterning rail or hydrophilic track (Figure 2.1). The gel can then be polymerized to create a patterned layer of hydrogel tens to hundreds of micrometers thick. The input of gel is powered by spontaneous capillary flow (SCF), which describes the surface tension-based flow of fluids in channel geometries that can have any number of open-air interfaces along the fluid path. [36, 40] The geometric control of the gel layer is obtained by abrupt changes in geometry (in the case of a patterning rail) or hydrophilicity (in the case of hydrophilic tracks) which prevent fluids from flowing past these capillary pinning points. Together, the principles of SCF and capillary pinning enable the creation of a patterned gel layer with simple laboratory equipment (e.g., pipettes) in existing laboratory platforms (e.g., well plates) without requiring actuators, electronics, or pressure sources.

Figure 2.2 shows a specific embodiment of the patterning technique where a patterning rail is used to define the outline of a virtual open microfluidic channel. The patterning rail is placed at the location where

the gel will be patterned and sits tens to hundreds of micrometers over the surface of the material below. The geometrical shape of the patterning area is designed to enable the spontaneous capillary flow of pre-gel solution throughout the open channel made between the patterning rail and the surface of the material below; capillary pinning enables the pre-gel solution to remain in the defined pattern. The patterning devices can be fabricated in hard plastic, such as resin that is 3D printed from a stereolithography 3D printer or polystyrene (PS) sheets that are CNC milled. The patterning device shown in Figure 2.2 fits inside of a 6-well plate, but the method is not limited to a 6-well plate form. The device sits flush to the floor of the well plate with spacers to control the height of the gel layer being formed (dotted red line in Figure 2.2Ai and iv, Figure A8, Figure A9) and pressure struts to maintain concentric alignment of the rail within the well.

In this chapter, we patterned 100-500 μm thick gel layers; numerical simulations of SCF suggest thinner layers (reduced *h* in Eq. 1) are achievable and, in fact, make it easier to satisfy the condition for SCF in our system which is defined by:

$$\frac{h}{w} < \frac{cos\theta_1 + cos\theta_2}{2} \qquad \text{(Eq 1)}$$

Where *h* is the height of the patterned layer (defined by the distance between the patterning area of the rail and the underlying substrate), *w* is the width of the rail perpendicular to the direction of flow, θ_1 is the contact angle of the hydrogel on the patterning device, and θ_2 is the contact angle of the hydrogel on the underlying substrate (conventionally equal to zero when flowing hydrogel over an existing hydrogel layer of the same type). To note, viscosity does not play a role in the condition for flow but does play a role in the dynamics of the flow. Higher viscosity pre-gel solutions will flow slower in the generation of a layer, ultimately extending fabrication times. A derivation of Eq. 1 from the generalized Cassie equation is provided in the Appendix A.

When pre-gel solution is loaded into a patterning setup, it fills the 'virtual channel', and remains suspended between the patterning device and the underlying substrate until a polymerization trigger is

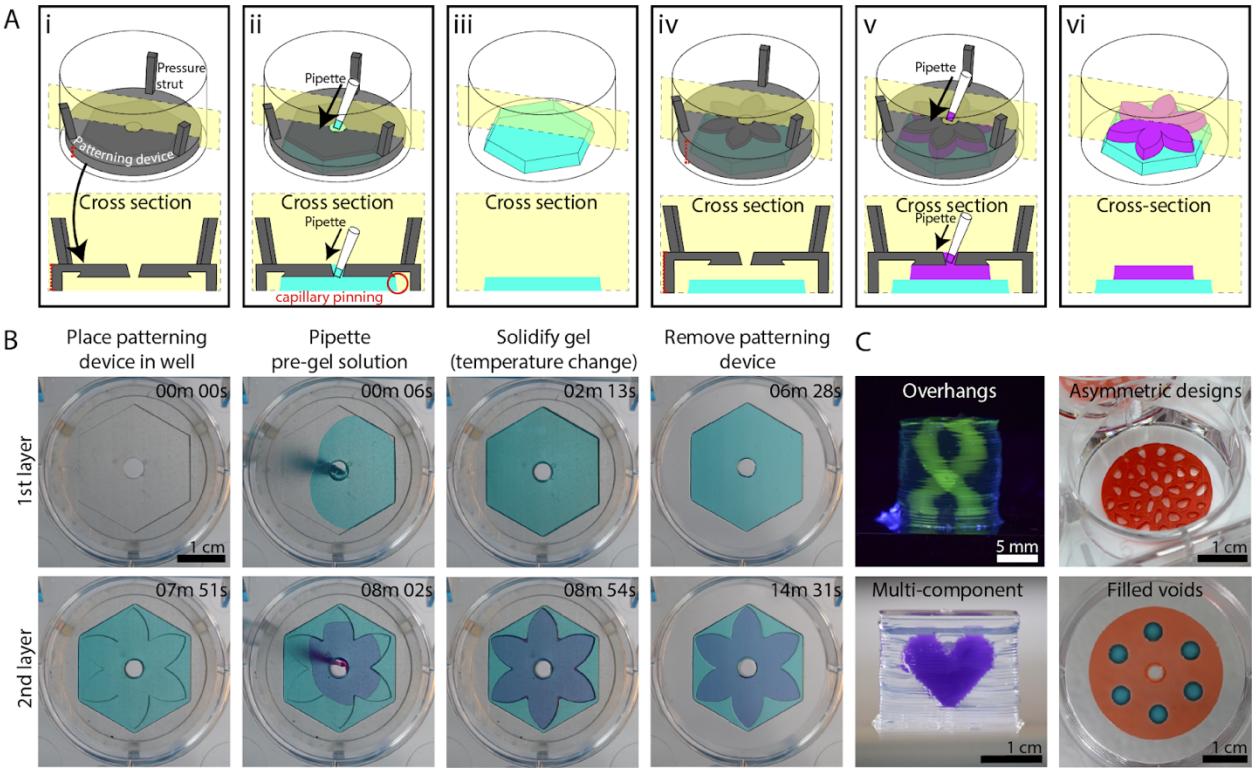

Figure 2.2. Rail-based open microfluidic layered patterning of unmodified hydrogels. (A) Schematic of patterning two layers of gel. (Ai) Patterning device (rail) is placed in a 6-well plate; the patterning region sits 250 µm above the well plate surface. Red dotted line on the left indicates portion of patterning device that is adjusted to determine the thickness of the gel layer. (Aii) Pre-gel solution is pipetted into the pipette port. (Aiii) Patterning device is removed after the pre-gel solution is solidified. (Aiv-Avi) Second layer is patterned using the same steps for the first layer. Red dotted line on the left in Aiv indicates distance between the well plate and the rail after an initial layer of gel is patterned. Note that the dotted line is longer than the red line seen in Ai. Cross-sections of patterning devices show capillary pinning (red circle) and 45° angle around the edges of the device to prevent capillary rise along the vertical face of the patterning device. A magnified schematic is included in Figure A8; an engineering drawing of the hexagon and petal devices is included in Figure A9. (B) Images of the patterning process for 1.5% low gelling temperature agarose dyed for visualization with teal and magenta India ink. Image was taken from the underside of a 6-well plate. (C) Various agarose structures built using rail-based open microfluidics to showcase the power of the method. Cylindrical structure with hollow unsupported winding tubes (double helix) (top, left), asymmetric geometries patterned in a well plate (top, right), a multicomponent structure (bottom, left), and a single layer of gel with islands of voids filled with a second gel in a single pipetting step (bottom, right).

introduced. Although temperature change was used for polymerization in this work, the ability to polymerize a layer after it has been patterned makes it possible to build multilayered structures of any hydrogel whose pre-gel solution can meet the condition for SCF. After a single layer of pre-gel solution is patterned and solidified (Figure 2.2Ai and 2.2Aii), the patterning device is removed (Figure 2.2Aiii), and a new patterning device is placed over the gel layer to define a new area for the next layer of gel (Figure

2.2Aiv). The patterning process is repeated for each additional layer (Figure 2.2Av and 2.2Avi). With this method we can deposit an entire layer in one pipetting step, as opposed to alternative nozzle-based 3D patterning methods which require multiple passes of material deposition for a single layer.

It is possible to pattern a pre-gel solution on top of an existing hydrogel layer using our method because capillary pinning still occurs at the junction of the edge of the patterning area and the previous hydrogel layer, maintaining a defined pattern (Figure 2.2B). However, gel overflow is observed for certain features (corresponding to Figure 2.2B), overflow of dispensed fluid at the edges of the 'flower' patterning device occurs because the surface tension of the pre-gel solution, which tends to favor a rounded fluid front, overcomes pinning at the acute internal angles of the patterning device. Due to the manual nature of our method in its current form, applications requiring only a few layers are more suitable for immediate use of the technology. However, we also present several structures with multiple layers (>30) to demonstrate the ability of our layer-by-layer fabrication method to create three-dimensional structures. Figure 2.2C highlights some of these features we achieved with our layered patterning method which include unsupported overhangs, asymmetric geometries, multicomponent structures and cell-laden patterns. These structures are described in more detail in the subsequent figures.

2.3 Patterning multicomponent structures with layer by layer open microfluidic patterning

The ability to pattern multiple materials in a single structure is of great interest for a variety of applications ranging from creating regions of varying material properties for studying molecular transport, [43, 44] to controlling the gel porosity in specific regions of a microfluidic device for use in chemical separation assays. [4] Patterning multiple materials is also of great importance to organotypic modelling. The cellular environment in biological tissue is heterogeneous in nature, and recapitulating this environment requires spatial control of cells in relation to multicomponent hydrogels and extracellular matrix materials. Our open microfluidic layered patterning method presents a new approach to building multicomponent structures. Figure 2.3A shows how different materials can be introduced at every layer to create a structure with differential material properties in the Z-direction. In Figure 2.3A, an agarose structure was erected

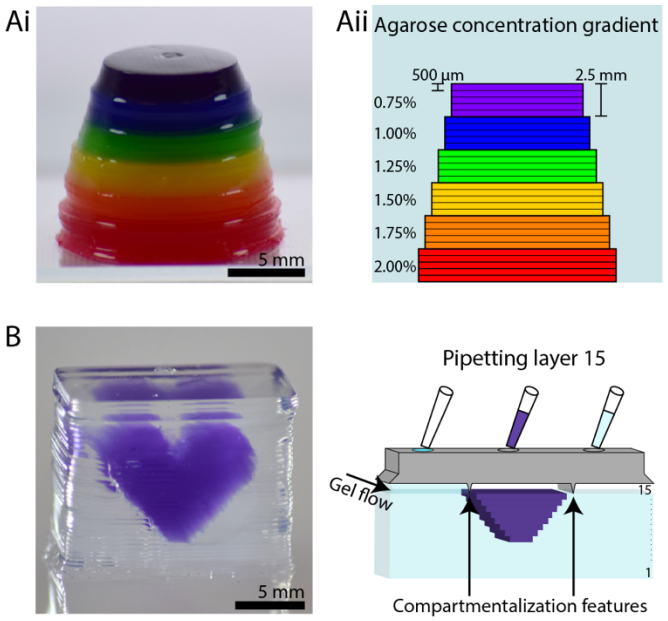

Figure 2.3. Constructing heterogeneous structures. (A) Structure with multiple agarose concentrations. (Ai) Photo of agarose structure (dyed for visualization, with each color representing a different concentration) in ascending layers. Layers are 500 µm thick, and each color contains 5 layers. (Aii) Cross-sectional schematic showing the agarose concentrations in each layer. (B) Purple agarose heart inside a colorless agarose cube demonstrating the ability to pattern materials of different composition *within* a layer (left). Schematic of patterning layer 15 of the 34-layered structure with compartmentalization features to segregate the different gels (right). Layers are 500 µm thick.

beginning with a concentration of 2% wt/v and decreasing 0.25% wt/v every five layers to a final concentration of 0.75% wt/v. Each concentration is dyed a different color for visualization. The resulting structure has a stepwise concentration gradient in the Z-direction. The agarose concentrations were chosen here as a proof of concept to demonstrate the ability to pattern different compositions across layers. These concentrations also fall within the range of relevant concentrations used for transport models of biological systems such as the brain extracellular space; our layered patterning method has the potential to be extended for brain extracellular matrix modeling application in future work. [44, 45]

The ability to pattern multiple materials *within the same layer* is essential to creating a structure with spatial organization in all three dimensions. Work by others to enable single layer printing of multiple gels through a multi-nozzle 3D printing system has demonstrated the interest of this capability in 3D bioprinting. [29, 46] To demonstrate the ability to pattern materials with different compositions within a layer using our method, we built a purple agarose heart within a colorless agarose cube (Figure 2.3B, left). In this case, we

added a simple ridge to the patterning rail to segregate the regions of different materials (purple and colorless agarose). Thus, different solutions agarose of agarose dyed different colors were allowed to flow within each layer in a defined pattern (Figure 2.3B, right).

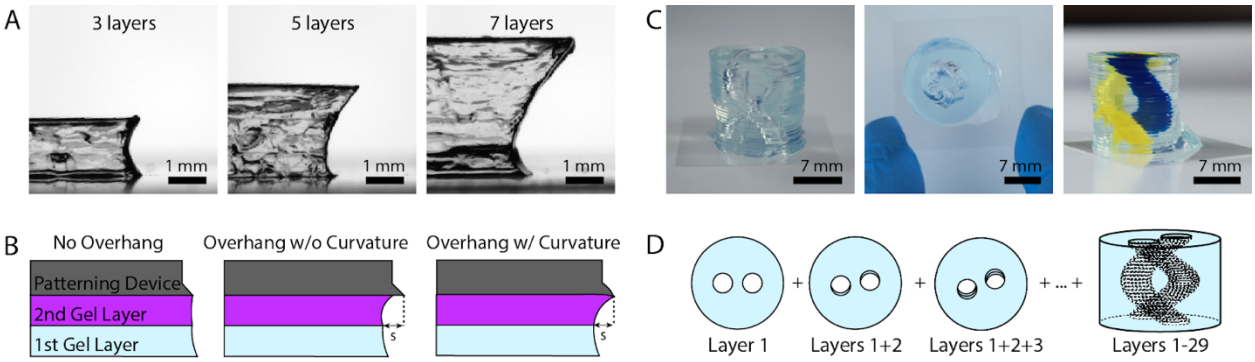

Figure 2.4. Rail-based open microfluidic layered patterning of overhanging features. (A) Imaging of a cross section of an overhanging agarose structure at three different points of production, 3 layers (left), 5 layers (center) and 7 layers (right). (B) Schematic for rail design of overhanging features showing no overhang, an overhang without curvature and an overhang with downward curvature; the latter rail design was used to print the structures shown in A and C. (C) Images of cylindrical structure with hollow unsupported winding tubes (double helix) made from agarose, showing side view (left), top down image (center), and side view where tubes are filled with yellow and blue India ink dyes for visualization (right). Full description of design in Appendix A and Figure A10. (D) Schematic showing the process for building the double helix structure, where the blue color represents the patterned agarose. Each layer is rotated about the center from the previous layer, forming a hollow helix within a cylinder of agarose.

2.4 Generation of unsupported overhanging features with open microfluidics

A design challenge for patterning three-dimensional hydrogel structures is building unsupported features (i.e., features that cantilever into air rather than building on base material underneath). Other systems for patterning soft materials have utilized sacrificial material as a support, which is removed in a post-processing step either physically or chemically. [23, 29, 47] The structural integrity of the desired product must be maintained after the supports are removed, which restricts the types of materials that can be used. Using our method, a dissolvable sacrificial gel approach could be employed; we also show that it is possible to create overhanging, unsupported structures without the use of sacrificial material by incrementally offsetting the patterning device from the edge of the previous layer such that each layer extends past the limits of the previous layer (Figure 2.4A). To exemplify this concept, the schematic in Figure 2.4B illustrates a rail design without an overhang (left) and with an overhang (center and right).

We found the length of overhang achievable was improved by the addition of a downward curvature to the edge of the patterning device to allow for favorable flow over the edge of the previous gel layer (Figure 2.4B, right). Without the added curvature, the bottom of the fluid front pins to the edge of the previous layer as expected, but the top of the advancing pre-gel solution does not continue along the patterning device (Figure 2.4B, center). The curvature decreases the relative ratio of the air-liquid interface to the patterning device-liquid interface; minimizing this ratio is favorable for SCF. [36] Thus, the agarose fluid front continues along the surface of the patterning device, increasing the overhang capacity. Each patterning device has a different radius of curvature based on the curvature of the previous patterning device. Detailed descriptions of how these dimensions were determined are included in the Appendix A and Figure A10, and the dimensions are given in Table A1. To fully demonstrate the capabilities of our method to produce geometries with overhanging features, we built an agarose cylinder with hollow winding tubes in the shape of a double helix (Figure 2.4C and 2.4D). The helix consists of 30 layers, each 500 μm thick, and has a total rotation of 270 degrees.

Previously, other fabrication methods have utilized a sacrificial material to create void spaces and channels through a three-dimensional hydrogel structure [29, 38] or have employed a casting method to create fluidic channels. [7] Furthermore, laser photoablation can be used to create microchannels through hydrogels with high resolution, [48] and recently multiphoton lithography has been used to photodegrade microchannels within cell-laden PEG-based hydrogels. [15] The approach we have taken here and the helix geometry proof of concept structure demonstrates the broader capacity to create gels with three-dimensional tubing and void spaces, thereby opening up the possibility of creating three-dimensional fluidic channels spanning multiple planes through a hydrogel structure without reliance on a sacrificial material or post-fabrication step.

2.5 Integrated fluidic channels within patterning device

We also demonstrate that it is possible to add open microfluidic functionality to the top of the patterning device, where the flow is also driven by capillary action. [49] This capability can be utilized as

another method by which multiple materials can be deposited in a single layer (Figure 2.5). We used open channels to deliver blue colored agarose to the voids in the red colored agarose layer below, which enables a single pipetting step to fill all six voids (Figure 2.5B).

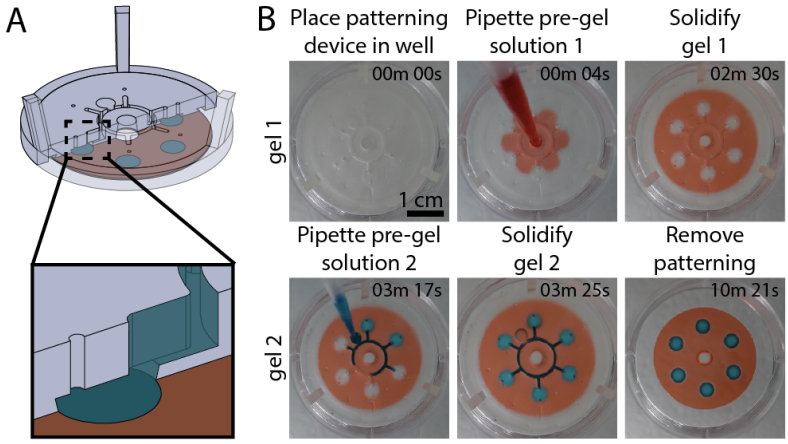

Figure 2.5. Integrated fluidic channels in patterning device for depositing second material in a layer. (A) Cross-sectional schematic representation of 'void-filling' patterning device with underlying layer. (B) Video stills of patterning red colored agarose (250 μm thick) and filling voids with blue colored agarose (750 μm thick).

2.6 Open microfluidic patterning of cell-laden type I collagen

Agarose is a useful hydrogel for characterizing the possible geometries and limitations of our patterning method as its structural properties make it ideal for withstanding a three-dimensional structure. Further there are many applications in which agarose patterning is useful, such as spatially defined microbial culture. [50] However, agarose does not contain extracellular matrix components and does not facilitate mammalian cell adhesion. Further, layer delamination may occur because agarose lacks intrinsic cross-linking characteristics, and the temperature dependent gelation of agarose can affect its flow depending on the starting temperature of the precursor solution. Given these limitations, we also characterized our method for use with other, cell compatible materials including unmodified type I collagen and engineered enzymatically degradable PEG-based hydrogels.

Many materials such as collagen do not have the mechanical properties necessary to create free-standing 3D structures without the use of a second support material. To overcome this challenge, we utilized

the ability to pattern a single layer with multiple materials to create an agarose 'support' structure for unmodified type I collagen (7.5 mg/mL). Type I collagen was chosen because it is abundant in biological systems. Here, we demonstrate an alternative method for patterning layers of commercially available concentrations of unmodified collagen (Figure 2.6). Briefly, we patterned an agarose border on each layer, which was subsequently filled with cell-free collagen. Cell-laden collagen was then patterned over the newly established layer of collagen (Figure A6). Figure 2.6 shows 130 confocal image stacks stitched together of Calcein AM stained human fetal lung fibroblasts in a type I collagen structure. Cells in this structure were 87% viable, quantified using live/dead (Calcein AM/ethidium homodimer) staining (Figure A5). The '3' and 'D' patterns represent two cell populations that were printed on two different layers, each 100 μm thick and separated by a 200 μm thick cell-free layer. A workflow schematic of the layer-by-layer collagen patterning process is shown in Figure A6.

2.7 Open microfluidic patterning of novel engineered hydrogels for dynamic 4D culture

Stimulus-responsive biomaterials, often referred to as "4D biomaterials", add a temporal dimension of control to a 3D material. [51, 52] Through well-defined molecular topology, these dynamic hydrogels can be chemically or physically modulated on demand in response to precise combination of environmental inputs (e.g., light, small molecules, cell-secreted enzymes, exogenous enzymes) following Boolean logic. [15, 53-56] Here, we introduce and utilize novel 4D peptide-polymer hydrogels that can be enzymatically degraded with cell-secreted matrix metalloproteases (MMPs) and/or exogenously added sortase (SrtA). Transpeptidation by SrtA has been demonstrated as a rapid, bio-orthogonal means of encoding dynamic behavior into gels but offers no spatial control over degradation. [57, 58] Here, we used our 3D patterning method to create a stimulus-responsive cell-laden PEG-based hydrogel multimaterial structure featuring different enzymatically degradable crosslinkers (Figure 2.7). Since these responsive PEG-peptide materials are formed through spontaneous reaction of two components in water (here, strain-promoted azide-alkyne cycloaddition), [41] their formation cannot readily be patterned using conventional techniques (e.g., extrusion, photopolymerization), which has placed limitations on their usage in tissue engineering.

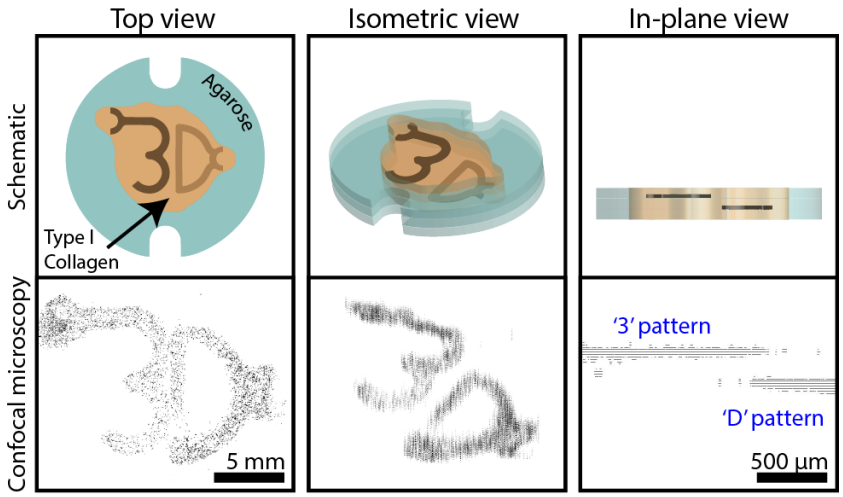

Figure 2.6. Schematics and confocal images of human fetal lung fibroblasts in a type I collagen structure. Cells were stained with Calcein AM (shown in black). The top view comprises 130 fields of view (which each contain 27 Z-stacked images) stitched together. Cells that make up the "3" and "D" are each printed in separate 100 µm thick collagen layers that are separated from each other by a 200 µm thick cell-free collagen layer. Z-step value was increased tenfold in isometric view for visualization purposes. Original confocal image file is included in Figure A5. Schematic of the workflow used to achieve this structure is shown in Figure A6; note: the additional features on the top left of the "3" and the right of the "D" were an intentional part of the design, used as loading ports for the pre-gel solution.

To demonstrate 3D fabrication of cell-laden multimaterial structures and their spatially coded responsiveness, we generated a structure whose inner cavity could undergo triggered degradation (Figure 2.7A). To achieve this geometry, the structure was fabricated with a PEG-based gel with two different crosslinkers; the crosslinker in the inner cavity was degradable by SrtA OR MMP, while the crosslinker in the outer structure could only be degraded by MMPs. The total height of the structure was 0.5 mm, allowing for diffusion of nutrients through the gel when the final structure was submerged in media after fabrication. A schematic of the fabrication process and dimensions can be found in Figure A11. The inner core height was designed as 100 µm with a width of either 1.0 mm or 0.5 mm. Confocal images in Figure 2.7 and Figure A12 are of the larger (1.0 mm designed width of degradable cavity) geometry, and Figure A13 shows confocal images of both geometries. Fluorescent HS5 cells were encapsulated in the gel multimaterial, with cells in the outer MMP-degradable regions expressing mCherry and those in the SrtA- OR MMP-degradable inner cavity expressing eGFP. Figure 2.7A shows the timeline and schematic of the fabrication; further details are included in the Experimental section. Briefly, cells were cultured in the patterned gel for

five days before SrtA treatment. At that point, the gel was treated with SrtA to facilitate degradation. The structure was incubated in DMEM media for an additional five days after the degradation before imaging. Confocal images before SrtA treatment (day 5) show the core of the structure intact with eGFP-expressing cells (green) distributed throughout the gel core and those expressing mCherry in the surrounding regions (Figure 2.7Ci). After triggered degradation of the inner cavity and extended culture (day 10), the resulting structure is a fully enclosed void space (Figure 2.7C and Figure A12), with released eGFP^{+}-cells settling to the bottom of the degraded core to form a monolayer (Figure 2.7Cii). Owing to the MMP-degradability of both the inner and outer layers, cells can actively remodel and spread within the hydrogel materials. As demonstrated, our generalizable patterning technique adds another dimension of control to responsive biomaterials; we view this as tremendously valuable for gel types that are incompatible with traditional additive manufacturing techniques, including the many that form through spontaneous reactions. [59]

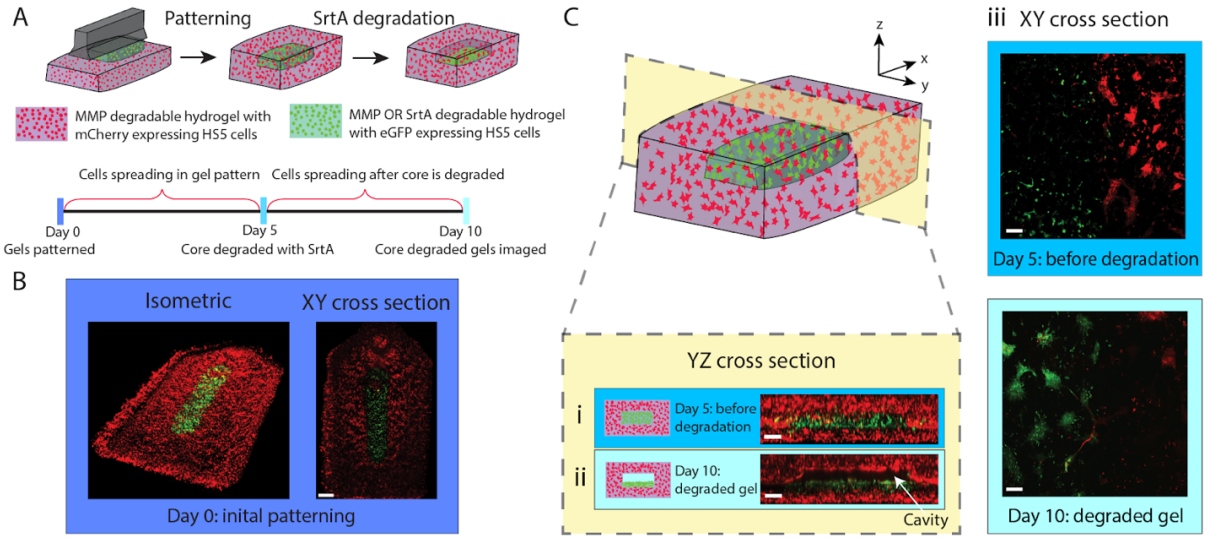

Figure 2.7. Layer-by-layer patterning of enzymatically degradable PEG-based hydrogel structures. (A) Timeline of degradation experiment, highlighting SrtA treatment on Day 5 that triggers degradation of the eGFP^{+}-cell-containing core. (B) Confocal images acquired immediately after multimaterial gel patterning. eGFP-expressing HS5 cells (green) were encapsulated in the MMP- OR SrtA-degradable core, mCherry-expressing cells (red) are in the surrounding MMP-only degradable hydrogel. Scale bar is 1 mm. (C) YZ cross-sectional view of gels (Ci) on Day 5 immediately preceding SrtA treatment, and (Cii) after 10 days of culture (5 days post core degradation), where released eGFP^{+}-cells settle to the bottom of the empty cavity to form a monolayer on the intact gel layer below. Scale bars are 200 µm. (Ciii) Confocal images (XY cross sections) at the interface between the bottom and middle layers on day 5 (prior to SrtA treatment) and day 10. eGFP^{+}-cells exhibit a 3D spread morphology on day 5, but transition to a 2D monolayer after release. Scale bars are 200 µm.

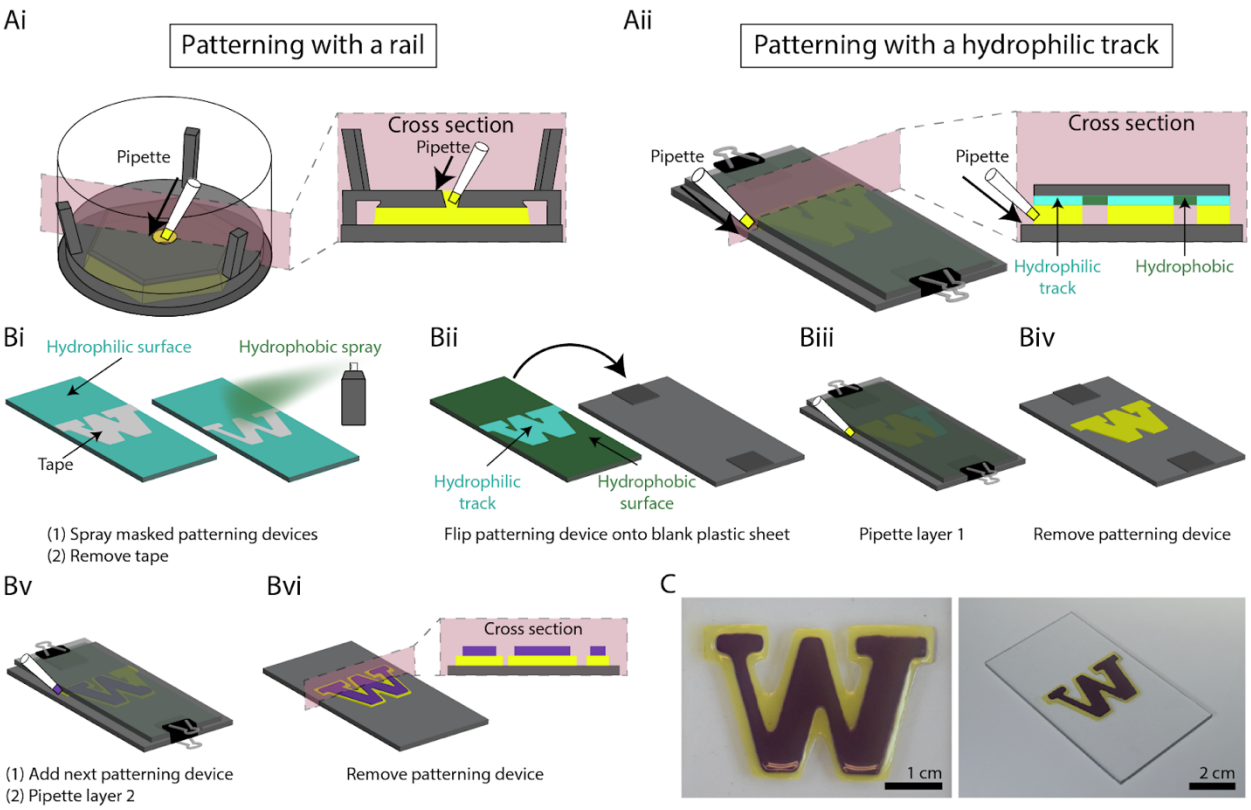

Figure 2.8. Layer-by-layer hydrogel patterning without a rail. (A) Overview of two patterning processes contrasting (Ai) patterning with a rail and (Aii) patterning with hydrophilic tracks. (Bi) Plasma treated polystyrene (PS) sheets were masked with tape, and a hydrophobic spray was applied. After the hydrophobic layer had set, the tape was removed. (Bii) The hydrophobic side of the PS sheet placed face down onto a clean, plasma treated PS sheet with stacked coverslips as spacers to create a gap between the two sheets. (Biii) The patterning device was secured to the spacers and bottom substrate with binder clips and the pre-gel solution was pipetted in the gap between the patterning device and bottom substrate at both sides of the 'W'. (Biv) The patterning device was removed after the gel solidified. (Bv) Additional coverslips were stacked on the existing spacers to create a larger gap for the second layer, and the second patterning device was aligned by eye, placed and secured with binder clips. The second layer of pre-gel solution was then pipetted in the same way. (Bvi) The patterning device was removed to reveal the 2-layered hydrogel structure. The thickness of each layer was 500 µm (C) Top view (left) and isometric (right) photo of two-layered agarose 'W'.

2.8 Layer by layer patterning with hydrophilic tracks

For each structure presented in Figures 2.2-2.7, we used a separate patterning rail (fabricated by 3D printing or CNC milling) for each layer (Figure 2.8Ai). While this method is convenient for development of our method, fluid patterning by SCF can also be achieved without a physical rail by using a flat surface

with patterned hydrophilic and hydrophobic regions to guide fluid flow by SCF into a desired pattern; the fluid flows along the hydrophilic tracks and pins at the hydrophilic/hydrophobic boundary (Figure 2.8Aii).

This concept builds on past work where localized hydrophilic/hydrophobic patterning on a single flat surface was used to constrain fluids to a hydrophilic pattern. [60, 61] Here, we extended this patterning concept to create a two-layered hydrogel structure, showing that the hydrophilic/hydrophobic patterning template can be removed after each hydrogel layer is created to iteratively build up multiple layers of hydrogel structures (Figure 2.8B). In the present embodiment, we plasma treated a polystyrene sheet and masked the area we wanted to preserve as hydrophilic with tape (i.e., the "W" shape shown in Figure 2.8Bi). A commercially available hydrophobic treatment spray was applied to create a hydrophobic background. The tape was then removed after the hydrophobic treatment, revealing a hydrophilic patterning region surrounded by a hydrophobic background. We built a two-layer hydrogel (agarose) "W" structure on a polystyrene base substrate. Using stacked, glass coverslips as spacers above the polystyrene base substrate, we created a 500 μm gap between the base substrate and the hydrophilic/hydrophobic patterning surface. The pre-gel solution flowed in this gap via SCF, as previously described, pinned at the interface between the hydrophilic and hydrophobic region creating the "W" pattern set by the hydrophilic region (Figure 2.8B-C). This result demonstrates that our open microfluidic layer-by-layer method can be implemented without a physical rail, opening up the potential for future embodiments in which the hydrophilic/hydrophobic regions are patterned via reversible or actuatable approaches.

2.9 Conclusion

A novel open microfluidic method for layer-by-layer patterning of 3D hydrogel objects has been demonstrated. Our method uses fundamentally different principles—surface tension forces and open microfluidics—from existing methods to pattern hydrogel structures. Hydrogel waste is minimized in our layer-by-layer patterning method because it uses simple pipettes (with no dead volume) rather than requiring large vats of material or dispensing containers common in some hydrogel 3D printing methods,

opening up the potential to use expensive hydrogels, rare cells such as primary patient samples, or precious reagents in small volume, a benefit of microfluidics.

We demonstrated the compatibility of our method with three materials: agarose, collagen, and PEG-based engineered hydrogels. Though each material type was amenable to 3D-patterned deposition, it is important to note that different gel precursors and patterned geometries have their own set of limitations and may require device optimization to achieve a desired structure. We fabricated structures that comprised representative features—specifically features that are enabled by additive manufacturing. In terms of feature geometry, we specifically found limitations in flowing around sharp corners as demonstrated in the roundedness of the acute angle of the "W" in Figure 2.8. Filling out sharp corners is also challenging such as the corner of a square, particularly at higher layer heights (Figure A1).

Complementing our efforts to define gel geometry with a physical rail, we have demonstrated that similar multilayer structures can be generated using patterned hydrophilic/hydrophobic surface coatings. Our hydrogel patterning method, used with surface chemistries that allow for rapid reversible patterning of hydrophilic and hydrophobic regions, could be amenable to rapid automation. Further improvements in processing time could be achieved through reaction conditions (e.g., temperature) optimized for specific gelation chemistries. Importantly, using the embodiment shown in the present chapter, we demonstrated layered patterning of cell-laden structures using standard cell culture materials and procedures without subjecting the fluid to external pressure, suggesting that this method has the potential to be extended for use with other cell types. Our capacity to control the location of different gel materials within and between layers suggests the possibility to create 3D organoid models by directing the patterning of cell types and culture materials in 3D space. Building open microfluidic channels directly into the patterning device (Figure 2.5) can enable efficient delivery of reagents, cells, or other components into void spaces with a single dispensing step. Moreover, as demonstrated, our method can be used to create overhanging structures and hollow tubes, extending the capability of adding fluidics (e.g., channels, voids) throughout the gel itself, thus opening up possibilities for complex three-dimensional models and systems. Finally, we demonstrated the capability to pattern engineered dynamic hydrogels that could not be extruded or photopolymerized,

enabling the 3D spatial control of multimaterial structures that respond dynamically to their environment, yielding a new breed of 4D functional materials.

2.10 Materials and methods

Patterning device design and fabrication (Figures 2.2-2.6): Patterning devices were designed in Solidworks 2017 and 3D printed out of clear resin (RS-F2-GPCL-04) using a Form 2 stereolithography 3D printer (Formlabs) (Figures 2.2-2.6) or milled (Figure 2.6) on a computer numerical control (CNC) mill (PCNC770, Tormach). The patterning devices were sonicated in isopropyl alcohol (IPA) for 10 minutes and again in clean IPA for 5 minutes to remove excess uncured resin. The devices were dried with compressed air and cured under a 395-405 nm 20W UV lamp (Quans) for 1 hour.

Plasma treating patterning devices (Figures 2.2-2.7): The patterning devices were plasma treated for increased wettability using a Zepto plasma treater (Diener Electronic). The chamber was pumped down to a pressure of 0.20 mbar, gas (free air) was supplied (4 min, 0.25 mbar), and power enabled (2 min, 200 W).

Agarose gel composition: Low gelling temperature agarose (MilliporeSigma) was dissolved in deionized water to a concentration of 15 mg/mL and dyed for visual aid with food dye (Spice Supreme), fluorescein labeled dextran (70,000 MW, Invitrogen), or India ink (Dr. Ph Martin's). All agarose structures used 1.5% wt/v gel except for the multicomponent structure in Figure 2.3A.

Fabrication of overhanging structures (Figure 2.4): For the seven-layer overhang structure, each layer height was 500 μm. Layers 2 and 3 were designed to be 239.9 μm of overhang, whereas the following layers were designed to be 479 μm of overhang (*s* in Figure 2.2B). A schematic of the patterning device design and detailed dimensions can be found in Appendix A.

Fabrication of hollow double helix (Figure 2.4): Using the patterning device in a 6-well plate, each layer was allowed to set at room temperature for approximately 10-20 minutes prior to removal of the patterning rail. Each helix was constructed over 2-3 days; the total fabrication time if done at once was about 10 hours. Sacrificial water was added to the empty wells in the 6-well plates to prevent drying when stored overnight. More details on the design of each layer can be found in Appendix A.

Cell culture of human fetal lung fibroblasts (Fig 2.6): Human fetal lung fibroblasts (HFL-1, ATCC) were cultured in T-75 tissue culture flasks (Falcon; Franklin Lakes, NJ, USA) with Dulbecco's Modified Eagle Medium supplemented with 10% fetal bovine serum and 1% penicillin/streptomycin at 37 °C and 5% CO2. Agarose prepared for cell culture experiments was dissolved in 1X PBS at 1.5% wt/v and autoclaved. Type I collagen solutions were neutralized by mixing rat tail collagen (Corning #354249) with 500 mM HEPES in a 9:1 ratio, respectively. Cell suspensions containing human fetal lung (HFL) fibroblasts (ATCC) at concentrations of ~9 million cells per mL in cell culture medium were then added to the collagen solutions in a 1:2 ratio, respectively, to give a final collagen concentration of 5 mg per mL and a final cell concentration of ~3 million cells per mL. Cell-laden structures were incubated at 37 °C, 5% CO2 for 24 hours in Dulbecco's modified eagle medium (Gibco) prior to imaging. Cells were stained with Calcein AM and ethidium homodimer (MilliporeSigma). Cell-laden structures were imaged with a Leica TCS SP5 II confocal microscope and a 17.9 μm Z-step. Images were processed in FIJI software.

Patterning type I collagen (Figure 2.6): Patterning collagen was achieved with the addition of a flattening step (Figure A6). This step involves placing a patterning device over the collagen layer prior to gelling such that the collagen will wet the pattern on the device, creating a flat surface to guide flow for the next layer. When the collagen is gelled and the device removed, the height of the resulting gel layer is precisely set in the shape and location of the pattern to be flowed in the next layer. Each layer was patterned at room temperature and immediately placed in a cell culture incubator until the next layer was patterned. The entire structure took ~5 hours to fabricate.

PEG hydrogel fabrication: PEG hydrogels were generated through strain-promoted azide-alkyne cycloaddition (SPAAC) between PEG-tetraBCN (4 mM) and peptide di-azide crosslinkers (8mM) with the inclusion of 1mM N_3-GRGDS-NH_2 to promote cell adhesion to the hydrogel. [15, 41] More information on hydrogel and peptide synthesis can be found in Appendix A. To prevent cell and gel adhesion to the rails upon removal, 3D printed patterning rails were not plasma treated and were incubated in 1% Bovine Serum Albumin (MilliporeSigma) in water for 1-2 hours prior to patterning. Gel precursors were mixed with cell

suspension, patterned using 3D printed rails, with each layer polymerized for 15 minutes at 37°C. The design consists of 3 layers, and 4 patterning steps and the entire fabrication process took ~1.5-2 hours.

HS5 cell culture in PEG hydrogels: HS5 transformed human bone-marrow stromal cells expressing either eGFP or mCherry were the generous gift of Dr. Brian Hayes at the Fred Hutchison Cancer Research Center. Cells were cultured in Dulbecco's Modified Growth Medium (DMEM) (Gibco) containing 10% Fetal Bovine Serum (FBS) and 1% Penicillin/Streptomycin and passaged at a 1:5 ratio at confluence. During passage, cells were encapsulated in 4 mM PEG gels as described above at a density of 20 x 10^6 cells/mL. Encapsulated cells were cultured for 5 days, degraded through treatment with an evolved Sortase A pentamutant [SrtA(5M)] [42] on day 5, and then cultured for an additional 5 days prior to imaging on day 10. Gels were imaged by confocal point scanning microscopy on a Leica SP8 microscope. Whole gel z-stacks were obtained at 10x magnification with a 5 μm z-step. Detector gain and laser power compensation were applied during acquisition to account for light attenuation through the gel.

PEG hydrogel degradation using SrtA (5M): A SrtA(5M) working solution consisting of 50 μM SrtA(5M), 18 mM triglycine (Chem Impex; Wood Dale, IL), and 1.8 mM $CaCl_2$ (Sigma Aldrich; St. Louis; MO) was prepared in 1X PBS. More information on recombinant expression and purification of the SrtA(5M) can be found in Appendix A. To initiate degradation of SrtA-susceptible regions, media was aspirated from the patterned gels and replaced with 600 μL of SrtA(5M) working solution. After 90 minutes of enzyme treatment, the SrtA(5M) working solution was aspirated from gels and replaced with DMEM supplemented with 10% FBS.

Hydrophobic coating for patterning (Figure 2.8): Rectangular polystyrene (PS) pieces were cut using a CNC mill (DATRON neo) to the same width as the designed "W" pattern. All PS pieces were plasma treated using the same protocol for the 3D printed patterning devices. The 'W' pattern, was cut from masking tape (3M) using a plotter cutter (Graphtec CE6000-40) and then applied to the plasma treated side of the PS, such that the edges of the 'W' lined up with the edges of the PS. Two coats of Step 1 of Rust-Oleum Neverwet™ hydrophobic treatment were applied, allowed to dry for 10 minutes, and then three coats of Step 2 were applied, and left to dry for an additional 10 minutes. The masking tape was removed,

revealing a hydrophilic pattern with hydrophobic surroundings. Neverwet™ may affect cell viability and we do not intend to use this reagent with cell culture.

Patterning hydrogels using hydrophilic/hydrophobic interfaces (Figure 2.8): Two No. 1.5 coverslips (Fisherbrand) were stacked on top of a PS base at both ends. Double-sided tape was placed between each coverslip to prevent slipping during assembly. The total height of the coverslips and double-sided tape was measured to be 500 μm with a caliber. The patterning piece (described above in the preceding section) was placed facedown over the coverslips and base. Binder clips were used to secure the PS layers and coverslips. A picture of the setup for the first layer can be found in Figure A7. 1.5% w/v agarose was dyed purple and yellow using India Ink (Dr. Ph Martin's). The first layer was patterned by placing the pipette at the edge of the hydrophilic patterning region in between the patterning piece and the base. Both ends of the W were used as inlets. The agarose was allowed to solidify for 10 minutes before the patterning device was removed. To achieve the second layer, two additional coverslips and double-sided tape were added to increase the distance between the base and the second patterning device, which was aligned by eye. The gel loading and setting process for the second layer was the same as for the first layer.

Image Processing: Images were processed using Adobe Photoshop CC 2018 using a uniform brightness/contrast adjustment.

2.11 References

1. D. J. Beebe, J. S. Moore, J. M. Bauer, Q. Yu, R. H. Liu, C. Devadoss and B.-H. Jo, *Nature*, 2000, **404**, 588-590.
2. S. B. Kim, Y. Zhang, S. M. Won, A. J. Bandodkar, Y. Sekine, Y. Xue, J. Koo, S. W. Harshman, J. A. Martin, J. M. Park, T. R. Ray, K. E. Crawford, K.-T. Lee, J. Choi, R. L. Pitsch, C. C. Grigsby, A. J. Strang, Y.-Y. Chen, S. Xu, J. Kim, A. Koh, J. S. Ha, Y. Huang, S. W. Kim and J. A. Rogers, *Small*, 2018, **14**, 1703334.
3. J. Choi, Y. Xue, W. Xia, T. R. Ray, J. T. Reeder, A. J. Bandodkar, D. Kang, S. Xu, Y. Huang and J. A. Rogers, *Lab on a chip*, 2017, **17**, 2572-2580.
4. A. E. Herr, A. V. Hatch, D. J. Throckmorton, H. M. Tran, J. S. Brennan, W. V. Giannobile and A. K. Singh, *Proceedings of the National Academy of Sciences*, 2007, **104**, 5268.
5. C.-C. Kang, K. A. Yamauchi, J. Vlassakis, E. Sinkala, T. A. Duncombe and A. E. Herr, *Nature Protocols*, 2016, **11**, 1508.

6. V. Chan, P. Zorlutuna, J. H. Jeong, H. Kong and R. Bashir, *Lab on a chip*, 2010, **10**, 2062-2070.
7. Y. Ling, J. Rubin, Y. Deng, C. Huang, U. Demirci, J. M. Karp and A. Khademhosseini, *Lab on a chip*, 2007, **7**, 756-762.
8. G. Ongo and D. Juncker, Kaohsiung, Taiwan, 2018.
9. B. H. Chueh, Y. Zheng, Y. S. Torisawa, A. Y. Hsiao, C. Ge, S. Hsiong, N. Huebsch, R. Franceschi, D. J. Mooney and S. Takayama, *Biomed Microdevices*, 2010, **12**, 145-151.
10. W.-G. Koh and M. V. Pishko, *Analytical and Bioanalytical Chemistry*, 2006, **385**, 1389-1397.
11. K. C. Hribar, K. Meggs, J. Liu, W. Zhu, X. Qu and S. Chen, *Scientific Reports*, 2015, **5**, 17203.
12. M. S. Hahn, J. S. Miller and J. L. West, *Advanced Materials*, 2006, **18**, 2679-2684.
13. V. A. Liu and S. N. Bhatia, *Biomedical Microdevices*, 2002, **4**, 257-266.
14. S. Khetan and J. A. Burdick, *Soft Matter*, 2011, **7**, 830-838.
15. C. K. Arakawa, B. A. Badeau, Y. Zheng and C. A. DeForest, *Advanced Materials*, 2017, **29**, 1703156.
16. J. Liu, D. Gao, H. F. Li and J. M. Lin, *Lab on a chip*, 2009, **9**, 1301-1305.
17. J. Decock, M. Schlenk and J.-B. Salmon, *Lab on a chip*, 2018, **18**, 1075-1083.
18. S. J. Bryant, J. L. Cuy, K. D. Hauch and B. D. Ratner, *Biomaterials*, 2007, **28**, 2978-2986.
19. G. Papavasiliou, P. Songprawat, V. Pérez-Luna, E. Hammes, M. Morris, Y.-C. Chiu and E. Brey, *Tissue Engineering Part C: Methods*, 2008, **14**, 129-140.
20. C. G. Williams, A. N. Malik, T. K. Kim, P. N. Manson and J. H. Elisseeff, *Biomaterials*, 2005, **26**, 1211-1218.
21. L. Xu, N. Sheybani, W. A. Yeudall and H. Yang, *Biomaterials Science*, 2015, **3**, 250-255.
22. T. Boland, X. Tao, B. J. Damon, B. Manley, P. Kesari, S. Jalota and S. Bhaduri, *Materials Science and Engineering: C*, 2007, **27**, 372-376.
23. C. Xu, W. Chai, Y. Huang and R. R. Markwald, *Biotechnology and Bioengineering*, 2012, **109**, 3152-3160.
24. T. Xu, W. Zhao, J.-M. Zhu, M. Z. Albanna, J. J. Yoo and A. Atala, *Biomaterials*, 2013, **34**, 130-139.
25. A. Bandyopadhyay, V. K. Dewangan, K. Y. Vajanthri, S. Poddar and S. K. Mahto, *Biocybernetics and Biomedical Engineering*, 2018, **38**, 158-169.
26. S. Sakai, K. Mochizuki, Y. Qu, M. Mail, M. Nakahata and M. Taya, *Biofabrication*, 2018, **10**, 045007.
27. J.-H. Shim, J.-S. Lee, J. Y. Kim and D.-W. Cho, *Journal of Micromechanics and Microengineering*, 2012, **22**, 085014.
28. F. Pati, J. Jang, D.-H. Ha, S. Won Kim, J.-W. Rhie, J.-H. Shim, D.-H. Kim and D.-W. Cho, *Nature Communications*, 2014, **5**, 3935.
29. T. J. Hinton, Q. Jallerat, R. N. Palchesko, J. H. Park, M. S. Grodzicki, H.-J. Shue, M. H. Ramadan, A. R. Hudson and A. W. Feinberg, *Sci Adv*, 2015, **1**, e1500758-e1500758.
30. R. Chang, J. Nam and W. Sun, *Tissue Engineering Part A*, 2008, **14**, 41-48.

31. K. Nair, M. Gandhi, S. Khalil, K. C. Yan, M. Marcolongo, K. Barbee and W. Sun, *Biotechnology Journal*, 2009, **4**, 1168-1177.

32. A. Blaeser, D. F. Duarte Campos, U. Puster, W. Richtering, M. M. Stevens and H. Fischer, *Advanced Healthcare Materials*, 2016, **5**, 326-333.

33. S. Cosson and M. P. Lutolf, *Scientific Reports*, 2014, **4**, 4462.

34. F. Chiellini, R. Bizzarri, C. K. Ober, D. Schmaljohann, T. Yu, R. Solaro and E. Chiellini, *Macromolecular Rapid Communications*, 2001, **22**, 1284-1287.

35. Y. Zheng, J. Chen, M. Craven, N. W. Choi, S. Totorica, A. Diaz-Santana, P. Kermani, B. Hempstead, C. Fischbach-Teschl, J. A. López and A. D. Stroock, *Proceedings of the National Academy of Sciences*, 2012, **109**, 9342.

36. B. P. Casavant, E. Berthier, A. B. Theberge, J. Berthier, S. I. Montanez-Sauri, L. L. Bischel, K. Brakke, C. J. Hedman, W. Bushman, N. P. Keller and D. J. Beebe, *Proceedings of the National Academy of Sciences*, 2013, **110**, 10111.

37. S. B. Berry, T. Zhang, J. H. Day, X. Su, I. Z. Wilson, E. Berthier and A. B. Theberge, *Lab on a chip*, 2017, **17**, 4253-4264.

38. W. Lee, V. Lee, S. Polio, P. Keegan, J.-H. Lee, K. Fischer, J.-K. Park and S.-S. Yoo, *Biotechnology and Bioengineering*, 2010, **105**, 1178-1186.

39. Y. Lee, J. W. Choi, J. Yu, D. Park, J. Ha, K. Son, S. Lee, M. Chung, H.-Y. Kim and N. L. Jeon, *Lab on a chip*, 2018, **18**, 2433-2440.

40. J. Berthier, K. A. Brakke and E. Berthier, *Open Microfluidics*, Scrivener Publishing LLC, Beverly, MA, USA 2016.

41. C. A. DeForest and D. A. Tirrell, *Nature Materials*, 2015, **14**, 523.

42. I. Chen, B. M. Dorr and D. R. Liu, *Proceedings of the National Academy of Sciences*, 2011, **108**, 11399.

43. E. J. Su, S. Jeeawoody and A. E. Herr, *APL Bioengineering*, 2019, **3**, 026101.

44. C. Curtis, D. Toghani, B. Wong and E. Nance, *Colloids and Surfaces B: Biointerfaces*, 2018, **170**, 673-682.

45. P. Zarrintaj, S. Manouchehri, Z. Ahmadi, M. R. Saeb, A. M. Urbanska, D. L. Kaplan and M. Mozafari, *Carbohydrate Polymers*, 2018, **187**, 66-84.

46. E. Sodupe-Ortega, A. Sanz-Garcia, A. Pernia-Espinoza and C. Escobedo-Lucea, *Materials*, 2018, **11**.

47. D. F. Duarte Campos, A. Blaeser, M. Weber, J. Jäkel, S. Neuss, W. Jahnen-Dechent and H. Fischer, *Biofabrication*, 2012, **5**, 015003.

48. N. Brandenberg and M. P. Lutolf, *Advanced Materials*, 2016, **28**, 7450-7456.

49. D. Juncker, H. Schmid, U. Drechsler, H. Wolf, M. Wolf, B. Michel, N. de Rooij and E. Delamarche, *Analytical Chemistry*, 2002, **74**, 6139-6144.

50. D. G. Priest, N. Tanaka, Y. Tanaka and Y. Taniguchi, *Scientific Reports*, 2017, **7**, 17750.

51. E. R. Ruskowitz and C. A. DeForest, *Nature Reviews Materials*, 2018, **3**, 17087.

52. Y. C. Li, Y. S. Zhang, A. Akpek, S. R. Shin and A. Khademhosseini, *Biofabrication*, 2016, **9**, 012001.

53. B. A. Badeau and C. A. DeForest, *Annual Review of Biomedical Engineering*, 2019, **21**, 241-265.

54. P. M. Gawade, J. A. Shadish, B. A. Badeau and C. A. DeForest, *Advanced Materials*, 2019, **31**, 1902462.

55. E. R. Ruskowitz, M. P. Comerford, B. A. Badeau and C. A. DeForest, *Biomaterials Science*, 2019, **7**, 542-546.

56. B. A. Badeau, M. P. Comerford, C. K. Arakawa, J. A. Shadish and C. A. DeForest, *Nature Chemistry*, 2018, **10**, 251.

57. J. Valdez, C. D. Cook, C. C. Ahrens, A. J. Wang, A. Brown, M. Kumar, L. Stockdale, D. Rothenberg, K. Renggli, E. Gordon, D. Lauffenburger, F. White and L. Griffith, *Biomaterials*, 2017, **130**, 90-103.

58. E. Cambria, K. Renggli, C. C. Ahrens, C. D. Cook, C. Kroll, A. T. Krueger, B. Imperiali and L. G. Griffith, *Biomacromolecules*, 2015, **16**, 2316-2326.

59. S. R. Caliari and J. A. Burdick, *Nature methods*, 2016, **13**, 405-414.

60. H. S. Lim, J. T. Han, D. Kwak, M. Jin and K. Cho, *Journal of the American Chemical Society*, 2006, **128**, 14458-14459.

61. J. Berthier and K. A. Brakke, *The Physics of Microdroplets*, Wiley, Hoboken, NJ, USA, 2012.

Chapter 3: Suspended Open Microfluidic Tissue Patterning[2]

Abstract: Combining suspended tissue constructs with the ability to control the 3D spatial composition would open new abilities to precisely control and study various biological processes, diseases, and therapeutic interventions. Here we present a novel open microfluidic suspended tissue patterning technique utilizing a removable open microfluidic patterning channel to pattern multiple spatial regions across a free-standing suspended tissue. The open microfluidic channel allows for the pipetting of different cell-ECM precursors and the capillary pinning ridges can be used to control the fluid front for patterning multiple regions in one tissue. Once the patterned tissue has begun to pull away from the open microfluidic channel walls, the patterning device can be removed to generate the suspended tissue. Here we demonstrate this technique to generate free-standing patterned tissues with multiple regional components using a variety of native ECM including fibrin and collagen. This technique offers a powerful tool for generating suspended tissue models with increased control over their geometry and composition, which can be used for a variety of applications, such as studying the interactions between two distinct regions of the tissue or generating a 3D model of a diseased region adjacent to a healthy region. We believe this technique has the potential to revolutionize the field of suspended tissue engineering.

3.1 Introduction

The ability to generate physiologically relevant tissue constructs *in vitro* is a significant driving force in the tissue engineering field. [1] These 3D tissue models offer a wide range of applications, from modeling tissue development to realizing clinical applications in tissue regeneration. [2] Towards the effort of generating *in vitro* 3D tissues for more accurate recapitulation of *in vivo* organ composition and function,

---

[2] *We would like to acknowledge L. G. Brown, S. Nguyen, P. Mulimani, A. Goldstein, R. C. Bretherton, A. Wu, C. A. DeForest, N. J. Sniadecki, E. Berthier, and A. B. Theberge "* Suspended Open Microfluidic Tissue Patterning*." In preparation*

AJH, and LGB designed method and conducted experiments. SN conducted experiments and assisted in designing method. PM designed and executed periodontal experiment. AG conducted experiments. RCB assisted in design and conducted experiment, AW collected preliminary data, CAD, NJS, ABT, and EB supervised and advised and AJH, LGB interpreted the results and wrote the manuscript.

cells are typically embedded within an extracellular matrix (ECM), which aid in modulating tissue architecture. However, these 3D models often lack mechanical forces, such as stress- and strain-induced mechanotransduction, that play a crucial role in cell morphology, alignment, proliferation, and differentiation. [3-5] To address this limitation, flexible cantilevers and pillars have been used to fabricate suspended 3D tissue structures that can experience tensile forces in real time; [6-9] these platforms have been used to develop engineered heart, [10, 11] muscle, [12, 13] and lung tissues, [14, 15] as well as wound healing skin models. [16] While being able to put these engineered tissues under a mechanical force is critical for understanding and studying these tissue types, what can further enhance the biological relevance and allow for more complex studies to recapitulate these tissues is the addition of spatial control across a suspended tissue. Tissues are typically not homogenous *in vivo*, they contain variation of cell type, ECM composition and shape and these variations in tissue compositions can also be different in certain disease processes. The ability to develop suspended 3D tissue constructs with precise cellular compositional control would improve the physiological relevance of *in vitro* tissue models that can be further used for drug testing and disease progression applications.

To achieve geometric control in 3D suspended tissue constructs, many biofabrication techniques, such as casting, [17] photopatterning, [18] and 3D bioprinting, [19] have been developed to recapitulate the complex structural and cellular composition of native tissues, but each method has limitations in either their geometric abilities, cellular distribution control, or compatibility with some native ECMs. [20] Microfluidic-based technologies have recently been realized in addition to these conventional tissue engineering methods due for their ability to introduce dynamic or perusable flow to 3D culture systems. [21] The ability to recapitulate mechanical forces needed for organotypic modeling has afforded microfluidics to be used in a wide range of applications, including disease modeling, [22] developing human-on-a-chip microsystems, [23] and controlled patterning of tissue microenvironments. [24-26] Recently, we developed a method for layer-by-layer 3D hydrogel patterning using 3D printed open microfluidic patterning devices. With this method, entire layers of hydrogel or ECM precursor gels with embedded cells can be flowed through a custom designed open microfluidic channel, where flow is driven

by surface tension and the shape of the patterned layer is controlled by the shape of the open microfluidic channel and capillary pinning ridges along the channel. [27] To this effect, open microfluidic methods can be used to pattern multiple regions comprising different cell types or ECMs, thereby generating spatially organized and complex tissue constructs that can provide better control over cell adhesion, migration, proliferation, and differentiation. [28] In open microfluidic systems, the flow of hydrogel precursors is achieved by passive forces, enabling patterning of non-extrudable or photopolymerizable hydrogels, which include native, unmodified ECMs such as fibrin and collagen, or custom-engineered hydrogels such as enzymatically degradable polyethylene glycol. [29]

Here in this work, we expand upon the open microfluidic hydrogel patterning method to generate a 3D patterned, multi-region suspended hydrogel culture. This suspended model is developed using a removable open microfluidic patterning device that interfaces two posts, generating a suspended hydrogel over an open space without the use of a sacrificial material. This technology expands on an existing model that uses casting to generate suspended engineered heart tissues, but our method offers the unique advantage of spatially controlled material and cell composition. [30, 31] Utilizing surface tension to drive flow and capillary pinning to stop flow, we can achieve control over the placement of tissue components to pattern multiple regions within a single suspended tissue. Next, taking advantage of the natural cellular behavior to contract and remodel ECM, cells pull away from the walls of the patterning device while remaining compacted on the suspended posts, thereby allowing gentle removal of the patterning device. This system can be used to unlock frontiers in modeling complex biological functions which require patterned/delineated tissue sections such as border regions between tissues (e.g., disease and healthy tissue borders), myotendinous junctions (e.g., bone-ligament or muscle-tendon interfaces), or recapitulating *in vivo* zonal patterning (e.g., modeling liver zonation or gradients).

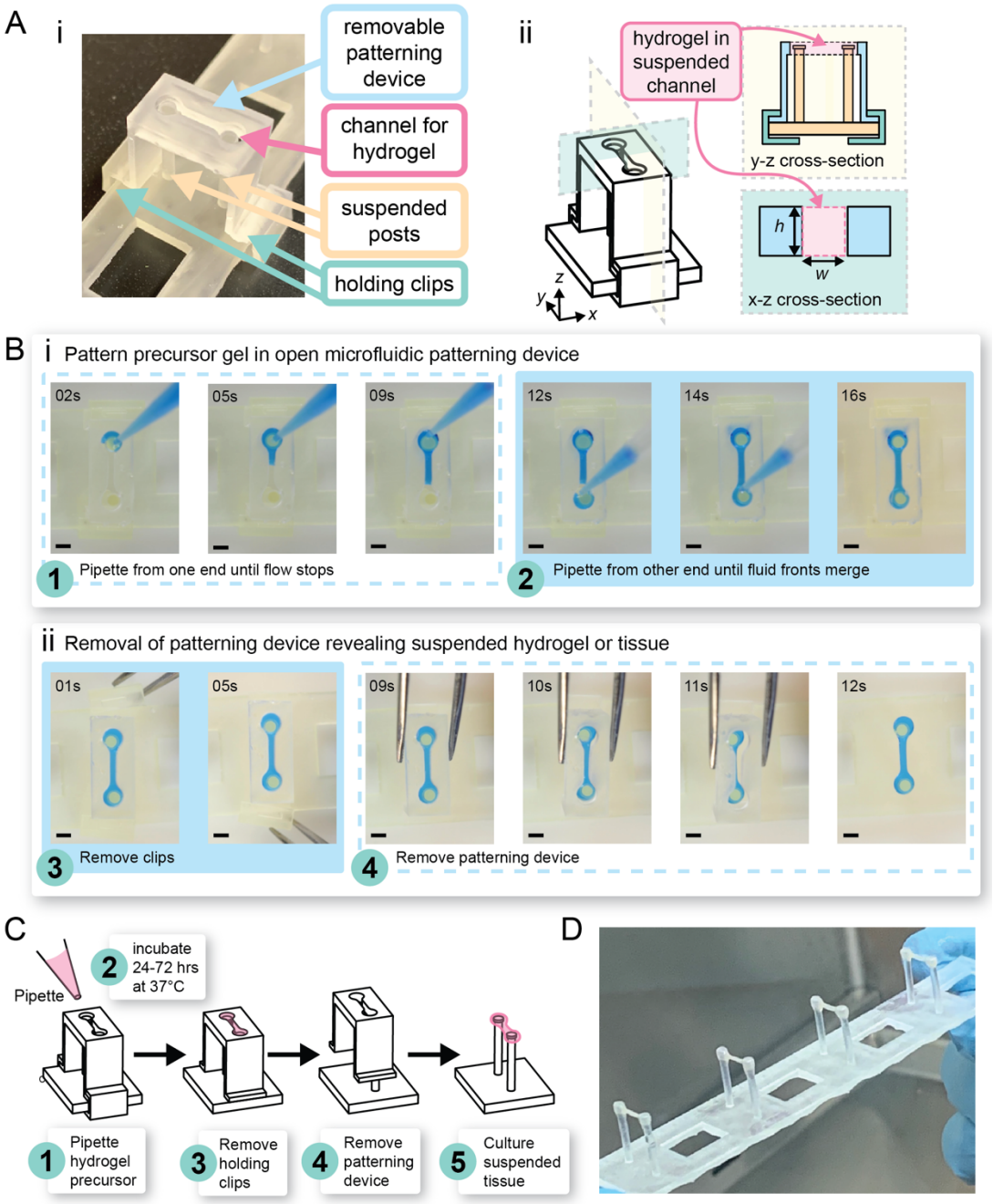

Figure 3.1. Suspended tissue open microfluidic patterning device design and workflow for patterning a single component tissue. (A) i) 3D printed patterning device components with ii) y-z cross-section (device side view) and x-z cross-section (channel cross-section view). (B) i) Process of patterning a precursor gel into the open microfluidic patterning device and ii) removing the holding clips and patterning device to reveal the suspended tissue construct. In this demonstration, 1.5% agarose dyed with blue food coloring was used. (C) Process of patterning cell-laden precursor gels. All scale bars are 2 mm. (D) Collagen laden with 3T3 fibroblast cells suspended between 3D printed posts, generated utilizing the open microfluidic suspended patterning method.

3.2 Open microfluidic patterning for the generation of suspended tissues

Our suspended open microfluidic patterning device has three main components: a suspended post array that fits within a 24-well plate, a removable patterning device, and holding clips (Figure 3.1Ai). The patterning device was designed to interface two suspended posts such that an open channel is formed around the two posts and each patterning device was attached to the post array using the holding clips (Figure 3.1Aii). Upon assembly of the device, suspended tissues are generated via a simple pipetting step into the open microfluidic channel, whereby the precursor ECM hydrogel solution laden with cells is flowed into the entire open channel via spontaneous capillary flow (Figure 3.1B). Once the cell-laden ECM is gelled and the tissue construct begins to pull away from the walls of the patterning device, the patterning device can be removed, and the construct can be cultured as a free-standing suspended tissue (Figure 3.1C).

Surface tension-driven and capillary forces hold the precursor cell laden-ECM solution suspended between the two walls of the open channel of the patterning device as the solution transitions from a fluid to hydrogel state. [29] After gelation, the entire assembled patterning device is placed within a 24-well plate with media. Before we can remove the holding clips and open patterning device from the post array, we first allow the cells to culture (anywhere between 2 to 48 h depending on cell and ECM type) until we observe the tissue pulling away from the channel walls of the patterning device. To this effect, we exploit the cell's natural behavior to remodel ECM and contract within an ECM, a phenomenon observed in other suspended tissue models to recapitulate vascularization and heart contractility. [32-35] Additionally, we coat the open microfluidic patterning device with 1% BSA, a common protein used for blocking, prior to pipetting the cell-ECM precursor gel to prevent cells from attaching to the channel walls and to further aid the tissue construct in contracting away from the device. At the same time, a T-shaped caps on each PDMS post anchors the cell-ECM tissue, such that it should remove from the walls of the patterning device and stay suspended between the posts. Once the tissue has visibly pulled away, we remove the assembled patterning device from culture and simply remove the holding clips that attach the patterning device to the post array and gently lift the patterning device, revealing the suspended cell laden ECM suspended between two posts. Thus far, we have successfully generated suspended tissues comprised of fibroblasts laden in

type I collagen (Figure 3.1D) and fibrin. However, for future target tissue models with different cell and ECM types, this patterning process must first be tested to verify compatibility with our device.

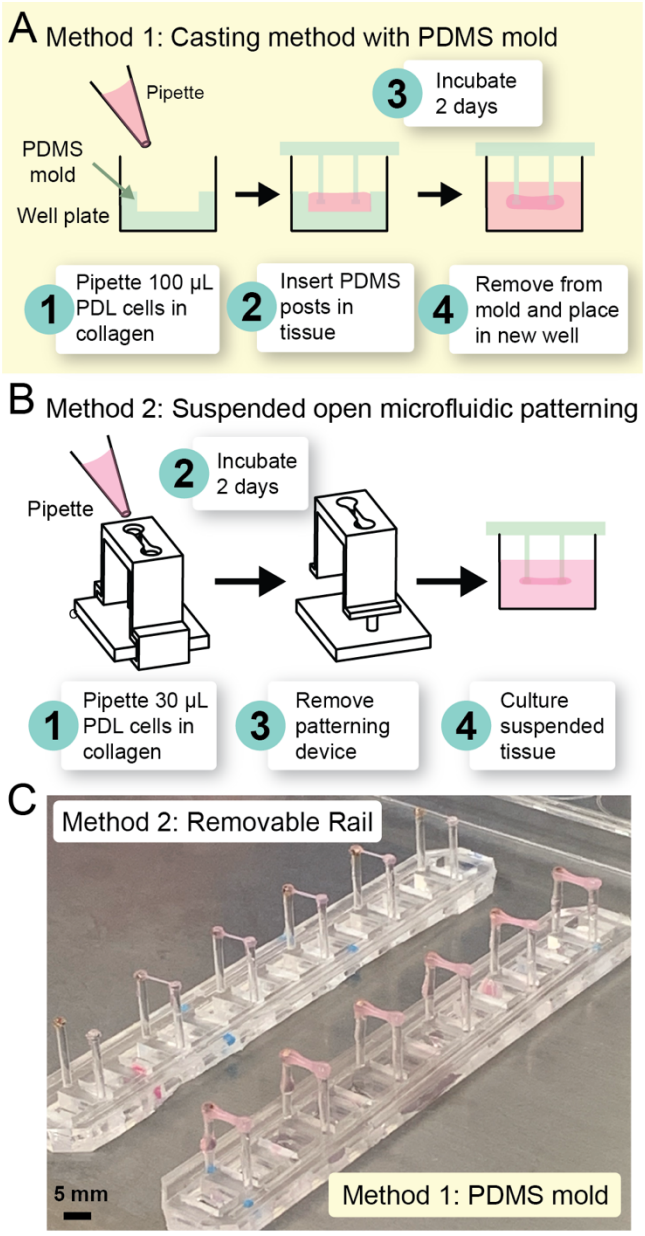

Figure 3.2. Comparing conventional casting method to our suspended tissue open microfluidic patterning device for generating suspended tissue constructs. (A) Process of casting suspended tissues with PDMS well-insert molds and PDMS post arrays. (B) Process of generating suspended tissues with our proposed method. (C) Side-by-side comparison of tissues generated using the casting method (right PDMS post array) and our method (left PDMS post array). Tissues generated using our method used ~30 µL of cell-ECM hydrogel and tissues generated using the casting method used ~100 µL of cell-ECM hydrogel. Both tissues composed of periodontal ligament cells at the same concentration in 5 mg/mL type 1 collagen.

3.3 Suspended open microfluidic patterning allows for increased control over 3D geometry

Our patterning method can generate similar tissues to a well-established casting method commonly used in tissue engineering applications for modeling myocardial [36, 37] and vascularized tissue. [38, 39] While the casting method is widely adopted due to its simplicity, our suspended open microfluidic method offers greater control over the geometry of the generated tissue. The schematic in Figure 3.2A illustrates the casting method comparing it to our open microfluidic suspended patterning method in Figure 3.2B. By changing the dimensions of the patterning channel, we can change the shape of the generated tissue if the cross-sectional dimensions of the channel follow the equation necessary for spontaneous capillary flow specific for this suspended channel geometry (Eq. 3.1), where *w* is the width (free perimeter) of the channel, *h* is the height (wetted perimeter) of the channel, and θ is the contact angle of the hydrogel to the surface of the channel. [27, 29] These dimensions can be visualized in the x-z cross-section in Figure 3.1Aii.

$$\frac{w}{h} < cos\ (\theta) \qquad \text{(Eq. 3.1)}$$

To demonstrate that our method can yield similar tissue constructs to conventional casting methods, we compared our suspended open microfluidic method with a casting method previously used by Bremner et al. to generate suspended collagen constructs laden with periodontal tissue (Figure 3.2A & 3.2B). [31] Compared to the casting method, which requires about 100 µL of cell-laden ECM, we can achieve thinner tissues (~30 µL of cell-ECM) by scaling down the size of the channels (Figure 3.2C). However, we can still achieve similar dimensions to the casting method by simply scaling up the dimensions of our open channel. The ability to easily scale up or down dimensions to generate tissues in variable sizes allows, in the case of thinner tissues, for a smaller volume—critical when you are considering using precious or rare cells or *de novo* hydrogel material. In the case of thicker tissues, a thicker tissue is beneficial for tissues to be cultured for longer periods of time and remain stable. The setup for both the open microfluidic and casting method had similar preparation and patterning times, with our setup offering additional control and customizability over geometry and volume.

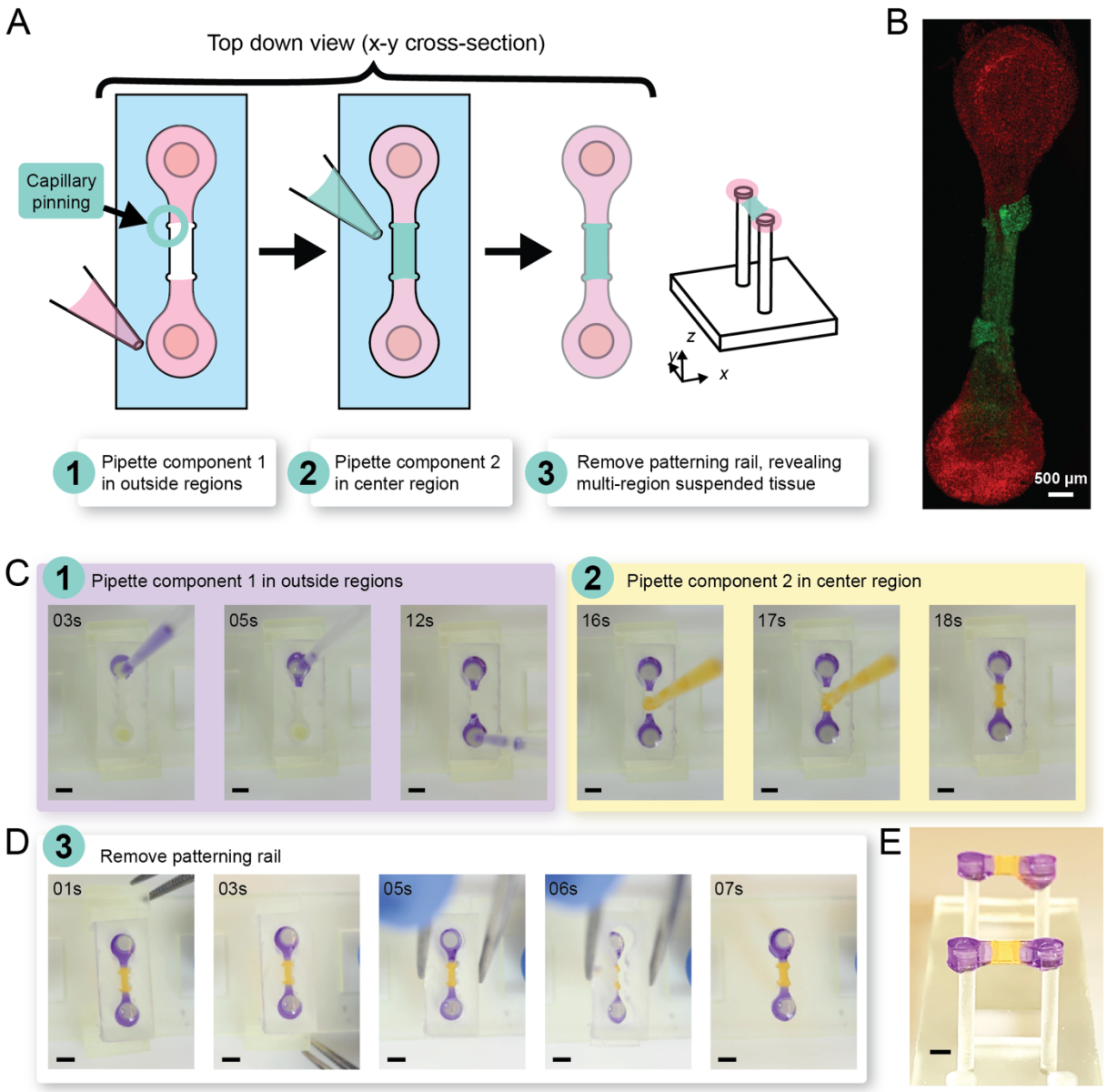

Figure 3.3. Utilizing capillary pinning ridges to generate multi-region suspended tissue constructs. (A) Schematic of the multi-region open microfluidic patterning device, which uses capillary pinning ridges to pin the fluid front before it reaches the altered geometrical shape of the channel. (B) Confocal microscopy image of fluorescently labeled 3T3 cells embedded in collagen to demonstrate successful patterning of multiple regions within a single tissue construct. The outer regions contained 3T3 cells dyed with CellTracker Red and the middle region contained 3T3 cells dyed with CellTracker Green, both of which stain the membranes of the cells. (C) Patterning process of multi-region tissue constructs and (D) subsequent removal of holding clips and patterning device. (E) Side view of suspended tissue constructs after removal of patterning device. In Part C-E, 1.5% agarose dyed with purple india ink dye was used in the outer regions and 1.5% agarose dyed with yellow india ink dye was used in the middle regions. All scale bars are 2 mm.

While the control over volume is notable, the major advantage of using an open microfluidic patterning system is the flexibility to pattern multiple regions within a single suspended construct. Since an open channel is used (i.e., a channel with no floor or ceiling), precursor gel can be pipetted anywhere along the length of the tissue (Figure 3.3). By adding capillary pinning ridges, as seen in Figure 3.3A, we can control where the precursor gel's fluid front stops due to the altered geometry of the channel at the pinning ridge location that lowers the magnitude of local capillary pressure driving flow (Figure 3.3C). [40] Once one region has been patterned, a second hydrogel precursor that is composed of a different cell type or ECM component can be pipetted into an adjacent region. The two regions can come together contiguously by breaking the capillary pinning on the ridge, either by using the tip of the pipette or by overfilling the channel. Generating two regions utilizing similar ECM and cell compositions (e.g., two separate cell types with similar propensity to contract ECM or two different ECMs, such as collagen and Matrigel, that have similar components and can bind together) will more easily form a contiguous tissue; it is necessary for the two interfaces to have the ability to integrate. Similar to the single component tissue construct described above, the patterning device and holding clips can be removed after the cell-ECM throughout the multiple regions have begun to pull away from the channel walls (Figure 3.3D). This is especially important to test with various cell-ECM compositions, since different regions along the patterning device can contract at different rates, either due to lower density of an ECM in one region or use of different types or concentrations of contractile cells.

3.5 Conclusions and future directions

Here we presented a method for generating multicomponent suspended tissue constructs utilizing a novel open microfluidics-based approach with a removable patterning device. Our open microfluidic suspended patterning method offers a versatile and customizable approach for generating suspended tissue models with increased control over the 3D geometry and composition of the generated tissues. We have demonstrated the feasibility of this approach for generating suspended tissues, including multi-component regions, for a variety of cell and extracellular matrix materials. We take the existing utility of the suspended

tissue constructs for mechanical manipulation of tissues and add regional control. Additionally, due to utilizing only a plastic patterning device and a simple pipetting step, we believe that this technique can be adopted by biologists and researchers, especially for those already employed in suspended tissue generation using casting methods. In the future, we plan to utilize rapid manufacturing techniques such as injection molding to produce more devices at lower cost, as well as utilize a more biologically-friendly plastic material such as polypropylene, a material used in standard tissue culture well-plates. This method has the potential to revolutionize the field of suspended tissue engineering by providing a powerful tool for generating suspended tissue models with increased control over their geometry and composition.

In recent years, tools have been developed to better understand the spatial distribution and heterogeneity of biological processes and identities in tissues. These tools, such as spatial transcriptomics and spatial histological analysis can be employed on patterned suspended tissues that are now possible to generate with open microfluidic suspended tissue patterning. Such a marriage of spatial patterning tools with spatial analysis will allow researchers to gain a better understanding of the interactions between two distinct regions within a suspended tissue construct. For example, the use of spatial transcriptomics can provide insight into the gene expression profiles of different regions of the tissue, while spatial histological analysis can provide a better understanding of the morphological features of the tissue, including the presence of different cell morphologies at the interface between two distinct regions. This can help to gain a better understanding of how the different regions interact, as well as to gain insight into the chemical and biological signaling that occurs at the border of the two regions.

In ongoing work, we continue to explore the potential of this method for generating a three-part periodontal tissue model. Further, we plan to employ these models to study various regional disease processes in engineered heart tissues. An example of such an application includes a scarred region representing a myocardial infarction adjacent to a healthy tissue region. Broadly, we believe we can use open microfluidic suspended patterning as a tool to model a diseased region adjacent to a healthy region by patterning two distinct regions, one containing the diseased cells and ECM components and the other containing healthy cells and ECM components. This allows researchers to study the interactions between

the two regions, such as the chemical and biological signaling that occurs at the interface. This can be used to gain a better understanding of the disease process and develop therapeutics. For example, we could use this technique with existing skeletal tissue models to create a 3D model of facioscapulohumeral dystrophy (FSHD) or other heterogeneous muscular dystrophies to better understand the disease and develop therapeutics.

3.6 Materials and methods

Device Design, Fabrication, and Sterilization: PDMS post arrays were fabricated as described in Leonard et al. [30] Briefly, uncured PDMS was poured into a 4-part acrylic mold to fabricate one array that contained six pairs of posts such that a single array could fit in a row of a 24-well plate. Glass capillary tubes were cut to the appropriate length and inserted into one side of the mold prior to curing such that each pair contained one rigid post. The posts were baked overnight at 65°C and then removed from the molds. Fabricated posts were 11 mm long and 1.5 mm in diameter with a cap structure (0.5 mm thick and 2.0 mm diameter) to aid in attachment of the cell-laden hydrogel of interest.

The open microfluidic patterning device and clips were designed in Solidworks 2020 and 3D printed out of clear resin using a Form 3B+ 3D printer (Formlabs Inc.). Dimensions of the open channel were designed to fit around the PDMS posts. Clips were designed to hold the patterning device in place during the tissue patterning process. The 3D printed parts (patterning device and clips) were cleaned in two separate FormWash units (Formlabs Inc.) with isopropyl alcohol (IPA) for 20 minutes and then another 10 minutes to remove excess uncured resin. The devices were dried with compressed air and cured under UV light at 60°C for 15 minutes in a FormCure (Formlabs Inc.).

To sterilize the PDMS posts, patterning devices, and clips for cell culture, all parts were first placed within a biosafety cabinet and UV sterilized for 20 minutes. The PDMS posts were additionally sterilized with 70% ethanol for five minutes by placing the tips of the posts in a 24-well plate, where each well contained 2 mL of 70% ethanol. The PDMS posts were then washed with sterile DI water twice for five minutes each.

Assembly of Suspended Tissue Open Microfluidic Patterning Devices: After sterilization, the patterning devices that were to be used with a cell-laden hydrogel or ECM were incubated in a solution of 1% bovine serum albumin (BSA) for 1 hour. After incubation, the 1% BSA solution was removed, and the patterning devices were allowed to fully dry prior to assembling the suspended tissue open microfluidic patterning devices (see Figure 3.1). The open microfluidic patterning devices was placed such that it surrounded the ends of each post, and the clips were used to hold the patterning device in place at the base of the PDMS post array.

Cell Culture of 3T3 Mouse Fibroblasts: Initial optimization experiments were conducted with NIH/3T3 mouse embryonic fibroblast cell line obtained from ATCC. The cells were maintained in a tissue culture flask containing Dulbecco's Modified Eagle Medium (DMEM) supplemented with 10% fetal bovine serum and 1% penicillin-streptomycin at 37°C, 5% CO_2. Culture medium was changed every other day until cells reached around 80-90% confluency, where the culture was rinsed with 1X PBS, followed by addition of TrypLE (Gibco). After incubation for 3 minutes at 37°C, the TrypLE was inactivated by diluting with cell culture medium. The fluid volume was centrifuged at 300 RCF for 3 minutes. The cells were resuspended in cell culture medium for further passaging or used for hydrogel encapsulation, as described below. For patterning, 3T3 cells were laden in desired hydrogel at a final concentration of $5.0x10^6$ cells/mL.

Patterning Type I Collagen: Following sterilization, PDMS posts were treated with 0.1% PEI for 10 minutes and then rinsed with sterile MilliQ water for five minutes. Next, the PDMS posts were treated for 30 minutes with 0.01% glutaraldehyde and then rinsed twice with MilliQ water for five minutes each. For each treatment step, 2 mL of the respective solution was placed in a 24-well plate so that the tips of each PDMS posts were in contact with the solution.

Collagen hydrogels were prepared by mixing a stock of rat tail collagen type I (Corning) in 0.02N acetic acid with sterile deionized water, 10X phosphate buffered saline (PBS), and 1N NaOH to achieve a final collagen density of 5 mg/mL. To generate the cell-laden collagen precursor gel for patterning, pelleted cells were resuspended in the neutralized collagen solution and then pipetted directly into the open microfluidic channel of the patterning device until the open channel was filled. The PDMS post array, with

the patterning device and clips assembled, was then placed upside down in a 24-well plate and 1X PBS was added as sacrificial liquid to surrounding wells to prevent drying out the cell-laden hydrogel. The well plate was incubated for 30 minutes at 37°C to allow the hydrogel to reach complete gelation. After gelation, 2 mL of culture medium was placed in each well. After 24 hours or once the collagen hydrogel visibly pulled away from the patterning device's channel walls, the clips and patterning devices were removed to reveal a suspended tissue between the PDMS posts. Culture medium was changed after the removal of the 3D printed patterning devices and then changed every other day.

Patterning Fibrin: Fibrinogen stock solutions were prepared at 50 mg/mL by dissolving 250 mg of powder fibrinogen from human plasma (Sigma-Aldrich) in 5 mL of warmed 0.9% NaCl in deionized water. The fibrinogen solution was then filter-sterilized with a 0.22 mm syringe filter. Thrombin stock solutions were prepared at 100 U/mL by dissolving 100 units of powder thrombin from human plasma (Sigma-Aldrich) in 1 mL of warmed 0.9% NaCl in deionized water. Fibrinogen and thrombin stock solutions were aliquoted and stored at -20°C until ready for use.

Fibrin hydrogels were prepared by mixing the cell suspension, fibrinogen, and thrombin on ice to obtain a final cell-laden fibrin gel concentration of 5 mg/mL at the desired cell concentration. Cell-laden fibrin gels were patterned immediately in our device due to rapid gelation of fibrin once mixed and removed from ice. The PDMS post array, with the patterning device and clips assembled, was then placed upside down in a 24-well plate and 1X PBS was added as sacrificial liquid to surrounding wells to prevent drying out the cell-laden hydrogel. The well plate was incubated for 30 minutes at 37°C to allow the hydrogel to reach complete gelation. After gelation, 2 mL of culture medium supplemented with 5 g/L 6-aminocaproic acid (Fisher) was placed in each well. After 24 hours or once the fibrin hydrogel visibly pulled away from the patterning device's channel walls, the clips and patterning devices were removed to reveal a suspended tissue between the PDMS posts. Culture medium supplemented with 5 g/L 6-aminocaproic acid was changed after the removal of the 3D printed patterning devices and then changed every other day.

3.6 References

1. Y. Park, K. M. Huh and S. W. Kang, *International Journal of Molecular Sciences*, 2021, **22**, 2491.
2. E. L. Elson and G. M. Genin, *Interface Focus,* 2016, **1**, 20150095.
3. B. D. Riehl, J. H. Park, I. K. Kwon and J. Y. Lim, *Tissue Eng Part B Rev*, 2012, **18**, 288–300.
4. W. Zhang, G. Huang and F. Xu, *Front Bioeng Biotechnol*, 2020, **8**, 1151.
5. J. Tomasek, G. Gabbiani, B. Hinz, C. Chaponnier and R. A. Brown, *Nature Reviews Molecular Cell Biology 2002 3:5*, 2002, **3**, 349–363.
6. W. R. Legant, A. Pathak, M. T. Yang, V. S. Deshpande, R. M. McMeeking and C. S. Chen, *Proc Natl Acad Sci U S A*, 2009, **106**, 10097–10102.
7. R. K. Christensen, C. von Halling Laier, A. Kiziltay, S. Wilson and N. B. Larsen, *Biomacromolecules*, 2020, **21**, 356–365.
8. N. Gaio, B. van Meer, W. Q. Solano, L. Bergers, A. van de Stolpe, C. Mummery, P. M. Sarro and R. Dekker, *Micromachines 2016, Vol. 7, Page 120*, 2016, **7**, 120.
9. J. Eyckmans and C. S. Chen, *J Cell Sci*, 2017, **130**, 63–70.
10. B. M. Ulmer, A. Stoehr, M. L. Schulze, S. Patel, M. Gucek, I. Mannhardt, S. Funcke, E. Murphy, T. Eschenhagen and A. Hansen, *Stem Cell Reports*, 2018, **10**, 834–847.
11. M. Lux, B. Andrée, T. Horvath, A. Nosko, D. Manikowski, D. Hilfiker-Kleiner, A. Haverich and A. Hilfiker, *Acta Biomater*, 2016, **30**, 177–187.
12. H. Vandenburgh, J. Shansky, F. Benesch-Lee, V. Barbata, J. Reid, L. Thorrez, R. Valentini and G. Crawford, *Muscle Nerve*, 2008, **37**, 438–447.
13. I.-C. Liao, J. B. Liu, N. Bursac and K. W. Leong, *Cellular and Molecular Bioengineering 2008 1:2*, 2008, **1**, 133–145.
14. Z. Chen, Q. Wang, M. Asmani, Y. Li, C. Liu, C. Li, J. M. Lippmann, Y. Wu and R. Zhao, *Scientific Reports 2016 6:1*, 2016, **6**, 1–11.
15. A. R. West, N. Zaman, D. J. Cole, M. J. Walker, W. R. Legant, T. Boudou, C. S. Chen, J. T. Favreau, G. R. Gaudette, E. A. Cowley and G. N. Maksym, *Am J Physiol Lung Cell Mol Physiol*, 2013, **304**, 4–16.
16. M. S. Sakar, J. Eyckmans, R. Pieters, D. Eberli, B. J. Nelson and C. S. Chen, *Nature Communications 2016 7:1*, 2016, **7**, 1–8.
17. Y. Ling, J. Rubin, Y. Deng, C. Huang, U. Demirci, J. M. Karp and A. Khademhosseini, *Lab Chip*, 2007, **7**, 756–762.
18. V. Chan, P. Zorlutuna, J. H. Jeong, H. Kong and R. Bashir, *Lab Chip*, 2010, **10**, 2062–2070.
19. S. v. Murphy and A. Atala, *Nature Biotechnology 2014 32:8*, 2014, **32**, 773–785.
20. R. Daniel Pedde, B. Mirani, A. Navaei, T. Styan, S. Wong, M. Mehrali, A. Thakur, N. Khadem Mohtaram, A. Bayati, A. Dolatshahi-Pirouz, M. Nikkhah, S. M. Willerth, M. Akbari, R. D. Pedde, B. Mirani, N. Khadem Mohtaram, M. Akbari, A. Navaei, M. Nikkhah, T. Styan, S. Wong, A. Bayati, S. M. Willerth, M. Mehrali, A. Thakur and A. Dolatshahi-Pirouz, *Advanced Materials*, 2017, **29**, 1606061.

21. M. Filippi, T. Buchner, O. Yasa, S. Weirich, R. K. Katzschmann, M. Filippi, T. Buchner, O. Yasa, S. Weirich and R. K. Katzschmann, *Advanced Materials*, 2022, **34**, 2108427.

22. Z. Li, J. Hui, P. Yang and H. Mao, *Biosensors 2022, Vol. 12, Page 370*, 2022, **12**, 370.

23. D. E. Ingber, *Nature Reviews Genetics 2022 23:8*, 2022, **23**, 467–491.

24. C. J. Demers, P. Soundararajan, P. Chennampally, G. A. Cox, J. Briscoe, S. D. Collins and R. L. Smith, *Development (Cambridge)*, 2016, **143**, 1884–1892.

25. C. Tu, B. Huang, J. Zhou, Y. Liang, J. Tian, L. Ji, X. Liang and X. Ye, *Micromachines 2017, Vol. 8, Page 1*, 2016, **8**, 1.

26. C. Su, Y. J. Chuah, H. B. Ong, H. M. Tay, R. Dalan and H. W. Hou, *Biosensors (Basel)*, 2021, **11**, 509.

27. U. N. Lee, J. H. Day, A. J. Haack, R. C. Bretherton, W. Lu, C. A. Deforest, A. B. Theberge and E. Berthier, *Lab Chip*, 2020, **20**, 525–536.

28. W. Tan and T. A. Desai, *Biomed Microdevices*, 2003, **5**, 235–244.

29. B. P. Casavant, E. Berthier, A. B. Theberge, J. Berthier, S. I. Montanez-Sauri, L. L. Bischel, K. Brakke, C. J. Hedman, W. Bushman, N. P. Keller and D. J. Beebe, *Proc Natl Acad Sci U S A*, 2013, **110**, 10111–10116.

30. A. Leonard, A. Bertero, J. D. Powers, K. M. Beussman, S. Bhandari, M. Regnier, C. E. Murry and N. J. Sniadecki, *J Mol Cell Cardiol*, 2018, **118**, 147–158.

31. S. Bremner, A. J. Goldstein, T. Higashi and N. J. Sniadecki, *Methods in Molecular Biology*, 2022, **2485**, 87–97.

32. W. P. Daley, S. B. Peters and M. Larsen, *J Cell Sci*, 2008, **121**, 255–264.

33. A. Lee, A. R. Hudson, D. J. Shiwarski, J. W. Tashman, T. J. Hinton, S. Yerneni, J. M. Bliley, P. G. Campbell and A. W. Feinberg, *Science (1979)*, 2019, **365**, 482–487.

34. M. A. Skylar-Scott, S. G. M. Uzel, L. L. Nam, J. H. Ahrens, R. L. Truby, S. Damaraju and J. A. Lewis, *Sci Adv*, , DOI:10.1126/SCIADV.AAW2459/SUPPL_FILE/AAW2459_SM.PDF.

35. C. Zuppinger, *Front Cardiovasc Med*, 2019, **6**, 87.

36. G. Vunjak Novakovic, T. Eschenhagen and C. Mummery, *Cold Spring Harb Perspect Med*, 2014, **4**, a014076.

37. M. L. Tomov, C. J. Gil, A. Cetnar, A. S. Theus, B. J. Lima, J. E. Nish, H. D. Bauser-Heaton and V. Serpooshan, *Curr Cardiol Rep*, 2019, **21**, 1–13.

38. J. S. Miller, K. R. Stevens, M. T. Yang, B. M. Baker, D. H. T. Nguyen, D. M. Cohen, E. Toro, A. A. Chen, P. A. Galie, X. Yu, R. Chaturvedi, S. N. Bhatia and C. S. Chen, *Nature Materials 2012 11:9*, 2012, **11**, 768–774.

39. M. J. J. van Velthoven, R. Ramadan, F. S. Zügel, B. J. Klotz, D. Gawlitta, P. F. Costa, J. Malda, M. D. Castilho, L. M. O. de Kort and P. de Graaf, *Tissue Eng Part C Methods*, 2020, **26**, 190–198.

40. A. Olanrewaju, M. Beaugrand, M. Yafia and D. Juncker, *Lab Chip*, 2018, **18**, 2323–2347.

Chapter 4: *home*RNA: a Self-Sampling Kit for the Collection and Stabilization of Blood RNA

Reproduced in part from A. J. Haack, F. Y. Lim*, D. S. Kennedy, J. H. Day, K. N. Adams, J. J. Lee, E. Berthier, A. B. Theberge, "*home*RNA: A Self-Sampling Kit for the Collection of Peripheral Blood and Stabilization of RNA." Analytical Chemistry, 2021, **93**, 13196-13203.*
** Equal contribution*

AJH and FYL designed and conducted the human subjects study with assistance from DSK, AJH designed, tested and engineered the stabilization tube with assistance from JHD, FYL conducted in lab experiments, JJL conducted preliminary work, KNA wrote and managed institutional review board applications, EB and ABT supervised the work and all authors interpreted the results.

Abstract: Gene expression analysis (e.g., targeted gene panels and transcriptomics) from whole blood can elucidate mechanisms of the immune function and aid in the discovery of biomarkers. Conventional venipuncture offers only a small snapshot of our broad immune landscape as immune responses may occur outside of the time and location parameters available for conventional venipuncture. A self-operated method that enables flexible sampling of liquid whole blood coupled with immediate stabilization of cellular RNA is instrumental in facilitating capture and preservation of acute or transient immune fluxes. To this end, we developed *home*RNA, a kit for self-collection of peripheral blood (~0.5 mL) and immediate stabilization of cellular RNA, using the Tasso-SST™ blood collection device with a specially designed stabilizer tube containing RNA*later*™. To assess the feasibility of *home*RNA for self-collection and stabilization of whole blood RNA, we conducted a pilot study (n = 47 participants) in which we sent *home*RNA to participants aged 21−69, located across 10 US states (94% successful blood collections, *n* = 61/65). Among participants who successfully collected blood, 93% reported no or minimal pain discomfort using the kit (*n* = 39/42), and 79% reported very easy/somewhat easy stabilization protocol (*n* = 33/42). Total RNA yield from the stabilized samples ranged between 0.20 and 5.99 μg (mean = 1.51 μg), and all but one RNA integrity number values were above 7.0 (mean = 8.1), indicating limited RNA degradation. The results from this study demonstrate the self-collection and RNA stabilization of whole blood with *home*RNA by participants themselves in their own home.

4.1 Introduction

Remote and contact-free laboratory testing is rapidly emerging as the new standard in patient care and clinical research, especially in light of the COVID-19 pandemic. However, blood sample collection remains a challenging procedure to perform remotely as venipuncture is resource-intensive, physically uncomfortable, and inflexible in regard to collection time and location. [1, 2] Remote self-administered blood collection, on the other hand, offers many practical advantages, including (1) expanded lab testing for rural and remote medicine applications (i.e., telemedicine), (2) convenience for clinical research studies as well as the ability to recruit participants that are not able to come to the clinic (due to work schedules, caregiver responsibilities, mobility challenges, etc.), (3) the ability to capture acute and transient biomarker fluxes (e.g., immediately following an acute exposure, an asthma attack, or a flare in an autoimmune disease), and (4) opportunities to conduct longitudinal research studies that require frequent sample collections from the same individual over a short time course (e.g., daily blood collections); to date, these applications have been limited due to the logistical challenges associated with in-person venipuncture. Here, we will describe *home*RNA: a new technology to enable at-home collection and stabilization of whole blood cellular RNA for gene expression analysis.

An important example of an existing technology aimed at remote blood sampling is the use of dried blood spot (DBS) sampling. In DBS sampling, a lancet-based finger prick is used to draw blood, which is applied to a sampling paper and left to dry. The sampling paper containing the DBS is then mailed back to the lab for analysis. [3] This technology has been applied to a variety of applications, including diagnostics and screening,4−9 therapeutic drug monitoring, [1,10,11] and other mechanistic biomolecule analysis. [12,13] Due to the increased use of DBS and convenience for remote sampling, tremendous research and development have been undertaken to improve the consistency and analysis of DBS samples. [5,14−16] In comparison to a DBS, a liquid blood sample can provide a larger volume of blood (>100 μL). An increased sample volume may be desirable for applications such as genomics, transcriptomics, or the detection of rare analytes. Further, if adequately stabilized, liquid samples may provide a greater quantity and better quality of the desired analyte than DBS samples, such as a higher yield of minimally degraded total whole blood

RNA. [17] Another burgeoning class of blood sample collection devices is lancet-based devices that collect from capillary beds in the arm. The user activates the lancet by pushing a button, which then causes blood to flow into a collection receptacle. [18−21] The Tasso-SST blood collection device used in this study falls under this category of sampling methods, along with the Seventh Sense biosampling device. [18−21] These devices collect larger volumes (>100 μL) than traditional finger-prick DBS sampling, and the sample is kept in a liquid form rather than dried on paper, which is ideal for analytics that require a higher volume liquid sample, such as transcriptomic analyses. Moreover, these devices are simple to use, and users report less pain while using these compared to a finger prick or traditional venipuncture. [18,19] However, lancet-based blood collection devices, such as the Tasso-SST, are more costly than a DBS sampling set up and require further stabilization of liquid blood for certain analytes such as RNA.

There is an obvious advantage to decentralizing blood collection beyond a phlebotomy clinic; consequently, there have been many technological advances in self-blood collection. However, blood collection is often only the first step in blood-based laboratory tests. In a traditional outpatient or research settings, after a phlebotomist draws blood, it is processed soon after in a lab by a technician. Blood is not a static tissue sample; it contains living cells that can continue reacting to changes in their ex vivo environment. Post collection sample handling is critical, and there have been numerous studies determining the best way to store, stabilize, and handle blood samples for various target analytes. [22−24] For transcriptomics profiling, RNA stabilization in liquid whole blood is particularly critical. Degradation of RNA by ribonucleases and rapid fluxes (induction and decay) of mRNA transcripts in response to the post collection ex vivo environment can be highly unfavorable for research intended to understand *in vivo* cellular expression landscapes. Further, these ex vivo changes can lead to an inaccurate representation of the *in vivo* transcriptome in question. [25, 26]

In a traditional outpatient venipuncture setting, stabilization of whole blood RNA is accomplished by collecting venous blood directly into vacutainers containing RNA stabilizers (e.g., Tempus or Paxgene) or immediately pipetting anticoagulated blood into RNA*later* containing vials. This procedure is incompatible with a self-sampling regime as users cannot be expected to pipette their own blood or do venipuncture into

a vacutainer tube on themselves. To fully enable remote sampling and transcriptomics profiling of liquid blood samples, one must eliminate the need for a phlebotomist-assisted blood draw and enable the patient or research participants to act as their own laboratory technician, allowing them to perform necessary steps to stabilize their blood sample without the use of pipettes, gloves, or syringes. In the present study, we accomplish this goal of both collection and RNA stabilization. We combine a commercially available lancet-based blood sampling device (Tasso-SST), a liquid RNA stabilizer (RNA*later*), and a custom-engineered fluid transfer and stabilizer tube into a single sampling unit that can be mailed to study participants. Participants collect a liquid sample (∼0.1−0.5 mL) of whole blood, stabilize it, and ship it back to the laboratory for analysis. To demonstrate our liquid stabilization technology, we chose to target total whole blood cellular RNA with RNA*later*. However, our technology is broadly generalizable in that a researcher interested in using a different stabilizer or targeting a different class of biomarkers can replace the stabilizer in the stabilizer tube with another liquid stabilizer.

To assess the usability and feasibility of this sampling methodology, we conducted a pilot study (n = 47 participants) to answer two fundamental research questions: (1) is the design and instructions for the kit comprehensive and user- friendly enough to allow users to collect and stabilize a sample of their own blood without in-person training? and (2) is the stabilization process sufficient to enable isolation of high-quality RNA suitable for standard gene expression analyses? In the pilot study, the *home*RNA kit was sent to 47 participants, aged between 21 and 69 and living across 10 different US states (WA, CA, CO, NE, WI, IN, PA, NY, MA, and ME). We demonstrated successful blood collection and RNA stabilization measured by total RNA yield and RNA integrity number (RIN). Additionally, we demonstrated expression analysis of two reference genes. Our kit and methodology open the potential for a new class of transcriptomics studies, enabling increased sampling frequency for longitudinal studies and access to populations that have been historically hard to reach.

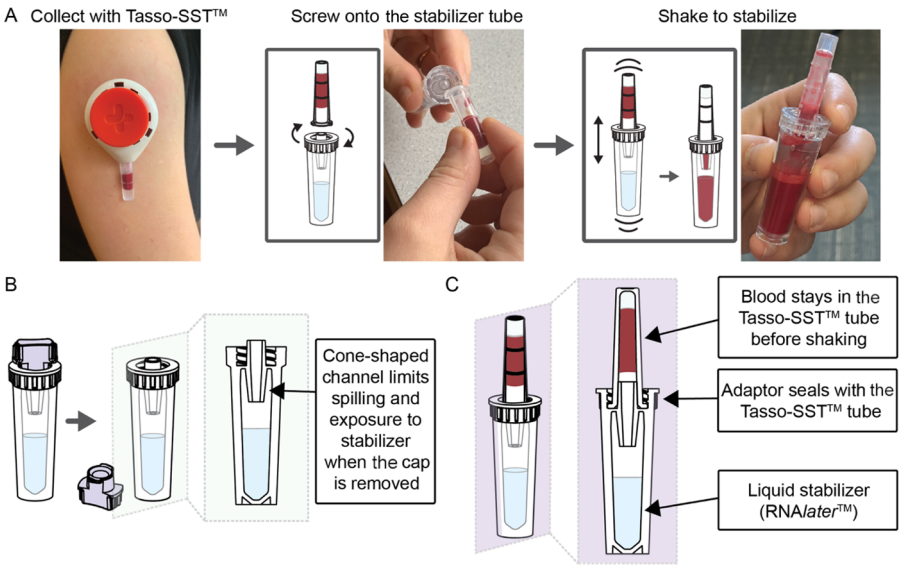

Figure 4.1. Workflow and design of *home*RNA blood collection and RNA stabilization kits. (A) Workflow for *home*RNA, where blood is first collected using the Tasso-SST, screwed on tightly to the stabilizer tube, and then shaken to mix with the stabilizer, RNA*later*. (B) Cross-sectional schematic of the stabilizer tube after the cap has been removed. (C) Cross-sectional schematic depicting a Tasso-SST blood collection tube filled with blood attached to the stabilizer tube, prior to shaking to mix the blood with the stabilizer.

4.2 Overarching design and considerations of the *home*RNA kit.

We developed *home*RNA to enable the self-collection of blood and immediate stabilization of RNA, an ability that opens new opportunities to probe immune responses to time- and location-specific stimuli outside of traditional venipuncture collection limitations. The two main components of *home*RNA include the Tasso-SST, which collects approximately 100−500 µL of blood from the upper arm and a stabilizer tube, designed to screw onto the detachable blood collection tube from the Tasso-SST device. Figure 4.1A summarizes the general workflow for collection and stabilization using *home*RNA. To operate the Tasso-SST, the device is first applied to the upper arm (Figure 4.1A), where it is held in place by an adhesive. The user then presses a red activator button deploying a lancet that quickly punctures the skin. Blood is then drawn into a detachable collection tube, which holds up to approximately 500 µL of blood. To stabilize the freshly drawn blood, the collection tube containing the blood is detached from the Tasso-SST device and screwed tightly onto the stabilizer tube, and the connected tubes are shaken to thoroughly mix the blood with the stabilizer. The stabilized blood sample is then packaged and mailed back to the lab for analysis.

The Tasso-SST was chosen as a method for blood collection due to its ability to be self-administered, its general ease of use, and the larger blood volume (>100 μL) it draws when compared to other devices in its category, making it suitable for applications requiring a greater amount of the starting material [e.g., RNA sequencing (RNA-Seq)]. Compared to other blood collection methods, users report lower pain thresholds when using the Tasso-SST or similar devices that collect from the upper arm. [18−21] The authors note that the serum separator tube (SST) gel (included in the Tasso-SST collection tube) is not necessary for RNA stabilization and analysis. In fact, a device or tube containing ethylenediamine- tetra acetic acid or another anticoagulant would be preferable to prevent clotting, and we note varying degrees of clotting observed in our returned samples. At the time of the study, the Tasso-SST was available for purchase. Therefore, it was chosen as the device to use as an initial proof of concept for demonstrating remote blood collection and RNA stabilization.

4.3 Design of the stabilizer tube.

The two primary design considerations for the stabilizer tube were (1) preventing exposure of the stabilizer solution and (2) preventing leaking or splashing when the blood and stabilizer solution are mixed. These design parameters are critical for home use, particularly to ensure that both the user's blood and stabilizer solution remain contained within the tubes throughout the stabilization process. To address these design problems, we designed (1) a spill-resistant stabilizer tube opening to mitigate user exposure (Figure 4.1B) and (2) an opening that seals tightly with the Tasso-SST (Figure 4.1C) to prevent leaking or splashing while mixing. Because of the small volume and shape (i.e., long and skinny) of the Tasso-SST blood collection tube, the blood sample remains in the tube even when it is inverted due to surface tension. This observation combined with a no-spill cone feature in the stabilizer tube allowed the user to easily tip the tubes sideways to connect them (Figure 4.1A) without causing either liquid (the stabilizer or the blood sample) to spill. However, the blood's tendency to remain in the Tasso-SST blood collection tube presented a nontrivial engineering challenge for mixing since to be stabilized, the blood needed to interface with the stabilizer liquid in the opposite tube (Figure 4.1C). However, when attached and shaken up and down, the

surface tension is broken as the two liquid interfaces (the blood and the stabilizer) come into contact, allowing for mixing. Because this mechanism for mixing required vigorous shaking across the two tubes' attachment point, a tight seal was critical. Leaking could also happen during the sample's return if the seal was inadequate. To achieve a tight seal, the stabilizer tube piece that attaches to the Tasso-SST collection tube was based on the design of the cap included with the Tasso-SST.

Surface tension was also utilized to design the opening of the stabilizer tube to achieve the first objective of preventing exposure to the stabilizer. The stabilizer tube was engineered with a fluidic cone-shaped channel at the connection point between the stabilizer tube and the Tasso-SST tube (Figure 4.1B). This fluidic cone takes advantage of surface tension to create a valve such that the stabilizer solution remains in the stabilizer tube when the tube is inverted. Figure 4.1 illustrates schematic cross sections of the stabilizer tube open (Figure 4.1B) and attached to the Tasso-SST collection tube (Figure 4.1C). The design of the stabilizer tube device was updated to facilitate easier mixing by altering the width of the opening at the bottom of the cone channel feature (Figure B4). The wider opening also enabled easier pipetting of the blood sample from the tube during processing. A new glue was also used to allow for easier fabrication. The new design and glue were used in the last two groups of participants (groups 6 and 7). Additional details on the design and fabrication of the stabilizer tube can be found in the Appendix B.

All components that comprised the stabilizer tube (tube, adapter, and cap) were injection-molded out of the same material (polycarbonate) to account for consistent material shrinkage during the injection molding process. Polycarbonate is commonly used in biological laboratory consumables and is known to be inert to most biological samples and reagents. Due to the nature of the injection molding process required for the adaptor piece (which included an internal thread feature), polystyrene and polypropylene, other commonly used materials in laboratory consumables, could not be used.

4.3 Stabilization of blood using RNA*later*

We assessed three RNA stabilizers commonly used in gene expression studies (Tempus, PAXgene, or RNA*later*) for both yield and quality of the total RNA isolated from stabilized blood samples over broad

storage conditions. Both Tempus and PAXgene are often used in blood gene expression studies due to the commercial availability of these stabilizers in vacutainer tubes, allowing for a direct drawing of venous blood into the stabilizers. On the contrary, RNA*later* is widely used to stabilize transcripts in laboratory specimens and extracted tissues but not commonly used in blood gene expression studies due to the lack of commercially available RNA*later* vacutainer tubes. However, since any RNA stabilizer can be put in the stabilizer tube in the *home*RNA kits, we were not limited to vacutainer tubes and therefore assessed all three common stabilizers for preserving transcripts from blood. We assessed these three stabilizers for both storage temperature and length, the two major variables that could significantly affect postcollection RNA yield and quality. In this study, we measured RNA quality with an RIN obtained on a Bioanalyzer 2100 coupled with its corresponding electropherogram profile. The RIN value is determined based on an algorithm that analyzes the electrophoretogram obtained from the capillary electrophoresis on the bioanalyzer chip. RIN values range from 1 to 10, where 10 represents entirely intact and nondegraded RNA. [27] Annotated examples of an electrophoretogram and digital gel obtained from one of the samples from this study are provided in the Appendix B in Figure B18. More information on the bioanalyzer, including examples of digital gels and electrophoretograms from samples with various RIN values can be found in the report by Schroeder et al. 2006. [27] This part of the study was performed in the lab using blood collected from venous draws so that we could expose blood samples collected from one donor to controlled temperatures for fixed periods.

Preliminary experiments showed that blood stabilized in RNA*later* offered comparable total RNA yield and highest RIN values (yield = 4.9 μg RIN = 8.4) compared to both Tempus (yield = 5.1 μg RIN = 7.1) and PAXgene (yield not detected, RIN = 1.0) after 7 days of storage at ambient temperature (Figure B5). Given these preliminary results, both RNA*later* and Tempus were assessed further for performance at a broader range of storage temperatures. As depicted in Figure 4.2 (see Figure B6 for electropherogram profiles), stabilization of blood using RNA*later* yielded better RIN values at higher temperatures. These parameters could be experienced with remote user-administered sampling methodologies. Further- more, the lack of corrosive (tartaric acid) and toxic (guanidine hydrochloride) stabilizing chemicals in RNA*later*

makes it an attractive choice for home-use or user-administered procedures. Due to high observed efficacy in stabilization for variable time and temperature profiles in our initial in-lab testing, coupled with user safety considerations, we chose to incorporate RNA*later* into the *home*RNA stabilizer tubes to accomplish stabilization of peripheral blood drawn with the Tasso-SST in the pilot study.

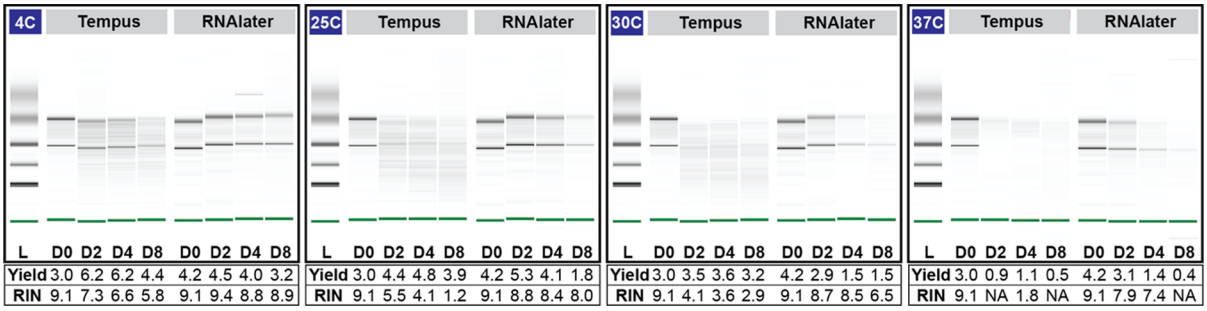

Figure 4.2. Performance of Tempus vs RNA*later* on total RNA yield and RNA quality. Effect of storage temperature and duration on total RNA yield (µg) and quality (RIN value) of samples stabilized in Tempus vs RNA*later*. Digital gel image of Tempus and RNA*later* stabilized blood stored at 4, 25, 30, and 37 °C over 8 days.

4.4 RNA returned from the *home*RNA kit reveals feasibility for disseminated sampling

We enrolled 47 participants in a pilot feasibility and usability study to demonstrate self-blood collection and RNA stabilization outside of a clinical or research setting. This study was approved by the University of Washington Institutional Review Board (IRB) under protocol STUDY00007868. All study procedures were performed after informed consent was obtained. The participants were asked to use either one or two *home*RNA kits each time they were sent kits, and some participants were sent kits on more than one occasion. With these considerations, 47 participants generated 60 samples. Details of which participants used one or two kits are given in the Appendix B (Table B3), and further details of which participants were included in two groups and how many samples came from each participant are included in the Appendix B dataset. *home*RNA kits were mailed to the participant's home where they collected, stabilized, and returned their own blood sample based solely on provided instructions in the kits and instructional video (see Appendix B). The stabilized samples were returned to the laboratory for analysis via mail. Therefore, they

had to remain stable throughout the shipping and the variability of temperature, pressure changes, and other mechanical stress inflicted during shipping.

Upon returning to the lab, total RNA was extracted from all stabilized blood samples and assessed for yield and quality (RIN values); 83% and 100% (n = 60 total samples) of blood samples returned from the pilot study offered a total RNA yield greater than 500 ng (a comfortable minimal cutoff value for large-scale transcriptomics analyses) and 100 ng (a comfort- able minimal cutoff value for expression analyses of a small panel of targeted genes), respectively (Figure 4.3A). These cutoff values for total yield obtained immediately after extraction may vary across studies depending on the choice of analysis methods [e.g., RT-PCR, digital droplet PCR (ddPCR), RNA- Seq, xMAP, and nCounter technologies] and preanalysis sample processing steps (e.g., globin depletion and RNA species enrichments) that will incur further yield losses. Based on our pilot study data, all self-drawn and self-stabilized peripheral blood samples using the *home*RNA blood kit offered sufficient yield for targeted small-gene panel profiling. The majority of the samples (83%, n = 50/60) also have sufficient yield for genome-wide transcriptional profiling analysis methods such as RNA-Seq.

We obtained RIN values for 85% of all isolated RNA (n = 51/60) samples (Figure 4.3B). We note that 15% (n = 9/60) of samples that were not scorable and did not afford a RIN value primarily due to the low total yield, resulting in low RNA concentrations in these samples (Figure B16). For samples that did not afford RIN values, a visual inspection of the digital gel images of these samples showed that 78% (n = 7/9) contain intact ribosomal RNA bands depicting good RNA integrity (Figure B17). The RIN values of all scorable RNA samples range between 6.8 and 9.6, with 53% (n = 27/51) of samples affording RIN values greater than or equal to 8.0 and all but one of the samples greater than 7.0 (n = 50/51) (Figure 4.3B). Similar to the minimum cutoff value for yield, RIN values and their suitability for downstream gene expression analyses vary widely based on the source of the tissue or sample from where the RNA is isolated. For example, formalin-fixed paraformaldehyde-embedded (FFPE) tissues and tissues containing high levels of ribonucleases (e.g., blood, liver, spleen, and kidney tissues) often afford lower RIN values due to the high degradation potential in these tissue types. A RIN value of 7.0 is the typical minimal cutoff value for

RNA-Seq applications. [17, 28] For highly degraded samples such as FFPE tissues that often have RIN values as low as 2.0, the fragment size distribution index (DV200) is frequently used to assess RNA quality and determine sample suitability for downstream gene expression analyses.29,30 Further, as there is interest in using RNA-Seq for lower yield or degraded samples (such as FFPE), there are many published techniques on methods to accomplish RNA-Seq in degraded samples. [28, 31] Despite whole blood being rich in ribonucleases, the remote self- collection and stabilization process of the *home*RNA blood kit still afforded high RIN values (RIN > 7.0) that, by themselves, render these samples suitable for a variety of gene expression analysis. Therefore, a DV200 index assessment was not necessary for assessment of these samples. The yield and quality of the RNA extracted from blood samples from our pilot study are well within the parameters for targeted small- gene panel profiling, and many of the samples even reach the higher thresholds set by sequencing facilities, conferring the convenience of outsourcing RNA-Seq for researchers interested in using our *home*RNA kit for their own out-of-clinic transcriptomics studies. Importantly, when compared to emerging remote self-sampling methodologies such as dried blood spotting, the *home*RNA collection process affords a better yield and quality that allows for a broader range of flexibility in analysis methodologies. [17, 32, 33]

Despite sufficient yield and high RIN values observed for the RNA samples isolated from the *home*RNA-stabilized blood, the presence of other residual chemical impurities that may have been introduced during the assembly process (e.g., the epoxy used for bonding) may affect downstream gene expression analyses. Thus, to further assess whether RNA isolated from *home*RNA-blood samples is compatible with downstream gene expression analysis protocols, expression of two reference genes (GAPDH and UBC) was measured from the isolated RNA samples (n = 23) using ddPCR. ddPCR was chosen as an analysis method due to its high protocol similarity to commonly used RT-PCR methods coupled with additional protocol requirements of maintaining droplet stability upon droplet generation. Select RNA samples with yield of 0.63− 5.44 μg and RIN values of 7.1−9.6 used for ddPCR analysis broadly represent the range of values for each of the two parameters observed in our pilot study. As shown in Figure B7, the mean values of total accepted droplets (TAD) for both GAPDH (TAD = 16,203; n = 23)

and UBC (TAD = 16,693; n = 22) reactions are comparable to that of the no-template control (TAD = 16,741; n = 4), suggesting that droplet stability is maintained throughout the amplification process. Both GAPDH and UBC depicted mean (SD) values of 4.1 × 103 (1.9 × 103) and 3.7 × 103 (1.6 × 103) copies/ng RNA- equivalent cDNA, respectively (Figure 4.3C). The variation in the observed copies can be attributed to biological variations in GAPDH and UBC gene expression within the study participants. Taken together, RNA yield, quality, and gene expression results obtained from *home*RNA blood RNA samples demonstrated successful preservation and expression analysis of blood mRNA transcripts from this user-operated home sampling methodology. Future studies on the use of the *home*RNA decentralized blood collection and stabilization technology to capture dynamic changes of immune responses to a variety of environmental stimuli and diseases will be of utmost interest to our group and the broader community.

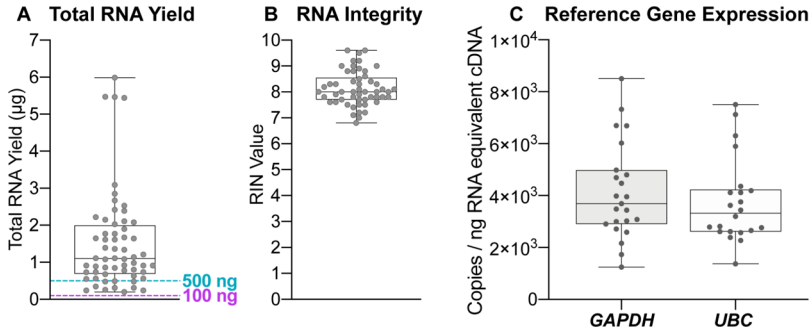

Figure 4.3. RNA yield and RIN value of peripheral blood samples self-collected and stabilized with *home*RNA. (A) Total RNA yield (µg), (B) RIN value, (C) droplet digital PCR of GAPDH and UBC from RNA isolated from peripheral blood samples collected and stabilized by participants in their home using *home*RNA.

4.5 Kit performance is robust across participant demography and mailing groups.

To assess the geographic distribution feasibility of this remote sampling methodology, *home*RNA blood kits were mailed from our lab (Seattle, WA) to various residential destinations in the West Coast, Midwest, and East Coast of the United States (Figure B8). Additionally, we mailed *home*RNA to various residential housing types in urban, suburban, and rural areas, including single-family unit houses and large multifamily apartmentcomplexes (where packages are typically held in the lobby or mail room). Demonstrating sampling from rural areas is important to expand research in places where participants traditionally needed to travel to phlebotomy labs located in other towns or cities. Such expansion would

enable research into immune events that may be more commonly triggered in rural populations, such as exposure to agricultural chemicals or wildfires.

*home*RNA kits were sent out in seven independent mailing groups from May to December 2020 (Table B3). Most kits were returned within 1−3 days after sample collection, but some kits were returned later, with one being returned as late as 15 days after collection (see Appendix B data set). Notably, this sample still yielded an RNA yield of 0.56 μg and a RIN value of 7.8, so even with over a 2 week delay, where the sample was in the mail, we recovered enough intact RNA for downstream analyses. From a usability perspective, differences between groups in terms of total RNA yield and RIN values were minimal (Figure B9), suggesting robustness to the remote sampling methodology afforded by the *home*RNA kit; slight variations in the instructions (e.g., changes in wording, updated graphics, and the inclusion of an instruc- tional video) did not dramatically change results, suggesting that the kit itself was relatively simple and intuitive to use. Finally, the RNA quality analysis parameters (total RNA yield and RIN values) were not markedly different across a range of age groups (Figure B10), gender (Figure B11), or body mass index (BMI) (Figure B12). Reported blood levels (which we use as an approximation for the volume collected) also were not markedly different between different ages, genders, or BMI (Figure B13), indicating consistency in blood collection with the Tasso-SST regardless of the participant demographic or BMI. While we demonstrated robustness across these parameters, we note that the pilot study did not collect information on participants' socioeconomic status or level of education. For future studies, we intend to evaluate the usability of the *home*RNA kit across a more diverse population and in geographical regions or during seasons that can incur more considerable variations in the high/low ambient temperatures as a notable limitation in our geographical sample set is that kits were not mailed to the hotter regions of the United States (e.g., the Southwest or South) during the summer months, and the majority of the samples were taken from the Seattle region; we are addressing this limitation in our ongoing studies.

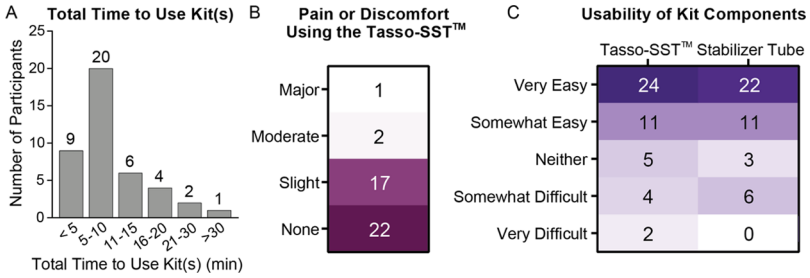

Figure 4.4. Survey responses to assess kit usability. (A) Histogram showing total self-estimated time required for each participant to use the kit from start to finish. (B) Participant ratings for the level of pain or discomfort using the Tasso-SST. Numbers represent the number of participants. (C) Participant ratings for the usability of the different kit components. Numbers represent the number of participants.

4.6 Participant survey responses indicate good usability of *home*RNA.

Ease of use and participant perception is critical for compliance, particularly for using this method in future longitudinal (multisample) studies. Usability was assessed through a user experience survey that the participants were asked to complete after using the kits. This survey was also used as a mechanism for feedback from the participants in order to iterate upon the instructions and kit components. Perception of the kits in terms of the time it takes to complete it, ease of use, and pain or discomfort was assessed (Figure 4.4). Metrics for measuring the performance of the kit were also assessed, including asking the participants to estimate how much blood was collected and the time the Tasso-SST was left on the arm as an approximation for the blood collection time (Figure 4.5).

Most of the participants who successfully collected blood using the Tasso-SST finished using their kits in less than 10 min (69%, n = 29/42, Figure 4.4A). Nearly all participants (93%, n = 39/42) reported either minimal pain or discomfort or no pain or discomfort while using the Tasso-SST, and the majority (52%, n = 22/42) reported no pain or discomfort.

Only three participants found the pain or discomfort to be rated as moderate (n = 2) or major (n = 1). Regarding the participant's perception of how easy the kits were to use, most of the participants reported the Tasso-SST and stabilizer tube to be easy to use or somewhat easy to use (76%, n = 35/46 and 79%, n = 36/42 for the Tasso-SST and stabilizer tube, respectively). Participants with close proximity to the project were excluded from this analysis; participants who failed to collect blood were excluded from the pain and

stabilizer tube usability but were included in the usability for the Tasso-SST (4 out of 47 total enrollment). In summary, feedback with regards to the pain experienced and usability was positive.

4.7 *home*RNA stabilized blood show sufficient RNA yield at a low sample volume.

To assess the possible correlation between estimated blood collection volume and total RNA yield, the participants were asked to estimate the levels of blood drawn into the Tasso-SST blood collection tube based on a provided blood tube image (depicted in Figure 4.5A(ii)). Estimated volumes for the four levels are as follows: level 1 = 100 µL, level 2 = 200 µL, level 3 = 300 µL, and level 4 > 400 µL. The majority of the participants reported blood collection at level 4 (52% n = 34/ 65). The reported blood level versus the RNA yield is plotted in Figure B14A. While there are very few samples at lower reported blood levels (level 1 and 2), there does not appear to be a strong correlation between the blood level reported and yield. This could be due to inaccuracies in reporting by participants, individual variability in RNA yield, or loss during the sample processing or blood clotting in the stabilizer tube. Notably, participants who reported collecting a low volume (level 1 ~100 µL) of blood still had RNA yields > 100 ng, with one sample as high as 2.85 µg. We have also included data on blood collection time, reported blood volume, and RNA yield in the Appendix B (Figures B14B and B15). In short, all collections, irrespective of the reported collection levels, afforded RNA yield sufficient for downstream gene expression analyses.

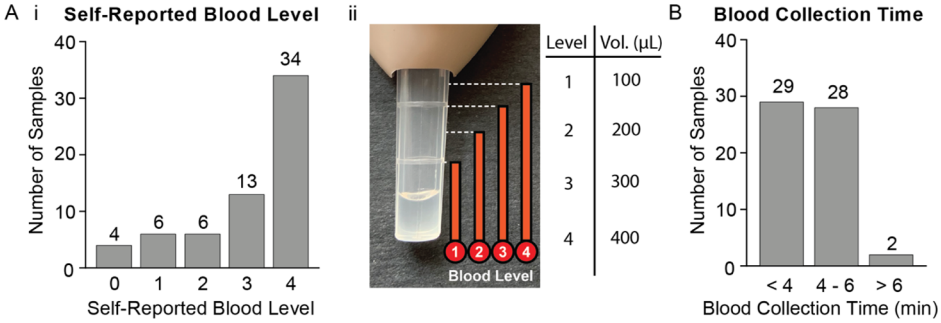

Figure 4.5. Survey responses to assess kit performance. (A) (i) Participant responses when asked to estimate the approximate blood level they filled the Tasso-SST blood collection tube based on the (ii) picture provided in the online survey. The volumes corresponding to each level are noted in (A(ii)). (B) Participant responses when asked how long they left the Tasso-SST blood collection tube on their arm this includes time before collection and after collection has stopped before removal of the device.

4.8 Conclusion

Our *home*RNA kit will enable translational researchers to ask fundamentally different biological and clinical questions than have to date been limited to clinic-based transcriptomics. Given the flexibility of this sampling system and low sample volume compared to venipuncture, future studies involving frequent sampling and sampling around a specific event (e.g., disease flare, environmental, or pathogen exposure) can be employed to better elucidate hard-to-capture expression signatures of the immune response. For example, we hope that our sampling platform enables us to observe and study early, transient, and dynamic changes in both the innate and adaptive arm of the immune system throughout the various stages of an infection in order to guide treatment or transmission control measures.

Critically, with *home*RNA, multiple samples can be taken from the same individual outside an in-patient setting more readily than with current methods, enabling easier comparison to an individual's own baseline. Coupling this with the ability to sample virtually anywhere, studies into a person's individualized response (i.e., compared to their own baseline) to an exposure or event in their daily environment are possible. Finally, we are excited to expand this technology to disseminated diagnostics, therapeutics, and clinical research into lower-resource or rural settings, which are often far from a phlebotomy clinic.

4.9 Materials and methods

Development and assembly of the *home*RNA blood collection and stabilization kit

Design process for the RNA stabilizer tube: The RNA stabilizer tube is assembled from three individual components: 1) a reagent vial to house the liquid stabilizer 2) an adaptor that interfaces both the reagent vial and the Tasso-SST blood tube and 3) a vial closure cap. Preliminary design iterations were generated on SolidWorks and 3D printed on a Form 3 3D printer (Formlabs) using clear resin (Formlabs). These preliminary designs were evaluated for leakage and spillage when tipped over or agitated. The mechanical agitation of shipping was simulated by placing the tube designs filled with water in a box and shaking. Designs were also tipped over without caps on to evaluate if fluid would easily spill out of the tube if an end user were to accidentally tip them over. The tubes were then inspected for leaking or spilling. The cone-

shaped channel design, which was ultimately used, performed notably better on leaking and spilling metrics in both the simulated shipping and knocking over tests, compared to a straight channel shape, or an inverted cone shaped channel where the opening on the bottom was wider than the top. The design of the adaptor piece was altered partway through the study (between group 5 and 6) to allow for easier mixing by increasing the diameter of the cone feature (Figure B4). The increased diameter also allowed for easier pipetting of the returned blood sample; the blood sample could be safely pipetted using a polypropylene Pasteur pipette (CELLTREAT) with a 2 mL manually adjustable pipette (Socorex) and a Pasteur pipette adaptor (DWK Life Sciences). Specific features of the stabilizer tube design include a cone channel feature in the adaptor piece (Figure 4.1B) to prevent contact between stabilizer reagent and the user during blood stabilization.

Design considerations for injection molding of the RNA stabilizer tube: Both tube designs were injection molded out of polycarbonate (PC: Makrolon 2407) by Protolabs, Inc (Maple Plain, MN). Several design considerations were optimized to include features important for the process of injection molding. Briefly these include, 1) adding a 2 degree draft to all vertical surfaces on all parts to allow for easier removal of the part from the mold, 2) thickening of the adaptor and vial piece to allow for mold ejection pin zones, 3) designing the shape of the cap piece to avoid overhangs, allowing for a two piece mold, and 4) designing the internal threads on adaptor piece, such that it required only a quarter turn to remove from the mold. Polycarbonate was chosen as the material for all three pieces as a consideration for constant material shrinkage, as the parts needed to fit together. Polycarbonate was chosen over other commonly used plastics due to the constraint on material caused by the internal thread feature in the adaptor piece; we note that polycarbonate is also a common material for biochemical samples containers.

Fabrication of the RNA stabilizer tube: For assembly, all components of the stabilizer tube are first cleaned via sonication in 70% ethanol (v/v) for 30 min and air dried. The adaptor was bonded onto the reagent vial using a UV curing glue (Damn Good® for the first 5 groups and Dymax MD® 1450-M-UR-SC for groups 6 and 7, Figure B3). The Dymax UV curing glue was ultimately chosen for the last iteration due to several design considerations. It has a lower viscosity making it suitable for fluid manipulation with a standard

micropipette, enabling faster and more consistent manual application of the glue to the bonding line. Further, the Dymax glue contains a color change indictor to aid in visualization for curing. Bonded parts were cured for 60 min at 395-405 nm UV Lamp (Quans) for all tubes used in all groups. The stabilizer tube was filled with 1.4 mL of RNA*later* (Thermo Fisher) as the stabilizing reagent, capped, and checked for leakage due to bonding defects before distribution to study participants. We did not observe any bonding defect leakage in tubes prepared for this study. RNA stabilizer tubes used in the feasibility pilot study were prepared within a week of being mailed to study participants.

Evaporative loss from stabilizer tubes: To assess evaporative loss, 8 stabilizer tubes were filled with 1.4 mL of RNA*later* and capped and left at room temperature for 8 weeks. Tubes were massed during initial setup before and after addition of RNA*later*, and were subsequently massed at week 1, 2, 3, 4, 5, and 8 (Figure B19). Less than 1% loss of RNA RNA*later* mass occurred in all 8 tubes at the 1-week timepoint, and therefore a week was chosen as the cutoff as experiments on evaporation of RNA*later* from prepared and capped tubes indicated less than 1% evaporative loss (Figure B19); in subsequent work, we have found that tubes filled with RNA*later* can be kept for 4 weeks while still allowing <5% v/v evaporative loss of RNA*later* (our 1-week cutoff in this study is unnecessarily stringent).

Kit components and assembly: All components included in the *home*RNA blood kit are listed in Table B1 and shown in Figure B1. The RNA stabilizer tube was labeled with a unique sample code and packaged into a transport bag with an absorbent material. A heat pack was included to increase blood flow to the upper arm (Medline). The stabilizer tube insert was designed to immobilize the stabilizer vial containing blood in a 50 mL conical tube during transport. The insert was designed on SolidWorks and 3D printed on a Form 3 3D printer (Formlabs) using clear resin. All kit components were placed in a rigid custom design mailer box fabricated via die-cutting (The BoxMaker, Inc.). A temperature strip (Propagate Pro) was affixed onto the outer side of the mailer box for temperature recording by study participants. A mailer bag with pre-printed return shipping label was also included with the outgoing package for specimen return to the lab. In brief, iterations were made to improve overall usability of the kit and clarity of the instructions for use. We included the final version of the instructions for use (IFU) at the end of this document.

RNA stabilization and isolation: For in-lab RNA stabilization experiments, fresh (< 8 hours post blood draw) whole venous blood drawn into EDTA-coated vacutainers (BD) was purchased from Bloodworks Northwest (Seattle, WA). Upon receipt, anti-coagulated whole blood was promptly transferred into either Tempus™, PAXgene®, or RNA*later*™ stabilizing reagents at their manufacturer's recommended stabilizer:blood ratios (v/v) of 2:1, 2:1, and 2.6:1 respectively. Stabilized blood was then incubated at various temperature ranges (4˚C, ambient, 30˚C, and 37˚C) and for a range of time periods (0-8 days) specific to each experiment as described in the results. At the end of the incubation period, total RNA was isolated from Tempus, PAXgene, and RNA*later* stabilized blood using Tempus Spin RNA Isolation Kit (Thermo Fisher), PAXgene, Blood RNA Kit (PreAnalytiX), and Ribopure - Blood RNA Isolation Kit (Thermo Fisher), respectively, according to manufacturer's protocol, and eluted in 50-100 µL volume.

For the at-home blood collection and stabilization feasibility study, Tasso-SST collected blood was stabilized in RNA*later* by the human subjects using the RNA stabilizer tube that interfaces with the Tasso-SST blood tube (Figure B2). Total RNA was isolated using the Ribopure™ - Blood RNA Isolation Kit (Thermo Fisher) according to manufacturer's protocol and eluted in 50-100 µL volume. RNA concentrations were obtained on a NanoDrop® ND-1000 spectrophotometer (Thermo Scientific). RNA integrity number (RIN) values were obtained on a Bioanalyzer 2100 (Agilent) using the RNA 6000 Nano Kit (Agilent) following the manufacturer's protocol. Initially, 1 µL of isolated RNA was added to the bioanalyzer chip to obtain a RIN value as described by the manufacturer's protocol. If a RIN was not obtained the sample was run again with 2 µL of isolated RNA. Details as to which RIN values were obtained with 1 µL or 2 µL are located in the supplemental dataset file included in the supplemental material in Haack, Lim 2021 [34]. Details on interpreting bioanalyzer data can be found in Schroeder et al.2006, [1] and a figure annotating the main components of an electrophoretogram profile and digital gel electrophoresis image of one of the samples collected in this study can be found in Figure B18. Isolated RNA was stored at -80oC until ready for further analyses.

Digital droplet PCR analysis: 1-3 µg of isolated RNA was digested with DNaseI (NEB) and 0.5 – 1.0 µg of DNA-free RNA was reverse transcribed into cDNA using Bio-Rad iScriptTM cDNA Synthesis Kit

(#1708891) according to manufacturer's protocol. ddPCRTM reactions were carried out in a total volume of 20 µL containing 10 µL of Bio-Rad 2X QX200TM ddPCRTM Evagreen ddPCRTM Supermix (#1864034), 25 ng of RNA-equivalent cDNA, and 180 nM of both forward and reverse primers (IDT). Primer sequences of both reference genes (GAPDH and UBC) analyzed in this study are listed in Table B4. Droplets were generated from the above reaction on a QX200TM droplet generator (Bio-Rad) using Bio-Rad QX200TM Droplet Generation Oil for Evagreen (#1864005) and Bio-Rad DG8TM cartridge (#1864008) and gasket (#1863009). 40 µL of the droplet suspensions were transferred to a Bio-Rad ddPCRTM 96-well semi-skirted plate (#12001925), sealed on a PX1TM (Bio-Rad) with a pierceable foil heat seal (#1814040) and cycled on a C1000 TouchTM 96-deep well reaction module thermal cycler (Bio-Rad). Thermal cycling conditions were as follows: initial denaturation and enzyme activation (95 oC, 5 mins), 40 cycles of denaturation (95 oC, 30 sec) followed by annealing and extension (55 oC, 1 min) at a 2 oC / sec ramp rate, signal stabilization (4 oC, 5 min) and enzyme deactivation (90 oC, 5 min), and finally held at 4 oC indefinitely. After PCR amplification, cycled droplets were read promptly on a QX200TM Droplet Reader (Bio-Rad). Extraction of raw fluorescence amplitude data, quantification of positive/negative droplets, and droplet visualization were performed using Bio-Rad's QuantaSoftTM software.

Pilot study: feasibility and usability assessment of the *home*RNA kit

Participant characteristics: This study was approved by the University of Washington Institutional Review Board (IRB) under protocol STUDY00007868. All study procedures were performed after informed consent was obtained. A total of 47 healthy volunteers between ages 21-69 years old were recruited via word of mouth or email to participate in the pilot study.

Human subjects study design: General study design: Study participants were enrolled in groups in order to iterate on the general usability of the *home*RNA kit, specifically on the kit components and the clarity of the IFU (Table B2). The study enrolled a total of five groups. In each group, participants were asked to self-collect and stabilize blood from their upper arm using the *home*RNA blood collection and stabilization kit. Each participant was also asked to complete a user experience survey that was designed to guide further

improvements to kit components and sampling parameters (e.g., ease of use, clarity of the IFU, mailing logistics, ambient temperature at collection site, etc.) Based on feedback, improvements were implemented in subsequent groups. Participants were asked to package their stabilized blood samples to be returned to the lab for analysis using the provided return mailer bag. Except for samples from group 1, where samples were picked up by the study team, all stabilized blood samples were mailed using next day delivery courier services (UPS). Unless specified, returned samples are stored at -20oC until ready for RNA extraction. Study data were collected and managed using REDCap electronic data capture tools2 hosted at the Institute of Translational Health Sciences. REDCap (Research Electronic Data Capture) is a secure, web- based application designed to support data capture for research studies, providing: 1) an intuitive interface for validated data entry; 2) audit trails for tracking data manipulation and export procedures; 3) automated export procedures for seamless data downloads to common statistical packages; and 4) procedures for importing data from external sources.

Group-specific study design: In order to assess effect(s) of storage length on total RNA yield and quality, participants in groups 1 (n = 4) and 2 (n = 5) and 7 (n = 5) were given two *home*RNA kits to be used, one on each arm. Participants were instructed to use the second kit promptly upon completion of the first kit and to complete a user experience survey. For group one and two, one vial of stabilized blood from each participant was frozen at -20oC immediately upon return to the lab, while the other was stored at ambient temperature for an additional three days prior to RNA extraction. Participants in groups 3-6 were given one *home*RNA kit and asked to perform the collection and stabilization procedure and complete a user experience survey. The first three groups were recruited locally (greater Seattle area) as well as group 6. To assess feasibility of the sampling pipeline across a wider geographical distribution, individuals from across the contiguous United States were recruited as participants for groups 4 (n = 13), 5 (n = 16) and 7 (n = 5). Some participants were included in two groups. Specific information as to which participants were included in which groups as well as how many collected samples came from each individual can be found in the supplemental dataset in Haack, Lim, et al.[34]. Taking into account participants completing two samples in one group and participant inclusion in two groups, 47 participants yielded 60 samples.

Inclusion and exclusion criteria for subject enrollment: Inclusion criteria included aged 18-75 years, between 105 - 230 lbs for those assigned female at birth and 135 - 250 lbs for those assigned male at birth. Exclusion criteria included pregnant individuals or those currently breastfeeding, individuals with skin disorders such as scabbing or psoriasis located on the upper arm, individuals with a blood platelet or coagulation disorder, or currently taking any blood platelet or anticoagulant medications, individuals who are immunosuppressed or taking any immunosuppressive medication, or individuals who reside in a correctional facility.

Recruitment and enrollment of subjects: Subjects were recruited by word of mouth, email, or posts on digital platforms advertising the study and invited to follow a link to a pre-screening survey which asked questions about the inclusion and exclusion criteria. A study team member then called the subject to confirm they met the inclusion and exclusion criteria and to answer any questions about the study. After signing an informed consent form on DocuSign, subjects enrolled into the study with an online form.

User experience survey: Subjects were asked to fill out a user experience survey after using their kit. The survey included questions about the timing in which they use the kit, the ambient temperature during use of the kit, the volume of blood collected based on how visually full the Tasso-SST blood tube was, and asked participants to rate their experience using the kit and provide any additional feedback on the kit or the process of receiving and returning the kit.

Instructions for Use: The final version of the instructions for use (IFU) is found at the end of appendix B. The IFU version published here was not used with any of the 7 sample groups, but rather the most mature version that was developed based on user feedback from the pilot study. The IFU was also designed by the authors of this study based in part on images from www.tassoinc.com available at the time of our study. These IFU are for the *home*RNA kit only and are not vetted by Tasso Inc.

Instructional video: Some groups (4-7) had the option to access an instructional video (linked to a QR code on their IFU). This is a 4 minute and 10 second video which features a member of our research group demonstrating proper use of the blood sampling and RNA stabilization kit. There is a voice-over narration

describing each step in detail. The QR code in the posted IFU links to the video and a link to the video can also be found here: https://youtu.be/iV3GZ8SmmuM

4.10 References

1. L. C. Martial, R. E. Aarnoutse, M. F. Schreuder, S. S. Henriet, R. J. M. Brüggemann, and M. A. Joore, *PLoS One*, 2016, **11**, e0167433.
2. C. A. James, M. D. Barfield, K. F. Maass, S. R. Patel and M. D. Anderson, *Nat. Med*, 2020, **26**, 1810.
3. P. Martinez and S. E. Zemore, *Addiction*, 2019, **114**, 1303−1308.
4. T. Prinsenberg, S. Rebers, A. Boyd, F. Zuure, M. Prins, M. van der Valk and J. Schinkel, *PLoS One*, 2020, **15**, e0231385.
5. C. Klumpp-Thomas, H. Kalish, M. Drew, S. Hunsberger, K. Snead, M. P. Fay, J. Mehalko, A. Shunmugavel, V. Wall, P. Frank, J. P. Denson, M. Hong, G. Gulten, S. Messing, J. Hicks, S. Michael, W. Gillette, M. D. Hall, M. J. Memoli, D. Esposito and K. Sadtler, *Nat. Commun.*, 2021, **12**, 113.
6. S. M. Lofgren, A. B. Morrissey, C. C. Chevallier, A. I. Malabeja, S. Edmonds, B. Amos, D. J. Sifuna, L. von Seidlein, W. Schimana, W. S. Stevens, J. A. Bartlett and J. A. Crump, *AIDS*, 2009, **23**, 2459− 2466.
7. S. Vázquez-Morón, B. Ardizone Jiménez, M. A. Jiménez-Sousa, J. M. Bellón, P. Ryan and S. Resino, *Sci. Rep.*, 2019, **9**, 7316.
8. M. D. Lim, *Am. J. Trop. Med. Hyg.*, 2018, **99**, 256−265.
9. J. Crossle, R. B. Elliot and P. Smith, *Lancet*, 1979, **313**, 472−474.
10. L. M. Geers, D. Cohen, L. M. Wehkamp, K. van Hateren, R. A. Koster, O. Y. Fedorenko, A. V. Semke, N. Bokhan, S. A. Ivanova, J. G. W. Kosterink, A. J. M. Loonen and D. J. Touw, *J. Clin. Psychiatry*, 2017, **78**, e1211– e1218.
11. T. Gaissmaier, M. Siebenhaar, V. Todorova, V. Hüllen and C. Hopf, *Analyst*, 2016, **141**, 892−901.
12. A. Koulman, P. Prentice, M. C. Y. Wong, L. Matthews, N. J. Bond, M. Eiden, J. L. Griffin and D. B. Dunger, *Metabolomics*, 2014, **10**, 1018−1025.
13. O. P. Trifonova, D. L. Maslov, E. E. Balashova and P. G. Lokhov, *Metabolites*, 2019, **9**, 277.
14. L. A. Leuthold, O. Heudi, J. Déglon, M. Raccuglia, M. Augsburger, F. Picard, O. Kretz and A. Thomas, *Anal. Chem.*, 2015, **87**, 2068−2071.
15. K. Li, J. C. Naviaux, J. M. Monk, L. Wang and R. K. Naviaux, *Metabolites*, 2020, **10**, 82.
16. K. Malsagova, A. Kopylov, A. Stepanov, T. Butkova, A. Izotov and A. Kaysheva, *Diagnostics*, 2020, **10**, 248.
17. M. J. Reust, M. H. Lee, J. Xiang, W. Zhang, D. Xu, T. Batson, T. Zhang, J. A. Downs and K. M. Dupnik, *Am. J. Trop. Med. Hyg.*, 2018, **98**, 1541−1546.
18. A. Catala, R. Culp-Hill, T. Nemkov, A. D'Alessandro, *Metabolomics*, 2018, **14**, 100.

19. T. M. Blicharz, P. Gong, B. M. Bunner, L. L. Chu, K. M. Leonard, J. A. Wakefield, R. E. Williams, M. Dadgar, C. A. Tagliabue, R. El Khaja, S. L. Marlin, R. Haghgooie, S. P. Davis, D. E. Chickering and H. Bernstein, *Nat. Biomed. Eng.*, 2018, **2**, 151−157.

20. B. Roadcap, A. Hussain, D. Dreyer, K. Carter, N. Dube, Y. Xu, M. Anderson, E. Berthier, F. Vazvaei, K. Bateman and E. Woolf, *Bioanalysis*, 2020, **12**, 893−904.

21. M. N. Fedoruk, *Bioanalysis*, 2020, **12**, 715−718.

22. L. A. Matheson, T. T. Duong, A. M. Rosenberg and R. S. M. Yeung, *J. Immunol. Methods*, 2008, **339**, 82−89.

23. N. Duale, G. Brunborg, K. S. Rønningen, T. Briese, J. Aarem, K. K. Aas, P. Magnus, C. Stoltenberg, E. Susser and W. Lipkin, *I. BMC Res. Notes*, 2012, **5**, 510.

24. A. Gautam, D. Donohue, A. Hoke, S. A. Miller, S. Srinivasan, B. Sowe, L. Detwiler, J. Lynch, M. Levangie, R. Hammamieh and M. Jett, *PLoS One*. 2019, **14**, No. e0225137.

25. L. Opitz, G. Salinas-Riester, M. Grade, K. Jung, P. Jo, G. Emons, B. M. Ghadimi, T. Beissbarth and J. Gaedcke, *BMC Med. Genomics*, 2010, **3**, 36.

26. A. T. Bender, B. P. Sullivan, L. Lillis and J. D. Posner, *J. Mol. Diagn.*, 2020, **22**, 1030−1040.

27. A. Schroeder, O. Mueller, S. Stocker, R. Salowsky, M. Leiber, M. Gassmann, S. Lightfoot, W. Menzel, M. Granzow, T. Ragg, *BMC Mol. Biol.*, 2006, **7**, 3.

28. B. Xiong, Y. Yang, F. R. Fineis and J. P. Wang, *Genome Biol.*, 2019, **20**, 75.

29. T. Matsubara, J. Soh, M. Morita, T. Uwabo, S. Tomida, T. Fujiwara, S. Kanazawa, S. Toyooka, and A. Hirasawa, *BioMed Res. Int.*, 2020, **2020**, 9349132.

30. I. Wimmer, A. R. Tröscher, F. Brunner, S. J. Rubino, C. G. Bien, H. L. Weiner, H. Lassmann and J. Bauer, *Sci. Rep.*, 2018, **8**, 6351.

31. S. Schuierer, W. Carbone, J. Knehr, V. Petitjean, A. Fernandez, M. Sultan and G. Roma, *BMC Genomics*, 2017, **18**, 442.

32. P. A. Combs and M. B. Eisen, *Peer J*, 2015, **3**, e869.

33. T. W. McDade, K. M. Ross, R. L. Fried, J. M. G. Arevalo, J. Ma, G. E. Miller and S. W. Cole, *Biodemogr. Soc. Biol*., 2016, **62**, 182−197.

34. A. J. Haack, F. Y. Lim, D. S. Kennedy, J. H. Day, K. N. Adams, J. J. Lee, E. Berthier and A. B. Theberge, *Anal. Chem.*, 2021, **93**, 13196–13203.

Chapter 5: At-home blood collection and stabilization in high temperature climates using *home*RNA

Reproduced in part from L.G. Brown, A. J. Haack*, D. S. Kennedy, K. N. Adams, J. E. Stolarczuk, M. G. Takezawa, E. Berthier, S. Thongpang, F. Y. Lim, D. Chaussabel, M. Garand, and A. B. Theberge, "At-home blood collection and stabilization in high temperature climates using* home*RNA" Frontiers in Digital Health, 2022, **4**, 903153.*
** Equal contribution*

LGB, AJH, EB, ST, DC, MG, and ABT contributed to the conception and design of the study. AJH, DSK, FYL, EB, and ABT developed home*RNA and the protocols implemented in home sampling in this manuscript. AJH, DSK, KNA, JS, and MGT conducted/contributed to the human subjects research with participants in the Western and South Central USA. DC and MG conducted the human subjects research with participants in Doha, Qatar. LGB, AJH, and MG performed the RNA extractions on samples and collected the RIN and yield data. LGB, AJH, JS, MGT, FYL, EB, ST, DC, MG, and ABT analyzed/interpreted the data. LGB, AJH, MG, and ABT prepared the figures and wrote the manuscript. All authors contributed to the article and approved the submitted version.*

Abstract: Expanding whole blood sample collection for transcriptome analysis beyond traditional phlebotomy clinics will open new frontiers for remote immune research and telemedicine. Determining the stability of RNA in blood samples exposed to high ambient temperatures (>30°C) is necessary for deploying home-sampling in settings with elevated temperatures (e.g., studying physiological response to natural disasters that occur in warm locations or in the summer). Recently, we have developed *home*RNA, a technology that allows for self-blood sampling and RNA stabilization remotely. *home*RNA consists of a lancet-based blood collection device, the Tasso-SST which collects up to 0.5 ml of blood from the upper arm, and a custom-built stabilization transfer tube containing RNA*later*. In this study, we investigated the robustness of our *home*RNA kit in high temperature settings via two small pilot studies in Doha, Qatar (no. participants = 8), and the Western and South Central USA during the summer of 2021, which included a heatwave of unusually high temperatures in some locations (no. participants = 11). Samples collected from participants in Doha were subjected to rapid external temperature fluctuations from being moved to and from air-conditioned areas and extreme heat environments (up to 41°C external temperature during brief temperature spikes). In the USA pilot study, regions varied in outdoor temperature highs (between 25°C and 43.4°C). All samples that returned a RNA integrity number (RIN) value from the Doha, Qatar group had a RIN ≥7.0, a typical integrity threshold for downstream transcriptomics analysis. RIN values for the Western and South Central USA samples (n = 12 samples) ranged from 6.9–8.7 with 9 out of 12 samples

reporting RINs ≥7.0. Overall, our pilot data suggest that *home*RNA can be used in some regions that experience elevated temperatures, opening up new geographical frontiers in disseminated transcriptome analysis for applications critical to telemedicine, global health, and expanded clinical research. Further studies, including our ongoing work in Qatar, USA, and Thailand, will continue to test the robustness of *home*RNA.

5.1 Introduction

Blood is a useful biofluid for transcriptome analysis, as it is relatively non-invasive to obtain and provides ample information for biomarker identification and analysis [1]. Consequently, whole blood RNA transcript analysis has emerged as an avenue for realizing the goals of personalized medicine [2, 3]. Key biomarkers discovered through blood transcriptomic studies have potential applications in novel therapeutics and diagnostics [4–8] and have provided new avenues for disease monitoring of chronic [9, 10], autoimmune [11, 12], and infectious diseases [13]. By combining home-sampling technologies and transcriptomics, one can further expand upon these applications, opening up both biomarker discovery through discovery-based research studies, and bring applications such as gene expression-based disease monitoring and diagnostics to home-based tests. Further, a technology that allows for remote blood transcriptomics would be enabling for increasing access to rural, remote, or underserved communities, for both research studies and telemedicine, and could be a powerful technology for enhancing global health efforts [2].

Conducting remote blood transcriptomics research presents several challenges. For example, while blood is relatively non- invasive to collect, conventional blood collection is limited to phlebotomy. Logistically, relying on phlebotomy for collection geographically confines blood collections to clinic/lab locations or research institutes. Several self-blood collection technologies have been developed for remote use, including fingersticks [8], dried blood spots [14–16], and lancet-based technologies that collect blood from the upper arm [17–21], such as the Tasso-SST device that we use in our home- sampling and RNA stabilization kits (including the work in this manuscript). Another major challenge of remote blood

transcriptomics is stabilization of whole blood RNA to minimize RNA degradation due to spontaneous degradation via autohydrolysis or degradation due to the presence of ribonucleases [22]. Toma et al. developed an at-home blood collection kit that collects 50µl of capillary blood via fingerstick and mixes with a proprietary RNA preservative solution at a 1:4 ratio [8]. To test the ability of the RNA preservative solution to preserve blood transcriptome, Toma et al. collected blood samples from participants (n = 3) and stored at ambient temperature (22°C) or −80°C for 0, 7, 14, and 28 days, with and without shipping. They found high correlation coefficients between gene expression levels from the samples in all conditions, demonstrating the efficacy of the RNA stabilization solution to preserve RNA integrity over 28 days [8].

To address this burgeoning need and develop technology for higher blood volumes than are possible with fingersticks, we have recently developed *home*RNA, a kit for the self-collection and stabilization of whole blood RNA, for use in disseminated whole blood transcriptome applications [23]. *home*RNA uses a blood collection device, the Tasso-SST, that collects capillary blood from the upper arm via a lancet; the blood collection tube from the Tasso system then interfaces with a custom engineered stabilizer tube that holds liquid stabilizer solution (RNA*later*) [23]. Previously, we demonstrated successful stabilization of RNA extracted from samples collected with *home*RNA in 47 participants in 10 USA states in a pilot feasibility study for validation of *home*RNA for remote blood collection and RNA stabilization. However, most of these samples were collected in regions with relatively moderate summer temperatures or during the fall/winter and thus we sought to test the *home*RNA sampling kit in regions with elevated temperatures. Our present study builds on a small body of prior work examining the effects of blood storage temperature on RNA quality; prior work largely focused on the effects of cold storage and did not examine temperatures above 25°C [24–26].

Establishing means to remotely probe the human whole blood transcriptome in elevated temperature settings has important implications, including enabling clinical research or personalized medicine applications in areas with high temperature and studying diseases/events that are specific to warm climates or warm times of year. For example, regions more highly burdened by tropical diseases would benefit from

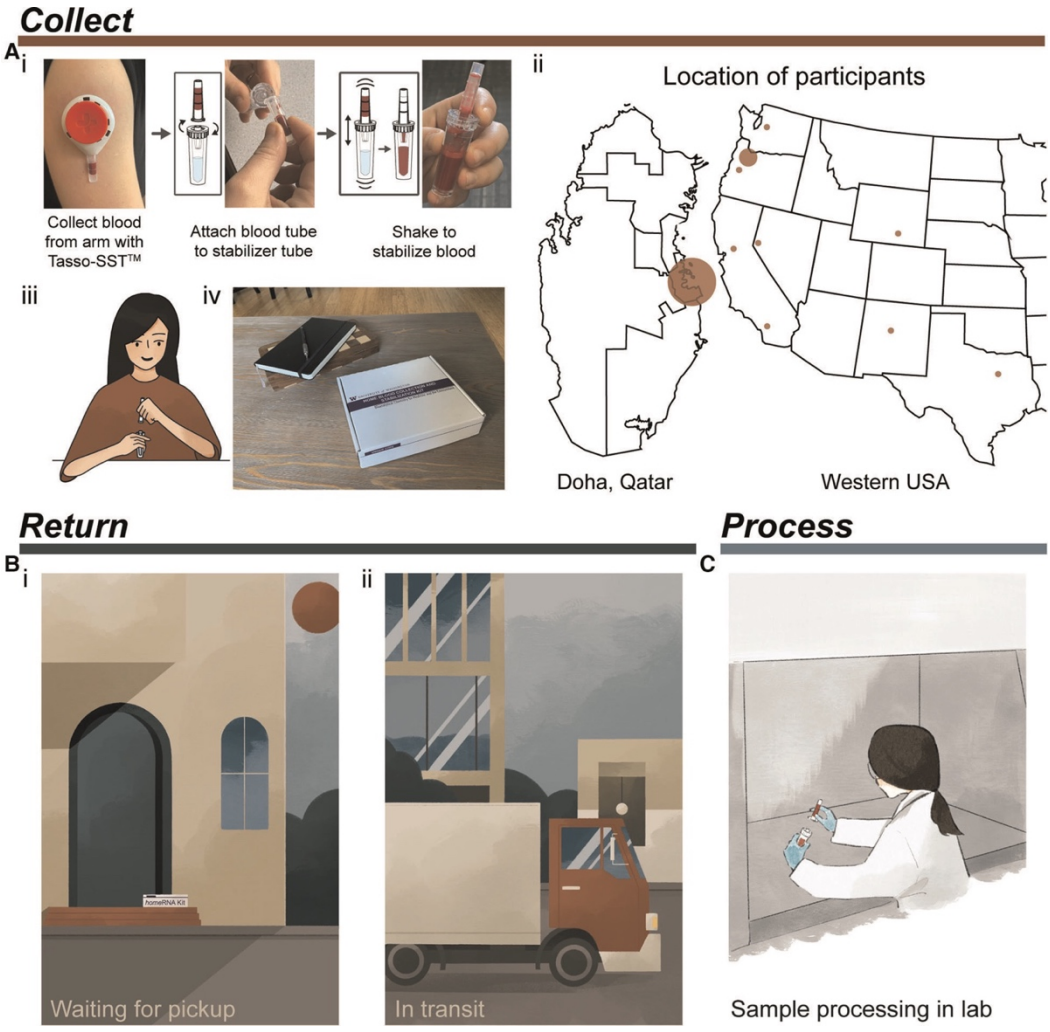

Figure 5.1. Typical process for using *home*RNA from collection to processing of samples. (A) Collection and stabilization of blood using *home*RNA. (i) Process of collecting blood from the upper arm with Tasso device and stabilizing the sample with the *home*RNA custom stabilizer tube. Image was reprinted with permission from Haack, Lim, et al. *home*RNA: A Self-Sampling Kit for the Collection of Peripheral Blood and Stabilization of RNA. Anal. Chem. 2021, 93, 39, 13196–13203. Copyright 2021 American Chemical Society [23]. (ii) Map depicting locations of participants in the small pilot studies conducted in Qatar and the Western and South Central USA. Note, participants in Qatar collected samples themselves in a lab setting. (iii) illustration demonstrating a participant connecting the Tasso blood tube and the *home*RNA stabilizer tube, (iv) *home*RNA kit on a coffee table, depicting a home setting for blood collection. (B) Illustration demonstrating two possible locations where samples may be exposed to high temperatures including (i) located on a front porch waiting to be picked up (which was the pickup location for many participants in the Western and South Central USA pilot study) and (ii) in transit in a delivery truck or courier service. (C) final step of sample processing for downstream analysis in a laboratory setting.

a better understanding of the stability of RNA because many of these areas often have persistently elevated temperatures. Further, even in regions with more moderate climates for part of the year, researchers may wish to conduct remote sampling studies in the summer months, particularly when tied to a specific seasonal

event. For example, a study aiming to understand wildfire smoke exposure in the Western and South Central USA would necessitate sampling in the summer months where temperatures are elevated, as these months are when wildfires occur. Overall, the ability to reliably stabilize RNA with *home*RNA in high temperature settings will open up remote transcriptome studies to regions with a warmer climate, whether seasonally or permanently.

We present here two small pilot studies exploring the application of *home*RNA in high temperature settings. In the first pilot study, *home*RNA was used by a small group in the city of Doha, Qatar before the sample was exposed to simulated shipping conditions of fluctuating temperatures. In the second study, *home*RNA was used at a regional scale, where participants used *home*RNA in their own homes during the summer months in several Western and South Central USA states, which included regions that are typically very hot [e.g., Reno, Nevada and Southern California) as well as the Pacific Northwest during the June 2021 heat wave. For samples collected from both studies, we examine quality control metrics typical to determining suitability of isolated RNA for downstream RNA transcript analysis, including the RNA integrity number (RIN) and total cellular RNA yield. In both the small pilot study in Qatar, and the small pilot study in the Western and South Central USA, we found satisfactory RIN values (RIN ≥7) in the majority of samples (84%, 16 out of 19 samples), with a RIN of 6.9 in the remaining 3 samples. Overall, our data demonstrate successful RNA stabilization as a function of yield and RIN values using *home*RNA in high temperature settings.

5.2 *home*RNA at high temperatures: An overview of two pilot studies

In this work, we tested the robustness of the *home*RNA kit by evaluating the stability of RNA transcripts in blood collected using the *home*RNA kits during high temperatures in the summer months (July-August) in two different regions: Doha, Qatar (in-lab collection with *home*RNA, followed by in-field sample exposure in a hot car to simulate conditions in a courier service) and the Western and South Central USA (remote collection with *home*RNA by participants in their home, shipped back to the lab). A typical logistical process of

collecting, stabilizing, shipping, and processing *home*RNA blood samples is outlined in Figure 5.1, including a schematic of how a user can collect and stabilize blood with *home*RNA. In each case, our study design was chosen based on how at-home clinical research studies would be performed in that region (i.e., a 3-hour car ride to simulate a courier service in Doha and overnight shipping via UPS in the USA). Specifically, in the Qatar pilot study we were interested in understanding if stabilized blood samples exposed to high temperature fluctuations in a region of the world that regularly experiences high temperatures would affect the quality of isolated blood RNA. The Qatar samples were collected in a laboratory setting which was air conditioned (to model the air-conditioned home environment typical in Qatar) and deliberately stressed in different temperature environments (i.e., collection at air-conditioned ambient temperature, exposure to external outdoor high temperatures, transportation conditions, etc. (Table C1)) to simulate shipping conditions that typically occur between remote blood collection and shipment back to the lab for analysis in Qatar. In Qatar, air conditioning is prevalent, and therefore samples may go from air-conditioned areas to extreme heat during shipping. Further, in Doha courier services (such as Uber) are a common method of moving packages around the city. The conditions we employed (Table C1) were chosen to mimic a typical car ride that the samples would experience in a courier service for shipments within the city itself; the length of the car ride (3h) is shorter than the time required to ship packages in the USA with UPS, but is relevant for courier services in Doha. Subsequently, the Western and South Central USA pilot study experienced real-world shipping conditions, in which participants were mailed *home*RNA kits from Seattle, WA to various states in the Western region of the USA during the summer (Table 5.1), yielding data from participants in a range of regions and temperatures to further test the applicability of *home*RNA in multiple high temperature environments.

The robustness of the *home*RNA kit to elevated ambient temperature exposures was validated by assessing isolated blood RNA quality with RNA integrity number (RIN) values. RIN values range between 1 and 10, with 1 referring to a completely degraded sample and 10 referring to an intact sample [27]. RIN values ≥7.0 are standard QC cut-offs for genome wide transcriptional profiling [28]. However, useful RNA sequencing data can still be obtained from more degraded samples (RIN values between 4 and 7) [29].

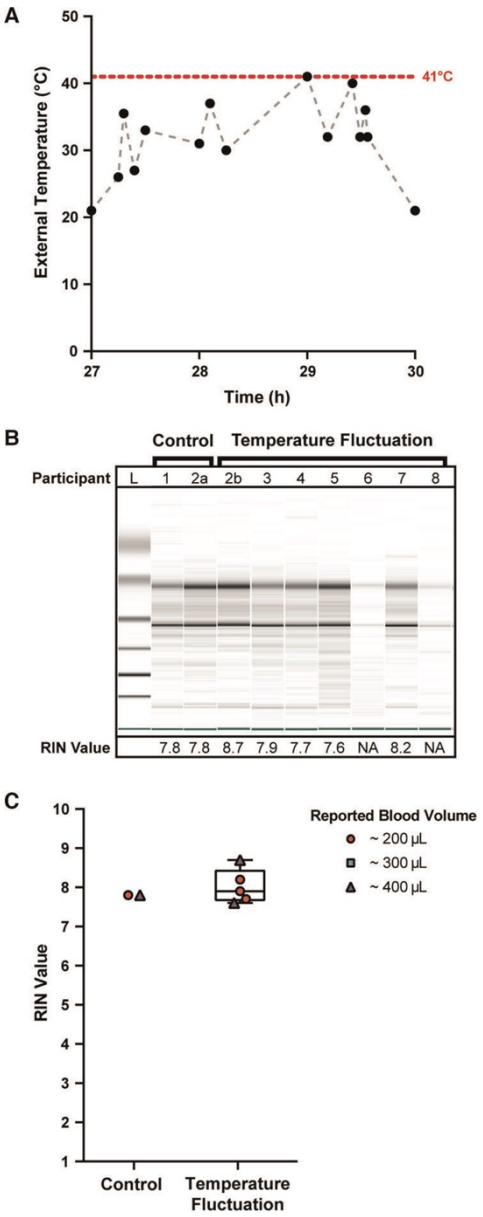

Figure 5.2. Quality of isolated RNA from stabilized *home*RNA samples exposed to high external temperature spikes in Doha, Qatar. (A) External temperature fluctuation experienced by self-collected and stabilized blood samples after storage at ambient temperature (21° C) for 27 h. External temperature reached a maximum of 41°C. Black data points indicate the measured temperature; gray dashed lines are included to connect the points to guide the eye only (transitions between temperatures may not be linear). (B) Digital gel image of RNA isolated from *home*RNA blood samples with corresponding RIN values. Samples 2a and 2b were from the same participant. Samples 1 and 2a did not undergo temperature fluctuations (they were frozen down at −80°C after overnight ambient temperature incubation to use as controls). (C) Scorable RIN values for each blood sample not exposed (control) and exposed (temperature fluctuation) to high temperature spikes along with the reported approximate blood volume collected by each participant. Participants 6 and 8 yielded too low of a RNA concentration to be detected using the RNA 6000 Nano kit.

5.3 *home*RNA for high temperature regions: A pilot study in Doha, Qatar

To understand the robustness of the *home*RNA device for use in clinical studies performed in Doha, Qatar, 8 participants in Doha, Qatar collected and stabilized their own blood in late August 2021. After blood collection and stabilization with the *home*RNA kit, each sample was incubated at room temperature (21°C) for 27 h, simulating time between remote blood collection and next-day sample pick up for shipment. After sitting out at room temperature, the stabilized blood samples were then exposed to fluctuating external temperatures in air-conditioned, indoor, and outdoor environments, as outlined in Figure 2A and Table C1, by driving the samples around Doha in a car. This setup mimics the change in environment and temperatures that the stabilized blood samples would experience in transit using a typical courier service (see rationale for design described at the beginning of the Results and Discussion). The samples underwent external changes in temperature between 21°C and 41°C over the course of three hours before storage at −80°C until the time of analysis (Figure 2A). Of the 8 participants, stabilized blood samples from 7 of the donors were exposed to these high environmental temperature spikes. Samples 1 and 2a (from participant 2 who was sampled twice: 2a for control and 2b for temperature stress) were frozen after overnight incubation at room temperature to serve as controls.

The quality of isolated RNA from all 9 blood samples (from 8 participants) was assessed to observe if the high external temperature spikes had adverse effects on the RNA stability in the *home*RNA platform. Of the 9 samples, 7 yielded scorable RIN values (Figure 5.2C). The two that did not yield a RIN value (participants 6 and 8) both reported collected blood volumes of ∼100 µl. We note that blood volume does not necessarily correlate with RNA yield (see Figure C5) and that variability in blood volume could result from device-to-device variability in the Tasso blood collection system and inaccuracy in participant reporting of the volume of collected blood. These two samples had low RNA concentrations beneath the limit of detection of the RNA 6000 Nano Kit (<5 ng/µl), but distinct 18S and 28S rRNA bands are noted in the digital gel (Figure 5.2B). The scorable RNA samples had RIN values between 7.6–8.7, demonstrating a sample quality suitable for downstream transcriptome (e.g., RNA-seq) analysis. Electropherograms obtained from the bioanalyzer can be found in the SI (Figure C1). RNA concentrations for the first 50 µl

elution were also obtained with the bioanalyzer (Figure C2). For the 5 samples that were exposed to temperature fluctuations and yielded a scorable RIN value, the RNA concentrations from the first 50 µl elution ranged from 21 ng/µl to 40 ng/µl (1,050–2,000 ng total cellular RNA in the first 50µl elution). The two samples that yielded a concentration less than the qualitative range (5 ng/µl) of the Nano 6000 kit (participant 6 and 8) both measured a concentration of 4 ng/µl (200 ng total cellular RNA in the first 50µl elution). Therefore, all samples, including the low concentration samples (participant 6 and 8), likely had at least 200 ng total yield of RNA in the first elution. In general, 500 ng is a comfortable minimal cutoff value for large-scale transcriptomics analyses such as standard RNA-Seq (with many facilities accepting lower amounts of RNA), and 100 ng is a comfortable minimal cutoff value for expression analyses of a small panel of targeted genes. For RNA-Seq, we note that different cutoff values exist (for example as low as 10–30 ng) depending on the method and whether cDNA amplification is performed.

The successful isolation and high quality of RNA from blood samples collected, stabilized, and analyzed in Doha suggests that the *home*RNA platform can be used for at-home clinical studies in Doha or places similar to Doha, a hot climate where air conditioning is commonplace in buildings and vehicles and fast courier services are available. In this setting, samples experience exposure to short term, high temperature fluctuations in external environmental conditions. Perhaps some researchers would assume that rapid temperature spikes would not affect the quality of RNA*later*TM- stabilized RNA, but we felt that it was necessary to conduct this field testing before using *home*RNA for clinical research in Doha. One important note regarding the experimental setup for this small pilot study is that the reported temperatures (Figure 5.2A, Table C1) are that of the local external environment (i.e., temperature inside the car, ambient outdoor temperature, etc.) rather than the temperature of the blood sample itself. It is possible that even though the external temperatures fluctuated markedly over the course of three hours with intervals of rapid but short increases or decreases in ambient temperatures, the blood sample itself may not have fully equilibrated to these observed external temperatures. Further experimentation, such as in-lab controlled temperature stress experiments, could further determine how spikes in external temperature affect the temperature of the blood sample itself.

5.4 *home*RNA for high temperature seasons: a pilot study in Western USA

To further assess the robustness of the *home*RNA kit in high temperature settings, 11 participants in various regions throughout the Western and South Central USA collected and stabilized their own blood and shipped it back to our lab for analysis. These samples were collected during the summer of 2021, which involved unusually high temperatures in some locations, and 2 of these samples were collected during the June 2021 heatwave in the Pacific Northwest region. Samples were collected at indoor ambient temperatures ranging between 21°C and 27°C (Table 5.1, Figure 5.3Bi). Typically, stabilized blood samples were shipped back the same day or the following day with overnight shipping. The logistics of the study were such that participants left their package in a designated pickup area; all participants chose to have their samples picked up from outside their homes; therefore, all the stabilized blood samples were also exposed to the outdoor ambient temperatures following indoor collection and stabilization (See Table 5.1 for pickup location). The duration of post-collection specimen storage prior to transit back to the lab (turnover duration) can be highly variable; this ranges from immediate transit (direct package handover a courier service driver) to overnight storage, in which these specimens can experience prolonged exposure to high ambient temperatures. This turnover duration is an important variable in temperature-dependent specimen stability and our data reflects the cumulative effect of variations in turnover duration experienced during real-world transits.

According to the day that each sample was collected and stabilized, the maximum outdoor temperature ("daily high") reported for the corresponding location of each participant (based on local weather reports found at Weather Underground) is included in Table 5.1. These outdoor temperatures spanned between 25°C and 44°C (Table 5.1, Figure 5.3Bii). We note that we do not know if the sample was outside during the daily high and further note that it is possible that the package was exposed to temperatures higher than the daily high, such as if it was placed in direct sunlight or if the temperature inside the pickup vehicle exceeded the daily high. Thus, the daily high is simply provided as a reference. In addition to the above, as noted in the Doha pilot study, the temperature of the blood sample may be different from the temperature of the external environment.

The quality of isolated RNA from 12 blood samples (from 11 participants) was assessed to observe how various temperature exposures (indoor, outdoor, shipping conditions, etc.) affected *home*RNA stability in a field test. 75% of the samples (9 out of 12 samples) yielded a RIN ≥7.0 (7.1–8.7) and the remaining yielded a RIN of 6.9 (Figure 5.3A). The RIN values demonstrate sufficient RNA quality for downstream transcriptomic analysis.

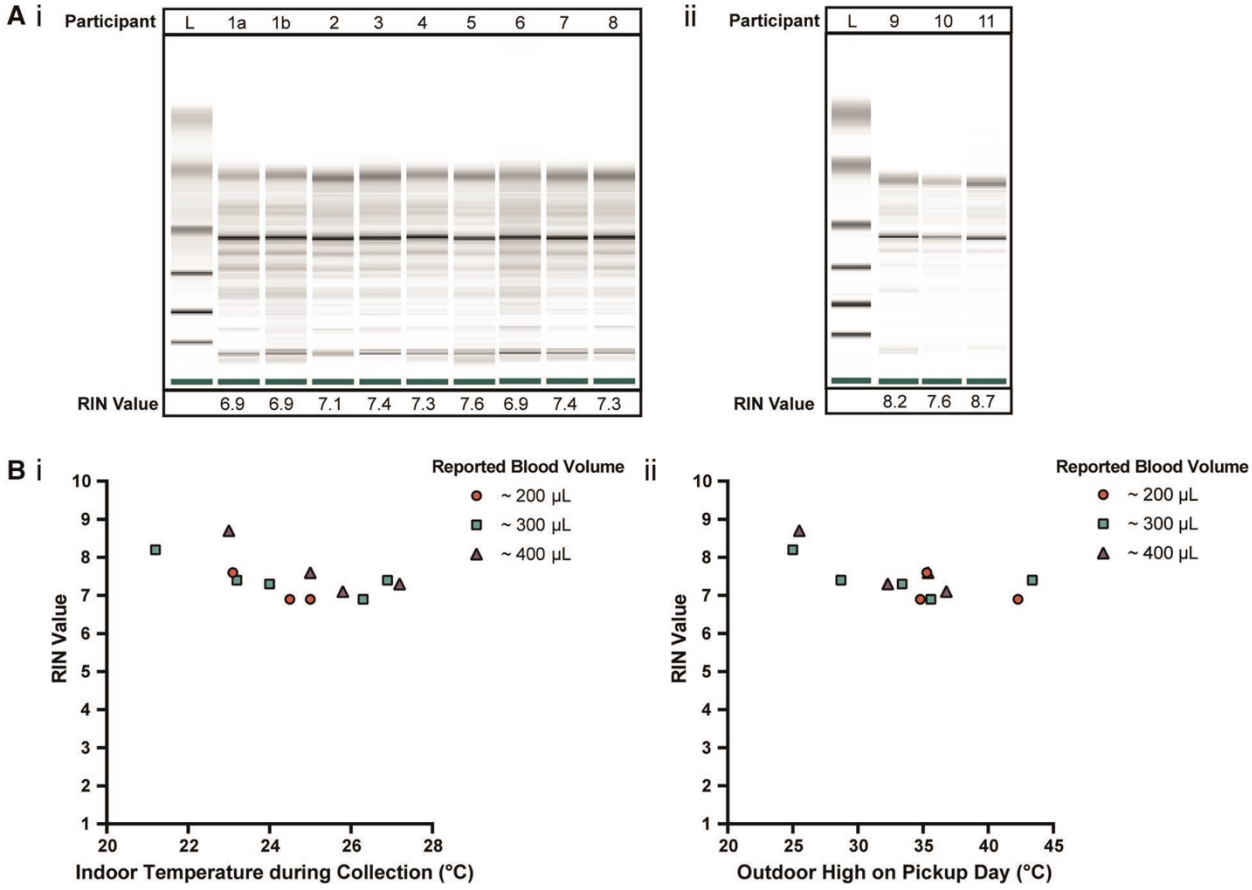

Figure 5.3. Quality of isolated RNA from stabilized *home*RNA samples collected during the summer in the Western and South Central USA. (A) Digital gel image of RNA isolated from *home*RNA stabilized blood samples with corresponding RIN values, with (i) samples diluted 1:5 with nuclease-free water and run with a RNA 6000 Pico kit and (ii) samples run with a RNA 6000 Nano kit without dilution. Participant 1 contributed two samples, 1a and 1b, that were collected and stabilized on different days and at different temperatures. (B) (i) RIN values from blood collected and stabilized at different indoor ambient temperatures during summer and (ii) RIN values according to the outdoor temperature high reported on the day of collection. Each participant was asked to report the approximate blood volume collected before stabilization based on Figure C6 in the collection survey. *home*RNA for high temperature seasons: A pilot study in Western and South Central USA

To observe how temperature at the time of collection and shipment affected the RNA integrity, RIN values were plotted against the respective indoor temperature at the time of collection and stabilization (Figure 5.3Bi) along with the local weather reports maximum outdoor temperature (Figure 5.3Bii). Indoor temperatures reported for the 12 samples range from 21.2–27.2°C. Indoor temperature at the time of collection (at least across the temperature range and small sample size used in this study) does not have a clear influence on the RIN value. Notably, there is overlap between the indoor temperatures reported here (Figure. 3B) and in our initial *home*RNA feasibility study [23]. In our previous pilot study conducted in 2020 [23], the majority of the samples were collected with an ambient indoor temperature between 18–25° C (n=43/53 analyzed returned samples where participants completed their surveys and provided indoor temperature data), with the other 9 samples ranging from 26–28°C, with 5 at 26°C, 1 at 27°C and 3 at 28°C. The results from the present study conducted in 2021 with respect to indoor temperature are plotted together with the results from our 2020 pilot study [23] with regards to RIN (Figure C5Ai) and total RNA yield (Figure C5Bi), in the Appendix C. There is also some overlap in the range of outdoor highs on pickup day in this study and our previous study conducted in 2020, but the samples collected in the 2021 study described here in the Western and South Central USA were picked up on days with a warmer outdoor high, on average. For the 2020 pilot study, the outdoor highs on pickup day ranged from 9–34.8°C, with a median outdoor high of 21.4°C, and only 7/60 total samples (collected from 47 total participants) had an outdoor high on the pickup day >30°C [23]. In contrast, the median and range of the outdoor high on pickup day was higher for the present 2021 study, ranging between 25–43.4°C, with a median of 35.1°C. The RIN (Figure C5Aii) and total RNA yield (Figure C5Bii) from the 2020 and 2021 studies are plotted together with respect to outdoor high on pickup day in Figure C5. All but one of the samples where a RIN was obtained in our 2020 pilot study yielded a RIN ≥7.0; the one sample with a RIN <7 was evaluated to a RIN of 6.8 [23]. With regards to the relationship between the outdoor high and RIN in the present study, the three samples with the lowest RIN (RIN of 6.9) correspond to outdoor daily high temperatures ≥34°C; however, four other samples corresponding to outdoor daily high temperatures ≥35°C returned RIN values ≥7.0.

Although RIN values were indicated as the main performance metric in this study, we acknowledge that other performance metrics (e.g., total yield and RNA concentration) may be used concurrently to guide sample selection for downstream analysis. In longitudinal studies with multiple collection time points, extremely low yields either due to low blood volume or low circulating WBCs can lead to exclusion of specific time points in the longitudinal data series. These missing-at-random (MAR) samples can be problematic in longitudinal studies as they create unbalanced data and biased estimates [30]. However, additional statistical approaches such as time-course gene set analysis (TcGSA) can be used to account for such heterogeneity in the dataset [30].

In studies where sampling is done in high temperature climates and samples are susceptible to variable levels of temperature-induced degradation, it is crucial that initial analysis of the genes of interest is performed to determine how their transcript levels change with respect to post- stabilization temperature stress as degradation may not occur uniformly within the sample [29]. Prior to complete sample stabilization, multiple RNA decay pathways may influence rate of decay for distinct transcript sets [31]. In such studies, alternative normalization strategies (e.g. using linear model framework to control for effects of RIN values) may be used to enable identification of biological meaningful expression signatures [29].

5.5 Conclusion

The ability to remotely collect and stabilize blood will expand future applications in the field of personalized medicine, particularly for analyzing blood transcriptomes that can give insight to disease progression/therapy response, immune response, and biomarker discovery. However, in order to establish the capability to do this, it is important to examine how exposure to various temperature conditions affects RNA stability. In this work, we conducted two small pilot studies to test the robustness of our *home*RNA at-home self-collection and stabilization blood kit to successfully preserve RNA integrity in high ambient temperature environments (>30°C) in two different study designs. These two pilot studies can inform clinical studies that could be run in places similar to Doha, Qatar (where samples are only exposed to short temperature spikes in transit) and the Western and South Central USA (where samples are in transit

overnight given the regional nature of the study). We demonstrated that the majority of these blood samples yielded sufficient RIN (≥7.0), which suggests the usability of these samples for downstream transcriptome analyses. Important limitations of the present work include relatively small sample sizes, although we note that this work follows on our larger study with 47 participants across the USA. [23] Further, we have several ongoing clinical studies in the USA, with >1,000 samples collected over the past year; these studies will eventually add to the literature on the robustness of *home*RNA across the USA through different seasons. It is also important to study the performance of *home*RNA in tropical climates where samples will undergo longer transit times and longer periods of sustained high temperatures than those expected in Doha; to this end, we have ongoing studies utilizing *home*RNA in urban and rural Thailand. As *home*RNA is applied to diagnosis and monitoring of specific diseases, it will be important to analyze the expression of genes of interest that could be affected by elevated temperatures (i.e., transcriptional levels of inflammatory genes or disease- specific genes) using controlled in-lab experiments prior to personalized medicine applications. To our knowledge, this is the first study to establish use of *home*RNA in sampling regions experiencing higher ambient temperatures, representing an initial validation study to extend the use of *home*RNA to warm environments.

5.6 Materials and Methods

*home*RNA for the collection and stabilization of whole blood cellular RNA

***Design and assembly of home*RNA:** The fabrication of the RNA stabilizer tube as an interface to the Tasso-SST blood tube has been described previously [23]. Briefly, the RNA stabilizer tube was designed to hold the RNA*later*TM stabilization solution and connect to the Tasso-SST blood collection tube for remote self-blood collection and RNA stabilization. The Tasso-SST blood collection tube does not contain an anticoagulant. We previously showed that Tasso-SST-mediated capillary blood collection, despite not having an anticoagulant, did not result in major compromise of RNA quality as measured by RIN values [23]. At the time of the development of the *home*RNA kit, the Tasso-SST was the only commercially available Tasso product for collecting liquid samples; we note that we do not use the serum separator tube

(SST) feature. The stabilizer tube was injection molded out of polycarbonate (PC: Makrolon 2407) by Protolabs, Inc (Maple Plain, MN). Details of the stabilizer tube components and design files can be found in Haack, Lim, et al. [23]. Prior to assembly of the stabilizer tube, all components were first cleaned via sonication in 70% ethanol (v/v) for 30 min and air dried. The stabilizer tube was filled with 1.3 ml RNA*later* (Thermo Fisher) stabilization solution and capped. The stabilizer tube insert was designed to hold the stabilizer tube containing blood in a 50 ml conical tube during transport. The insert also allows for facile centrifugation of the sample in the 50 ml standard conical tube when it arrives in a laboratory setting, as it centers and immobilizes the *home*RNA sample tube relative to the 50ml tube. The insert was injection molded out of polycarbonate (PC: Makrolon 2407) by Protolabs, Inc (Maple Plain, MN). All other components included in the *home*RNA blood kit and the Instruction for Use (IFU) are listed previously [23] and included in the Appendix of this chapter for easy reference. All kit components were placed in a rigid custom design mailer box fabricated via die-cutting (The BoxMaker, Inc.) [23].

High temperature fluctuations in *home*RNA collected samples: A small pilot study in Doha, Qatar

Participant recruitment and demographics*:* Healthy adult volunteers (18 years or older) were recruited in Doha, Qatar via word of mouth under a protocol approved by Sidra Medicine Institutional Review Board study number 1609004823. Written informed consent was obtained from all participants. In total, the study enrolled 8 participants between the ages of 29 and 53 (7 male and 1 female).

Temperature fluctuations of* home*RNA collected and stabilized blood samples*:* Participants were asked to collect and stabilize 1–2 whole blood samples using *home*RNA in a laboratory setting. The stabilizer vial containing the stabilized blood was placed in the 50ml conical tube with the insert provided in the *home*RNA kits (see design and assembly of *home*RNA above). Next the 50 ml tube containing the stabilized blood samples was placed in a sealed bag (provided in the kit) inside the *home*RNA cardboard package, and then incubated at ambient temperature (21°C) for 27 h to simulate the amount of time that might pass between blood collection at home and a scheduled pickup time from a courier service. Samples 1a (from participant 1 who was sampled twice) and 2 were frozen at −80°C after incubation at ambient room temperature for 27 h. The remaining 6 samples, after 27 h incubation at ambient temperature, underwent

3h of exposure to cycling temperatures in air-conditioned, indoor, and outdoor environments to simulate shipping conditions of the *home*RNA kit from remote site to lab. Each sample was exposed to a low of 21°C and a high of 41°C (with the elevated temperatures occurring as brief temperature spikes, see Table C1 and rationale for this temperature exposure/study design provided in the Results and Discussion) over the course of 27–30h after blood collection and stabilization.

_home_RNA collection during summer months: A small pilot study in the Western and South Central USA

***Participant recruitment and demographics**:* Healthy adult volunteers (18 years or older) were recruited from US states that historically experience wildfire smoke (i.e., the Western USA) via word of mouth under a protocol approved by University of Washington Institutional Review Board (STUDY00012463). 11 participants between the ages of 20 and 56 years old were enrolled (4 male and 7 female) and collected samples used in this study. Note: these samples were collected as part of a larger ongoing study our research group is performing to investigate the effects of wildfire smoke exposure on inflammation. These 12 samples (from 11 participants) were chosen to capture a range of temperatures including the warmest temperatures experienced by our participants in summer 2021. Written informed consent was obtained from all participants. Participants were located in 7 states, including California, Nevada, New Mexico, Texas, Oregon, Washington, and Wyoming. Samples were collected between June and July of 2021, including samples (n = 2) that were collected during the June 2021 heat wave in the Pacific Northwest.

***Participant blood self-collection and stabilization**:* Participants were asked to self-collect and stabilize blood from their upper arm using the *home*RNA blood collection and stabilization kit. Each participant was also asked to complete a survey with each collection that included information about the ambient temperature during collection and the approximate blood level (see Figure C6). Participants were asked to package their stabilized blood samples to be returned to the lab for analysis using the provided return mailer bag (per instructions including containment in a 50 ml conical tube, plastic bag, and the *home*RNA kit cardboard box). Participants left their sample outside for pickup between the hours of 12:00 PM and 3:00 PM. All stabilized blood samples were mailed using next day delivery courier services (United Parcel

Service, UPS). Returned samples were delivered to a −20°C freezer and subsequently stored at −80°C prior to RNA extraction.

Temperature data collection*:* Participants were provided with a temperature monitor (ThermPro) and were asked to record the temperature at the time of sampling to obtain the indoor temperature data (Figure 5.3Bi). We collected the maximum temperature from the day the sample was picked up as the outdoor high on pickup day (Figure 5.3Bii). Temperature data was obtained from the daily high reported from the closest weather station on the day of the pickup. The weather station data was obtained from Weather Underground.

Table 5.1: Participant and sampling information for the Western USA pilot study

Participant	Self-Reported Blood Volume (µL)	Indoor Temperature at Sampling (°C)	Outdoor Temperature High on Pickup Day (°C)	Location of Sampling	Month of Sampling	Total Yield (ug)	RIN
1A	200	25.0	42.3	Albany, OR	Late June	0.7	6.9
1B	300	26.3	35.6	Albany, OR	Early July	0.8	6.9
2	400	25.8	36.8	Davis, CA	Late July	1.1	7.1
3	300	23.2	28.7	Seattle, WA	Early August	0.8	7.4
4	300	24.0	33.4	Dallas, TX	Early July	0.7	7.3
5	200	23.1	35.3	Laramie, WY	Late July	0.5	7.6
6	200	24.5	34.8	Pasadena CA	Mid July	0.8	6.9
7	300	26.9	43.4	Portland, OR	Late June	0.5	7.4
8	400	27.2	32.3	Reno, NV	Early August	1.0	7.3
9	300	21.2	25.0	Albuquerque, NM	Late June	1.9	8.2
10	400	25.0	35.4	Portland, OR	Late July	1.8	7.6
11	400	23.0	25.5	Portland, OR	Late July	1.6	8.7

RNA isolation and assessment of RNA integrity from *home*RNA-stabilized whole blood

RNA isolation

For both small pilot studies in Doha, Qatar and the Western and South Central USA, total cellular RNA was isolated using the RibopureTM - Blood RNA Isolation Kit (Thermo Fisher) according to manufacturer's protocol and eluted in two 50 µl aliquots. Prior to removing the stabilized blood from the collection tube, the 50 ml conical tube holding the *home*RNA device was briefly centrifuged 10 s at 50 g. Isolated RNA was stored at −80°C until ready for further analysis.

Assessment of yield and RNA integrity of total cellular RNA in the Western and South Central USA: For the pilot study in the USA, RIN values of the first 50 µl elution were obtained on a Bioanalyzer 2100 (Agilent). The Agilent 2100 Bioanalyzer uses proprietary, built-in software to calculate RIN values, which is based on the relative peak height and shape of the 18S and 28S rRNA fragments in the resulting electropherogram after separation. All samples were assessed using the RNA 6000 Nano Kit. Samples with returned concentrations below the quantitative range (<25 ng/µl) of the RNA 6000 Nano Kit were further analyzed using the RNA 6000 Pico kit. For these low concentration samples, only values provided by the Pico kit were used in the data analysis. Samples 9–11 had sufficient RNA concentration to be within the quantitative range of the RNA 6000 Nano Kit (25–500 ng/µl), whereas RNA concentration from the first elution from samples 1–8 were below this threshold and were therefore diluted 1:5 with nuclease free water to be within the quantitative range for the RNA 6000 Pico Kit (50–5,000 pg/µl). RNA concentration was measured for both isolated RNA aliquots using a Cytation 5 Multi-Mode Reader (Agilent Biotek Instruments) with a Take3 Micro-Volume Plate at the wavelengths of 260, 280, and 320 nm (Figure C4).

Assessment of yield and RNA integrity of total cellular RNA in Qatar: For the pilot study in Qatar, RNA integrity number (RIN) values and RNA concentration of the first 50 µl elution were obtained on a Bioanalyzer 2100 (Agilent) using the RNA 6000 Nano Kit (Agilent) for all samples. For samples analyzed in Qatar, additional assays on the Pico kit were not performed on samples with concentrations below the qualitative range of the Nano kit. The bioanalyzer was used to obtain the RNA concentration from the first 50 µl elution of the RNA isolation protocol (Figure C2).

5.7 References

1. S. Mohr and C. C. Liew, *Trends Mol Med*, 2007, **13**, 422–432.
2. D. Chaussabel, *Semin Immunol*, 2015, **27**, 58–66.
3. B. Heidecker and J. M. Hare, *Heart Fail. Rev.*, 2007, **12**, 1–11.
4. H. Runne, A. Kuhn, E. J. Wild, W. Pratyaksha, M. Kristiansen, J. D. Isaacs, E. Régulier, M. Delorenzi, S. J. Tabrizi and R. Luthi-Carter, *Proc. Natl. Acad. Sci. U. S. A.*, 2007, **104**, 14424–14429.
5. C.-X. Li, J. Chen, S.-K. Lv, J.-H. Li, L.-L. Li and X. Hu, *Mediators Inflamm.*, 2021, **2021**, 6635925.

6. C. C. Liew, J. Ma, H. C. Tang, R. Zheng and A. A. Dempsey, *J. Lab. Clin. Med.*, 2006, **147**, 126–132.

7. S. A. Byron, K. R. van Keuren-Jensen, D. M. Engelthaler, J. D. Carpten and D. W. Craig, *Nature Reviews Genetics 2016 17:5*, 2016, **17**, 257–271.

8. R. Toma, N. Duval, B. Pelle, M. M. Parks, V. Gopu, P. J. Torres, F. R. Camacho, N. Shen, S. Krishnan, A. Hatch, H. Tily, A. Perlina, G. Banavar and M. Vuyisich, *Biotechniques*, 2020, **69**, 289–301.

9. T. Ahmad, M. Fiuzat, G. M. Felker and C. O'Connor, *Nat. Rev. Cardiol.*, 2012, **9**, 347–359.

10. I. v Yang, L. G. Luna, J. Cotter, J. Talbert, S. M. Leach, R. Kidd, J. Turner, N. Kummer, D. Kervitsky, K. K. Brown, K. Boon, M. I. Schwarz, D. A. Schwartz and M. P. Steele, *PLoS One*, 2012, **7**, e37708.

11. P. D. Burbelo, M. J. Iadarola, I. Alevizos and M. R. Sapio, *Mol. Diagn. Ther.*, 2016, **20**, 415–427.

12. B. Mesko, S. Poliska and L. Nagy, *Trends Mol Med*, 2011, **17**, 223–233.

13. R. Bayaa, M. D. B. Ndiaye, C. Chedid, E. Kokhreidze, N. Tukvadze, S. Banu, M. K. M. Uddin, S. Biswas, R. Nasrin, P. Ranaivomanana, A. H. Raherinandrasana, J. Rakotonirina, V. Rasolofo, G. Delogu, F. de Maio, D. Goletti, H. Endtz, F. Ader, M. Hamze, M. B. Ismail, S. Pouzol, N. Rakotosamimanana, J. Hoffmann and H. working group within the G. network, *Sci. Rep.*, 2021, **11**, 13646.

14. P. Martinez and S. E. Zemore, *Addiction*, 2019, **114**, 1303–1308.

15. J. Hicks, C. Klumpp-Thomas, H. Kalish, A. Shunmugavel, J. Mehalko, J.-P. Denson, K. R. Snead, M. Drew, K. S. Corbett, B. S. Graham, M. D. Hall, M. J. Memoli, D. Esposito and K. Sadtler, *J. Clin. Immunol.*, 2021, **41**, 906–913.

16. K. Li, J. C. Naviaux, J. M. Monk, L. Wang and R. K. Naviaux, *Metabolites*, , DOI:10.3390/metabo10030082.

17. A. Catala, R. Culp-Hill, T. Nemkov and A. D'Alessandro, *Metabolomics*, 2018, **14**, 100.

18. T. M. Blicharz, P. Gong, B. M. Bunner, L. L. Chu, K. M. Leonard, J. A. Wakefield, R. E. Williams, M. Dadgar, C. A. Tagliabue, R. el Khaja, S. L. Marlin, R. Haghgooie, S. P. Davis, D. E. Chickering and H. Bernstein, *Nat Biomed Eng*, 2018, **2**, 151–157.

19. M. N. Fedoruk, *Bioanalysis*, 2020, **12**, 715–718.

20. A. Vusirikala, H. Whitaker, S. Jones, E. Tessier, R. Borrow, E. Linley, K. Hoschler, F. Baawuah, S. Ahmad, N. Andrews, M. Ramsay, S. N. Ladhani, K. E. Brown and G. Amirthalingam, *J Infect*, 2021, **83**, 104–111.

21. K. J. Williams, J. Lutman, C. McCaughey and S. K. Fischer, *Bioanalysis*, 2021, **13**, 679–691.

22. J. Tenhunen, *Hydrolysis of single-stranded RNA in aqueous solutions-effect on quantitative hybridizations*, 1989, vol. 3.

23. A. J. Haack, F. Y. Lim, D. S. Kennedy, J. H. Day, K. N. Adams, J. J. Lee, E. Berthier and A. B. Theberge, *Anal. Chem.*, 2021, **93**, 13196–13203.

24. L.-H. Huang, P.-H. Lin, K.-W. Tsai, L.-J. Wang, Y.-H. Huang, H.-C. Kuo, S.-C. Li, H. L-h, L. P-h, T. K-w, W. L-j, H. Y-h and K. H-c, *PLoS One*, 2017, **12**, e0184692.

25. N. Duale, W. I. Lipkin, T. Briese, J. Aarem, K. S. Rønningen, K. K. Aas, P. Magnus, K. Harbak, E. Susser and G. Brunborg, *BMC Res. Notes*, 2014, **7**, 633.

26. Y. Shen, R. Li, F. Tian, Z. Chen, N. Lu, Y. Bai, Q. Ge and Z. Lu, *Onco Targets Ther*, 2018, **11**, 3573–3581.

27. A. Schroeder, O. Mueller, S. Stocker, R. Salowsky, M. Leiber, M. Gassmann, S. Lightfoot, W. Menzel, M. Granzow and T. Ragg, *BMC Mol. Biol.*, 2006, **7**, 3.

28. K. R. Kukurba and S. B. Montgomery, *Cold Spring Harb Protoc*, 2015, **2015**, pdb.top084970.

29. I. Gallego Romero, A. A. Pai, J. Tung and Y. Gilad, *BMC Biol.*, 2014, **12**, 42.

30. B. P. Hejblum, J. Skinner and R. Thiébaut, *PLoS Comput Biol*, 2015, **11**, e1004310.

31. A. C. Tuck, A. Rankova, A. B. Arpat, L. A. Liechti, D. Hess, V. Iesmantavicius, V. Castelo-Szekely, D. Gatfield and M. Bühler, *Mol Cell*, 2020, **77**, 1222-1236.e13.

Chapter 6: Assessing the Effects of Wildfire Smoke Exposure with *home*RNA: A Flexible and Responsive Approach[3]

Abstract: Wildfire smoke is becoming an increasingly pressing problem, with the frequency, size, and intensity of wildfire events projected to increase; this has led to an increase in the population of people who experience non-work-related wildfire smoke exposure at greater intensities. As a result, there is an urgent need to understand the impacts of wildfire smoke from a mechanistic perspective on systemic inflammation. Investigating the effects of wildfire smoke via blood biomarker and transcriptome analysis is challenging due to the unpredictable nature of wildfires and the logistical difficulty of conducting a clinical study in remote areas. Here, we describe a flexible feasibility study design to investigate the effects of wildfire smoke exposure using a novel *home*RNA kit to collect longitudinal blood samples from 58 participants located in the Western, Southwest and Midwestern United States, many of whom (n=18) were located in the Methow Valley, WA. Samples were collected throughout the wildfire season, as well as 3 and 6 months after the wildfire season, to assess the effects of wildfire smoke both directly after and several months after smoke exposure. This study design shows that *home*RNA kits enable targeted regional response to wildfire smoke; flexibly allowing participants to collect blood samples throughout the year, even during emergency evacuations when some participants chose to take their *home*RNA kits with them. RNA integrity numbers (RINs) from the *home*RNA-stabilized samples were suitable for downstream analysis (e.g., NanoString, 3'

[3] *We would like to acknowledge Y. Zeng*, L. G. Brown*, D. S. Kennedy, K. N. Adams, J. W. MacDonald, T. K. Bammler, I. H, Jeacopello, J. E. Stolarczuk, M. G. Takezawa, G. W. Hassan, F. Y. Lim, D. Chaussabel, N. A. Errett, E. Walker, E. Berthier, and A. B. Theberge, for their help in the preparation of this thesis chapter.*
** Equal contribution*

AJH, EB and ABT contributed to the conception and design of the study. KNA, AJH, DSK, EB and ABT designed and executed the human subjects study. AJH, DSK, FYL, EB, and ABT developed home*RNA and the protocols implemented in home sampling in this chapter. AJH, DSK, KNA, JS, GWH and MGT conducted/contributed to the human subjects research and collection of samples. YZ and LGB performed the RNA extractions on samples and collected the RIN and yield data. AJH, YZ, LGB, JWM, TKB, JS, EB, DC, and ABT analyzed/interpreted the data. AJH, YZ, LGB, JS, IHJ and ABT prepared the figures and wrote the chapter.*

RNA-seq). The study suggests that *home*RNA is a suitable tool for investigating the effects of wildfire smoke on overall health, as well as for investigating the impacts of wildfire smoke from a mechanistic perspective, particularly on systemic inflammation.

6.1 Introduction

The frequency, size, and intensity of wildfire events have increased dramatically in the past decades across the western United States and are projected to continue increasing by 56% through 2100. [1] The Methow Valley in Washington state, for example, experienced one of its worst summers for wildfire smoke in 2021 as smoke from nearby wildfires blanketed the region, causing several days of "hazardous" air quality category (the highest category of Air Quality Index (AQI) >301; for reference, a good air quality is AQI<50); an unprecedented level of smoke exposure for the already historically wildfire smoke-impacted region. Wildfire smoke is associated with adverse health effects across the population, particularly children and older adults. [2-4] Smoke from wildfires impacts human health via smoke particulate matter (e.g., PM_{10}, $PM_{2.5}$), toxic substances (e.g., carbon monoxide, volatile organic compounds), and aerosolized microbes (e.g., bacteria, fungi). [5] Exposure to wildfire smoke can lead to acute respiratory symptoms, acute bronchitis, and can exacerbate existing chronic obstructive pulmonary disease (COPD) and asthma. [6-8] Moreover, smoke exposure has been proposed as a proximal mediator for elevated and chronic inflammation implicated in several chronic diseases, including the development of chronic lung diseases such as COPD, [8-11] asthma, [12, 13] cancer, [14-16] kidney disease, [17] heart disease [16, 18] and metabolic syndrome. [18, 19]

In addition to investigating the effects of wildfire smoke on overall health, there has also been a push to understand the impacts of wildfire smoke, from a mechanistic perspective, particularly on respiratory tract and systemic inflammation. [20-24] Several studies have investigated targeted panels of blood-based biomarkers such as cytokines in the firefighter population, which implicate inflammatory activation acutely in response to work-related smoke exposure. [20, 23, 25] One study by Swiston et al.

investigated inflammatory responses in 52 seasonal firefighters during shifts fighting wildfires through blood and sputum collection, with samples taken within 4 hours of completing a fire-fighting shift. Changes included an increase in proinflammatory cytokines such as interleukin 6 (IL-6), interleukin 8 (IL-8) and monocyte chemotactic protein-1 (MCP-1), indicating acute changes in cytokines in blood towards inflammatory activation. [20] A smaller study (n=12) on firefighters working at prescribed burns saw further increases in inflammatory markers from dried blood spot (DBS) samples taken immediately before (i.e., the morning of) and immediately after (i.e., the evening of) working on prescribed burns. This study detected increases in inflammatory biomarkers IL-1β, IL-8, CRP, SAA, ICAM-1, and VCAM-1, with a >1.5-fold increase in IL-8, CRP and ICAM-1. [23] These studies implicate immune activation acutely in response to extreme exposures seen by wildland firefighters; these results invite a question into whether similar changes occur in the general population by individuals who routinely are exposed to prolonged and high levels of wildfire smoke by nature of where they live, and additionally, how prolonged are these effects. As the intensity and area of wildfire smoke coverage is predicted to increase, [26] the population of people who experience wildfire smoke exposure because of where they live will continue to increase. Studies examining the broader immune implications of non-work-related wildfire smoke exposure are needed.

In addition to expansion of study population, expanding the number and type of biomarkers probed can bring additional insight. With continued advances in technologies aimed at probing the transcriptome (e.g., RNA-Seq, 3'RNA-Seq and NanoString), there is an opportunity for a broader probe into immune activation via mRNA analysis, which will complement the existing research on individual cytokines. Animal studies with targeted gene panels reveal gene expression changes in blood RNA in monkeys (84 gene panel) [27] and otters (13 gene panel) [28] exposed to wildfire smoke. While miRNA [29, 30] and DNA methylation [13, 31-34] have been investigated in the blood of humans and animals [35] exposed to wildfire smoke or air pollution, suggesting epigenetic regulation in response to smoke exposure, to our knowledge, large scale gene expression changes via mRNA transcriptomic analysis in humans in response to wildfire smoke have not yet been reported.

Investigating a transcriptome-wide response to wildfire smoke on the general population is difficult due to the logistical challenges inherent with conducting such a study. In firefighters, regular smoke exposure is expected, and in the case of controlled burns, the timing of smoke exposure can be predicted, making enrollment and logistics of studying this population simpler. In contrast to controlled burns, wildfires are unpredictable, and thereby running a clinic-based blood draw study would require either (1) relying on historical data to choose a location that has infrastructure to support clinic-based blood draws (i.e., an urban or suburban environment), which has a historically high prevalence of wildfire smoke, (2) setting up a multi-site study, or (3) relying on retrospective studies or capturing smoke exposure incidentally on a study investigating a different question where longitudinal blood samples are collected. [22, 36] These factors make designing and executing studies into wildfire smoke logistically challenging. Having a single location runs the risk of no smoke exposure occurring during the study period. Setting up a multi-site study with multiple clinic-based phlebotomy sites or mobile phlebotomists would increase the logistical burden of the study design but would increase the likelihood that some study participants would be exposed. Finally, many cases of wildfire smoke exposure occur in remote locations, which may be inaccessible for mobile phlebotomists or require study participants to travel large distances for each blood draw time point, increasing burden on participants and making longitudinal studies infeasible.

To address this challenge, we have developed *home*RNA: a self-sampling kit that allows for the collection of blood and stabilization of RNA by study participants themselves in their own home, which will be later shipped back to the lab for downstream analysis. [37] *home*RNA enables targeted regional response to disasters without relying on predicting where the disaster would occur (as would be required for a clinic-based blood draw or remote phlebotomy study design). Multiple kits can be mailed to participants within a day of an event occurring (such as a wildfire smoke event) and can be used by participants over several time points upon receiving. With this remote study design with *home*RNA, we can collect snapshots of a participant's inflammatory responses before, during, and after an exposure in their own homes—flexibility that has not previously been possible with clinic-based blood draws.

*home*RNA makes use of a commercially available lancet-based blood sampling device, the Tasso device, which collects up to 0.5 mL of blood from the upper arm; the RNA stabilizing effect is achieved by a custom-built stabilizer tube, designed to interface with the Tasso blood tube (Figure 4.1A). The stabilizer tube contains RNA*later*™, which is mixed with blood in the blood collection compartment to stabilize the RNA when the user shakes the assembled tubes (Figure 4.1A). Previously, in a pilot study testing the feasibility of *home*RNA for home-sampling and RNA stabilization, we validated the kit in 41 participants across 10 states, receiving blood samples with RNA yields and RNA integrity numbers (RINs) suitable for most standard downstream analysis (e.g., RNA sequencing (RNA-Seq), or targeted gene panels such as those used with technologies such as NanoString). [37] The total RNA yield was > 500 ng for 83% of samples, and >100 ng for all samples (Figure 4.3A), and RIN values > 7 for all but one sample (Figure 4.3B), indicating sufficient RNA quality and quantity for downstream analysis.

As our initial pilot study [37] demonstrated that the *home*RNA kits can be deployed "on demand" across the U.S, here, we apply this feature to collect *home*RNA stabilized samples in response to wildfires. Beginning in June 2021, we enrolled 58 individuals throughout the Western United States, with many participants located in the Methow Valley, WA (n=18), a region with historically impactful wildfire seasons, to study their inflammatory response to wildfire smoke exposure. One unique advantage of *home*RNA is the responsive and flexible blood sampling, as study participants can collect blood and stabilize RNA in their own homes. Some participants even chose to collect blood samples despite needing to relocate amid an emergency evacuation due to the portability of the kits, which further demonstrated the flexibility of using *home*RNA in response to disasters. Besides the *home*RNA kits, the study design itself is also flexible: by recruiting participants in a diverse geographical range, we can combat the unpredictability of knowing when and where a wildfire event may occur. With a disseminated study design, we can also sample participants from multiple regions at the same time who may or may not be experiencing wildfire smoke, allowing for a diverse range of $PM_{2.5}$ exposures to be analyzed.

In this study, we collected samples from participants who were exposed to varying levels of wildfire smoke throughout the wildfire season to study the short-term effects, as well as 3 and 6 months after the

wildfire season to assess months-long effects of wildfire smoke. An overview of the study design and timeline for collection is summarized in Figure 6.1. Currently, RNA has been extracted from a subset of participant's (*n*=33/58) *home*RNA-stabilized samples, with RINs suitable to conduct 3'RNA-Seq analysis (>6) for most extracted samples (94%, *n*=402/427). We are currently analyzing 300 samples from 28 individuals, with 3' RNA sequencing. Participants in this selected subset of 28 individuals were exposed to varying levels of wildfire smoke with samples collected throughout the wildfire season, as well as additional samples collected 3 and 6 months after the wildfire season to assess months-long effects of wildfire smoke.

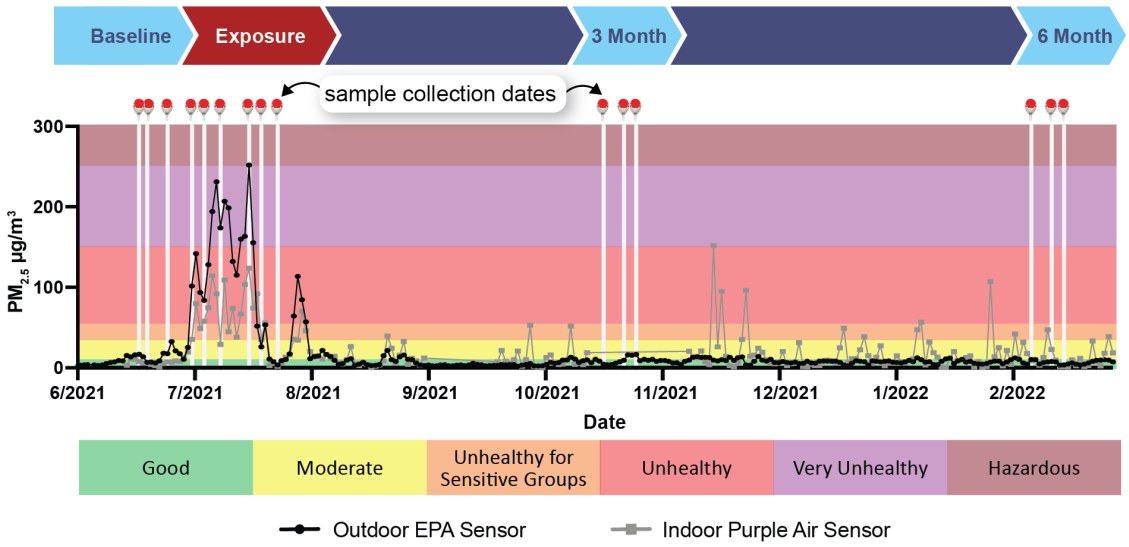

Figure 6.1. Study design for using *home*RNA throughout wildfire season. Samples are collected before, during and after wildfire smoke exposure as depicted as an annotated timeline schematic. Timeline corresponds to sample collection in response to $PM_{2.5}$ exposure where outdoor $PM_{2.5}$ collected from the nearest outdoor EPA sensor and the indoor $PM_{2.5}$ collected purple air sensor located in the participant's home. White vertical lines indicate dates in which a blood sample was taken. Data is collected from a participant located in the Methow Valley.

6.2 *home*RNA enables remote responsive sampling throughout wildfire season

The immune response to wildfire smoke exposure is difficult to capture, largely due to the unpredictable nature of wildfires. Smoke exposure can occur in remote areas and can quickly move from one region to another depending on many factors. Setting up a large-scale study to study wildfire smoke exposure in the general population using traditional phlebotomy sampling is difficult as it either limits

participant enrollment to a specific region where an academic or clinic laboratory is located that can provide phlebotomy blood draws or requires complicated logistics to set up multiple or remote phlebotomy blood draw locations while requiring study participants to go physically to a blood draw location during a smoke event. Utilizing *home*RNA as we have done in this study allows for facile remote study logistics and broad recruitment, while allowing for participants to sample in their own home easily throughout a yearlong study.

Furthermore, to understand the effect of wildfire smoke on immune activation and inflammatory responses, it is helpful to have a baseline measurement of the inflammatory transcriptome prior to wildfire smoke exposure. This is especially important, given recent studies showing that immune gene regulation can persist as long as three months after exposure. [38] However, if a study is located only in one location, collecting baseline samples before any smoke exposure has occurred could be logistically risky from a study design perspective, as there is always a chance that no smoke exposure will occur in that region in a given wildfire season. Previous studies utilize several strategies to allow for the collection of a baseline while de-risking the possibility that a wildfire smoke event will not occur. Apart from utilizing a firefighter population who will more than likely be exposed to smoke, [20, 23, 25, 29] another strategy is using controlled burns as a proxy for wildfire smoke exposure [23, 38, 39] as these can be more readily predicted, but many studies have found varying responses to controlled burns versus a true wildfire event. [38] As such, many existing literature on wildfire smoke exposure where blood samples are collected are either missing a baseline measurement as they only begin sampling after smoke exposure has occurred, [31] take place over multiple sites over multiple years, [39, 40] or take place in a region prone to wildfire smoke. [13, 33, 38] Other studies that do contain a pre-smoke exposure sample, are collected incidentally; study participants were enrolled in a separate study in which longitudinal samples were being collected, while a subset of participants happens to have experienced wildfire smoke exposure during the study period. [22, 31, 36]

*home*RNA kits provide an additional strategy by enabling fully remote, flexible, and responsive sampling throughout a wildfire season. To de-risk the possibility of smoke exposure not occurring, we took a dual approach of enrolling participants broadly throughout the American West, while also utilizing a more

targeted enrollment strategy in the Methow Valley region in Washington state, a region that historically has had high wildfire smoke exposures yearly. [41-44] We enrolled participants broadly throughout the American West, Southwest and Midwest, with the total of the 58 participants representing multiple regions, ranging from the Pacific Northwest, Northern and Southern California, and areas of the Midwest and Southwest including Montana, Wyoming and Texas (Figure 6.2). While enrolling broadly, the plurality of study participants were located in the Methow Valley region (n=18). This recruitment geography not only reduces the risk of a wildfire not occurring in a single study location, but also makes it possible to collect samples from participants who are getting exposed to wildfire smoke and those that are not, allowing for a more comprehensive understanding of the effects of wildfire smoke.

In addition, *home*RNA kits provide flexibility to participants, making it easier for them to collect samples even when it's a stressful event such as a wildfire occurring nearby. This contrasts with needing to go to a clinic to get a blood draw, which can be difficult or even impossible in the event of a natural disaster. Notably, at one point in the study, some participants needed to evacuate due to the locations of their homes with regards to a wildfire. Some of these participants chose to take their *home*RNA kits with them and continued sampling; such anecdotes exemplifies the flexible nature of *home*RNA and remote study design and the potential utility of such tools for the study of natural disasters broadly.

The study design does have limitations, such as the fact that other factors may affect immune activation throughout the year, including seasonal changes. However, we were able to collect samples from people who did not experience smoke exposure throughout the year which may help to correct for this confounding factor. Another concern was that participants would not remain enrolled throughout the study due to the prolonged year-long nature and requirement to collect up to 15 blood samples with the *home*RNA kit. Nonetheless, the study participants reported that the *home*RNA kit was easy to use, and most participants remained in the study (n=58/62 originally enrolled) even though it was a 10-month longitudinal study. Furthermore, many participants indicated in their survey responses that they would like to be contacted for enrollment for an additional year. *home*RNA enables fully remote, flexible, and responsive sampling throughout a wildfire season.

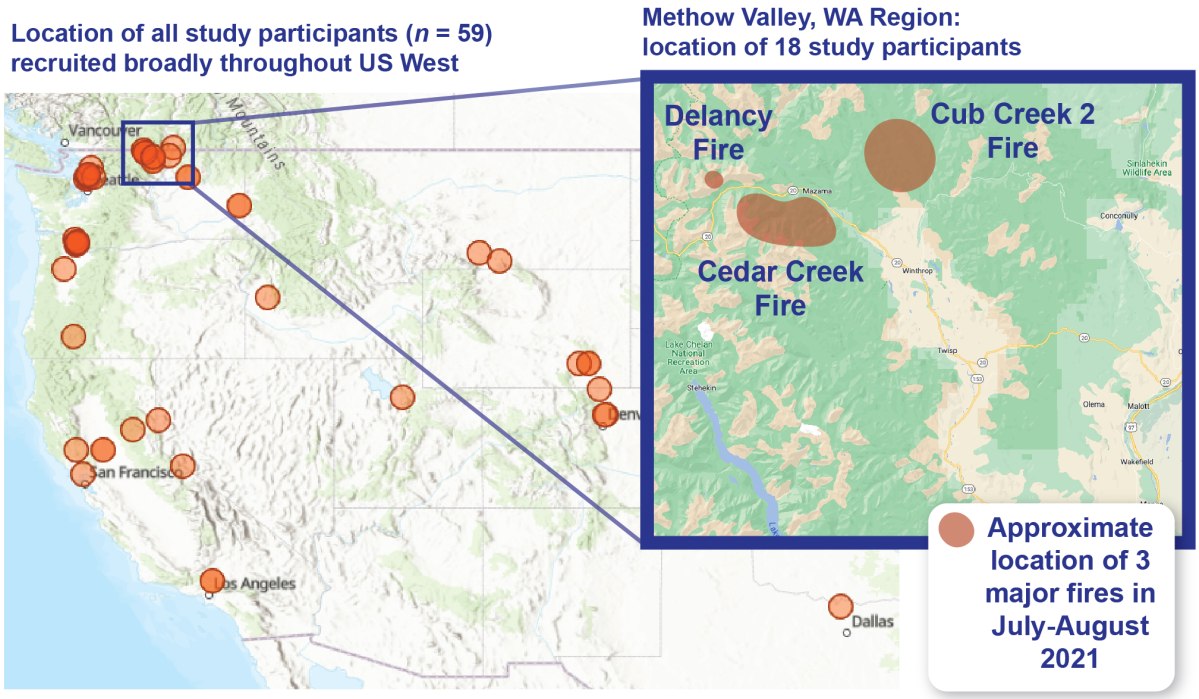

Figure 6.2. Location of study participants. Each participant is represented by an orange circle. Darker shade of orange indicates multiple participants within a small distance, as the circles overlap. Inset depicts the Methow Valley region where 18 participants are located, and the approximate location of 3 major fires in July-August of 2021 in the region, the Cedar Creek, Delancy and Cub Creek fire. Fire map area estimated based on InciWeb. (inciweb.nwcg.gov). Map generated with arcGIS software, where each participant's reported zip code was used to generate coordinates (arcgis.com).

6.3 EPA $PM_{2.5}$ sensors and PurpleAir sensors enable collection of wildfire smoke exposure data

The current practice to quantify wildfire smoke exposure for the public is by measuring the concentration of $PM_{2.5}$ at ground level. $PM_{2.5}$ is particulate matter with an aerodynamic diameter of 2.5 µm or smaller, commonly referred to as fine particulate matter. The size of particles is directly related to health outcomes. PM_{10}, particles with a diameter between 10 and 2.5 µm, can enter the lungs but are a small portion of wildfire smoke. [45] $PM_{2.5}$ can penetrate deeper into the lungs and be absorbed by the bloodstream making it a greater health concern. Vincente et al. reported that 90% of the total mass of wildfire smoke is particulate pollution. [45]

Most research used to understand possible negative health effects of wildfire smoke comes from research into particle pollution in ambient air. As of 2020, there were 2,498 ground monitoring sites within the US tracking $PM_{2.5}$, PM_{10}, and other pollutants such as ozone. The intended use of these monitors was

for states, local governments, and tribal agencies to measure ambient air quality in accordance with the 1970 Clean Air Act (U.S.C. 42). This in-place infrastructure for ambient air monitoring has shown to be an important tool for tracking wildfire smoke and led to websites like Air Now that have specific wildfire tracking maps that the public can visit at airnow.gov/wildfires/.

To ensure accurate and consistent reporting, the U.S. Federal Reference Method (FRM) determines the type of measurement. $PM_{2.5}$ is measured gravimetrically; fine particles are collected on a filter that is weighed before and after sampling. Regulations require agencies to use equipment calibrated for temperature, humidity, and weight. Measurements are reported to the EPA in units of $\mu g/m^3$. To make it easier for the public to understand, the EPA converts the concentration of $PM_{2.5}$ to the Air Quality Index (AQI) which reports values from 0 to 500 and categorical indicators of "Good", "Moderate", "Unhealthy for Sensitive Groups", "Unhealthy", "Very Unhealthy", and "Hazardous". Current thresholds, set by the EPA for public health, recommend an average annual fine particle standard of no more than 12 $\mu g/m^3$ and an average 24-hour standard of no more than 35 $\mu g/m^3$. [46] Below this threshold corresponds to the "good" air quality index range.

Using the nearest EPA sensor to each study participant, we make an estimate of the average daily $PM_{2.5}$ exposure for each participant. The average daily $PM_{2.5}$ data from a subset of participants (n=9) is plotted in Figure 6.3, along with the dates for which each sample was collected plotted as a vertical white line. By utilizing the nearest EPA sensor data to each study participant, we can acquire an understanding of a daily average $PM_{2.5}$ value for each study participant. This also creates a standardized way of estimating exposure (barring sensor to sensor differences in $PM_{2.5}$ measurement) by utilizing an EPA sensor which has some standardization on how the $PM_{2.5}$ measurement is made.

However, the methodology of using a single nearest EPA sensor has many limitations. For one, the distance each participant lives to the exact location of an EPA sensor varies amongst the study participants. For example, many participants, particularly those who were located within the Methow Valley live closest to the same sensor, and therefore have the same outdoor $PM_{2.5}$ exposure by means of the way that we measured outdoor $PM_{2.5}$ exposure. However, because they vary in distance from the sensor, it is more likely

that the $PM_{2.5}$ exposure differs amongst the participants and the accuracy likely follows how close they live to the sensor. Variations in terrain, wind and other weather patterns may further complicate the actual outdoor exposure accuracy, beyond simply distance to sensor.

Indoor air quality can also vary greatly from outdoor air quality and the difference between indoor and outdoor air quality may further be different based on an individual home's ventilation. We capture indoor air values for a subset of participants (n=15) from the use of a PurpleAir Indoor air monitor, and therefore we can gain a better understanding for these 15 participants of the indoor air quality. Qualitatively examining the $PM_{2.5}$ graphs for indoor air quality for participants in the Methow Valley who experienced smoke from the same fires, participants 1 and 2 (from the same household) compared to participant 3 or participant 4 (Figure 6.3A-D), even for the same outdoor air quality EPA sensor, the indoor air quality varies greatly between households. Participant 6, who was also located in the Methow Valley but closer to a different EPA sensor had a much lower indoor $PM_{2.5}$ compared to their outdoor exposure (Figure 6.3F). The indoor air $PM_{2.5}$ average daily values are plotted in Figure for participants where data was available (Figure 6.3 A-D, F, G, I).

Finally, it is important to note that individual behavior also changes each individual's effective $PM_{2.5}$ exposure. For example, two study participants who are located near each other and are closest to the same EPA sensor may experience vastly different effective $PM_{2.5}$ exposures. One participant may work from home, will have spent most of their time indoors in a well-ventilated home with an effective HVAC system, while additionally utilizing HEPA filters in their homes and using N95 masks when they did need to go outdoors. This participant is likely to have been exposed to a much lower amount of smoke particulates compared to another participant who may need to work outdoors throughout the heavy smoke exposure, does not wear an N95 mask or have effective HVAC or HEPA-based filters in their home.

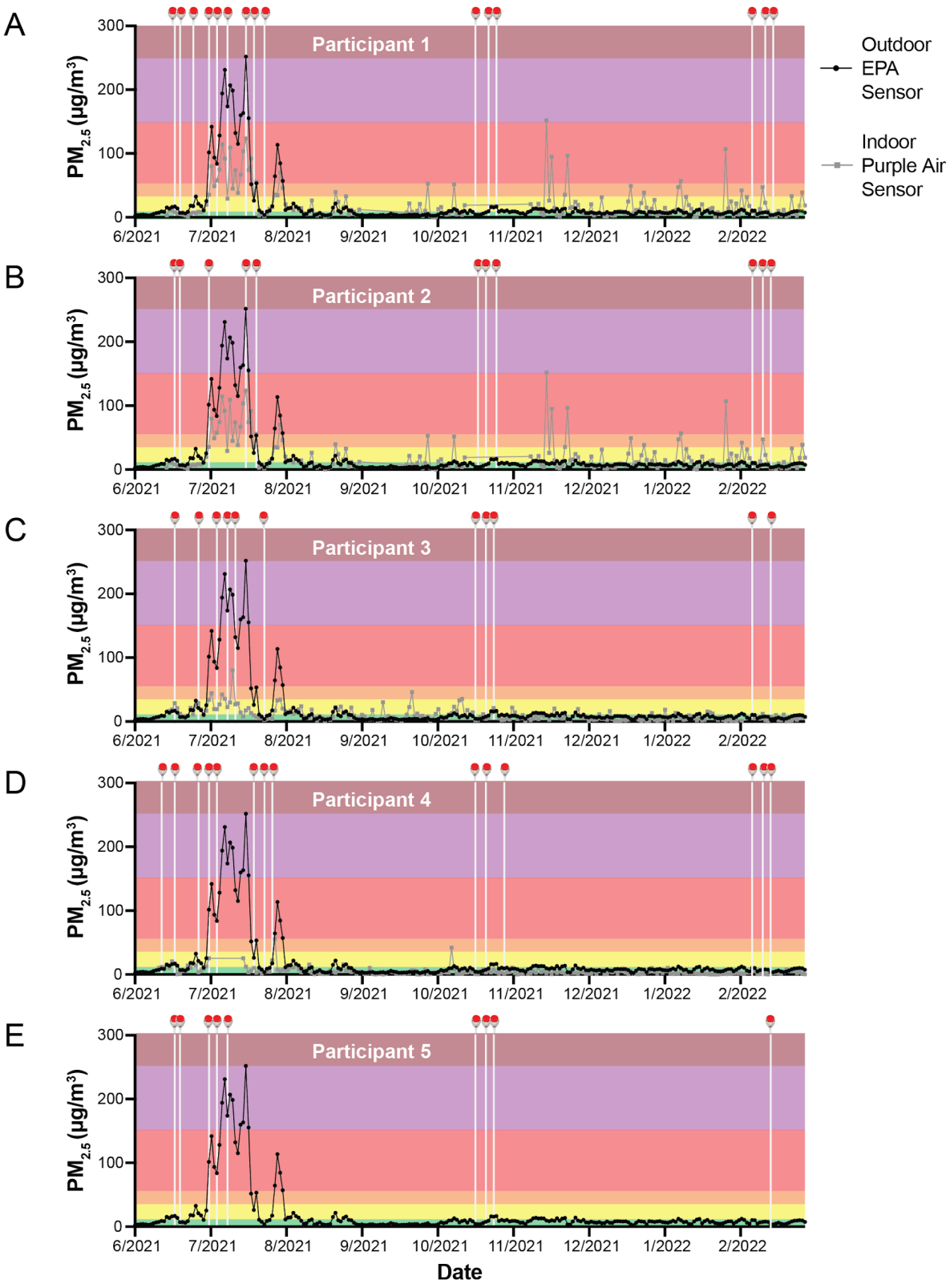
A
Participant 1
B
Participant 2
C
Participant 3
D
Participant 4
E
Participant 5
PM2.5 (µg/m3)
300
200
100
0
6/2021
7/2021
8/2021
9/2021
10/2021
11/2021
12/2021
1/2022
2/2022
Date
Outdoor EPA Sensor
Indoor Purple Air Sensor

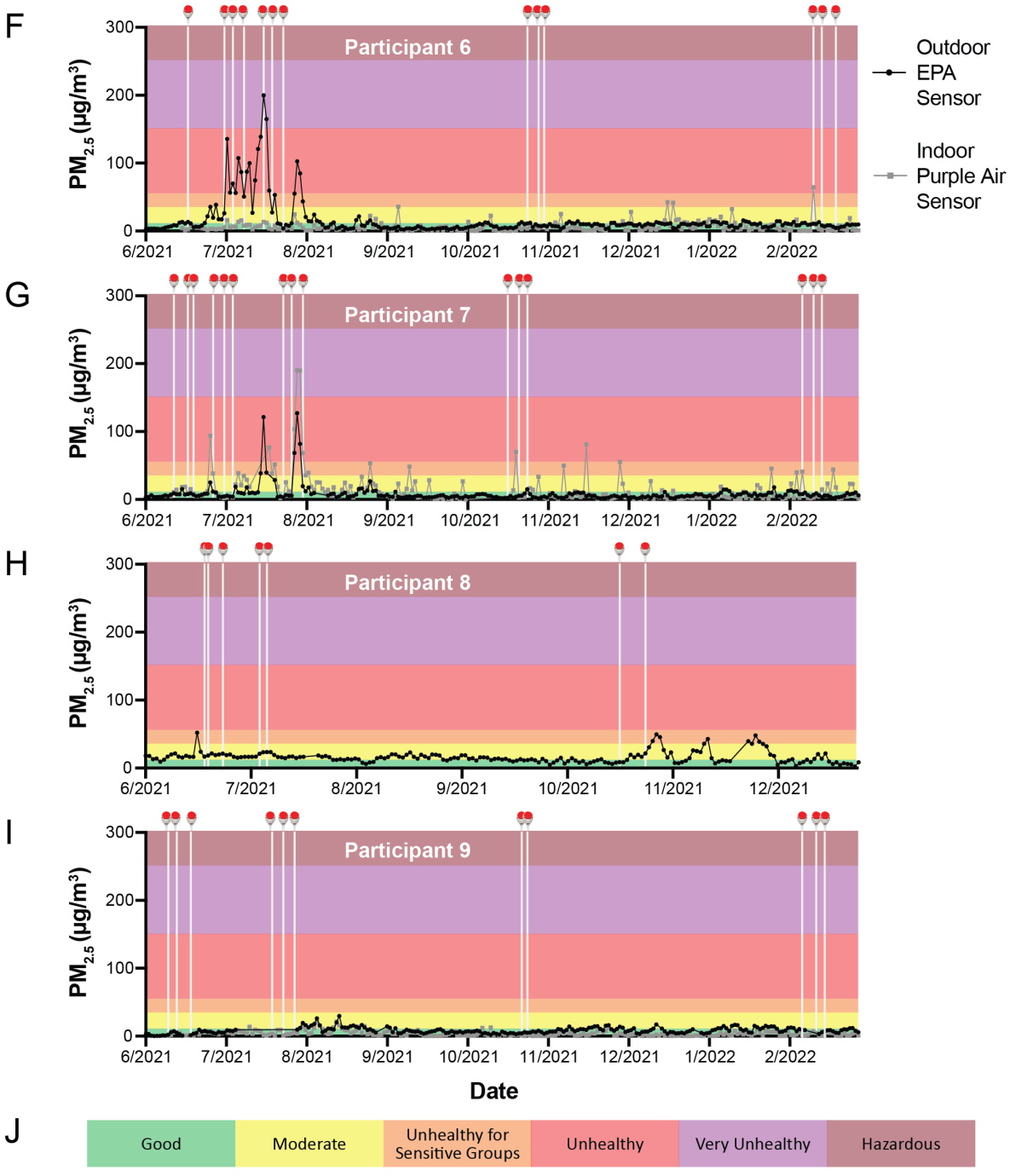

Figure 6.3. Subset of participant's $PM_{2.5}$ exposure across study period with relation to sampling timepoints. (A) through (I) indicated participant 1-9 individual exposure plotted against the sampling timepoints indicated by white vertical lines. Outdoor EPA sensor is plotted in black in indoor PurpleAir sensor (if available) plotted in grey. Participant 1 (A) and 2 (B) were from the same household. (A-E) Participant 1 – 5 had the same nearest outdoor EPA sensor in the Methow Valley. (F) Participant 6 was also in the Methow Valley but was closer to a different sensor. (G) Participant 7 was located in central Washington State, and participant 7 (H) and 8 (I) were located in southern and northern California, respectively. (J) color scheme key for all charts corresponding to the EPA air quality categories.

6.6 Materials and Methods

***home*RNA kit assembly and contents:** *home*RNA is a self-sampling kit for the collection and stabilization of blood RNA, utilizing the Tasso-SST™ blood collection device and specially designed stabilizer tube containing RNA*later*™. The kit includes components for self-collection of peripheral blood and immediate stabilization of cellular RNA. We describe the components and workflow of assembling and using the *home*RNA kit in detail in Haack, Lim, et al., [37] which describes a small pilot feasibility study in which we characterized the use of *home*RNA for remote blood collection and RNA stabilization.

The stabilizer tube was injection molded out of polycarbonate (PC: Makrolon 2407) by Protolabs, Inc (Maple Plain, MN) and was designed to hold a stabilization solution and connect to the commercially available Tasso-SST™ blood collection tube. The stabilizer tube was filled with 1.3 mL RNA*later*™ (Thermo Fisher) stabilization solution and capped. The stabilizer tube insert was injection molded out of polycarbonate (PC: Makrolon 2407) by Protolabs, Inc (Maple Plain, MN) and was designed to hold the stabilizer tube containing blood in a 50 mL conical tube during transport. All components were cleaned via sonication in 70% ethanol (v/v) for 30 min and air dried prior to assembly. Finally, all kit components were placed in a rigid custom design mailer box (The BoxMaker, Inc.). Detailed design files for the stabilizer tube and insert can be found in Haack, Lim, et al. [37]

***home*RNA workflow:** The workflow of the *home*RNA device is described in detail in Haack, Lim, et al. (Ch. 4)[37]. Briefly, to use the *home*RNA kit, participants collected capillary blood from their upper arm using a Tasso-SST™ device provided in the *home*RNA kit. Prior to stabilizing the blood, participants were asked to estimate the volume of blood collected based on a photo of the Tasso SSTTM tube in the sample collection survey (Fig Xi). The participants then stabilized the blood in RNA*later*™ by interfacing the RNA stabilizer tubes with the Tasso-SST™ blood tube and shaking to mix the blood with the stabilizer. After mixing, the stabilized blood sample is placed inside of a 50 mL conical tube containing an insert to hold the sample tube in place, which is then packaged and mailed back to the lab for analysis.

Participant recruitment and demographics: This study was approved by the University of Washington Institutional Review Board (IRB) under protocol STUDY00012463. All study procedures were performed

after informed consent was obtained. A total of 63 volunteers between ages 20-77 years old were enrolled between June and August 2021. Of these, 58 completed at least one sample collection and continued in the study. By design, more participants were enrolled than we plan to analyze to increase the likelihood that a subset of participants would experience smoke exposure. Of the 58 participants that completed at least 1 sample, 28 were selected for further analysis. 18 participants were located in the Methow Valley Region in WA state and 14 of these were selected for further analysis.

Of the 28 participants selected for further sample analysis, 10 reported male sex at birth, and 18 reported female sex at birth. At the time of enrollment, the age range from 22 to 77 years old. 14 participants from the Methow Valley region were selected for further sample analysis, and 14 from outside of the Methow Valley region. Every individual inside the Methow Valley region experienced high levels of smoke exposure in 2021. Of those outside of the Methow Valley region, 4 experienced some smoke exposure in 2021, and 9 experienced little to no smoke exposure in 2021 but were sampled at similar times as the participants from the Methow Valley Region.

Study Design of Enrollment: After completing a screening survey online including information on eligibility for the study and zipcode, individuals were invited to complete the process for informed consent and enrollment by the study team. Preference was given to those located in the Methow Valley region. To ensure an adequate distribution of participants outside of the Methow Valley region (in order to increase the likelihood that a subset of participants would experience wildfire smoke exposure), enrollment was then offered to individuals in order to increase geographic diversity while preventing an excess of participants from one region.

Study Design of timeline of sample collection and logistics: Throughout the study, participants were sent a package containing 3 *home*RNA kits, and given a schedule for when to use each kit. Typically, each of the 3 samples was taken 3 to 4 days apart, and returned immediately via overnight shipping, if available.

Baseline samples: Immediately upon enrollment participants were sent three samples to serve as the baseline pre-wildfire smoke exposure time point.

Sampling throughout wildfire season: Location of wildfires, smoke plumes, and $PM_{2.5}$ values were monitored throughout the wildfire season. If smoke was present in a participant's zip code, participants were sent a box with 3 kits and asked to sample every 3-4 days. During the smoke event in Methow Valley WA, participants outside of this region who were not experiencing smoke exposure were asked to sample at similar times to those located in a Methow Valley. Because participants were asked to take a total of three samples 3 to 4 days apart, sampling lasted for about 1.5 weeks, thereby capturing different time points during a particular fire (in other words, a day before a spike in $PM_{2.5}$ value, the day of the spike in $PM_{2.5}$ value, or a few days after, when $PM_{2.5}$ values had returned down towards moderate to low values).

Sampling after wildfire season: All participants were sent 3 additional *home*RNA kits between October-early November (3 months after wildfire event in Methow Valley region in Washington), then again in February-April (approximately 6 months after the wildfire event in Methow Valley region in Washington).

$PM_{2.5}$ data collection: $PM_{2.5}$ data was estimated using the nearest outdoor EPA sensor for each participant and utilizing a provided indoor PurpleAir air monitor if available.

$PM_{2.5}$ outdoor data collection: Daily averages of $PM_{2.5}$ data were collected for each day of the study period from the closest EPA sensor to each participant's home address. The closest sensor was calculated based on the participants home latitude and longitude and mapped to the closest EPA sensor based on the reported latitude and longitude of the sensor, which can be found at https://www.epa.gov/outdoor-air-quality-data/download-daily-data.

$PM_{2.5}$ indoor data collection: A subset of participants (*n=15*) were provided with indoor purple air monitors (PurpleAir indoor monitor) and the study team was provided with the sensor ID. Data for the study period was downloaded from the PurpleAir website (purpleair.com), and the daily average $PM_{2.5}$ was calculated for each day of the study period.

Survey data collection: Participants were surveyed throughout the study period. Specific surveys are described below:

Enrollment Survey: Survey was taken immediately after informed consent was given, and asked participants for information about participant demographics, participant home address for the purpose of

sending samples and tracking $PM_{2.5}$ data, and asked the participant to report information on underlying health conditions, recent vaccinations and medications that may affect immune activation.

Baseline Survey: This survey was given with the first sample that was taken, whether it was before the first wildfire smoke exposure or not. Information collected in the survey included all of the information included in every sample collection survey (see "*Sample Collection Surveys"* below). If, for the first sample, a participant was experiencing smoke exposure, they were additionally asked the questions that are specific to smoke exposure (see "*Smoke Exposure Survey"* below). Additional information in the baseline survey included information on exposures a participant may have experienced in the past year, a participant's occupation, including whether or not the participant's occupation requires them to work outdoors, and asks the participant about typical daily activities and to list general activities they engage in as a means of reducing psychological stress. Questions on daily activities and stress were adapted from standardized surveys on stress assessment available on PhenX.

Sample Collection Surveys: every sample collection survey included questions about sample collection metrics (e.g., estimating how much blood was collected, time to collect) and usability questions (how easy the kit was to use and pain level using the Tasso device). Each time a participant took a blood sample they were also asked about the presence of any symptoms related to smoke exposure (the list of symptoms was adopted from a standardized survey in PhenX for wildfire smoke exposure), they were asked to rate their stress levels compared to normal, they were asked to estimate hours of sleep, and they were asked about whether or not they were able to engage in their normal daily activities. If a participant is included in the group that received an indoor PurpleAir $PM_{2.5}$ monitor, they were asked to report the value on a $PM_{2.5}$ air monitor at the time of collection. Participants were also asked about the date and time in which they took the blood sample.

Smoke Exposure Surveys: if a study participant was using the *home*RNA kit during a period of time in which they were experiencing smoke exposure, they were asked all the same questions and the sample collection survey (see "*Sample Collection Surveys"* above) and were additionally asked question specifically towards behaviors that would affect smoke exposure. These questions included asking the

participants to estimate how much time they spent outdoors, in a car or bus, and indoors. It also asked participants if they utilize any mitigation strategies, including the use of a HEPA filter, an N95 mask, or simply avoiding going outside or doing activities such as vacuuming.

Closing Survey: participants were given a final survey at the end of the study period. The survey included demographics and behavior questions, including if a participant had a major change in behavior or health status throughout the entirety of the study. Participants were also asked to list any periods of time in which they may have been in a different location (e.g., on vacation), that would have caused them to experience either higher or lower smoke exposure or pollution than they would have if they had stayed home.

Sample processing: Upon arrival at the lab, the packaged *home*RNA kit was initially stored at -20°C by direct delivery to a -20°C freezer. Within a week, the 50 mL conical tube containing the stabilized blood sample was removed from the kit and the RNA*later* stabilized sample was stored at -80°C until ready for further analysis. Total cellular RNA was isolated from selected samples using the Ribopure™ - Blood RNA Isolation Kit (Thermo Fisher) according to manufacturer's protocol and eluted in two 50 µL aliquots. Isolated RNA was stored at -80°C until ready for further analysis.

The RIN scores of the first 50 µL elution for all extracted RNA samples were obtained on a Bioanalyzer 2100 (Agilent) using the Agilent RNA 6000 Pico Kit, using a 1:20 dilution in nuclease free water to ensure the RNA concentration was in the qualitative range for the Agilent RNA 6000 Pico Kit. RNA concentration of the first 50 µL elution was measured using the Qubit Flex Fluorometer (Thermo Fisher) using the Qubit RNA High Sensitivity Assay Kit.

6.7 Conclusion

We demonstrated that *home*RNA facilitated an effective and flexible approach to studying the effects of wildfire smoke on human health. The *home*RNA kits enabled participants to collect samples in their own homes, allowing for a fully disseminated study. By enabling fully remote, flexible, and responsive sampling throughout a wildfire season, *home*RNA kits provide an opportunity to capture different time points during a particular fire, as well as to collect samples from participants who are exposed to wildfire

smoke and those that are not, allowing for comparisons across exposure groups. The study also retained over 95% of participants, with some participants even choosing to continue to use *home*RNA even after evacuation, demonstrating the feasibility of the *home*RNA kits and this study design to conduct longitudinal studies on health effects of wildfires and other hazards and disasters. Most samples where RNA was isolated also had suitable quality assessment metrics (RIN ≥ 6) for downstream analysis with 3'RNA-Seq, indicating that this study design can help elucidate inflammatory gene response to wildfire smoke in the general population.

Understanding the inflammatory gene response to smoke exposure and evaluating the impacts of protective measures, such as portable air cleaners, is essential for protecting public health and informing policy decisions. Further studies utilizing *home*RNA kits in a larger study population could provide more information on the health effects of wildfire smoke and their socio-economic, occupational, and household-level determinants, as well as the associated effect of protective measures.

6.8 References

1. M. D. Hurteau, A. L. Westerling, C. Wiedinmyer and B. P. Bryant, Environ Sci Technol, 2014, **48**, 2298–2304.
2. J. A. Hutchinson, J. Vargo, M. Milet, N. H. F. French, M. Billmire, J. Johnson and S. Hoshiko, *PLoS Med*, 2018, **15**, 1–21.
3. S. M. Holm, M. D. Miller and J. R. Balmes, *Journal of Exposure Science & Environmental Epidemiology 2020 31:1*, 2020, **31**, 1–20.
4. C. E. Reid, M. Brauer, F. H. Johnston, M. Jerrett, J. R. Balmes and C. T. Elliott, *Environ Health Perspect*, 2016, **124**, 1334–1343.
5. L. N. Kobziar and G. R. Thompson, *Science (1979)*, 2020, **370**, 1408–1410.
6. S. Henry, M. B. Ospina, L. Dennett and A. Hicks, *Int J Environ Res Public Health*, 2021, **18**, 8799.
7. M. C. Mirabelli, N. Künzli, E. Avol, F. D. Gilliland, W. J. Gauderman, R. McConnell and J. M. Peters, *Epidemiology*, 2009, **20**, 451.
8. E. R. Sutherland, B. J. Make, S. Vedal, L. Zhang, S. J. Dutton, J. R. Murphy and P. E. Silkoff, *Journal of Allergy and Clinical Immunology*, 2005, **115**, 420–422.
9. E. Roscioli, R. Hamon, S. E. Lester, H. P. A. Jersmann, P. N. Reynolds and S. Hodge, *Respir Res*,

2018, **19**, 1–13.

10. G. Lee, T. C. Walser and S. M. Dubinett, *Curr Opin Pulm Med*, 2009, **15**, 303–307.
11. J. Zhao, M. Li, Z. Wang, J. Chen, J. Zhao, Y. Xu, X. Wei, J. Wang and J. Xie, *Respir Res*, 2019, **20**, 1–13.
12. J. R. Murdoch and C. M. Lloyd, *Mutat Res*, 2010, **690**, 24–39.
13. M. Prunicki, L. Stell, D. Dinakarpandian, M. de Planell-Saguer, R. W. Lucas, S. K. Hammond, J. R. Balmes, X. Zhou, T. Paglino, C. Sabatti, R. L. Miller and K. C. Nadeau, *Clin Epigenetics*, 2018, **10**, 2.
14. L. M. Coussens and Z. Werb, *Nature*, 2002, **420**, 860–867.
15. G. Lee, T. C. Walser and S. M. Dubinett, *Curr Opin Pulm Med*, 2009, **15**, 303–307.
16. K. M. Navarro, M. T. Kleinman, C. E. Mackay, T. E. Reinhardt, J. R. Balmes, G. A. Broyles, R. D. Ottmar, L. P. Naher and J. W. Domitrovich, *Environ Res*, 2019, **173**, 462–468.
17. S. Mihai, E. Codrici, I. D. Popescu, A. M. Enciu, L. Albulescu, L. G. Necula, C. Mambet, G. Anton and C. Tanase, *J Immunol Res*, , DOI:10.1155/2018/2180373.
18. A. Lopez-Candales, P. M. H. Burgos, D. F. Hernandez-Suarez and D. Harris, *J Nat Sci*.
19. K. Esposito and D. Giugliano, *Nutrition, Metabolism and Cardiovascular Diseases*, 2004, **14**, 228–232.
20. J. R. Swiston, W. Davidson, S. Attridge, G. T. Li, M. Brauer and S. F. van Eeden, *European Respiratory Journal*, 2008, **32**, 129–138.
21. H. Jia, Y. Liu, D. Guo, W. He, L. Zhao and S. Xia, *Environ Toxicol*, 2021, **36**, 298–307.
22. K. Huttunen, T. Siponen, I. Salonen, T. Yli-Tuomi, M. Aurela, H. Dufva, R. Hillamo, E. Linkola, J. Pekkanen, A. Pennanen, A. Peters, R. O. Salonen, A. Schneider, P. Tiittanen, M. R. Hirvonen and T. Lanki, *Environ Res*, 2012, **116**, 44–51.
23. A. M. Hejl, O. Adetona, D. Diaz-Sanchez, J. D. Carter, A. A. Commodore, S. L. Rathbun and L. P. Naeher, *J Occup Environ Hyg*, 2013, **10**, 173–180.
24. G. Mu, M. Zhou, B. Wang, L. Cao, S. Yang, W. Qiu, X. Nie, Z. Ye, Y. Zhou and W. Chen, *Science of The Total Environment*, 2021, **755**, 142522.
25. A. M. Adetona, O. Adetona, R. M. Gogal, D. DIaz-Sanchez, S. L. Rathbun and L. P. Naeher, *J Occup Environ Med*, 2017, **59**, 679–690.
26. W. E. Cascio, *Science of The Total Environment*, 2018, **624**, 586–595.
27. C. Black, J. E. Gerriets, J. H. Fontaine, R. W. Harper, N. J. Kenyon, F. Tablin, E. S. Schelegle and L. A. Miller, *Am J Respir Cell Mol Biol*, 2017, **56**, 657–666.
28. L. Bowen, A. K. Miles, C. A. Kolden, J. A. Saarinen, J. L. Bodkin, M. J. Murray and M. T. Tinker, *Mar Mamm Sci*, 2015, **31**, 191–210.
29. A. M. Jung, J. Zhou, S. C. Beitel, S. R. Littau, J. J. Gulotta, D. D. Wallentine, P. K. Moore and J. L. Burgess, *J Expo Sci Environ Epidemiol*, 2021, **31**, 900–912.
30. X. Du, Q. Zhang, Y. Jiang, X. Zhu, Y. Zhang, C. Liu, Y. Niu, J. Cai, R. Chen and H. Kan, *Environ Int*, , DOI:10.1016/j.envint.2022.107430.
31. R. Xu, S. Li, Y. Wu, X. Yue, E. M. Wong, M. C. Southey, J. L. Hopper, M. J. Abramson, S. Li and

Y. Guo, *Environ Int*, 2023, **171**, 107704.

32. M. Prunicki, R. Kelsey, J. Lee, X. Zhou, E. Smith, F. Haddad, J. Wu and K. Nadeau, *Allergy*, 2019, **74**, 1989.

33. M. Prunicki, S. Miller, A. Hopkins, M. Poulin, H. Movassagh, L. Yan and K. C. Nadeau, *The Journal of Immunology*, 2020, **204**, 146.17-146.17.

34. L. Williams, J. Mouat, A. Goodrich, E. Angel, S. Raffuse, J. LaSalle and R. Schmidt, *ISEE Conference Abstracts*, , DOI:10.1289/ISEE.2022.O-OP-143.

35. A. P. Brown, L. Cai, B. I. Laufer, L. A. Miller, J. M. LaSalle and H. Ji, *Environ Int*, , DOI:10.1016/j.envint.2021.106993.

36. A. M. Parenteau, N. v. Alen, J. La, A. T. Luck, D. J. Teichrow, E. M. Daang, A. T. Nissen, L. B. K. Deer and C. E. Hostinar, *New Dir Child Adolesc Dev*, 2022, **2022**, 125–154.

37. A. J. Haack, F. Y. Lim, D. S. Kennedy, J. H. Day, K. N. Adams, J. J. Lee, E. Berthier and A. B. Theberge, *Anal Chem*, 2021, **93**, 13196–13203.

38. M. Prunicki, R. Kelsey, J. Lee, X. Zhou, E. Smith, F. Haddad, J. Wu and K. Nadeau, *Allergy*, 2019, **74**, 1989.

39. D. O'Keeffe, M. Dennekamp, L. Straney, M. Mazhar, T. O'Dwyer, A. Haikerwal, F. Reisen, M. J. Abramson and F. Johnston, *BMC Public Health*, 2016, **16**, 1–7.

40. T. O'dwyer, M. J. Abramson, L. Straney, F. Salimi, F. Johnston, A. J. Wheeler, D. O'keeffe, A. Haikerwal, F. Reisen, I. Hopper and M. Dennekamp, *Int J Environ Res Public Health*, 2021, **18**, 1–10.

41. A. Durkin, R. Gonzalez, T. B. Isaksen, E. Walker and N. A. Errett, *International Journal of Environmental Research and Public Health 2020, Vol. 17, Page 8393*, 2020, **17**, 8393.

42. A. Doubleday, J. Schulte, L. Sheppard, M. Kadlec, R. Dhammapala, J. Fox and T. Busch Isaksen, *Environ Health*, 2020, **19**, 1–10.

43. N. A. Errett, H. A. Roop, C. Pendergrast, C. B. Kramer, A. Doubleday, K. A. Tran and T. M. B. Isaksen, *Int J Environ Res Public Health*, , DOI:10.3390/IJERPH16132398.

44. A. Humphreys, E. G. Walker, G. N. Bratman and N. A. Errett, *BMC Public Health*, , DOI:10.1186/S12889-021-12411-2.

45. A. Vicente, C. Alves, A. I. Calvo, A. P. Fernandes, T. Nunes, C. Monteiro, S. M. Almeida and C. Pio, *Atmos Environ*, 2013, **71**, 295–303.

46. Clean Air Act Requirements and History | US EPA, https://www.epa.gov/clean-air-act-overview/clean-air-act-requirements-and-history, (accessed 28 January 2023).

47. B. P. Hejblum, J. Skinner and R. Thiébaut, *PLoS Comput Biol*, 2015, **11**, e1004310.

48. D. Rinchai, S. Deola, G. Zoppoli, B. S. A. Kabeer, S. Taleb, I. Pavlovski, S. Maacha, G. Gentilcore, M. Toufiq, L. Mathew, L. Liu, F. R. Vempalli, G. Mubarak, S. Lorenz, I. Sivieri, G. Cirmena, C. Dentone, P. Cuccarolo, D. R. Giacobbe, F. Baldi, A. Garbarino, B. Cigolini, P. Cremonesi, M. Bedognetti, A. Ballestrero, M. Bassetti, B. P. Hejblum, T. Augustine, N. van Panhuys, R. Thiebaut, R. Branco, T. Chew, M. Shojaei, K. Short, C. G. Feng, S. M. Zughaier, A. de Maria, B. Tang, A. Ait Hssain, D. Bedognetti, J.-C. Grivel and D. Chaussabel, *Sci Adv*, 2022, **8**, 21.

Chapter 7: Conclusions and Future Directions

The technologies presented in this dissertation have potential to impact a diverse set of interdisciplinary applications towards the goal of understanding human health and disease mechanisms. Open microfluidic patterning methods and *home*RNA are both actively being used in many studies across a broad range of topics in medicine and human health. Open microfluidic patterning is currently being used to develop skeletal tissue disease models, periodontal models, and cardiac disease models. Similarly, *home*RNA is being used in many human subjects studies investigating a range of questions from the host-viral interactions to autoimmune flares.

With open microfluidic patterning we open up a new paradigm for formation of specially controlled 3D engineered tissues. Using surface tension to drive flow and achieve spatial control, additional materials in geometries become possible to pattern. This has implications for forming tissues made from biologically relevant native ECMs such as collagen or fibrin, but also opens up a potential new class of "4D" tissues by enabling special control of a stimuli responsive ECM materials that are not photo-polymerizable or extrudable. Current investigations in this area include utilizing and enzymatically degradable polyethylene glycol combined with the layer by layer open microfluidic patterning method to generate pre-endothelialized vasculature within a patterned tissue.

We also introduce a method for suspended tissue generation or multiple regions can be patterned across an unsupported suspended tissue, adding an additional control of mechanical manipulation of patterned tissues. The patterning mechanism was designed to directly interface with suspended post models which are currently used to generate tissue models via casting methods, thereby this method can be easily directly adopted by users to add elements of patterning to these tissue models. In fact, investigations developing a multi tissue type periodontal model and a skeletal tissue model to investigate the border between diseased and healthy tissues are currently underway. By opening of the ability to pattern with additional materials (i.e., stimuli responsive) and the ability to create additional geometries (i.e., suspended multi region tissues), open microfluidics patterning enables not only spatial control but also temporal, chemical, and mechanical control, thus achieving an unprecedented user defined control over tissues.

In addition to applications in *in vitro* tissue models, I applied engineering and fluidic design to home-based blood sampling in RNA stabilization through the development of the *home*RNA kit, thus expanding the potential to study human health and disease outside of the laboratory and into the home. We have demonstrated that *home*RNA can be used as a tool for dynamic and responsive sampling during wildfire smoke exposure events and future work aims at expanding the use of *home*RNA to other disasters. *home*RNA is also being used for studies investigating the host-response to SARS-CoV-2 infections and for capturing inflammatory changes in individuals with rheumatoid arthritis, particularly in response to flare triggers.

Along with ongoing remote studies using *home*RNA to investigate the immune response to various events, further development is currently underway on *home*RNA itself. This development includes investigating temperature related effects of *home*RNA stabilized blood with controlled temperature in-lab experiments and shipping experiments with continuous temperature monitors. Further, we plan to expand the blood stabilization process to other biological molecules, such as proteins, miRNA, etc. thus further expanding the possibilities for probing systemic biological responses to remote events.

A. Appendix for Chapter 2

Reproduced in part from U. N. Lee, J. H. Day,* A. J. Haack,* R. C. Bretherton, W. Lu, C. A. DeForest,[#] A. B. Theberge,[#] and E. Berthier,[#] "Layer-by-layer fabrication of 3D hydrogel structures using open microfluidics." Lab on a Chip, 2020, **20**, 525–536.*
**Equal contribution*
[#]Co-corresponding authors

Extended Materials and Methods

Derivation for SCF condition in rail-based microchannels

In the case where a channel is comprised of multiple surfaces with different materials and unique contact angles, the condition for advancement of a fluid in the channel is given by a condition on the Cassie Angle, θ^*(1a), referred to as the Generalized Cassie law (1b), where f_i is the fraction of the channel's cross-sectional perimeter composed of a material i, and θ_i is the contact angle of material i.

$$\cos(\theta^*) = \sum_i f_i \cos(\theta_i) \quad \text{(Eq. 1a)}$$

$$\cos(\theta^*) > 0 \quad \text{(Eq. 1b)}$$

Given the cross-sectional geometry of a rail-based channel and the convention that the contact angle of fluid on air is 90°, Eq. 1 can be rewritten as:

(Eq. 2)

Where w_1 is the width of the channel ceiling, w_2 is the width of the channel floor, and h is the distance between the channel ceiling and the floor. Assuming that $w_1 = w_2$, Eq. 2 reduces down to:

$$\frac{h}{w_1} < \frac{\cos(\theta_1) + \cos(\theta_2)}{2} \quad \text{(Eq. 3)}$$

where h is the height of the patterned layer (defined by the distance between the patterning area of the patterning device and the underlying substrate), θ_1 is the contact angle of the patterning device, and θ_2 is the contact angle of the underlying substrate.

Design of hollow double helix

The helix consists of a total of 30 layers of agarose (including the base layer), which were all patterned via SCF and rail-based technology. Each layer looks like a button with two holes, that is rotated about the center for each subsequent layer. Figure A10A illustrates a top-down schematic for the helix design. The length, *d*, is the diameter of the holes, which is 3 mm for all layers on both sides. *r* is the distance from the center of the design to the center of the holes on both sides, and for all layers is 2.5 mm. The angle of rotation about the center of the design is denoted by ϕ, and the maximum overhang length is denoted by *s*. For the first two layers, the angle of rotation, ϕ, is 5 degrees with a designed overhang, *s*, of 240 μm to establish the overhang. After the overhang was established, the remaining layers were rotated 10 degrees for a total designed maximum overhang of 479 μm. A new device was used for each layer with an alignment marker for consistency in the degree of rotation. The helix was designed to include a curvature that outlined the two holes which allowed for SCF to continue to the edge of the desired overhang. These values can be found in Table A1.

Imaging of hollow double helix

A Nikon DSLR camera was used to take images of the double helix. The helices were removed from the well plate with a spatula and placed on a standard No. 1.5, 25 mm square coverslip (Fisherbrand). A 1 mL syringe with a 18 gauge needle with 18 gauge PTFE tubing attached to reach the bottom of the helices was used to load the helices with dye. A syringe with a 25 gauge needle was used to remove any air pockets that formed from filling the hollow tubes with dye. During loading, the tubing damaged the walls of the agarose and these irregularities filled with dye (Figure 4C, right). Yellow and blue India ink dye (Dr. Ph. Martin's Bombay India Ink) was used to fill the helix (Figure 4C, right), and dextran with fluorescein 70,000 MW in DI water at 10 mg/mL (Invitrogen) was used to fill a separate helix in Figure 2C. To take the photo in Figure 2C, the fluorescent dye was excited using a 365 nm lamp (Spectroline). Helix images were processed using Adobe Photoshop CC 2018 using a uniform brightness/contrasts adjustment.

Imaging and design of overhanging cross sections

The cross-sectional images shown in Figure 4A were designed such that the overhang and curvature of each layer corresponded to the maximum overhang in the first seven layers of the helix. The curvature information can be found in Table C1 where the first seven layers correspond to the overhang cross section device, as well as the first seven layers of the helix. To image the cross section, a smooth edge was cut using a coverslip (Fisherbrand) and the overhang was transferred to another coverslip for imaging with a DSA25E goniometer (Kruss). The images in Figure 4A are separately constructed agarose structures, cut and imaged at different stages.

Design of curvature for overhanging features

In order to achieve spontaneous capillary flow for all layers of the seven layered overhanging structure (Figure 4A) and the hollow double helix structure (Figure 4C, Figure 2C), the geometry of curvature was adjusted for each layer. If each layer had the same curvature, then the maximum distance (air gap) between the two layers would become great enough that spontaneous capillary flow is inhibited. This concept is illustrated in Figure C3C, as denoted by the red arrow. However, by applying a calculation to change the curvature dimensions of the current layer based upon the dimensions of the previous layer, the distance between layers can be minimized allowing for SCF, illustrated by the reduction of the double-headed red arrow length (Figure C3C). Note that the overhang dimensions for the seven layered overhanging structure in Figure 4A are the same as the dimensions for the first seven layers of the helix. The calculation was made as follows: for the first overhanging layer, layer 2, the radius of curvature is set to 1 mm. Every subsequent layer's radius of curvature is increased by 0.5 mm, i.e., layer 3 is 1.5 mm, layer 4 is 2 mm, etc. Take any layer, n where $n > 1$, and the radius of curvature, r_n is then given by Eq. 4.

$$r_n = 0.5n \qquad \text{(Eq. 4)}$$

Layer 1 has no radius of curvature, as it is not an overhanging layer. The curvature of layer n was designed such that the curvature began at half the distance of the x-component of the previous layer, x_{n-1}, which is illustrated in the diagram below.

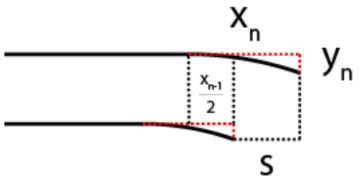

Note that s is the designed maximum overhang, which for the helix design is also denoted by s in Figure C3A. The s component of the curvature for layer n, x_n, is then given by taking one half of the x-component of the previous layer, and adding this to the maximum overhang, s, described in Eq. 5.

$$x_n = \frac{x_{n-1}}{2} + s \quad \text{(Eq. 5)}$$

Note that the maximum overhang, s is set by the angle of rotation for the helix (ϕ in Figure C10A). Using the calculated x-component and the radius of curvature for layer n, the y-component of the curvature can then be derived. The schematic below shows the geometrical schematic to calculate these layers.

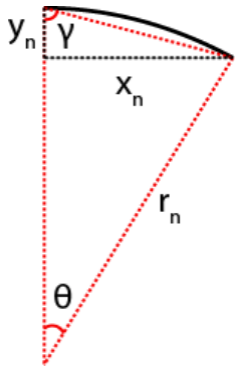

To calculate the angle, θ, which represents the arc angle of the circle that encompasses the curvature, the geometric relation of the radius of curvature, r_n, to the x-component of the curvature was used, and described in Eq. 6 where θ is in degrees.

$$\theta = \arcsin\left(\frac{x_n}{r_n}\right) \quad \text{(Eq. 6)}$$

Using this angle and the fact that the red dotted triangle is an isosceles triangle, the value of angle γ could be calculated using Eq. 7, where γ and θ are in degrees.

$$\gamma = \frac{180 - \theta}{2} \quad \text{(Eq. 7)}$$

Then, the value of y_n can be calculated using Eq. 8.

$$y_n = \frac{x_n}{\tan(\gamma)} \quad \text{(Eq. 8)}$$

These calculations were applied to all layers to derive the values in Table C1. Note that the first overhanging layer, layer 2, was set such that the curvature began at the edge of layer 1.

Enzymatically degradable hydrogels synthetic information

Chemical reagents were obtained from either Sigma-Aldrich or Fisher Scientific unless otherwise noted. Amino acids for peptide synthesis were purchased from ChemPep and associated coupling reagents from Chem-Impex.

Peptides were synthesized using standard Fmoc Solid Phase Peptide Synthesis (SPPS) on a microwave-assisted Liberty1 automated peptide synthesizer. Fmoc groups were deprotected in 20% piperidine (v/v) in N,N dimethylformamide (DMF) with 0.1 M 1-hydroxybenzotriazole (HOBt) at 90°C for 90 seconds. Fmoc-protected amino acids (1 mmol; 4x) were coupled in a solution of 1-[Bis(dimethylamino)methylene]-1H-1,2,3-triazolo[4,5-b]pyridinium3-oxide hexafluorophosphate (HATU; 1 mmol; 4x) and diisopropylethylamine (DIEA; 2 mmol; 8x) in a mixture of 20% N-methyl-2-pyrrolidone (NMP) in DMF at 75°C for 5 minutes.

Semi-preparative scale reversed-phase high-pressure liquid chromatography (RP-HPLC) was conducted on a Dionex Ultimate 3000 with 220 nm and 280 nm detection wavelengths, through a Thermo 5 μm Sychronis silica 250x21.2 mm C18 column. Pure fractions were lyophilized using a LABCONCO FreeZone 2.5 plus freeze-dryer equipped with a LABCONCO rotary vane 117 vacuum pump. Matrix-assisted laser desorption/ionization time of flight (MALDI-TOF) mass spectrometry was performed on samples suspended in a matrix of α-cyano-4- hydroxycinnamic acid:2,5-dihydroxy benzoic acid (2:1) using a Bruker AutoFlex II mass spectrometer in reflectron positive mode with detector range set to 600-3000 Da.

Four-arm poly(ethylene glycol) (MW = 20,000 Da) end-functionalized with bicyclononyne (PEG-tetraBCN) and N_3-GRGDS-NH_2 peptide were synthesized as previously described [1,2].

Recombinant Expression and Purification of SrtA(5M)

pET30b-5M SrtA was a gift from Hidde Ploegh (Addgene plasmid # 51140 ; http://n2t.net/addgene:51140 ; RRID:Addgene_51140). Chemically competent BL21 *E. coli* cells were transformed with the pET30b-5M SrtA plasmid, expanded in 1 L of Luria broth at 37°C under agitation at 200 RPM, and induced using 0.5 mM Isopropyl-beta-D-thiogalactoside when OD600 of the bacterial culture reached 0.6, measured on a Thermo Fisher Nanodrop 2000 spectrophotometer. After overnight culture at 17°C and 200 RPM agitation, cells were pelleted, resuspended in lysis buffer (20 mM Tris; 50 mM NaCl; 10 mM imidazole; 40 mL) on ice, and lysed by sonication (6 x 3 min cycles; 30% amplitude, 33% duty cycle and 3 min resting). The soluble lysate fraction was incubated with 3 mL Ni-NTA Agarose Beads (GoldBio) for 1hr at 4°C in a gravity column. The resin and bound His-tagged protein were washed in wash buffer (20 mM Tris; 50 mM NaCl; 20 mM imidazole; 5 x 20 mL), then purified SrtA was eluted in elution buffer (20 mM Tris; 50 mM NaCl; 20 mM imidazole; 20 x 1 mL). Protein was then dialyzed against PBS with Thermo Fisher SnakeSkin Dialysis Tubing (MWCO ~10 kDa) to remove Tris and imidazole. Protein was then spin concentrated in an Amicon centrifugal column (MWCO ~10 kDa), glycerol was added to 20% wt/vol, and aliquots were stored at -80°C prior to use. Protein identity and purity were confirmed using SDS-PAGE and whole protein ESI-MS (Expected 17.8 kDa, Observed 17.8 kDa).

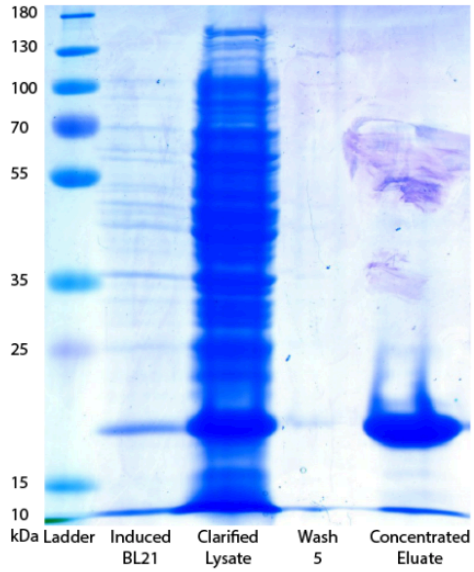

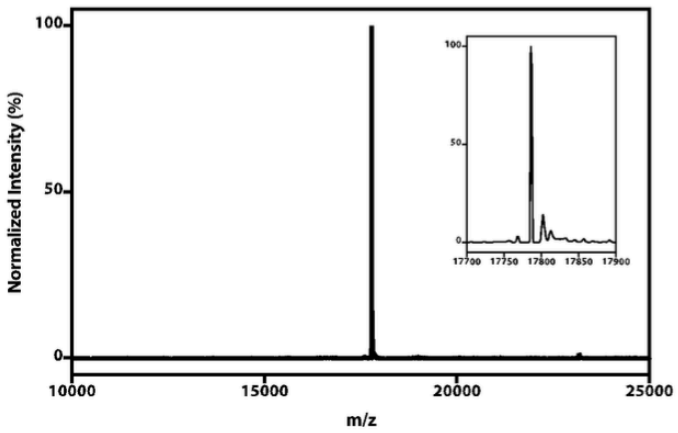

SrtA(5M) protein purification was evaluated by SDS-PAGE, revealing a strong 18 kDa band corresponding to the protein (left). Protein Identity was verified by mass spectrometry (right).

Synthesis of N_3-RGPQGIWGQGRK(N_3)-NH_2 and N_3-RGPQGIWGQLPETGGRK(N_3)-NH_2

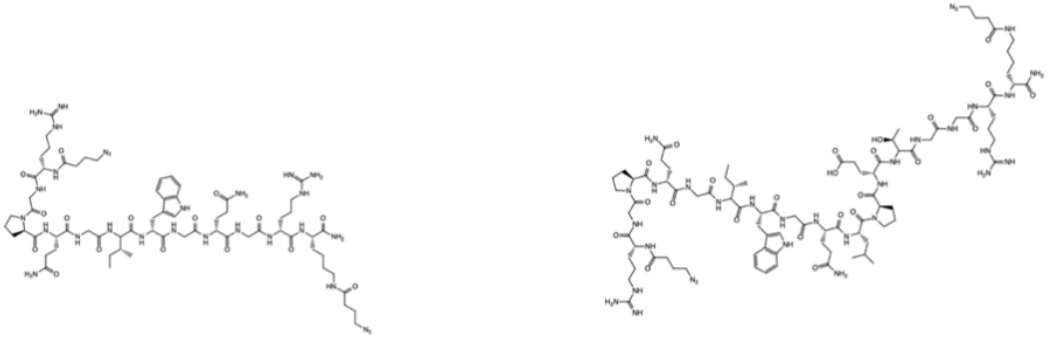

Chemical structures of the MMP-degradable peptide N_3-RGPQGIWGQGRK(N_3)-NH_2 (left) and the MMP OR SrtA degradable peptide N_3-RGPQGIWGQLPETGGRK(N_3)-NH_2 (right)

The peptides H-RGPQGIWGQGRK(Dde)-NH_2 and H-RGPQGIWGQLPETGGRK(Dde)-NH_2 were synthesized by Fmoc SPPS at 0.25 mmol scale on rink amide resin. The Dde protecting group was cleaved from resin-bound peptide using 2% hydrazine (3 x 10 min). 4-azidobutanoic acid (4x; 259 mg; 2 mmol) was conjugated to the free amines on the N-terminus and deprotected Lysine though *in situ* ester activation using a solution of HATU (3.95X; 750 mg; 1.97 mmol) and diisopropylethylamine (DIEA; 8X; 1.38 mL; 4 mmol) for 90 minutes [1]. Resin was then thrice washed with DMF and thrice with dichloromethane (DCM) prior to peptide cleavage from resin [95%/2.5%/2.5% Trifluoracetic Acid (TFA)/ Triisopropylsilane (TIS)/ H_2O]. Crude peptide product was precipitated in ice-cold diethyl ether and dried under N_2 prior to purification by RP-HPLC (55-minute gradient of 5-100% acetonitrile in water). Lyophilization yielded the pure final products (N_3-RGPQGIWGQGRK(N_3)-NH_2 and N_3-RGPQGIWGQLPETGGRK(N_3)-NH_2), each as a light-yellow solid. Peptide identity was confirmed using MALDI-TOF.

Peptide Sequence	Expected Mass (Da)	Observed Mass (Da)	Yield (mg)	Yield (mmol)	Yield (%)
N_3-RGPQGIWGQGRK(N_3)-NH_2	1559.83	1560.36	52.5	0.033	13.2
N_3-RGPQGIWGQLPETGGRK(N_3)-NH_2	2056.08	2058.47	51.2	0.025	9.9

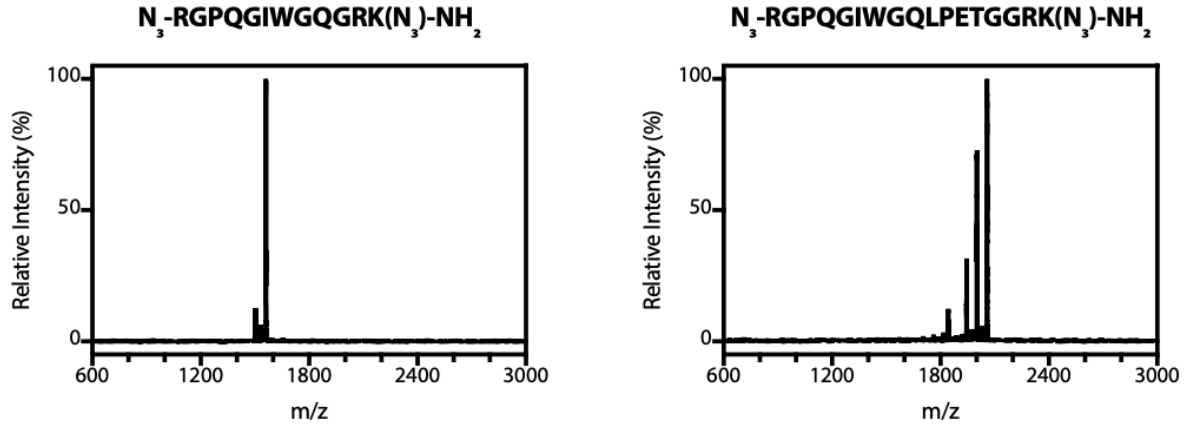

MALDI mass spectra for the synthesized and HPLC purified peptides.

Preparation of Patterning Rails for cell-encapsulated PEG hydrogel patterning.
Rails were printed with a Form 2 3D printer. Devices were sterilized under UV light for 1 hour. To prevent hydrogel or cell adhesion, the devices were incubated in 1% Bovine Serum Albumin (BSA) for 1-2 hours, and allowed to fully air dry prior to use.

References

1. DeForest, C.A.; Tirrell, D.A. A photoreversible protein-patterning approach for guiding stem cell fate in three-dimensional gels. *Nat. Mater.* **2015**, *14*, 523–531.
2. Arakawa, C.K.; Badeau, B.A.; Zheng, Y.; DeForest, C.A. Multicellular Vascularized Engineered Tissues through User-Programmable Biomaterial Photodegradation. *Adv. Mater.* **2017**, *29*, 1703156.
3. Bellis, S.L. Advantages of RGD peptides for directing cell association with biomaterials. *Biomaterials* **2011**, *32*, 4205–4210.

Supplementary Figures

Note: Figures A1-4 are demonstrations of the resolution in agarose structures achievable with the Form 2 3D printer that we used to fabricate the rail structures and is not inherent to the 3D patterning method presented in this paper.

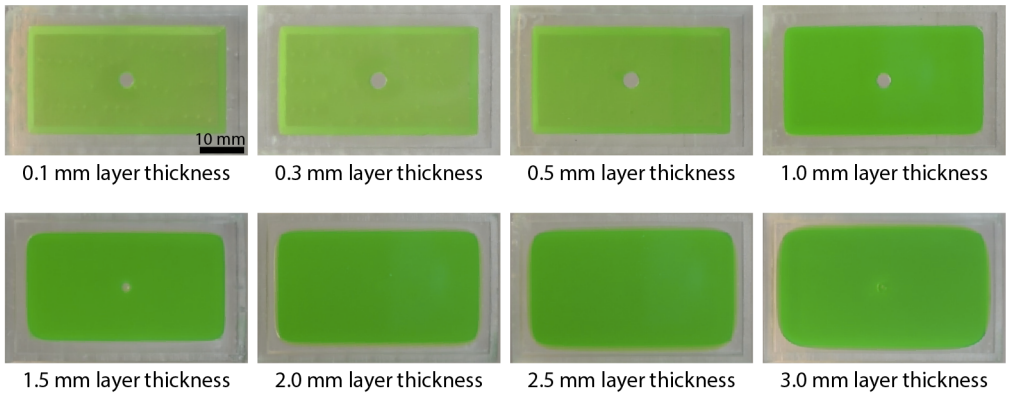

Figure A1. Effects of increasing layer thickness on capillary pinning at corners. At layer thickness 0.1, 0.3, and 0.5 mm the agarose fully fills to the corner of the patterning device. At 1.0 mm and above, agarose is unable to pin at the corners of the patterning device. Images are taken from the underside of single layers of patterned agarose. Images are representative of n=3.

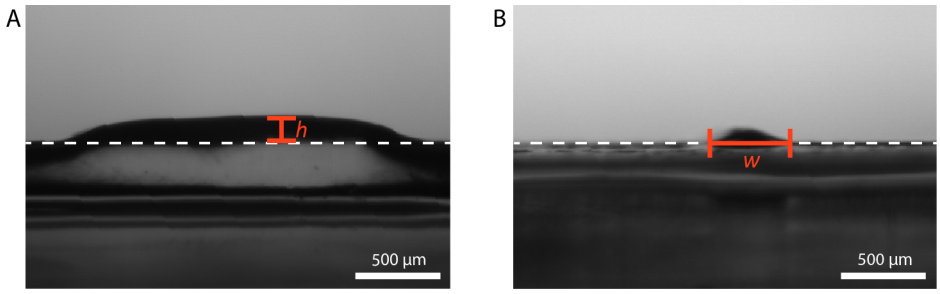

Figure A2. Cross-sectional images of minimum height and width of a layer. (A) Minimum layer height, *h*, was meausred from the baseline (dotted line) to the highest point on the gel layer. The average minimum height was 140 ± 19 µm. (B) Minimum feature width, *w*, was measured at the base of the top layer. The average minimum width was 660 ± 210 µm. At larger widths there was better control over deviations in the width (1292 ± 46 µm). All data are reported as mean ± SD for n=3.

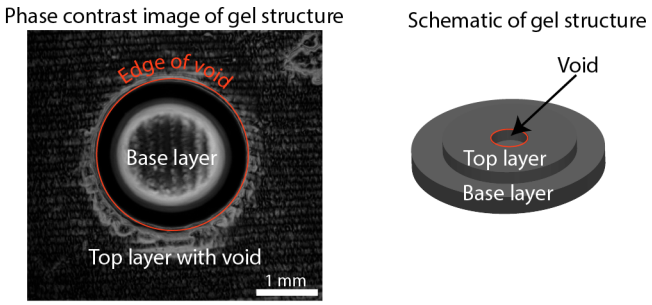

Figure A3. Minimum diameter of void. Red indicates the circle used to measure the diameter of the void. Minimum diameter of void is 1256 ± 18 µm. Data are reported as mean ± SD for n=3. Phase contrast images were taken with a Zeiss Primovert inverted microscope with a MU1403B camera (AmScope).

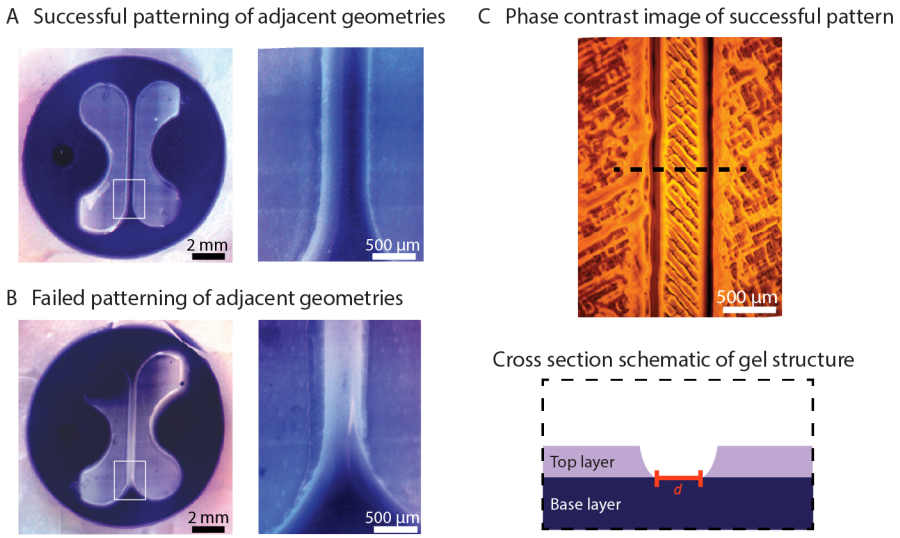

Figure A4. Minimum spacing between two independently patterned geometries (white) over a base layer of gel (purple) is 270 ± 49 µm. (A) Successful patterning of adjacent geometries. (B) Failed patterning of adjacent geometries. (C) Representative image of phase contrast image of agarose structure. Dotted line indicates cross section of the gel in schematic where *d* indates the area of measurement on the gel. Phase contrast images were taken with a Zeiss Primovert inverted microscope with a MU1403B camera (AmScope). All data are reported as mean ± SD for n=3.

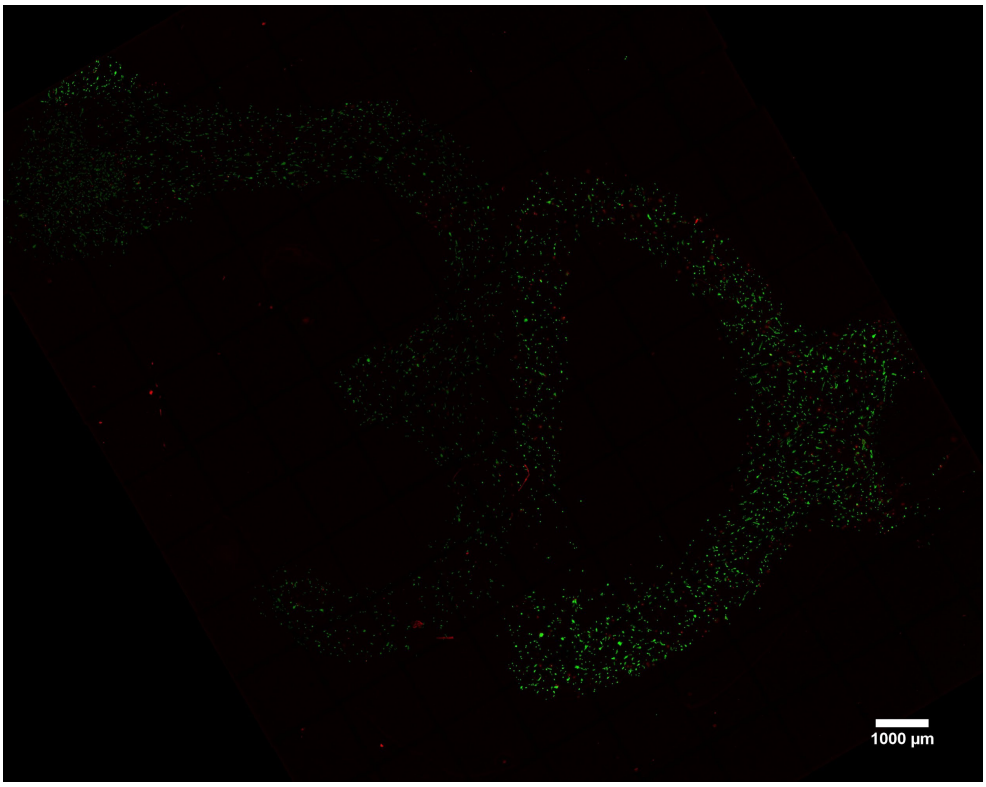

Figure A5. Confocal images showing live/dead staining of human fetal lung fibroblast cells in 3D collagen structure from Figure 2.6. Image comprises 130 fields of view (which each contain 27 Z-stacked images) stitched together. Green is Calcein AM, which stains the cytoplasm of live cells, and red is ethidium homodimer, which stains the nuclei of dead cells. Viability (87% over all, 93% and 86% in the '3' and D' patterns, respectively) was quantified in FIJI image processing software (using a minimum cell area of 25 px^2 for the live and dead stains and a minimum circularity of 0.25 for the dead stain).

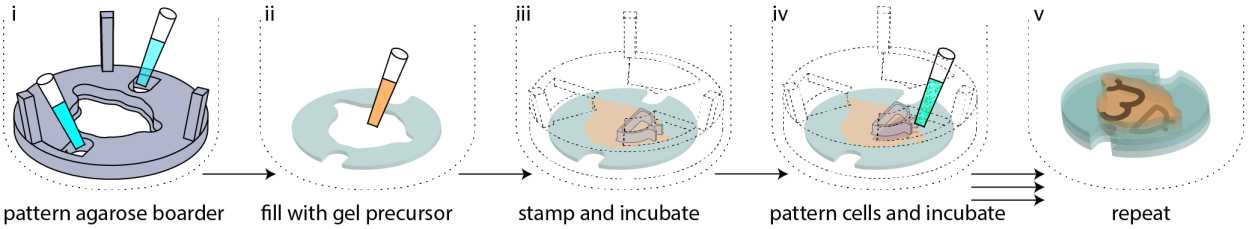

Figure A6. Schematic workflow of agarose and collagen patterning process used to make the cell-laden collagen structure in Figure 2.6. (i) A 200 m tall agarose border is patterned in a 6-well plate. (ii) The agarose border is then filled with collagen gel precursor. (iii) A 200 m tall 'D' patterning device is then placed in the well, which precisely sets the height of the collagen fill to 200 m (the patterning device is shown as two parts for visualization purposes, where the main device component is shown in dotted lines and the 'D' patterning component is shown in transparent grey). The well plate is then incubated with the device in place for 10 minutes to polymerize the collagen. (iv) The previous patterning device is then removed, and an identical, 300 m tall patterning device is placed in the same position. 8 L of cell-laden collagen gel precursor solution is then pipetted into the loading region of the patterning device, at which point the gel precursor solution flows through the 'D' pattern. These 4 steps are repeated once more with a '3' pattern, and then again with no pattern to yield (v) the final structure. As described in the manuscript, the final structure consists of a first cell-free layer that is 200 m tall, then a cell-laden collagen layer containing the 'D' pattern that is 100 m tall, then a cell-free layer that is 200 m tall, then a finally cell-laden collagen '3' pattern that is 100 m tall, then a cell-free layer.

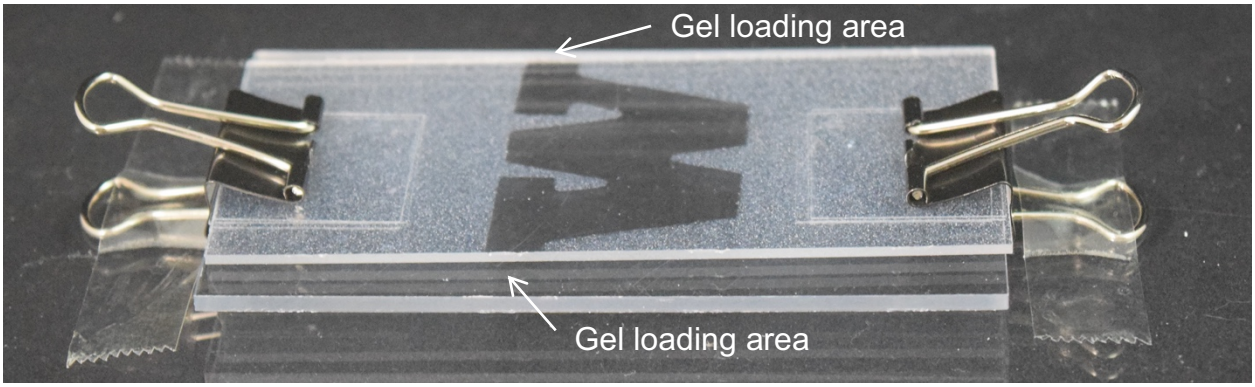

Figure A7. Set up of Figure 8Aii before pre-gel solution is pipetted into gel loading are

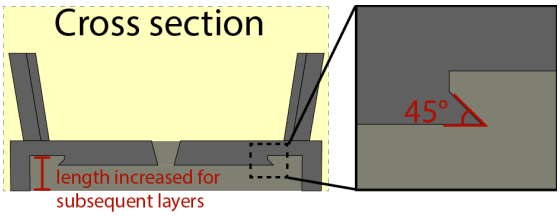

Figure A8. Cross section of patterning device with inset of 45° angled edge to prevent capillary rise. If the patterning device contained a simple 90° angled edge rather than the 45° angled edge shown here, the pre-gel solution would wet the vertical edge of the patterning device due to capillary rise. The diagram also shows the portion of patterning device that is adjusted to increase the height of the patterning area for subsequent layers of hydrogel.

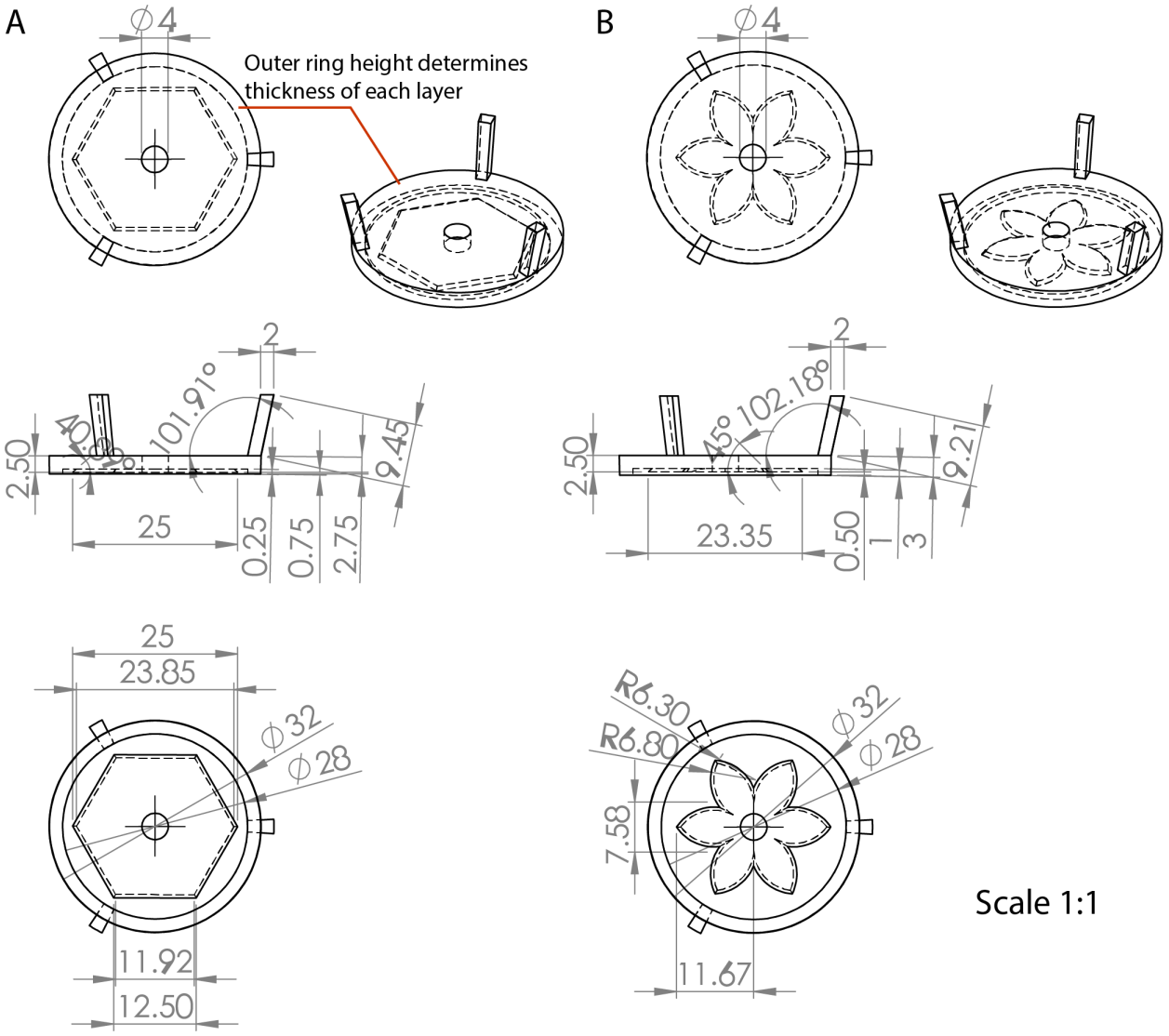

Figure A9. Schematic diagrams illustrating the dimensions of the patterning devices in Figure 2B. (A) First layer hexagon pattern. Red lines indicate the ring ('foot' of the device) that sits flush to the well plate floor which is adjusted for each patterning device to determine layer thickness. (B) Second layer flower pattern.

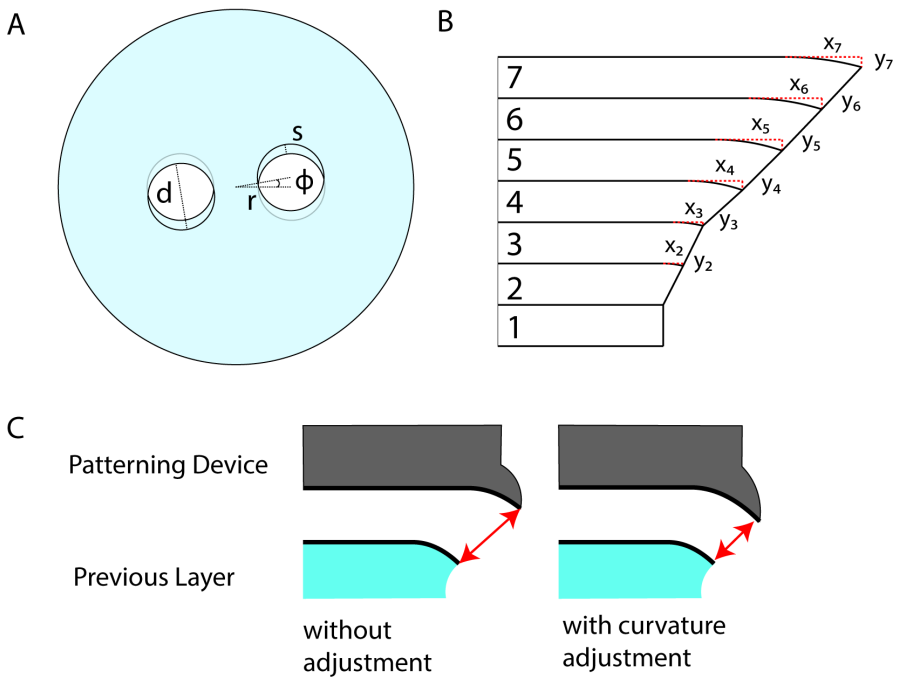

Figure A10. Schematic of helix and overhang design used to make the structures shown in Figure 4 of the manuscript. (A) Dimensions of each design parameter where is diameter of hole, is distance from center of the design to the center of the hole, is the angle of rotation from layer to layer, and is the maximum overhang length. (B) Schematic of the overhang design for 7 layers, showing the curvatures for each layer. Note: there is no curvature for the first layer. (C) The effect of adjusting the curvature based on the previous curvature on the distance between the two layers, as denoted by the red arrows, which limits the surface capillary flow to the edge of the overhang. The left diagram shows the same curvature for both layers and the right diagram shows curvature adjustment on the patterning device based on the previous layer.

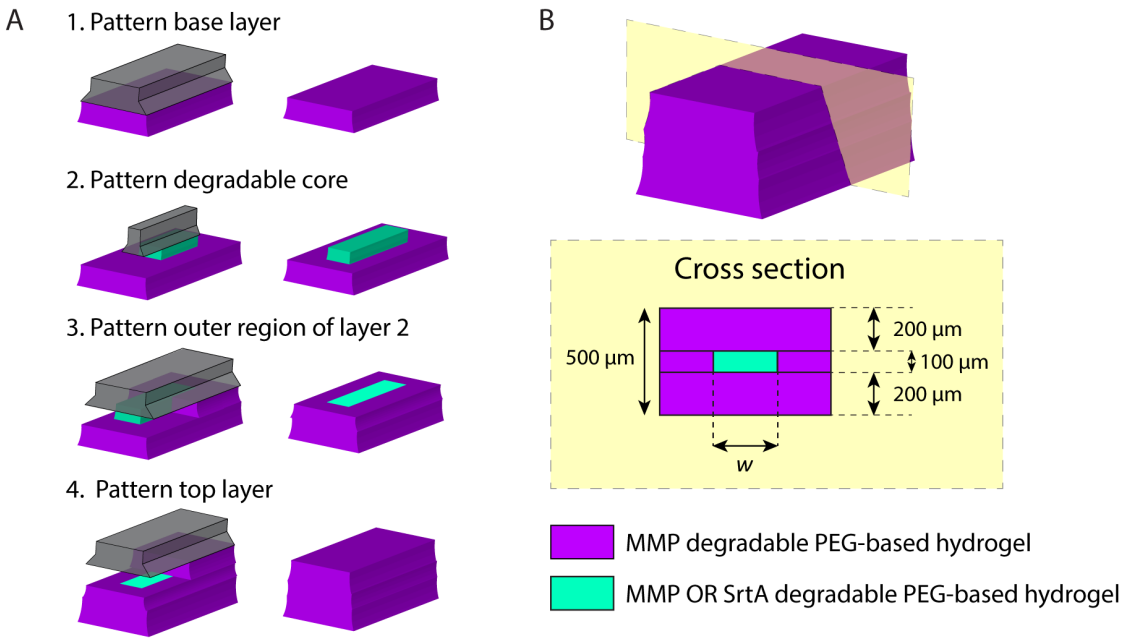

Figure A11. 3D open microfluidic fabrication of PEG-based structure with a enzymatically degradable core. (A) Workflow of fabrication. The gel structure was fabricated in four steps to create a three layered structure consisting of a matrix metalloproteinase (MMP) OR sortase (SrtA) degradable core (teal gel) surrounded entirely by a MMP only degradable gel (purple gel). The middle layer consisting of the core was patterned in two steps, with the SrtA OR MMP degradable core patterned first. (B) Cross section showing dimensions of gel. The total height was designed as 500 m with the middle layer designed as 100 m. The width of the core, *w*, was either 1.0 mm or 0.5 mm.

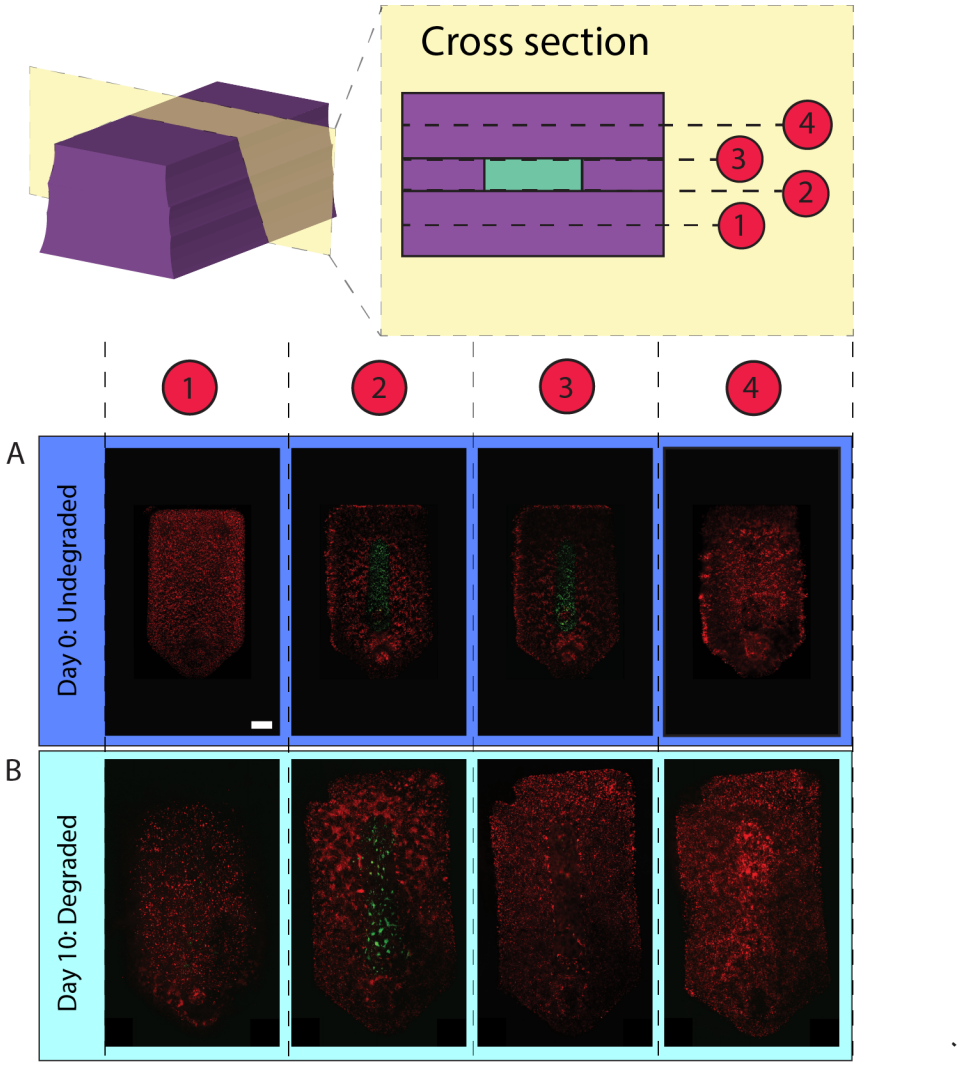

Figure A12. Confocal slices of multiple top-down views of the structure shown in Figure 7. Slice 1-4 is denoted on the cross section schematic with dotted lines. (A) Slices taken from gel just after encapsulation and patterning with no SrtA degradation. (B) Slices taken from gel on day 10 of culture, after SrtA degradation on day 5. eGFP expressing cells are not found in at the top of the middle layer (cross section 3), as the cells have settled to the bottom of the cavity. Scale bar is 1 mm.

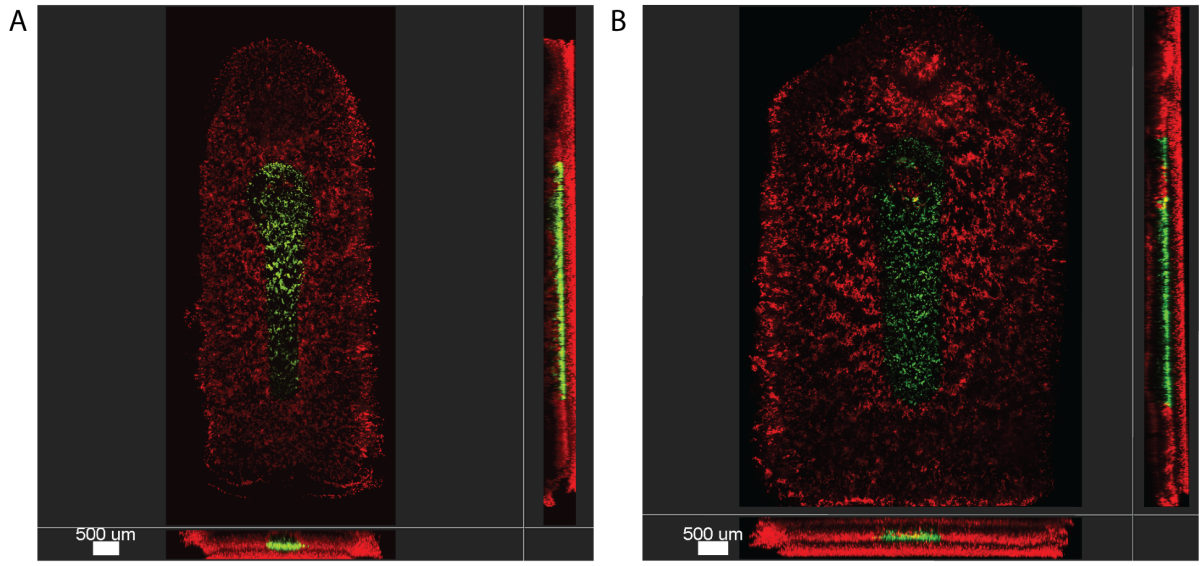

Figure A13. Confocal images of different degradable core geometries. (A) Degradable core width designed with a width of 0.5 mm, and the outside structure was designed with a width of 2.5 mm (B) Degradable core width designed with a width of 1.0 mm with an outside structure designed with a width of 4.5 mm. Scale bars apply to all planes of imaging.

Table A1. Calculated designed curvature values for all patterning devices used for double helix structure.*

Layer	Rotation angle, ϕ (degree)**	Maximum overhang*** (m)	Radius of curvature (mm)	Horizontal length of curvature, x (m)	Vertical length of curvature, y (m)
1	0	0	0	0	0
2	5	239.9	1.0	239.9	29.2
3	5	239.9	1.5	359.9	43.8
4	10	479.4	2.0	659.3	111.8
5	10	479.4	2.5	809.1	134.5
6	10	479.4	3.0	884.0	133.2
7	10	479.4	3.5	921.4	123.5
8	10	479.4	4.0	940.1	112.0
9	10	479.4	4.5	949.5	101.3
10	10	479.4	5.0	954.2	91.9
11	10	479.4	5.5	956.5	83.8
12	10	479.4	6.0	957.7	76.9
13	10	479.4	6.5	958.3	71.0
14	10	479.4	7.0	958.6	65.9
15	10	479.4	7.5	958.7	61.5
16	10	479.4	8.0	958.7	57.7
17	10	479.4	8.5	958.7	54.2
18	10	479.4	9.0	958.7	51.2
19	10	479.4	9.5	958.7	48.5
20	10	479.4	10.0	958.7	46.1
21	10	479.4	10.5	958.7	43.9
22	10	479.4	11.0	958.7	41.9
23	10	479.4	11.5	958.7	40.0
24	10	479.4	12.0	958.7	38.4
25	10	479.4	12.5	958.7	36.8
26	10	479.4	13.0	958.7	35.4
27	10	479.4	13.5	958.7	34.1
28	10	479.4	14.0	958.7	32.9
29	10	479.4	14.5	958.7	31.7

*First seven layers curvature and overhang information also corresponds to the cross section device in Figure 2.4A.
**Rotation angle represents the rotation change from the previous layer. Values are in degrees.
***Maximum overhang corresponds to *s* in Figure A10A.

B. Appendix for Chapter 4

Reproduced in part from A. J. Haack, F. Y. Lim*, D. S. Kennedy, J. H. Day, K. N. Adams, J. J. Lee, E. Berthier, A. B. Theberge, "*home*RNA: A Self-Sampling Kit for the Collection of Peripheral Blood and Stabilization of RNA." Analytical Chemistry, 2021,* ***93****, 13196-13203.*
** Equal contribution*

SUPPLEMENTAL TABLES AND FIGURES:

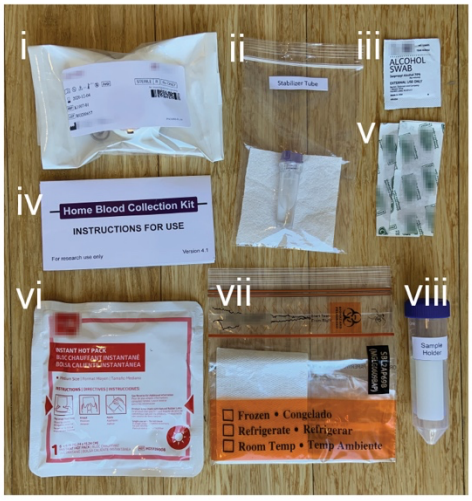

Figure B1. Components of the *home*RNA kit. Kit components include i) the Tasso-SST device, ii) the stabilizer tube containing RNA*later* iii) alcohol wipes iv) instructions for use, v) sterile bandages, vi) hot pack for warming the arm prior to application of the Tasso-SST, vii) sample return bag and viii) sample holder with 3D printed insert to hold the sample tube in place.

Table B1. Components of the *home*RNA blood kit

Kit Component	**Manufacturer(s)**	**Quantity**
Sterile Tasso-SST™ blood collection device	Tasso, Inc.	1
RNA stabilizer tube	Our Lab	1
Instant heat pack	Medline Industries, Inc.	1
Sterile Alcohol Wipe	Covidien, BD	2
Sterile bandage	Band-Aid, Curad	1
Specimen transport bag with absorbent pad	Minigrip	1
50 mL conical tube with stabilizer tube insert	BD, Our Lab	1
Instructions for use	Our Lab	1
Blood-stabilizer mixing instruction card	Our Lab	1

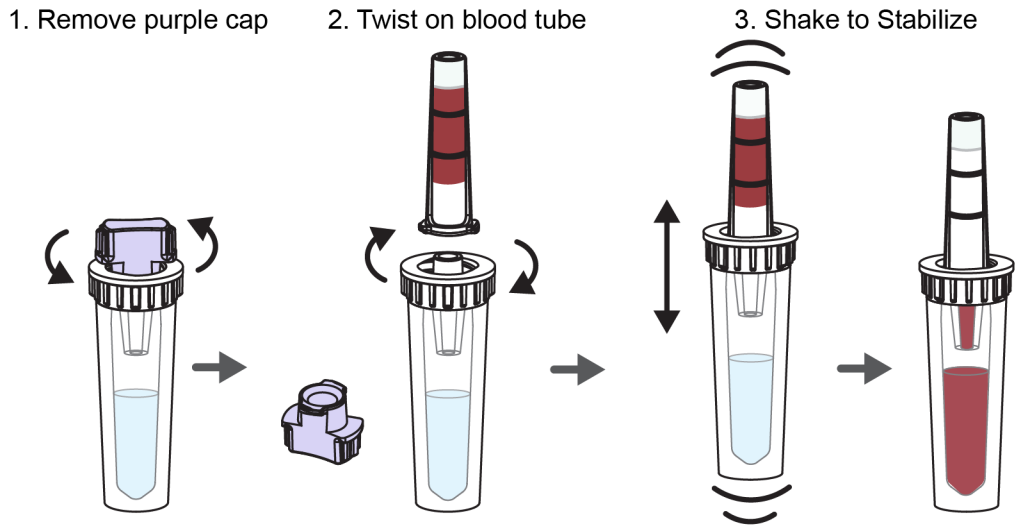

Figure B2. Schematic workflow of the stabilization process. The steps for stabilizing a blood sample collected with the Tasso-SST are as follows: 1) removal of the purple cap, 2) twisting on the Tasso-SST blood tube with the blood sample, 3) shaking up and down vigorously to mix the sample with the stabilizer resulting in RNA stabilized blood.

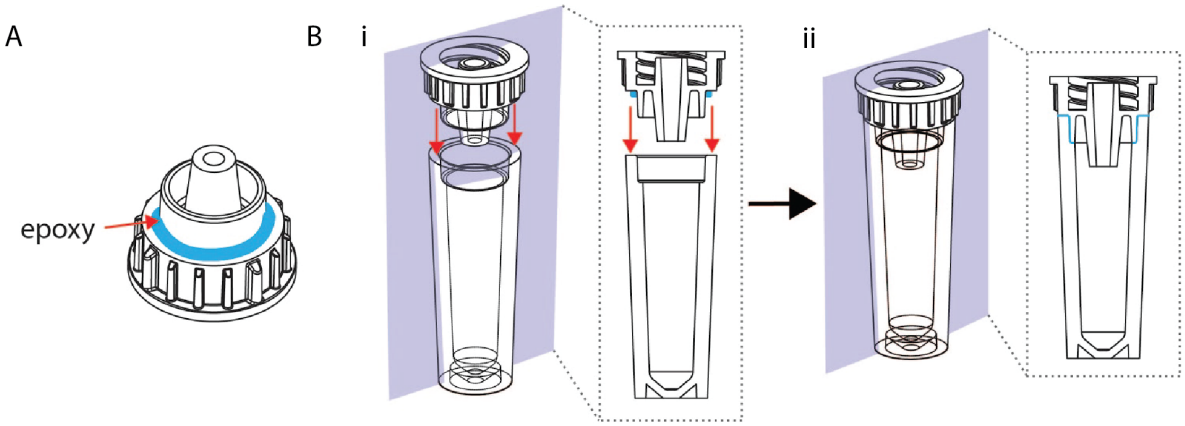

Figure B3. Fabrication of stabilizer tube. A) Location where UV epoxy (blue) is applied to the adaptor piece. B) Mating of the adaptor piece with the vial piece showing location of glue before (i) and after (ii) inserting the adaptor piece into the vial piece. Glue is then cured with a 395-405 UV lamp as described in the materials and methods.

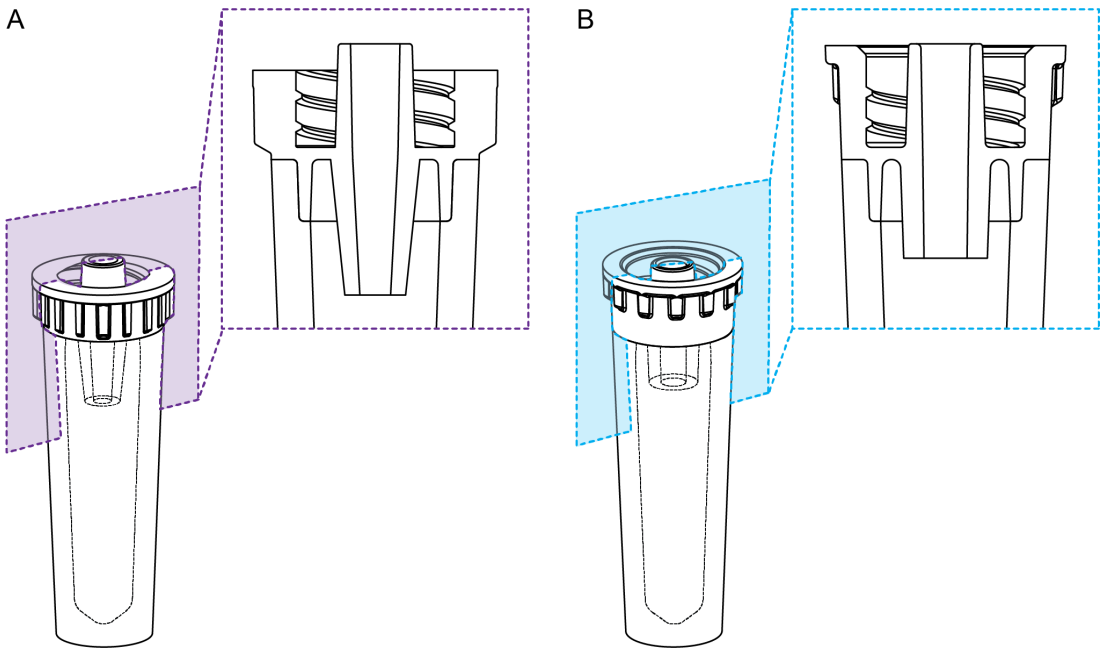

Figure B4. Tube adaptor design. A) Tube adaptor design used for groups 1-5. B) Tube adaptor used in groups 6-7. The tube design use for groups six and seven features a wider opening for easier mixing and pipetting.

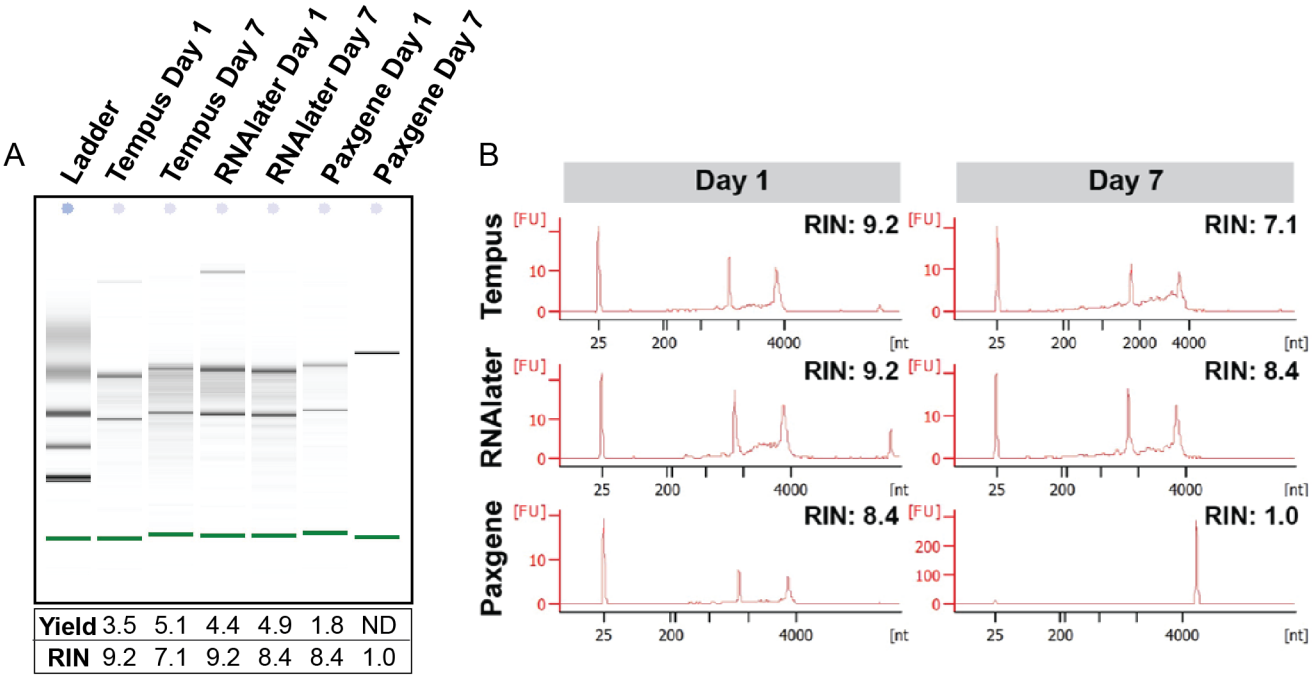

Figure B5. Performance of select RNA stabilizers on total RNA yield and RNA quality over 7 days at room temperature. A) Digital gel image, total RNA yield (µg), RIN values and B) electrophoretogram of RNA isolated from blood stabilized in Tempus, Paxgene and RNA*later* for seven days at ambient temperature.

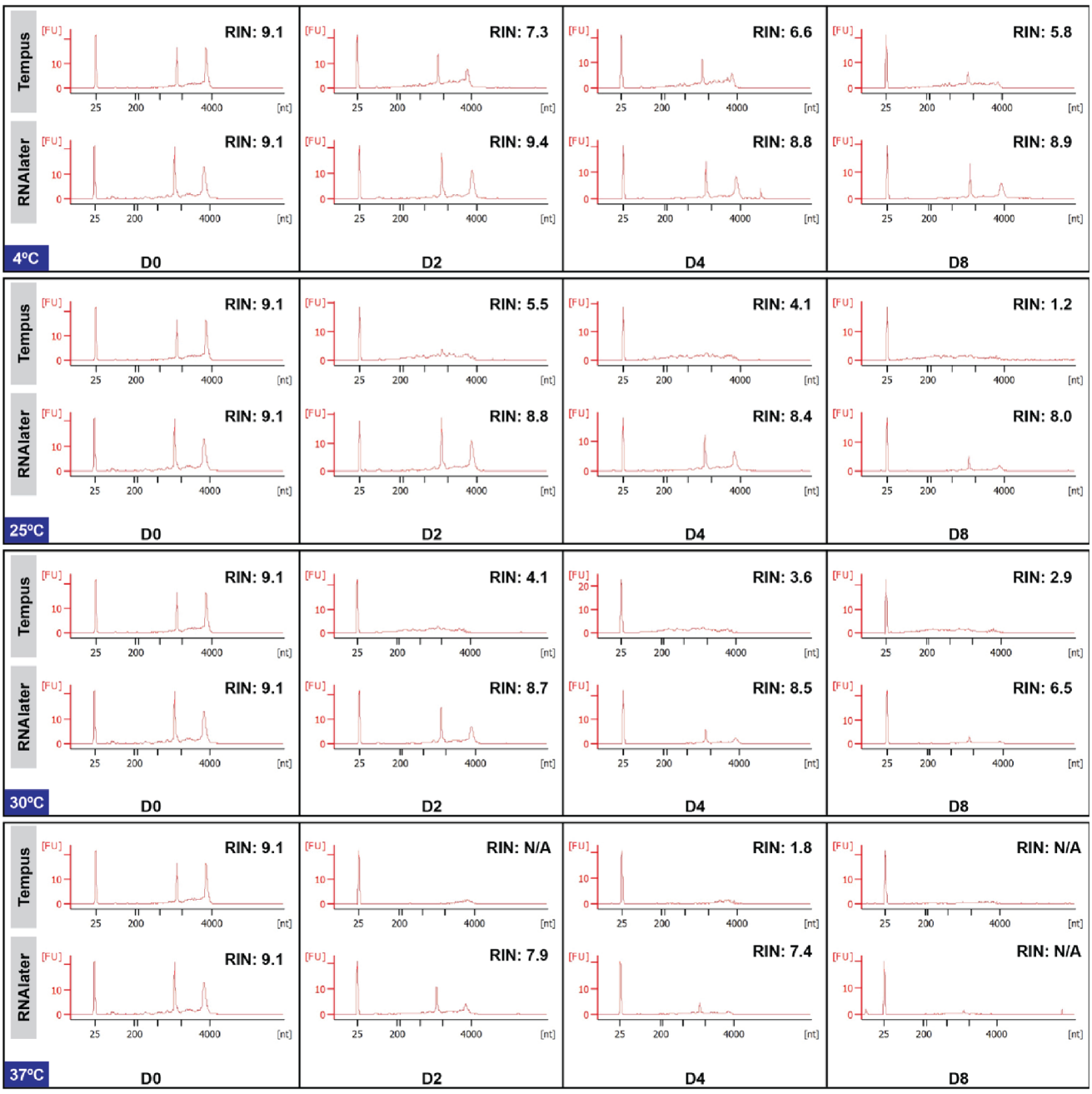

Figure B6. Electropherogram of RNA samples extracted from blood stored at various temperatures. Electropherogram of TempusTM and RNAlaterTM stabilized blood stored at 4°C, 25°C, 30°C and 37°C over 8 days.

Table B2. Components included in each group

Group	IFU version	Video provided	Card with mixing instruction	Tasso-SST™	Stabilizer Tube	Adaptor 1 or 2	Hot Pack	Alcohol wipe, bandages	Sample Return bag	Sample Holder
1	3.1	No	No	Yes	Yes	1	Yes	Yes	Yes	No
2	3.3	No	No	Yes	Yes	1	Yes	Yes	Yes	No
3	3.4	No	No	Yes	Yes	1	Yes	Yes	Yes	No
4	4.1	Yes	Yes	Yes	Yes	1	Yes	Yes	Yes	Yes
5	5.2	Yes	Yes	Yes	Yes	1	Yes	Yes	Yes	Yes
6	5.2	Yes	Yes	Yes	Yes	2	Yes	Yes	Yes	Yes
7	5.4	Yes	Yes	Yes	Yes	2	Yes	Yes	Yes	Yes

Table B3. Logistics for different groups

Group	Time of Year Group was sent out	Shipped or Hand Delivered and Picked up	Number of Subjects	Subjects sent one or two kits
1	Late May, 2020	Hand delivered and picked up- Seattle Area	4	2 kits
2	Mid June, 2020	Shipped- Seattle Area	5	2 kits
3	Mid July, 2020	Shipped -Seattle Area	4	1 kit
4	Mid August, 2020	Shipped- Nationally (WA, NY, PA, IN)	13	1 kit
5	Mid September, 2020	Shipped- Nationally (WA, CO, CA, NE, ME, WI, MA)	16	1 kit
6	Early November 2020	Shipped – Seattle Area	5	1 kit
7	Early December 2020	Shipped – Nationally (WA, CA)	5	2 kits

Table B4. Primer sequences used in gene expression analysis.

Gene	Description	NCBI Ref Seq	Primer Sequence (For and Rev)	T_m
GAPDH	Glyceraldehyde – 3 – phosphate dehydrogenase	NM_002046.7	5’-TGCACCACCAACTGCTTAGC-3’	58ºC
			5’- GGCATGGACTGTGGTCATGAG-3’	58ºC
UBC	Ubiquitin C	NM_021009.7	5’-ATTTGGGTCGCAGTTCTTG-3’	56ºC
			5’-TGCCTTGACATTCTCGATGGT-3’	56ºC

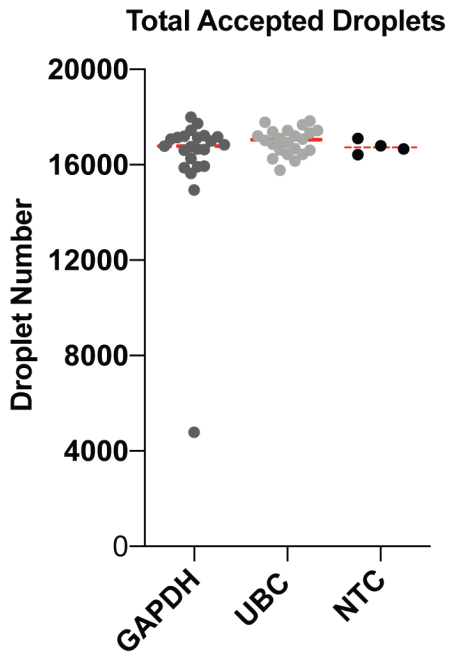

Figure B7. Total Accepted Droplets of GAPDH and UBC ddPCR reactions. NTC represents no template control.

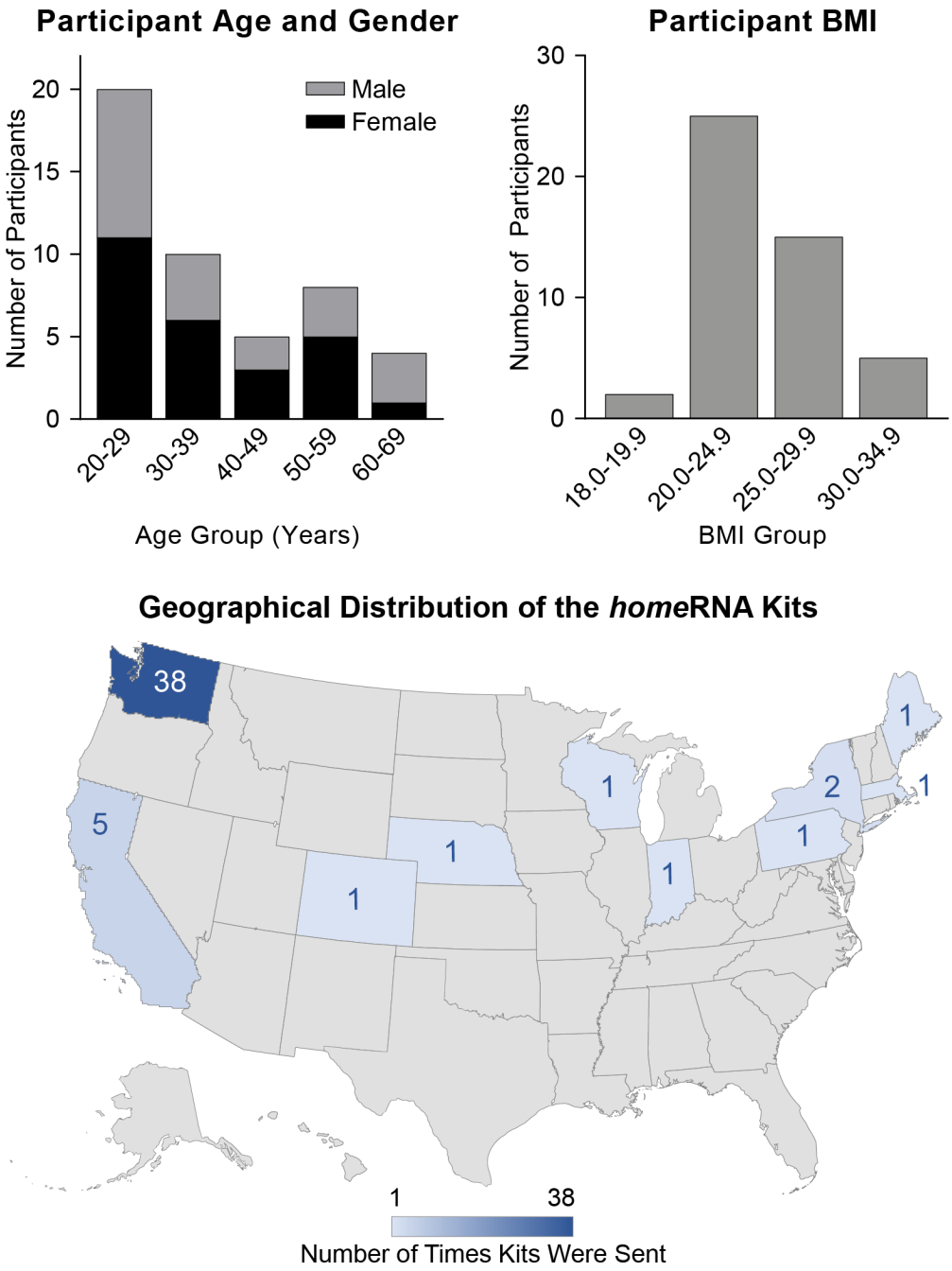

Figure B8. Age, gender, BMI and region of participants. A) Age and gender distribution of participants. B) BMI distribuiton of participants. C) Location by state where *home*RNA kits were sent.

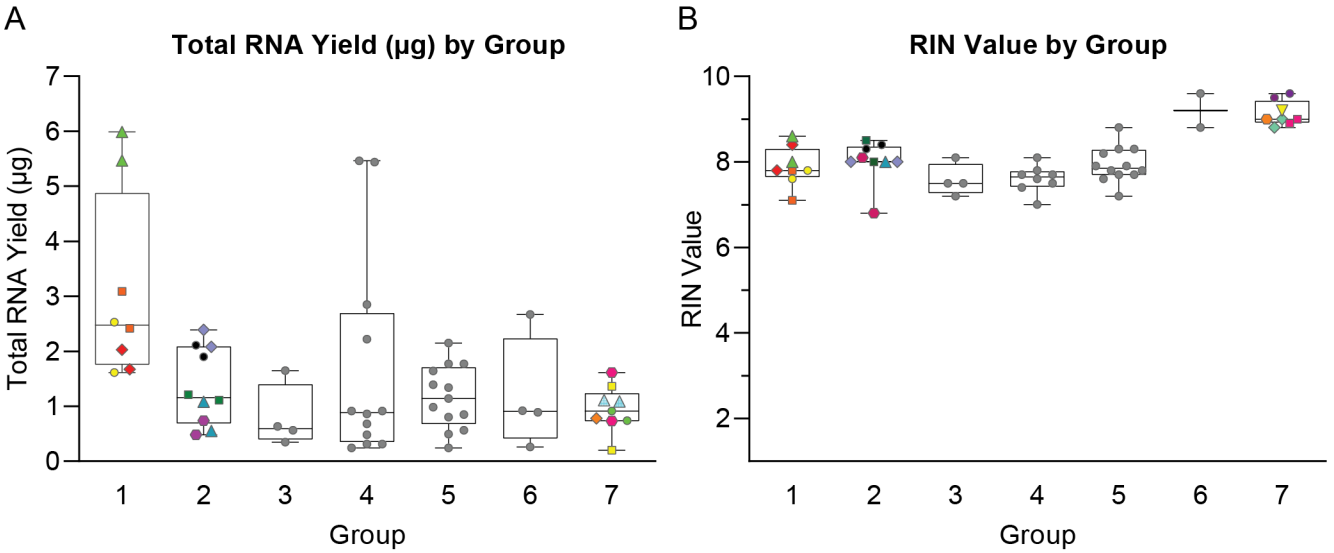

Figure B9. RNA quantity and quality parameters by participant group. A) Total RNA yield and B) RIN value by participant group. Grey circles represent a single sample from a single participant. For group 1 and 2 and 7, each participant collected two samples, which are both plotted and represented by a different color and shape for each participant. Box and whisker plots represent full range, interquartile range, and median.

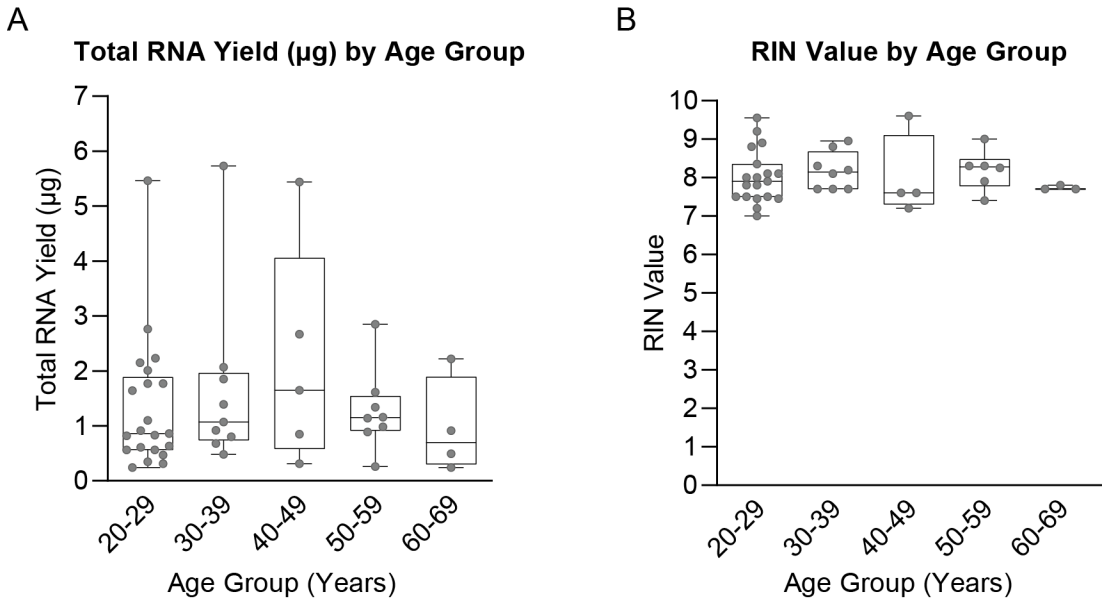

Figure B10. RNA quantity and quality parameters by age group. A) Total RNA yield and B) RIN value by age group. The samples taken where each participant collected and stabilized two samples were averaged, and the mean is plotted here. Box and whisker plots represent full range, interquartile range, and median.

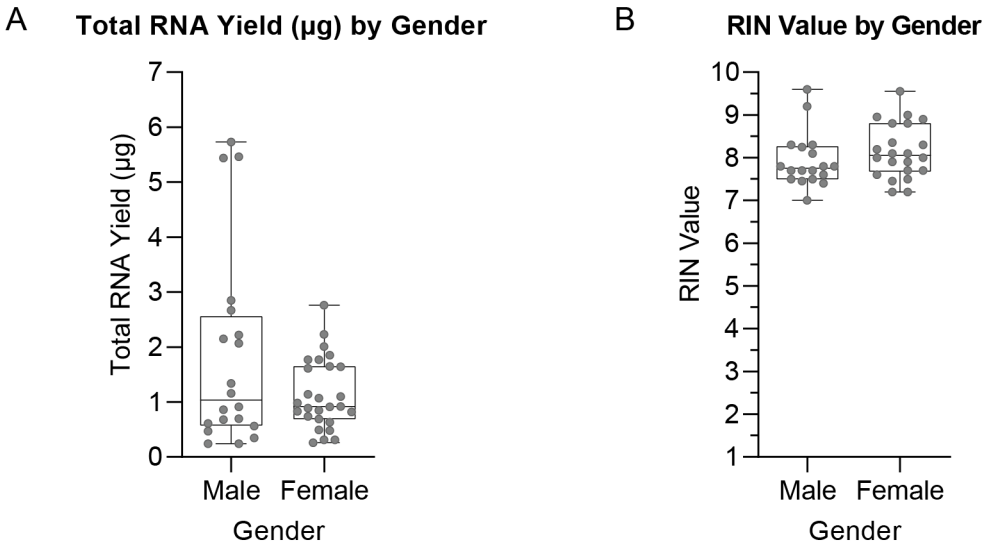

Figure B11. RNA quantity and quality parameters by gender. A) Total RNA yield and B) RIN value by gender. The samples taken where each participant collected and stabilized two samples were averaged, and the mean is plotted here. Box and whisker plots represent full range, interquartile range, and median.

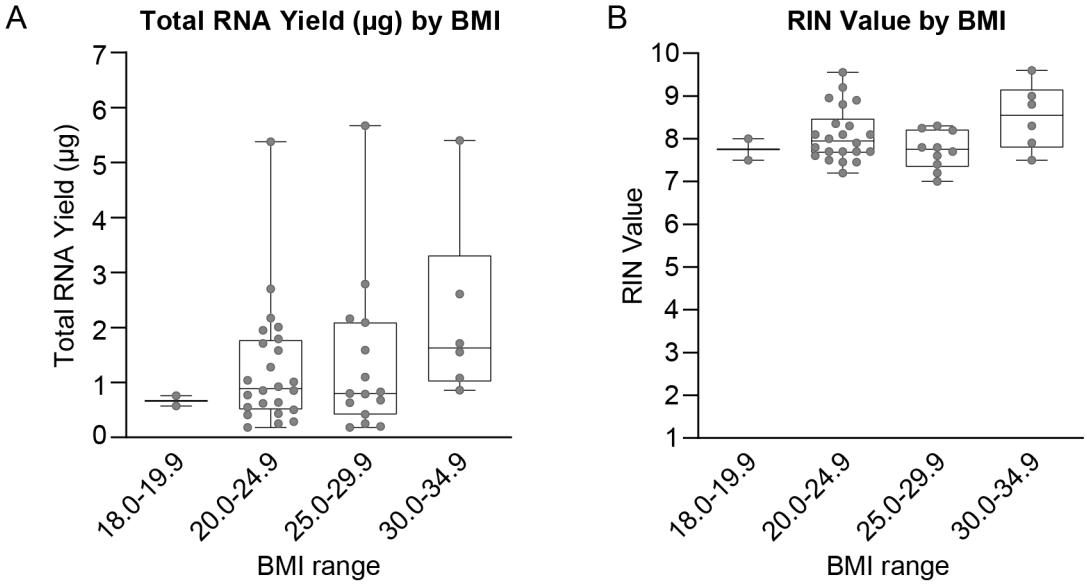

Figure B12. RNA quantity and quality parameters by BMI. A) Total RNA yield and B) RIN value by BMI. The samples taken where each participant collected and stabilized two samples were averaged, and the mean is plotted here. Box and whisker plots represent full range, interquartile range, and median.

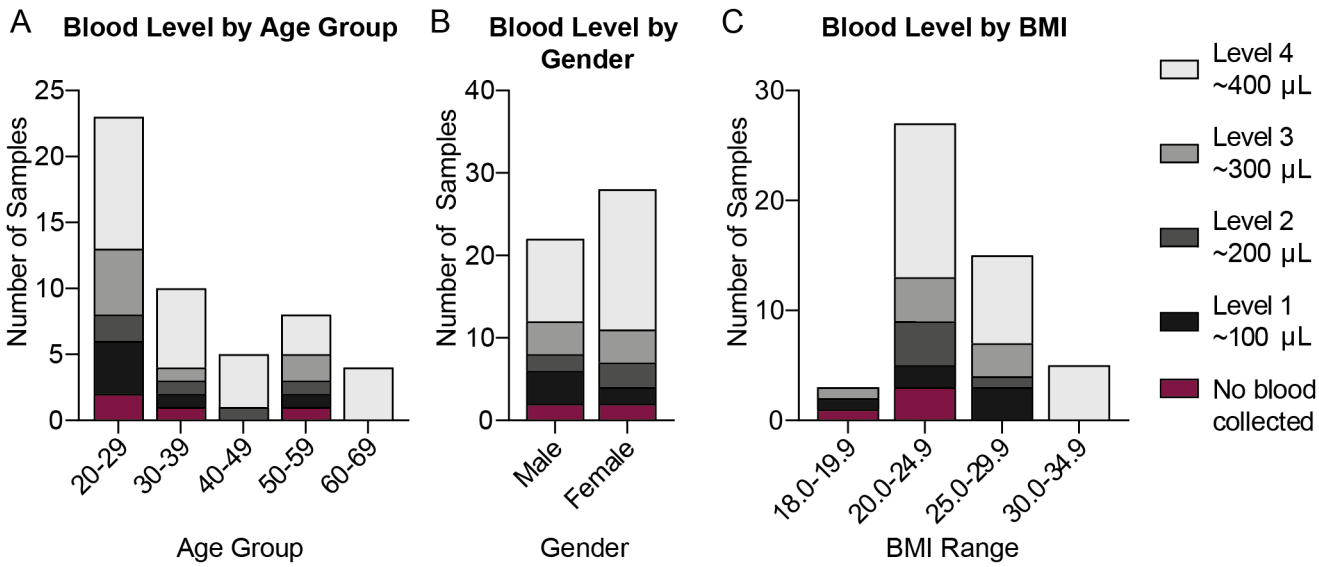

Figure B13. Reported blood level by participant demographics. Reported blood level by A) age B) gender and C) BMI of participants.

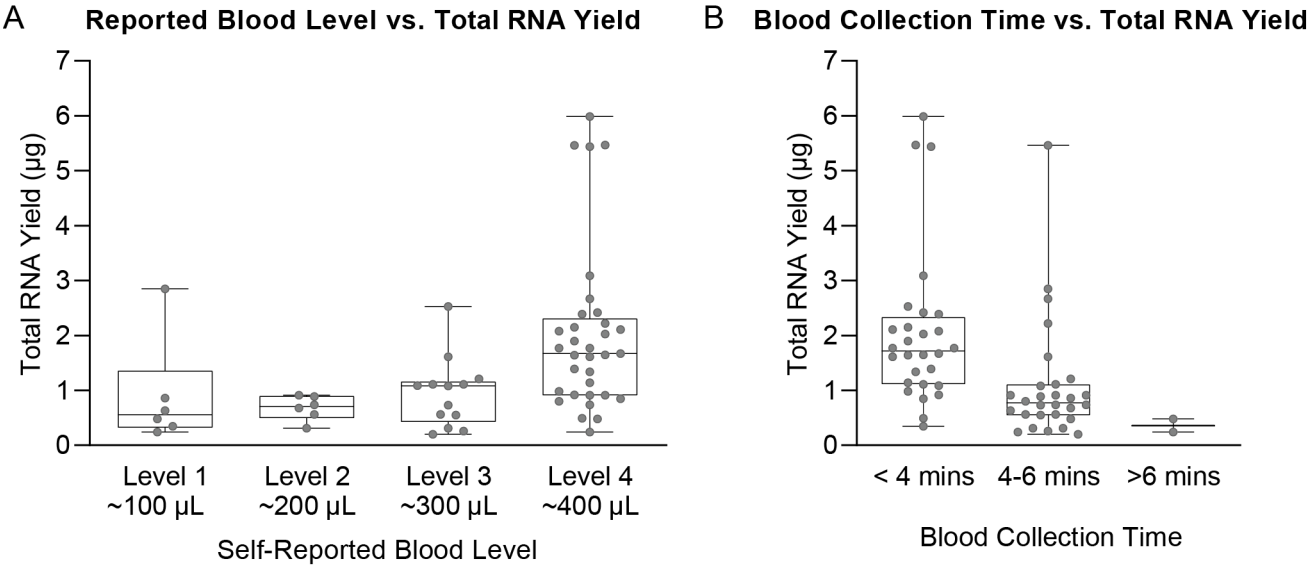

Figure B14. Total RNA yield in relation to responses to surveys on collection parameters. A) Reported blood level vs. total RNA yield. B) Blood collection time vs. total RNA yield, where time includes the total time the Tasso-SST device was left on the arm. Box and whisker plots represent full range, interquartile range, and median.

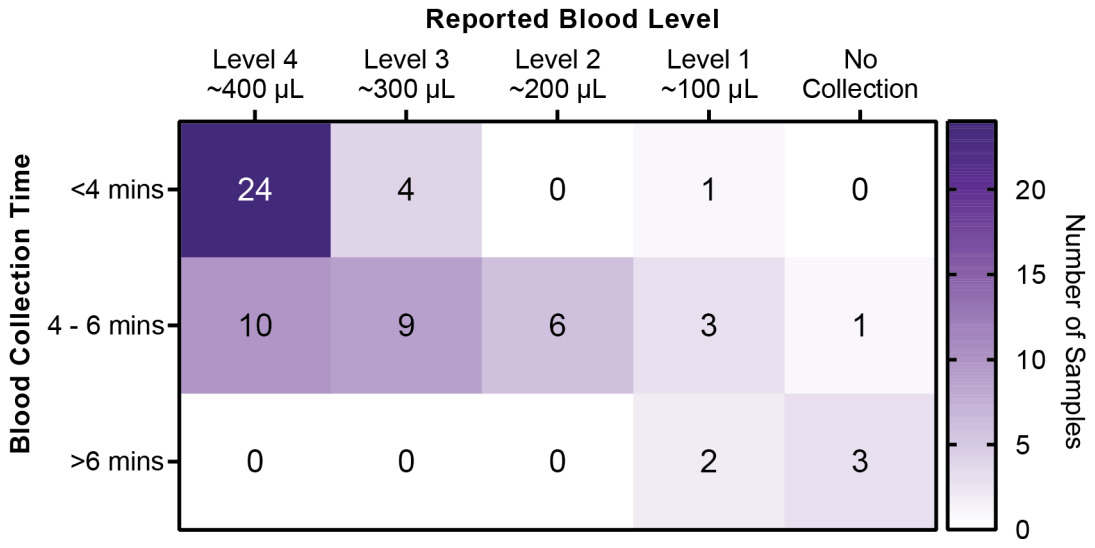

Figure B15. Reported blood level vs blood collection time.

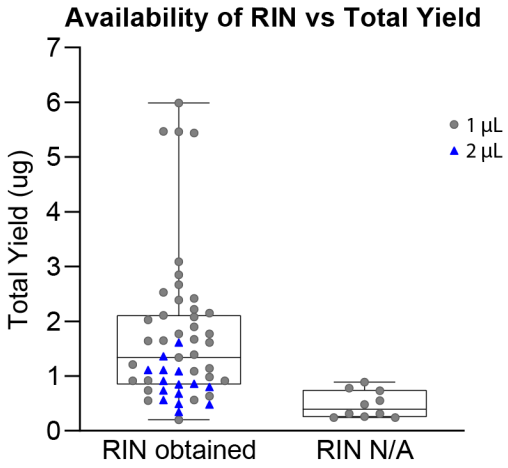

Figure B16. Availability of RIN based on total yield. Blue triangles represent samples where 2 µL of isolated RNA were added to the bioanalyzer chip. Grey circles represent where 1 µL was added to the bioanalyzer chip.

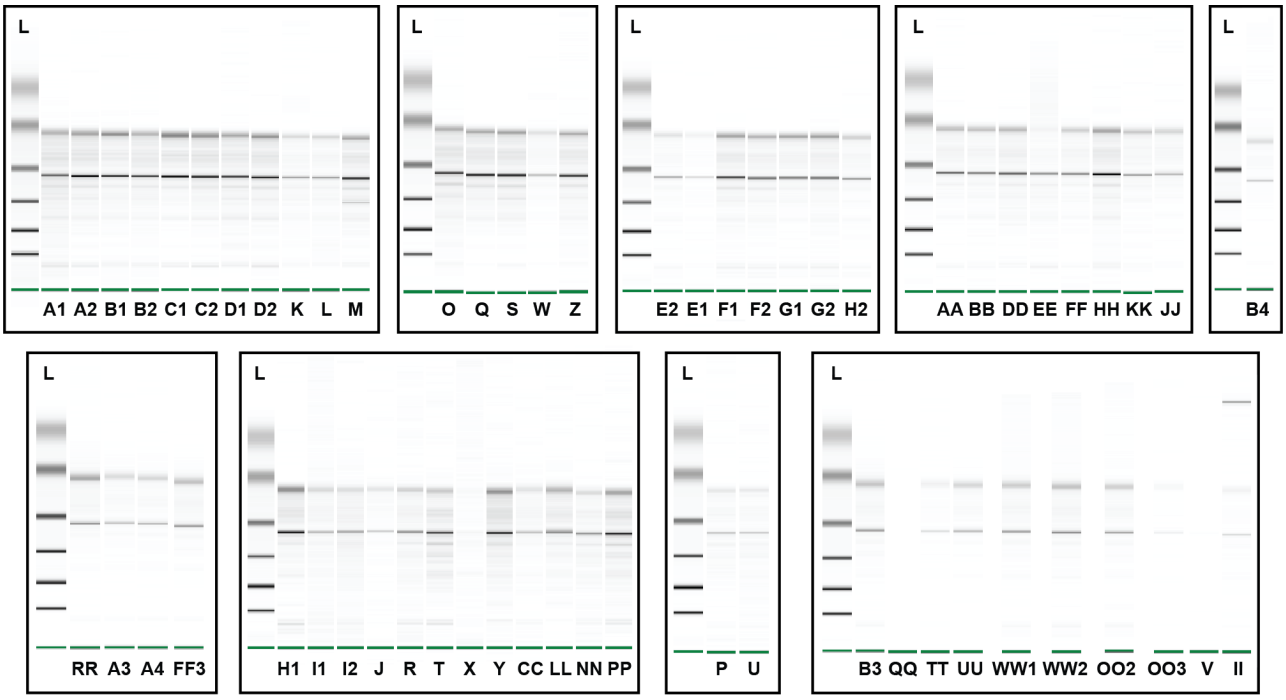

Figure B17. Digital gel images of all samples obtained from the Bioanalzyer 2100. Additional sample information corresponding to the letter code are located in the supplemental dataset in Haack, Lim, et al. [3].

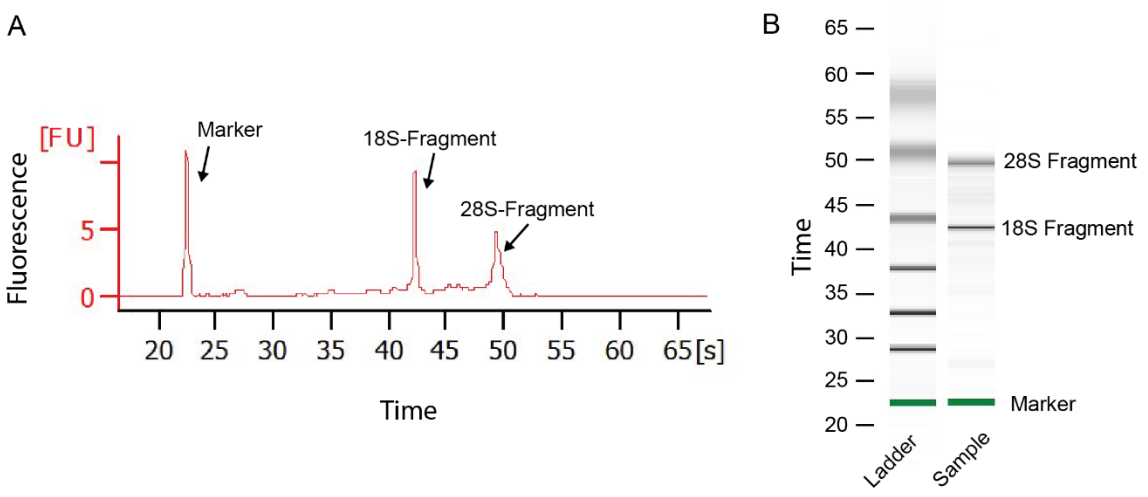

Figure B18. General Information on Bioanalyzer Profile. A) Electrophoretogram and B) Digital gel electrophoresis image obtained from Sample B1 annotated with the marker and two other major peaks that help determine RIN including the 18-S fragment peak, and the 28-S fragment peak. More information on interpreting bioanalyzer data, including examples of electrophoretograms obtained from samples with various RIN values can be found in Schroeder 2006. [1]

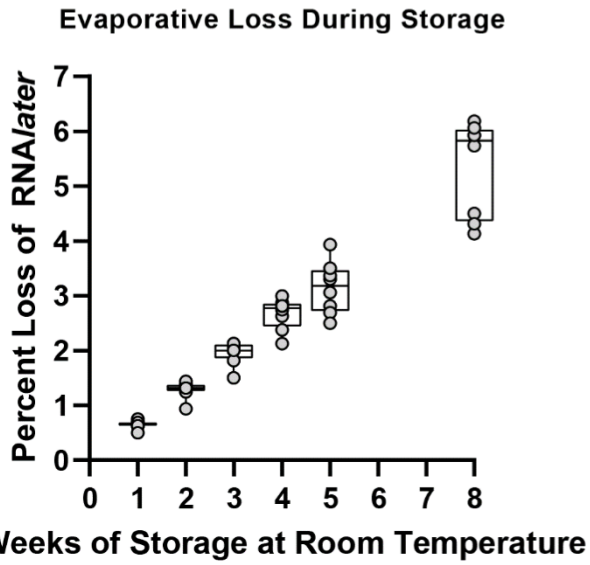

Figure B19. Evaporative Loss During Storage. Percentage loss by weight of RNA*later* at 1, 2, 3, 4, 5, and 8 weeks storage in the *home*RNA tube at room temperature. Box and whisker plots represent full range, interquartile range, and median.

REFERENCES:

1. Schroeder, A.; Mueller, O.; Stocker, S.; Salowsky, R.; Leiber, M.; Gassmann, M.; Lightfoot, S.; Menzel, W.; Granzow, M.; Ragg, T., The RIN: an RNA integrity number for assigning integrity values to RNA measurements. BMC Mol. Biol 2006, 7 (3), 1-14.

2. Harris, P. A.; Taylor, R.; Thielke, R.; Payne, J.; Gonzalez, N.; Conde, J. G., Research electronic data capture (REDCap)--a metadata-driven methodology and workflow process for providing translational research informatics support. J Biomed Inform 2009, 42 (2), 377-81

3. A. J. Haack, F. Y. Lim, D. S. Kennedy, J. H. Day, K. N. Adams, J. J. Lee, E. Berthier and A. B. Theberge, *Anal. Chem.*, 2021, **93**, 13196–13203.

C. Appendix for Chapter 5

Reproduced in part from L.G. Brown, A. J. Haack*, D. S. Kennedy, K. N. Adams, J. E. Stolarczuk, M. G. Takezawa, E. Berthier, S. Thongpang, F. Y. Lim, D. Chaussabel, M. Garand, and A. B. Theberge, "At-home blood collection and stabilization in high temperature climates using* home*RNA" Frontiers in Digital Health, 2022, **4**, 903153.*
** Equal contribution*

Table C1: Experimental timeline and external temperature conditions for Doha, Qatar pilot study

Time (h)	Event / Procedure	External Temperature (℃)	Location
0	Overnight hold at room temperature	21	Lab, Research
27	Start in lab	21	Lab, Research
27.25	Transport outside to car	26	Outside
27.3	In car - A/C started	35.5	Indoor parking
27.4	In car - A/C on	27	Indoor parking
27.5	In car - driving with some sun exposure	33	Driving
28	In car - A/C stopped	31	Outdoor parking - moderate sun exposure
28.1	In car - A/C restarted	37	Outdoor parking - moderate sun exposure
28.25	Car stopped - A/C off	30	Outdoor parking - covered
29	Car restarted - A/C on	41	Outdoor parking - covered
29.19	Car stopped - A/C off	32	Home parking - covered
29.42	Car restarted - A/C on	40	Home parking - covered
29.49	Car stopped - A/C off - Walking to Lab	32	Indoor parking
29.54	Enter building	36	Research
29.56	Office	32	Office, Research
30	Transferring blood from stabilizer tube to store	21	Lab, Research
30.3	Storing sample	-80	Lab, Research

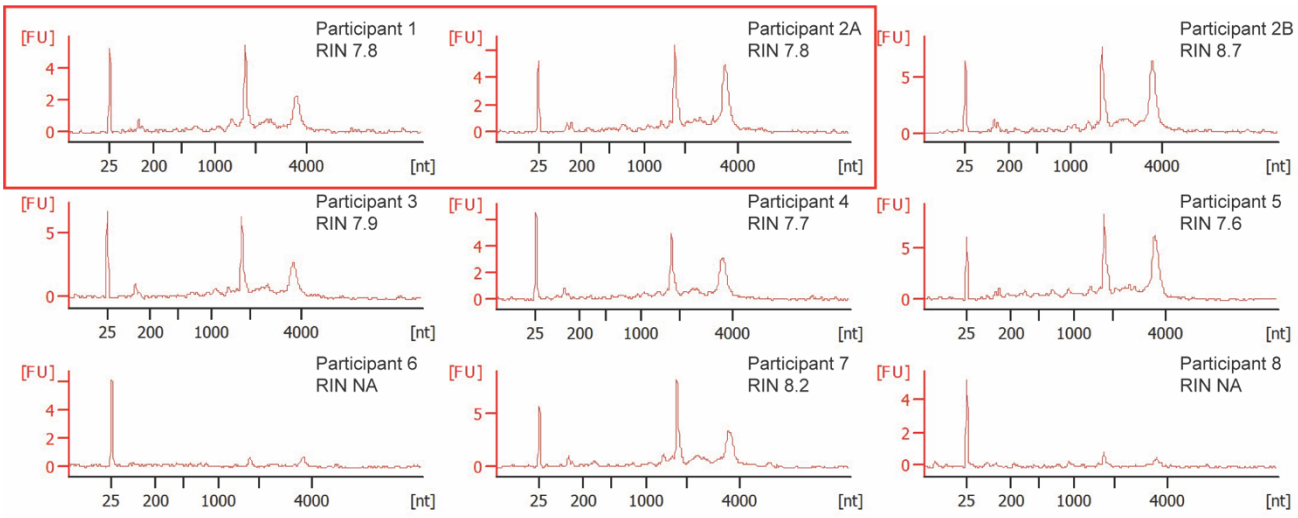

Figure C1. Electropherograms of isolated RNA from stabilized *home*RNA samples in Doha, Qatar. Electropherograms were obtained as raw data using a RNA 6000 Nano Kit on an Agilent 2100 bioanalyzer, which uses fluorescence to detect the marker (~25 nt), 18S rRNA fragments (~1900 nt), and 28S rRNA fragments (~3900 nt). The RIN algorithm then uses these peaks to assign a RIN value to the corresponding sample. The electropherograms are used to generate a gel image, as seen in **Figure 2B**. Samples 1 and 2A in the red box correspond to control samples.

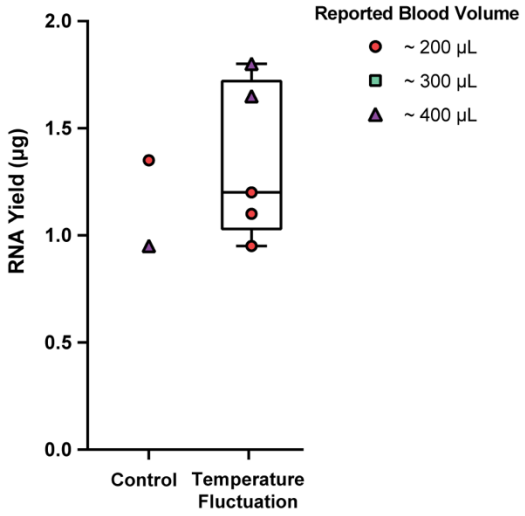

Figure C2. Yield of isolated RNA from stabilized *home*RNA samples in Doha, Qatar. Reported yields were obtained from bioanalyzer measurements by taking the reported concentration from the first 50 µL elution. For the two samples (from participant 6 and 8) that did not have scorable RIN values, yields were not included on the graph since their concentrations were below the lower limit of the qualitative range of the RNA 6000 Nano kit (5 ng/µL). However, for reference, the bioanalyzer reported 4 ng/µL for participants 6 and 8. While concentrations from the Agilent 2100 Bioanalyzer are not typically used for obtaining yield, a threshold value of 200-500 ng total yield is typically needed for downstream analysis such as RNA sequencing. Therefore, an exact value is less important and the bioanalyzer can be used to obtain approximate RNA concentration ranges.

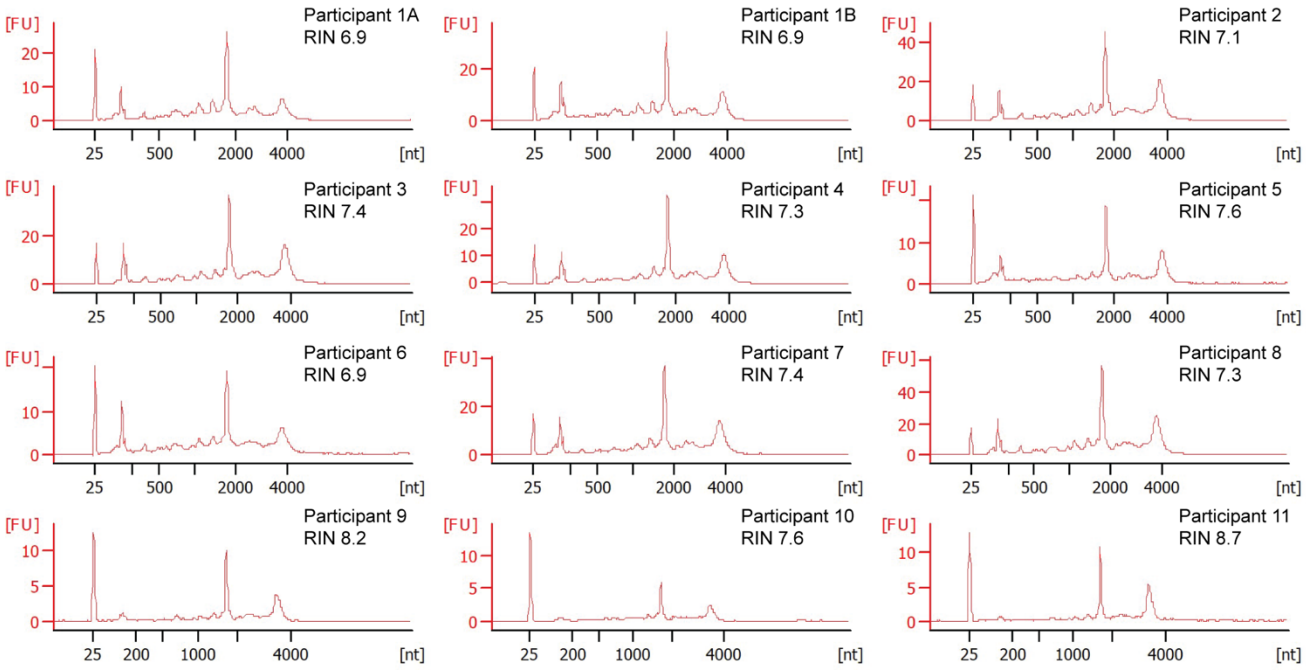

Figure C3. Electropherograms of isolated RNA from stabilized *home*RNA samples in the Western and South Central USA. Electropherograms were obtained as raw data using a RNA 6000 Pico Kit for samples 1-8 and a RNA 6000 Nano Kit for samples 9-11 on an Agilent 2100 bioanalyzer. For samples 1-8, the RNA 6000 Pico kit uses fluorescence to detect the marker (~25 nt), 5S rRNA fragments (~150 nt), 18S rRNA fragments (~1900 nt), and 28S rRNA fragments (~3900 nt). The RNA 6000 Nano kit detects the same peaks with the exception of the 5S rRNA fragment peaks. The RIN algorithm then uses these peaks to assign a RIN value to the corresponding sample. The electropherograms are used to generate a gel image, as seen in **Figure 3A**.

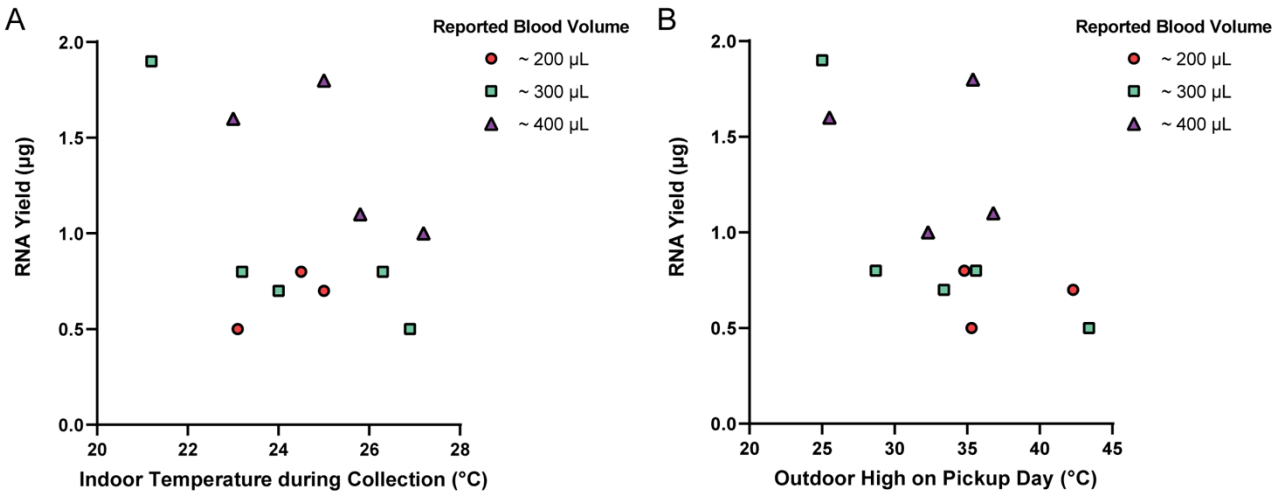

Figure C4. Total yield of isolated RNA from stabilized *home*RNA samples collected, stabilized, and shipped at high temperatures in Western and South Central USA. Reported total yields were obtained by measuring both 50 µL elutions from the RNA isolation protocol (see Methods and Materials) on Cytation 5 Multi-Mode Reader and adding them together to obtain a total yield. Each total yield is reported with the corresponding A) indoor ambient temperature at the time of collection and B) reported outdoor temperature high on the pickup day.

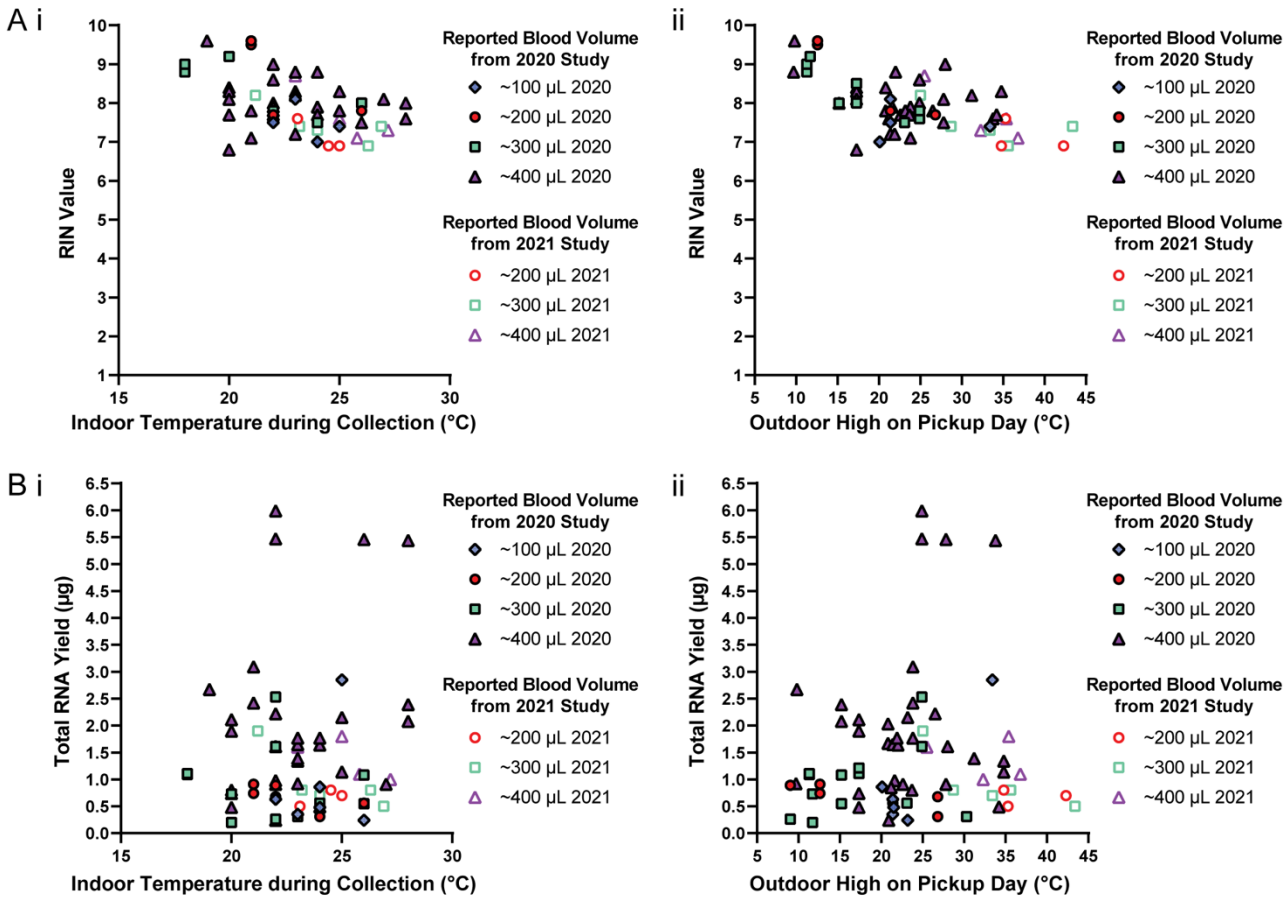

Figure C5. RNA quality and quantity versus temperature, combining data from the present study (summer 2021) from our previous pilot study (summer 2020, Haack, Lim, et al. 2021) (1). A) RIN values versus i) indoor temperature and ii) outdoor high on pickup day. A) Total RNA yield versus i) indoor temperature and ii) outdoor high on pickup day.

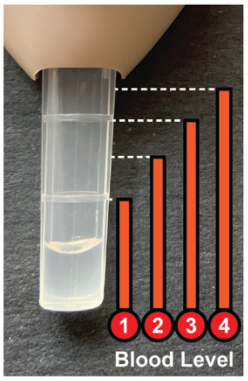

Level	Vol. (µL)
1	100
2	200
3	300
4	400

Figure C6. Reported blood level volumes. Study participants for both the Qatar and Western and South Central USA groups were asked to report the approximate volume with each blood collection with the Tasso-SST™ based on this picture provided in the survey that they completed with sampling. Image was reprinted with permission from Haack, Lim, et al. *home*RNA: A Self-Sampling Kit for the Collection of Peripheral Blood and Stabilization of RNA**.** *Anal. Chem.* 2021, 93, 39, 13196–13203. Copyright 2021 American Chemical Society. (1)

References

1. Haack AJ, Lim FY, Kennedy DS, Day JH, Adams KN, Lee JJ, Berthier E, Theberge AB. *home*RNA: A Self-Sampling Kit for the Collection of Peripheral Blood and Stabilization of RNA. *Anal Chem* (2021) **93**:13196–13203. doi: 10.1021/acs.analchem.1c02008

PREPARE DEVICES AND APPLICATION SITE

FIRST TIME USERS

Please watch the instructional video provided at

https://www.youtube.com/watch?v=iV3GZ8SmmuM

1. Wash hands and get a timer.

You will use a timer in Steps 2 and 10.

2. Apply hot pack to upper arm for 2 minutes.

Warming helps your blood flow better.

3. Clean arm with alcohol wipe.

4. Open the stabilizer tube by twisting off the purple cap.

5. Open Tasso pouch by pulling apart white and clear layers.

Discard cap in pouch.

COLLECT BLOOD USING TASSO-SST

6. Remove clear plastic cover over the red button.

7. Peel paper tab behind the red button.

Keep the tube pointing down.

8. Stick device to shoulder.

Do not remove once it is on.

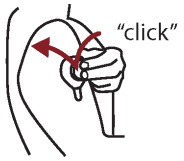

9. Press button quickly and firmly until it can't go any farther. Wait 2 seconds then let go.

10. Start a 5 minute timer.

Keep arm at your side. You wont see blood right away. It can take up to a minute for blood to flow.

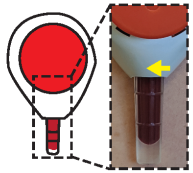

11. After 5 minutes or when the tube fills, *whichever comes first*, peel off the device.

12. Remove tube by firmly twisting a quarter turn and pulling down.

This may take a bit of finger strength.

MIX AND PACKAGE

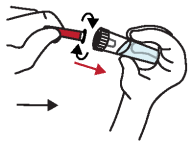

13. Bring together the blood tube and stabilizer tube and screw these together tightly.

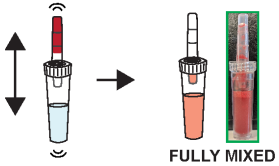

14. With the stabilizer tube on the bottom, shake hard up and down to mix. Stop when mixed.

Some fluid may remain in blood tube. When mixed, the color is the same. See insert for details.

DO NOT DISCONNECT TUBES.

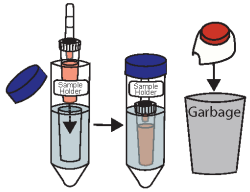

15. Place sample in sample holder. Throw away used Tasso device.

16. Place blood sample in the specimen bag. Wash your hands with soap and water

17. Fill out the online Collection Survey that was emailed to you.

You will need the Unique Code on the box.

18. After filling out the survey, place your sample back in the box, and return using the provided shipping return bag.

Figure C7. Instructions for use for *home*RNA

For research use only

INSTRUCTIONS FOR USE

Home Blood Collection Kit

INTENDED USE

TASSO-SST is a single use blood collection device that is intended for the self collection of capillary blood from the upper arm of adults (18 years or older). The stabilizer tube contains liquid that is intended for stabilizing the collected blood. The home blood sampling kit is for academic research use.

STORAGE

Store at 15 - 30ºC (60 - 80ºF) in a dry place.

WARNINGS

- The TASSO-SST is a sterile device. Do not open until use.
- The TASSO-SST device contains sharps. Handle with care.
- For external use only.
- Keep out of reach of children.
- Use while seated as fainting may occur during blood sampling procedure.
- Do not activate the red button until device is firmly on skin.
- Wipe application site with alcohol wipe to reduce infection risk.
- Always use a new unopened pouch of Tasso-SST. Do not re-use.

ONLINE SYMPTOM AND COLLECTION SURVEY

Please check your e-mail or text message based on the preference you has listed for a link to fill out the daily use online survey.
If you cannot find the link, e-mail us at [redacted]

If you need assistance please contact us at bcmeresearch@uw.edu or call [redacted]

Thank you for participating in our study!

KIT CONTENTS

Make sure your kit contains all components listed below

1) Tasso-SST device

2) Stabilizer tube

3) Alcohol wipes
4) Hot pack
5) Bandage
6) Specimen bag
7) Sample Holder
8) Mail return bag